$B\pi$ Excited State Contamination in B Meson Observables Obtained from Lattice QCD

Dissertation

zur Erlangung des akademischen Grades

doctor rerum naturalium
(Dr. rer. nat.)

im Fach Physik
Spezialisierung: Theoretische Physik

eingereicht an der
Mathematisch-Naturwissenschaftlichen Fakultät der Humboldt-Universität zu Berlin

von

M. Sc. Alexander Roland Broll

Präsidentin der Humboldt-Universität zu Berlin
Prof. Dr. Julia von Blumenthal

Dekanin der Mathematisch-Naturwissenschaftlichen Fakultät
Prof. Dr. Caren Tischendorf

Gutachter:
1. Prof. Dr. Rainer Sommer
2. Prof. Dr. Agostino Patella
3. Assoc. Prof. Dr. Christopher Aubin

Tag der mündlichen Prüfung: 04.12.2023

Abstract

Lattice simulations of Quantum Chromodynamics allow for a fully non-perturbative computation of correlation functions of hadronic operators. The numerical result of a correlator is a superposition of contributions from the ground state as well as excited states. Oftentimes only the ground state is of interest, of which matrix elements and the energy can be determined. If the ground state and the excited states cannot be disentangled in the numerical data, a systematic error might enter the extracted quantities. The aim of this thesis is to analytically determine the contributions of the dominant excited states in correlation functions involving B mesons using an effective field theory. The computations will be carried out in Heavy Meson Chiral Perturbation Theory, a theory which shares its symmetries with Heavy Quark Effective Theory. Besides an expansion in small energies of the interacting particles, this theory also involves an expansion in inverse powers of the heavy meson mass. The focus of this work is on flavour-changing processes of the weak interactions, which are proportional to CKM matrix elements. Those are free parameters of the Standard Model of particle physics and relevant in the search of new physics.

The computations and derivations in this thesis are carried out in the static limit, in which all $1/m_B$ corrections are neglected, and to next-to-leading order in the chiral expansion. The most important results are on the one hand the expressions for the quark bilinears $\bar{q}\,\Gamma Q$, where q is a light quark and Q a heavy quark, in the effective theory. On the other hand, the contributions of $B\pi$ excited states to several correlation functions, which are needed for extracting B physics observables, are computed. These observables are the B meson mass, its decay constant, the $B^*B\pi$ coupling, where B^* is a vector B meson, the $B \to \pi$ vector form factors $h_\perp$ and $h_\parallel$, and the parameter $\hat{B}_d$ which enters in B^0-$\bar{B}^0$ oscillations. With one exception, the excited states lead to an overestimation of the ground state, but yet unknown low energy constants enter some of the results. These can in principle be determined from lattice correlation functions which were identified with the help of the effective theory. For $h_\perp$ on the other hand, the result is quite different: the excited states lead to a strong underestimation of the form factor, and the size of this deviation also strongly depends on the momentum of the final state pion. It is possible that this result can explain the discrepancy between inclusive and exclusive determinations of $|V_{ub}|$.

Using the effective theory, it is also possible to study the effect of smeared interpolating fields. Empirical studies on the lattice show that local interpolating fields, i.e. fields which are defined on a single lattice site, lead to a larger excited states contamination compared to smeared interpolating fields which are spread out over neighbouring lattice sites. In the effective theory, the effect of smearing is captured by using different low energy constants for local and smeared interpolating fields. The numerical values of these constants depend on the smearing procedure and the level of smearing, and can in principle be determined from suitable lattice correlation functions. These correlators were also identified in the effective theory.

Zusammenfassung

Gittersimulationen der Quantenchromodynamik ermöglichen eine vollständig nichtperturbative Berechnung von Korrelationsfunktionen hadronischer Operatoren. Das numerische Resultat des Korrelators ist eine Superposition von Beiträgen sowohl des Grundzustands als auch von angeregten Zuständen. Von Interesse ist häufig nur der Grundzustand, von dem Matrixelemente und die Energie bestimmt werden. Können der Grundzustand und die angeregten Zustände nicht sauber in den numerischen Daten getrennt werden, kann dies zu einem systematischen Fehler in den extrahierten Größen führen. Ziel dieser Dissertation ist die Beiträge der dominanten angeregten Zustände in Korrelationsfunktionen mit B Mesonen analytisch in einer effektiven Feldtheorie zu bestimmten. Dies wird in der Chiralen Störungstheorie für Schwere Mesonen durchgeführt, die die Symmetrien der Effektiven Theorie Schwerer Quarks teilt. Neben einer Entwicklung in kleinen Energien der wechselwirkenden Teilchen beruht diese auch auf einer Entwicklung in inversen Potenzen der Masse der schweren Mesonen. Der Fokus dieser Arbeit liegt hierbei besonders auf Flavour-veränderenden Prozessen der schwachen Wechselwirkung, die proportional zu CKM Matrixelementen sind. Diese sind freie Parameter des Standardmodells der Teilchenphysik und relevant in der Suche nach neuer Physik.

Die Rechnungen und Herleitungen in dieser Dissertation wurden im statischen Limes, in dem alle Korrekturen durch die Masse des schweren Mesons vernachlässigt werden, sowie zur nächstführenden Ordnung in der chiralen Entwicklung durchgeführt. Die wichtigsten Resultate sind dabei zum einen die expliziten Ausdrücke für die Quark-Bilineare $\bar{q}\,\Gamma Q$, wobei q ein leichtes und Q ein schweres Quark ist, in der effektiven Theorie. Zum anderen werden die Beiträge der angeregten $B\pi$ Zustände zu den für verschiedene Observablen relevanten Korrelationsfunktionen berechnet. Diese sind die Masse des B Mesons, seine Zerfallskonstante, die $B^*B\pi$ Kopplungskonstante, wobei B^* ein Vektor-B-Meson ist, die $B \to \pi$ Vektorformfaktoren $h_\perp$ und $h_\parallel$ sowie der Parameter $\hat{B}_d$, der in B^0-$\bar{B}^0$ Oszillationen auftritt. Bis auf eine Ausnahme führen die angeregten Zustände zu einer Überschätzung des Grundzustands um einige Prozent, wobei in manchen Resultaten derzeit unbekannte Niedrigenergie-Konstanten beitragen. Zur Bestimmung der numerischen Werte derselben wurden Korrelationsfunktionen bestimmt aus denen sie prinzipiell in Gittersimulationen extrahiert werden können. Für $h_\perp$ andererseits ergibt sich ein anderes Bild: durch die angeregten Zustände kommt es zu einer starken Unterschätzung des Formfaktors, zusätzlich hängt das Ergebnis noch stark vom Impuls des Pions im Endzustand ab. Möglicherweise kann dieses Resultat die Diskrepanz zwischen inklusiven und exklusiven Bestimmungen von $|V_{ub}|$ erklären.

Mittels der effektiven Theorie lässt sich auch die Wirkung von geschmierten interpolierenden Feldern untersuchen. Erfahrungen aus Gittersimulationen zeigen, dass lokale interpolierende Felder, die nur auf einem Gitterpunkt sitzen, eine stärkere Kontamination durch angeregte Zustände zeigen, als solche die über mehrere aneinandergrenze Gitterstellen verteilt sind. Die Wirkung des Schmierens manifestiert sich in der effektiven Theorie durch verschiedene Niedrigenergie-Konstanten für lokale und geschmierte interpolierende Felder. Die Werte dieser Konstanten hängen sowohl von der Art der Verschmierung als auch der Stärke ab und können im Prinzip mittels geeigneter Korrelationsfunktionen, die in der effektiven Theorie identifiziert wurden, in Gittersimulationen bestimmt werden.

Contents

1. Introduction **7**

2. Quantum Chromodynamics in the Continuum and on a Lattice **11**
2.1. Basics of Quantum Chromodynamics . . . 11
2.1.1. Chiral Symmetry . . . 15
2.2. QCD on a Lattice . . . 21
2.2.1. Excited States Contamination of Correlation Functions . . . 26
2.2.2. Smeared Interpolating Fields . . . 29
2.2.3. Summation Method . . . 29
2.3. Heavy Quark Effective Theory . . . 30
2.3.1. Matching HQET Currents to QCD . . . 34
2.4. Flavour Changing Interactions . . . 37
2.4.1. Leptonic B Meson Decays . . . 38
2.4.2. Semileptonic B Meson Decays . . . 38
2.4.3. B^0-$\bar{B}^0$ Oscillations . . . 40

3. Chiral Perturbation Theory **43**
3.1. Basics of Chiral Perturbation Theory . . . 43
3.2. Heavy Meson Chiral Perturbation Theory . . . 46

4. Excited States Contamination of Light and Heavy Meson Two-Point Functions **51**
4.1. Heavy-Light Currents and Densities . . . 52
4.1.1. Matching Smeared Interpolating Fields to Chiral Perturbation Theory 55
4.2. B Meson Two-Point Function . . . 56
4.2.1. Effective Mass . . . 62
4.2.2. Effective Decay Constant . . . 62
4.3. Pion and Kaon Two-Point Functions . . . 64

5. Excited States Contamination of Hadronic B Meson Matrix Elements **69**
5.1. $B^*B\pi$ Coupling Constant . . . 69
5.1.1. Correlation Functions for the Determination of the NLO LEC γ . . . 72
5.2. $B \to \pi$ Vector Form Factors . . . 76
5.2.1. $h_\perp$ . . . 78
5.2.2. $h_\parallel$ . . . 81
5.2.3. Comparing the Excited States Contamination of Different Ratios . . . 83
5.2.4. Extracting β_1 and β_2 from the Form Factors . . . 86
5.3. B^0-$\bar{B}^0$ Oscillations . . . 88
5.3.1. O_L and O_M in HM ChPT . . . 90
5.3.2. Excited States Contamination of B^0-$\bar{B}^0$ Mixing Matrix Elements . . . 95
5.3.3. Correlation Functions for the Determination of the LECs ω_1, $\hat{\eta}$, and $\hat{\phi}$ 98

6. Conclusions and Outlook **101**

Appendices **107**

A. Feynman Rules **109**

B. Higher Order Corrections of the B Meson Two-Point Function **115**

C. Higher Order Corrections of $\delta h_\perp$ **121**

Bibliography **125**

1. Introduction

The Standard Model (SM) of particle physics is currently the most accurate theory describing the interactions of elementary particles at energy ranges accessible in today's particle physics experiments. It explains how the matter particles, known as leptons and quarks, interact via three of the four fundamental forces. The forces themselves are mediated by gauge bosons: the photon is responsible for the electromagnetic interactions of particles, the Z^0 and $W^\pm$ mediate the weak interactions, and the strong force is due to gluon exchange. The strong force only acts on quarks and gluons, and binds them into hadrons, such as protons and neutrons which are the building blocks of atomic nuclei, at low energies. Another ingredient of the SM is the Higgs boson, the latest elementary particle discovered in experiments [1, 2], which is central in giving masses to the Z^0 and $W^\pm$ gauge bosons as well as the quarks and half of the leptons via the Higgs mechanism [3–5].

The excellent agreement of almost all experimental results and SM predictions as exemplified in the reviews of the Particle Data Group [6] shows that the SM is indeed an accurate description of elementary particle physics at the energy scales that can be accessed in today's experiments. It is nonetheless possible that unknown new particles exist whose contributions to physical processes at low energy scales are highly suppressed, but become more and more important as the energy scale is increased. It is therefore an important task to search for tensions between experimental results and theory predictions in order to identify physics Beyond the Standard Model (BSM). This can be done by making use of the parameters of the SM.

The SM Lagrangian depends on a number of free parameters. Only after extracting them from experiments, it is possible to make concrete predictions for other elementary particle physics processes. These free parameters include, amongst others, the masses of the elementary particles, and the gauge couplings, such as the elementary charge e of electromagnetic interactions. The parameters which are relevant for the present thesis are the elements of the Cabibbo-Kobayashi-Maskawa (CKM) matrix [7, 8]. The importance of these matrix elements is the following: the quarks come in six different flavours, which are divided into three up-type quarks $U_i = (u, c, t)$ with electric charge $2/3e$, and three down-type quarks $D_i = (d, s, b)$ with electric charge $-1/3e$. The weak interactions are the only interactions which can change the flavour of a quark, they allow for transitions between up-type U_i and down-type D_j quarks, the probability of which is proportional to the square of the absolute value of the CKM matrix element V_{ij}. The important point is that this matrix element enters *every* process which includes this transition and can therefore potentially be extracted from several processes. If no new particles would exist, all extracted values for a given CKM matrix element should agree. However, if at least one not yet discovered particle contributes to one of the processes, the SM calculations are not applicable anymore and the value of V_{ij} determined from it can deviate from the other values.

One such transition, which will play a role in this thesis, is the decay of a bottom quark into an up quark, $b \to u$, which is proportional to the CKM matrix element V_{ub}. In nature, the strong interactions bind the quarks into hadrons, and this transition can, among other processes, be observed in semileptonic decays of B mesons which are quark-anti-quark bound states of a b and a light quark. $|V_{ub}|$ can be extracted from exclusive decays with a fixed final state hadron, e.g. $B \to \pi\ell\bar{\nu}_\ell$ with a lepton ℓ and an anti-neutrino $\bar{\nu}_\ell$, or one can consider the inclusive decay rate for the process $B \to X_u\ell\bar{\nu}_\ell$, where X_u is any hadronic state which

contains the up-quark of the considered quark transition. The values presented by the Particle Data Group [6] for $|V_{ub}|$ extracted from these two processes agree at the $1.4\,\sigma$-level, while the errors are both of the order of 5%. It will be interesting to see if a significant tension between these two values will emerge when the errors are brought down to the sub-percent level in the future.

Processes involving hadrons such as B mesons cannot be (reliably) computed in perturbation theory at low energies. The coupling constant of Quantum Chromodynamics (QCD), the theory describing the strong force, increases for decreasing energy [9, 10] until it reaches a value at which a series expansion in it breaks down. Furthermore, there are also hadronic observables such as the proton mass which cannot be computed in perturbation theory. A fully non-perturbative approach to QCD is therefore needed to describe low energy hadronic processes. The most prominent tool for this task is lattice QCD [11], an approach in which hadronic correlation functions are computed numerically in a discretised and finite Euclidean spacetime. This comes with the drawback that all quantities that are extracted from these correlators have to be extrapolated to the continuum and infinite volume limit. These extrapolations have to be done with care, otherwise *systematic* errors can enter the results and lead to incorrect values of observables or SM parameters, such as CKM matrix elements, which require input from the lattice.

This thesis is devoted to the study of another kind of systematic errors in lattice simulations: *excited states contaminations*. These arise in the following way: correlation functions are vacuum expectation values of operators which are used to create and destroy particles, as well as operators which mediate interactions between those particles. The form of the operators is dictated by the quantum numbers of the particle they are interpolating, such as spin, parity, and flavour content. For a pseudoscalar B meson, which is a bound state of a bottom b quark and light quark $\bar{q}$, a suitable interpolating field is given by $\bar{q}\gamma_5 b$ with the Dirac matrix γ_5. It turns out that this operator does not only create and destroy B mesons, but also other states of QCD such as $B^*\pi$ multi-particle states, where B^* is a vector B meson and π a pseudoscalar pion. These two particles can be coupled in such a way that the combined state has the same quantum numbers as a B meson state, and the operator $\bar{q}\gamma_5 b$ can therefore couple to it. Even worse, the operator can couple to every (multi-)particle state which has the same quantum numbers as a B meson. As a consequence, correlation functions are a linear combination of contributions from an infinite number of (multi-)particle states. Disentangling the relevant ground state from the excited states contributions in numerical results of correlation functions is a significant but also error-prone task in lattice QCD. This is often done by using multi-state fits or solving a Generalised Eigenvalue Problem (GEVP) [12, 13]. These are methods which need lattice correlation functions as input. It is far more desirable to have analytic expressions for the effects of at least the dominant excited states on correlation functions. This begs the question in which theoretical framework this can be done, since QCD can be ruled out for the very reason that lattice QCD is needed in the first place for the computation of hadronic observables and correlation functions. The answer is Chiral Perturbation Theory (ChPT) [14–16], the low energy effective theory of QCD, which describes the interaction of the lightest hadrons: pions ($m_\pi \approx 140\,\text{MeV}$), kaons ($m_K \approx 500\,\text{MeV}$), and the eta meson ($m_\eta \approx 550\,\text{MeV}$). These are the particles one expects to enter in the dominant excited states contamination of correlation functions. The coupling of these particles to the lightest nucleons has also been worked out [17, 18]. On this basis, the excited states contamination of several nucleon correlation functions were successfully predicted in [19–26], proving that this approach for estimating excited states is viable.

The aim of this thesis is to extend this approach to the excited states contamination of B meson correlation functions. Chiral Perturbation Theory itself is not capable of describing the interactions of B mesons with a mass of $m_B \approx 5\,\text{GeV}$, it needs to be augmented to

accommodate heavy particles. A theory which can do this has been worked out in the past and is known as Heavy Meson Chiral Perturbation Theory (HM ChPT) [27–30]. It is based on an expansion in inverse powers of the heavy meson mass, a feature it shares with the underlying Heavy Quark Effective Theory (HQET) [31–39] which is an expansion in inverse powers of the heavy quark mass. This connection indeed proves useful when the analogues of quark bilinears such as $\bar{q}\gamma_5 b$ are derived in HM ChPT. The main results of this thesis are the analytic expressions for the asymptotically dominant excited states contamination of matrix elements relevant for weak interaction processes of B mesons. These are: i) the B meson decay constant which enters in the leptonic decay $B \to \tau\bar{\nu}_\tau$ which allows for a determination of $|V_{ub}|$; ii) the $B \to \pi$ vector form factors relevant for the semileptonic decays $B \to \pi\ell\bar{\nu}_\ell$ which can also be used for extracting the same CKM matrix element. It turns out that there is an exceptionally large excited state in one of the form factors, a result which might help to explain the slight tensions between inclusive and exclusive determinations of $|V_{ub}|$ alluded to earlier; and iii) the hadronic matrix elements needed for the description of B^0-$\bar{B}^0$ oscillations, from which the product of CKM matrix elements $|V_{tb}V_{td}|^2$ can be extracted. Some of the results depend on Low Energy Constants (LECs) for which numerical values have not been determined yet. Some suitable correlation functions have been found using HM ChPT, from which they can in principle be determined in a lattice simulation, but for the present thesis their influence was only estimated using naive power counting.

This thesis is structured as follows: Ch. 2 presents the basics of Quantum Chromodynamics. Whereas Sec. 2.1 is concerned with the continuum theory and chiral symmetry, Sec. 2.2 focuses on the lattice formulation of QCD and introduces, amongst other things, the excited states contamination of lattice correlation functions. In Sec. 2.3, Heavy Quark Effective Theory is introduced before Sec. 2.4 gives an overview of the weak interaction processes for which the calculations of the later chapters are relevant. Ch. 3 gives an overview of Chiral Perturbation Theory and Heavy Meson ChPT. In Ch. 4, the interpolating fields for heavy-light B mesons are derived. Using those, the excited states contaminations of the B meson two-point function, the B meson mass, and the B meson decay constant are computed. The influence of excited states on the pion and kaon two-point functions is also investigated. Ch. 5 is concerned with the excited states contamination of B meson matrix elements. First, the matrix element is considered from which g, the sole low energy constant of the HM ChPT Lagranigan in the chiral and static limit, is extracted. This is followd by a discussion of the $B \to \pi$ vector form factors, which are relevant for the determination of V_{ub} from semileptonic B decays. Finally, hadronic matrix elements relevant for B^0-$\bar{B}^0$ oscillations are considered. Strategies for the determination of yet unknown LECs are also presented where applicable. Final conclusions are drawn in Ch. 6.

2. Quantum Chromodynamics in the Continuum and on a Lattice

2.1. Basics of Quantum Chromodynamics

Quantum Chromodynamics is a Quantum Field Theory (QFT) describing the interaction of quarks and gluons, known as the strong interaction. It is responsible for the formation of mesons, baryons, and other quark bound states collectively denoted as hadrons, and also plays a role in the binding of protons and neutrons in atomic nuclei.

QCD is a Yang-Mills theory [40] coupled minimally to fermions transforming in the fundamental and anti-fundamental representation of the gauge group. The group is the non-abelian Lie group $\mathrm{SU}(3)_\mathrm{C}$, where C stands for colour, and the fermions can have the colour charges 'red', 'green', and 'blue' whereas the anti-quarks carry anti-colour charges. The fermions are called quarks and come in six different species, often referred to as flavours. They are grouped into up-type quarks $U_i = (u, c, t)$ and down-type quarks $D_i = (d, s, b)$, depending on whether their electric charge is the same as the charge of the up quark ($Q_u = 2/3\, e$) or the down quark ($Q_d = -1/3\, e$).

The QCD Lagrangian in Euclidean spacetime is given by

$$\mathcal{L}_\mathrm{QCD} = -\frac{1}{4g_\mathrm{s}^2} G^a_{\mu\nu} G^a_{\mu\nu} + \sum_f \bar{q}_f (\not{D} + m_f) q_f \,, \tag{2.1}$$

with the field strength tensor,

$$G^a_{\mu\nu} = \partial_\mu A^a_\nu - \partial_\nu A^a_\mu + f^{abc} A^b_\mu A^c_\nu \,, \tag{2.2}$$

of the gauge fields, the gluons A^a_μ, and the covariant derivative is defined as

$$D_\mu = \partial_\mu - \mathrm{i} A^a_\mu T^a \,. \tag{2.3}$$

Here and in the following, the Einstein summation convention is used in which a summation over twice appearing indices is implied. $\not{D}$ is short for $D_\mu \gamma_\mu$ with the gamma matrices γ_μ which form a representation of the Euclidean Clifford algebra in four dimensions. The T^a are the generators of $\mathrm{SU}(3)_\mathrm{C}$ which can be defined to be one half of the Gell-Mann matrices λ^a. They then fulfil the relation

$$\mathrm{Tr}\left[T^a T^b\right] = \frac{\delta^{ab}}{2} \,. \tag{2.4}$$

In the Standard Model of particle physics, the fermion masses m_f are generated by the Higgs mechanism [3–5]: the quarks are coupled via a Yukawa coupling to the Higgs field which acquires a vacuum expectation value after spontaneous electroweak symmetry breaking. This generates mass terms for the quarks and interaction terms with the Higgs boson which both depend on the strength of the Yukawa couplings. In pure QCD, the quarks are vector-like and an explicit mass term is allowed.

The remaining constant in the QCD Lagrangian (2.1) is the strong coupling constant g_s. It describes the interaction strength between the quarks and the gauge field of the theory. This can be seen by rescaling

$$A^a_\mu \to g_\mathrm{s} A^a_\mu \tag{2.5}$$

to obtain the standard form of the Lagrangian.

The form of the terms in the Lagrangian is dictated by two principles: renormalisability and the symmetries of the theory. The concept of renormalisation will be introduced below, for now it suffices to say that a theory is renormalisable if all observables computed from it can be made finite after adjusting a finite number of counterterms. On the other hand, all terms which are not invariant under the symmetries of the theory cannot be part of the Lagrangian. For QCD, the most relevant symmetries are Poincaré symmetry and the $\mathrm{SU}(3)_\mathrm{C}$ gauge symmetry.

In principle, one can add another term to the Lagrangian which violates CP symmetry, the combination of charge conjugation and parity,

$$\Delta\mathcal{L} = \frac{\theta}{64\pi^2}\varepsilon_{\mu\nu\rho\sigma}G^a_{\mu\nu}G^a_{\rho\sigma}\,, \tag{2.6}$$

but experiments put tight constraints on the parameter θ. A non-zero neutron electric dipole moment d_N for example would be explained by a non-zero value for this so-called vacuum angle, but experiments show that it is very small and compatible with zero [41, 42]. As a consequence, one has the bound $|\theta| \leq 10^{-10}$ [6] and for this reason this additional contribution to the Lagrangian will be neglected in the following.

Upon closer inspection, it turns out that the theory as is is ill-defined: When computing observables in perturbation theory using the QCD Lagrangian, one would sooner or later be confronted with divergent integrals and thus infinite results which is in contradiction with the finite values measured in experiments. This apparent paradox is resolved by observing that all parameters (and also the fields themselves) receive quantum corrections so that the values of the so-called bare parameters of the Lagrangian have no physical relevance. Instead, one *renormalises* the theory by adjusting the n bare parameters so that n observables assume their physical value. To do so, one first has to *regularise* the divergences. The most used regularisation scheme in perturbation theory is dimensional regularisation [43, 44] in which integrals are evaluated in $d = 4 - 2\varepsilon$ dimensions and divergences then appear as poles in ε. The bare parameters of the Lagrangian as well as other renormalisation constants from e.g. local composite operators[1] are then adjusted in the result of the n chosen observables so that all poles cancel and the remaining finite values match experiments after removing the regulator. This is normally written as an equation relating bare and renormalised parameters via renormalisation constants Z_i

$$\bar{g}_\mathrm{s} = Z_g(\varepsilon, \bar{g}_\mathrm{s})\, g_\mathrm{s}\,, \qquad \bar{m}_f = Z_m(\varepsilon, \bar{g}_\mathrm{s})\, m_f\,. \tag{2.7}$$

The regularisation in the computed result for the observable can be removed by taking $\varepsilon \to 0$ and the theory is renormalised up to the given order in perturbation theory in $\bar{g}_\mathrm{s}$ to which the n observables have been computed. It should be noted that different renormalisation schemes exist which all lead to the same result for the observables. They differ by how the constants Z_i are chosen, e.g. without a dependence on the quark masses as presented here. The same procedure can also be used with other regularisation schemes such as a discretisation of spacetime or Pauli-Villars regularisation [46].

All regularisation schemes have one thing in common: they introduce a dimensionful scale μ. In dimensional regularisation this scale is introduced to keep the mass dimension of integrals and parameters constant when switching from 4 to d dimensions. Depending on the

[1] Local composite operators are products of field operators at a single spacetime point, e.g. the quark vector current $\bar{q}_1(x)\gamma_\mu q_2(x)$. Products of operators defined at the same spacetime point need special treatment, the renormalisation involves mixing with operators of the same and lower mass dimension, see e.g. [45] for more information.

renormalisation scheme used, the renormalised parameters of the theory become functions of this energy scale.[2] For example, the renormalised coupling $\bar{g}_\mathrm{s}$ of QCD varies as a function of the energy scale μ. This is encoded in the β function, which is defined as

$$\beta(\bar{g}_\mathrm{s}) = \mu \frac{\mathrm{d}\bar{g}_\mathrm{s}}{\mathrm{d}\mu} = -b_0 \bar{g}_\mathrm{s}^3 - b_1 \bar{g}_\mathrm{s}^5 + \mathcal{O}(\bar{g}_\mathrm{s}^7)\,. \tag{2.8}$$

The first two coefficients b_0 and b_1 of the perturbative expansion do not depend on the chosen renormalisation scheme, but higher order coefficients do. The QCD β function shows a qualitatively different behaviour compared to its analogue in Quantum Electrodynamics (QED): whereas the latter has a positive β function, it is negative in QCD [9, 10]. This implies that the coupling strength decreases as μ is increased. Since one chooses μ to be of the order of the typical energy E of the physical process one wants to describe,[3] this means that $\bar{g}_\mathrm{s}$ decreases as a function of this energy. This behaviour is known as *asymptotic freedom*, since for large energies the coupling goes to zero and one recovers a free field theory. On the other hand, the value of $\bar{g}_\mathrm{s}$ increases for decreasing energy scales and is responsible for confinement: the coupling between quarks becomes so strong that they have to form colour-singlet bound states, the hadrons. A perturbative description of the theory is not possible and one has to take advantage of nonperturbative tools e.g. lattice simulations. Lattice field theory is a regularisation scheme in which the inverse of the small lattice spacing a defines an ultraviolet cutoff of the theory. An introduction to lattice QCD will be given in Sec. 2.2.

At first sight, it seems like physical observables which necessarily depend on the parameters of the theory are functions of the renormalisation scale μ. But this scale is arbitrary and should thus not affect anything that can be measured in experiments. It turns out that the scale dependence can be eliminated, which can be concluded from the renormalisation group equations: the starting point is that any renormalised physical observable O does not depend on the scale μ, so they have to satisfy the Callan-Symanzik equations [47, 48]

$$0 = \mu \frac{\mathrm{d}O}{\mathrm{d}\mu} = \left(\mu \frac{\partial}{\partial \mu} + \beta(\bar{g}_\mathrm{s}) \frac{\partial}{\partial \bar{g}_\mathrm{s}} + \tau(\bar{g}_\mathrm{s}) \bar{m}_f \frac{\partial}{\partial \bar{m}_f} \right) O\,, \tag{2.9}$$

where a sum over the renormalised quark masses $\bar{m}_f$ is implied and a dependence on kinematical variables is suppressed. The anomalous dimension of the quark masses is defined as

$$\tau(\bar{g}_\mathrm{s}) = \frac{\mu}{\bar{m}_f} \frac{\mathrm{d}\bar{m}_f}{\mathrm{d}\mu}\,, \qquad \tau(\bar{g}_\mathrm{s}) = -d_0 \bar{g}_\mathrm{s}^2 + \mathcal{O}(\bar{g}_\mathrm{s}^4)\,. \tag{2.10}$$

The coefficients of τ depend on the renormalisation scheme, except for the leading order coefficient d_0. Every function satisfying Eq. (2.9) is called a Renormalisation Group Invariant (RGI).

Since O does not depend on the renormalisation scale μ, it should be possible to eliminate the μ-dependent renormalised gauge coupling and quark masses. To do so, one defines the following special solutions to the renormalisation group equations, $\Lambda(\mu, \bar{g}_\mathrm{s})$ and $M_i(\bar{g}_\mathrm{s}, \bar{m}_i)$ which depends on only a single quark mass $\bar{m}_i$, which satisfy

$$\left(\mu \frac{\partial}{\partial \mu} + \beta(\bar{g}_\mathrm{s}) \frac{\partial}{\partial \bar{g}_\mathrm{s}} \right) \Lambda = 0\,, \qquad \left(\beta(\bar{g}_\mathrm{s}) \frac{\partial}{\partial \bar{g}_\mathrm{s}} + \tau(\bar{g}_\mathrm{s}) \bar{m}_i \frac{\partial}{\partial \bar{m}_i} \right) M_i = 0\,. \tag{2.11}$$

[2] This dependence is most of the time kept implicit in the following. If a parameter can be measured directly in experiments, one can choose a scheme in which it is truly a constant, e.g. the elementary charge e and electron mass m_e in the on-shell scheme.

[3] The perturbative expansion can contain terms proportional to powers of $\log(E/\mu)$. These need to be kept under control by choosing E/μ close to unity.

The solutions to these equations are given by

$$\Lambda = \mu \left(b_0 \bar{g}_\mathrm{s}^2\right)^{-\frac{b_1}{2b_0^2}} e^{-\frac{1}{2b_0\bar{g}_\mathrm{s}^2}} \exp\left(-\int_0^{\bar{g}_\mathrm{s}} \mathrm{d}x \left[\frac{1}{\beta(x)} + \frac{1}{b_0 x^3} - \frac{b_1}{b_0^2 x}\right]\right) , \tag{2.12}$$

$$M_i = \bar{m}_i \left(2b_0 \bar{g}_\mathrm{s}^2\right)^{-\frac{d_0}{2b_0}} \exp\left(-\int_0^{\bar{g}_\mathrm{s}} \mathrm{d}x \left[\frac{\tau(x)}{\beta(x)} - \frac{d_0}{b_0 x}\right]\right) . \tag{2.13}$$

The first equation relates the renormalised, dimensionless coupling $\bar{g}_\mathrm{s}$ to a constant Λ of mass dimension one. This is known as dimensional transmutation and signals that QCD dynamically generates an additional energy scale through quantum effects. At least perturbatively, one can invert the equation and thus replace $\bar{g}_\mathrm{s}$ by a function of Λ. The second equation can be used to eliminate $\bar{m}_i$ in favour of the constant M_i. These are the fundamental constant parameters of QCD and every observable can be expressed as functions of only them and kinematical variables. Λ still depends on the renormalisation scheme chosen, whereas the masses M_i do not.

But it is not only possible to find the renormalisation group invariant parameters of a theory, but one can also define RGI local composite operators such as currents. This will become relevant in Sec. 2.3.1 and other parts of this thesis where correlation functions of currents and interpolating fields for quark bilinears are considered. By definition, an RGI operator is an operator whose matrix elements do not depend on the renormalisation scale μ. In order to define them, one needs the anomalous dimension of the operator which comes about in the following way: a bare current J_ν is related to the renormalised current $J_{\mathrm{R},\nu}$ via a renormalisation constant Z_J

$$J_\nu = Z_J(\varepsilon, \bar{g}_\mathrm{s})\, J_{\mathrm{R},\nu} \,. \tag{2.14}$$

This is a simplification: in general, a composite operator can mix under renormalisation with operators of the same or (in massive theories) lower mass dimension and the same quantum numbers. The renormalisation constant Z is then a matrix, but this complication is not needed here. Since the arbitrary scale μ is only introduced by the regularisation procedure, the bare current does not depend on it. One thus has

$$0 = \mu \frac{\mathrm{d}J_\nu}{\mathrm{d}\mu} = \mu \frac{\mathrm{d}Z_J}{\mathrm{d}\mu} J_{\mathrm{R},\nu} + \mu Z_J \frac{\mathrm{d}J_{\mathrm{R},\nu}}{\mathrm{d}\mu} \tag{2.15}$$

From this, one then defines the anomalous dimension γ_J to satisfy

$$\gamma_J J_{\mathrm{R},\nu} = \mu \frac{\mathrm{d}J_{\mathrm{R},\nu}}{\mathrm{d}\mu} = -\frac{\mu}{Z_J} \frac{\mathrm{d}Z_J}{\mathrm{d}\mu} J_{\mathrm{R},\nu} \,, \tag{2.16}$$

and its perturbative expansion reads

$$\gamma_J = -\gamma_J^{(0)}\, \bar{g}_\mathrm{s}^2 + \mathcal{O}(\bar{g}_\mathrm{s}^4) \,. \tag{2.17}$$

$\gamma_J^{(0)}$ is independent of the renormalisation scheme, but higher order coefficients are not. It can be seen from Eq. (2.16) that the derivative of the renormalised current J_R w.r.t. the scale μ is not zero, but proportional to the anomalous dimension. It follows that the renormalised current does not satisfy Eq. (2.9), the differential equation of a renormalisation group invariant. This can be remedied by defining the RGI product

$$J_{\mathrm{RGI},\nu} = \varphi_J J_{\mathrm{R},\nu} \,. \tag{2.18}$$

where the function φ_J is independent of the masses, has no explicit dependence on μ, and is a solution to the equation

$$\left(\beta\frac{\partial}{\partial\bar{g}_\mathrm{s}}+\gamma_J\right)\varphi_J=0\,. \tag{2.19}$$

A suitably normalised solution reads

$$\varphi_J=(2b_0\bar{g}_\mathrm{s}^2)^{-\frac{\gamma_0^J}{2b_0}}\exp\left(-\int\limits_0^{\bar{g}_\mathrm{s}}\mathrm{d}x\,\left[\frac{\gamma_J(x)}{\beta(x)}-\frac{\gamma_0^J}{b_0x}\right]\right)\,. \tag{2.20}$$

The so defined current $J_{\mathrm{RGI},\nu}$ does not depend on μ and also not on the chosen renormalisation scheme.

Time-ordered products of these currents and other local (composite) operators can be inserted between vacuum states to form correlation functions. These can be used to extract e.g. S matrix elements of an operator between asymptotic in- and out states. An especially useful result is that these correlation functions can be expressed as a path integral:

$$\langle\mathcal{T}\{\mathcal{O}_1(x_1)\cdots\mathcal{O}_n(x_n)\}\rangle=\frac{1}{\mathcal{Z}}\int\mathcal{D}\left[\Phi\right]\,e^{-S[\Phi]}\mathcal{O}_1[\Phi(x_1)]\cdots\mathcal{O}_n[\Phi(x_n)]\,, \tag{2.21}$$

$$\mathcal{Z}=\int\mathcal{D}\left[\Phi\right]\,e^{-S[\Phi]}\,. \tag{2.22}$$

Here, Φ denotes the collection of all fields of the theory and S is the action which is defined as the spacetime integral of the Lagrangian. $\mathcal{T}$ denotes the time-ordering operator which orders the operators in descending order according to their times t_i and includes appropriate sign factors if fermionic operators have to be swapped. This operator will be suppressed in the following. The Hilbert space operators on the l.h.s. of the equation turn into functionals of the fields on the r.h.s. and are integrated over all field configurations. This representation of correlators is used in lattice field theory as will be explained in Sec. 2.2.

2.1.1. Chiral Symmetry

Global symmetries are integral ingredients of the Standard Model: as long as the symmetries are not spontaneously broken, particles transform in irreducible representations of symmetry groups and they thus shape the particle spectrum. In QCD, there is an important global, approximate symmetry which is known as chiral symmetry. An approximate symmetry is a symmetry which is broken explicitly by a term in the Lagrangian which is not invariant under the symmetry transformation and is proportional to a 'small' parameter. If this parameter has mass dimension one, like the mass of a particle, this means that it should be small compared to the relevant energy scale of the theory as will be explained later. This approximate symmetry of QCD is the basis for Chiral Perturbation Theory, an Effective Field Theory (EFT) for QCD at low energies, which will be described in detail in Ch. 3. A comprehensive overview of this topic can be found in [49], a summary of the most relevant points is presented in this section.

Chiral symmetry is based on the concept of chirality, i.e. left- and right-handed particles. These particles transform in distinct representations of the Lorentz group: the $\left(\frac{1}{2},0\right)$ and $\left(0,\frac{1}{2}\right)$ representation, respectively. In four spacetime dimensions, they are represented by two-component spinors. The quarks of QCD are usually defined to be Dirac fermions which transform as the direct sum of a left- and right-handed Weyl spinor, i.e. $\left(\frac{1}{2},0\right)\oplus\left(0,\frac{1}{2}\right)$, and are represented by four-component spinors. In order to project to particles with definite chirality, one can use the projectors

$$P_\mathrm{L}=\frac{1}{2}\left(\mathbb{1}-\gamma^5\right)\,,\qquad P_\mathrm{R}=\frac{1}{2}\left(\mathbb{1}+\gamma^5\right)\,. \tag{2.23}$$

As the subscript suggests, the effect of acting with P_L (P_R) on a Dirac spinor is to only retain the part which transforms as a left-handed (right-handed) particle. In equations

$$P_\mathrm{L}\Psi = \Psi_\mathrm{L}\,, \qquad\qquad P_\mathrm{R}\Psi = \Psi_\mathrm{R}\,. \tag{2.24}$$

Setting all quark masses in the QCD Lagrangian with for now n_f flavours to zero, it is readily shown that quarks of different chirality do not interact:[4]

$$\mathcal{L}_{m_f=0} = -\frac{1}{4g_\mathrm{s}^2}G^a_{\mu\nu}G^a_{\mu\nu} + \sum_{f=1}^{n_f}\left(\bar{q}_{f,\mathrm{L}}\not{D}q_{f,\mathrm{L}} + \bar{q}_{f,\mathrm{R}}\not{D}q_{f,\mathrm{R}}\right)\,. \tag{2.25}$$

As long as one does not include electroweak interactions, the n_f left-handed quarks are now indistinguishable and the same is true for the right-handed fields. Neglecting the masses of the lightest quarks, u, d, and to some degree s, is a very good approximation since their RGI masses are small compared to the proton mass of nearly 1 GeV which can be taken as the typical QCD scale. In the classical theory, a rotation of the left-handed particles by a generic constant $\mathrm{U}(n_f)_\mathrm{L}$ matrix, and the right-handed particles by a different $\mathrm{U}(n_f)_\mathrm{R}$ matrix then leaves the Lagrangian invariant. Factoring the U(1) elements one ends up with the symmetry group $\mathrm{SU}(n_f)_\mathrm{L}\times\mathrm{SU}(n_f)_\mathrm{R}\times\mathrm{U}(1)_\mathrm{L}\times\mathrm{U}(1)_\mathrm{R}$. The transformation of the quarks under this symmetry group is given by

$$q_\mathrm{L} \to e^{-\mathrm{i}\theta_L}e^{-\mathrm{i}\theta^a_L T^a_\mathrm{L}}\,q_\mathrm{L}\,, \qquad\qquad \bar{q}_\mathrm{L} \to \bar{q}_\mathrm{L}e^{\mathrm{i}\theta^a_L T^a_\mathrm{L}}e^{\mathrm{i}\theta_L}\,, \tag{2.26}$$

$$q_\mathrm{R} \to e^{-\mathrm{i}\theta_R}e^{-\mathrm{i}\theta^a_R T^a_\mathrm{R}}\,q_\mathrm{R}\,, \qquad\qquad \bar{q}_\mathrm{R} \to \bar{q}_\mathrm{R}e^{\mathrm{i}\theta^a_R T^a_\mathrm{R}}e^{\mathrm{i}\theta_R}\,. \tag{2.27}$$

Here, T^a_L (T^a_R) are the hermitian and traceless generators of $\mathrm{SU}(n_f)_\mathrm{L}$ ($\mathrm{SU}(n_f)_\mathrm{R}$) and the qs and $\bar{q}$s are n_f component vectors in flavour space. It is convenient to redefine the U(1) transformations: 'vector' transformations $\mathrm{U}(1)_\mathrm{V}$ are defined by setting $\theta_\mathrm{L} = \theta_\mathrm{R}$, and 'axial vector' transformations $\mathrm{U}(1)_\mathrm{A}$ are defined by $\theta_\mathrm{L} = -\theta_\mathrm{R}$. Note that explicit, non-degenerate mass terms for the quarks would break the symmetry completely except for the $\mathrm{U}(1)_\mathrm{V}$ symmetry. This symmetry is known to be responsible for baryon number conservation. As usual, one can derive conserved currents and conserved charges using Noether's theorem. It is common to write them in the following form

$$V^a_\mu = R^a_\mu + L^a_\mu = \bar{q}\gamma_\mu T^a q\,, \tag{2.28}$$

$$A^a_\mu = R^a_\mu - L^a_\mu = \bar{q}\gamma_\mu\gamma_5 T^a q\,, \tag{2.29}$$

$$V_\mu = R_\mu + L_\mu = \bar{q}\gamma_\mu q\,, \tag{2.30}$$

$$A_\mu = R_\mu - L_\mu = \bar{q}\gamma_\mu\gamma_5 q\,. \tag{2.31}$$

V^a_μ and A^a_μ are the isovector vector and axial vector currents, respectively. T^a stands for the generators of the $SU(n_f)$ flavour group, which are e.g. given by $T^a = \sigma^a/2$ for $n_f = 2$ and $T^a = \lambda^a/2$ for $n_f = 3$ with the Pauli (σ^a) and Gell-Mann (λ^a) matrices, respectively. Since the currents are conserved, their divergences vanish. This is not true for the isoscalar, i.e. U(1), axial current A_μ in the quantum theory since $\mathrm{U}(1)_\mathrm{A}$ transformations do not leave the path integral measure invariant. Instead, one finds for its divergence [50–52]

$$\partial_\mu A_\mu = \frac{3g_\mathrm{s}^2}{32\pi^2}\varepsilon_{\mu\nu\rho\sigma}G_{a,\mu\nu}G_{a,\rho\sigma}\,. \tag{2.32}$$

The term on the right-hand side is related to the topological charge. The two U(1) symmetries will not be of interest in the following and will be ignored from now on.

[4] Note that the following considerations are naive in the sense that they are solely based on the QCD Lagrangian and do not include the effects of a regularisation scheme.

The conservation of axial and vector currents has an interesting implication for the particle spectrum (this line of argument follows [49]): since the conserved charges

$$Q_{\mathrm{V}}^a = \int \mathrm{d}^3\vec{x}\, V_0^a(\vec{x},t)\,, \qquad Q_{\mathrm{A}}^a = \int \mathrm{d}^3\vec{x}\, A_0^a(\vec{x},t)\,, \tag{2.33}$$

commute with the Hamiltonian, one can show that the three states

$$|\psi\rangle\ , \qquad Q_{\mathrm{V}}^a\,|\psi\rangle\ , \qquad Q_{\mathrm{A}}^a\,|\psi\rangle \tag{2.34}$$

all have the same energy. If the state $|\psi\rangle$ is chosen to be a positive parity eigenstate, one would expect mass degenerate states of opposite parity. The reason is that Q_{A}^a changes sign under a parity transformation since its definition involves the time component of an axial vector, whereas Q_{V}^a does not. This means that $Q_{\mathrm{A}}^a\,|\psi\rangle$ is a negative parity eigenstate which is mass degenerate with the two positive parity states $|\psi\rangle$ and $Q_{\mathrm{V}}^a\,|\psi\rangle$. But this is not observed in experiments: there are no partners of opposite parity and equal or similar masses for the pions or the proton which are all bound states of the lightest quarks. A possible way out of this apparent contradiction is the postulate that the symmetry is *spontaneously broken* by the ground state of the theory. In other words, the Lagrangian is invariant under the full symmetry group, but the ground state is not and is rather transformed into another degenerate state by some of the symmetry transformations. A consequence of the spontaneous breaking of a global symmetry is the appearance of massless spin 0 particles in the spectrum of the theory. This result is known as Goldstone's theorem [53–55] and the massless particles are called Goldstone bosons. In general, if the Lagrangian is invariant under a group G with N generators, but the ground state is only left invariant by a subgroup H of G with M generators, then the spectrum will contain $N-M$ (the number of 'broken generators') Goldstone bosons.

In order to apply these considerations to the chiral theory discussed above, one first needs to establish which subgroup of the symmetry is spontaneously broken. The Vafa-Witten theorem [56] forbids the spontaneous breaking of vector symmetries in vector-like gauge theories without a vacuum θ-angle. This only leaves the axial symmetry transformations and implies that they do not leave the vacuum state invariant. According to Goldstone's theorem, there needs to be at least one non-vanishing vacuum expectation value for the commutator of the axial charge and a second operator $\mathcal{O}$ in order for this to be true.

$$\langle 0|[Q_{\mathrm{A}}^a,\mathcal{O}]|0\rangle = \langle 0|Q_{\mathrm{A}}^a\mathcal{O}|0\rangle - \langle 0|\mathcal{O}Q_{\mathrm{A}}^a|0\rangle \neq 0 \tag{2.35}$$

Inserting a complete set of states between Q_{A}^a and $\mathcal{O}$ and demanding that the expression does not vanish implies that $\mathcal{O}$ should have the same quantum numbers as Q_{A}^a in order to have a non-zero overlap with the same states $|\pi^a\rangle$ as the axial charge (it is assumed that the vacuum expectation value of the operators are zero). These states are the Goldstone modes of the spontaneously broken symmetry. In QCD, the pseudoscalar density

$$P^a = \bar{q}\gamma_5 T^a q \tag{2.36}$$

satisfies these requirements. Working with the lightest three flavours of QCD for the moment and setting their masses to zero, an explicit calculation yields (see [49] for more information)

$$\left\langle 0\middle|\left[Q_{\mathrm{A}}^a, P^b\right]\middle|0\right\rangle = \delta^{ab}(c_u^a\,\langle 0|\bar{u}u|0\rangle + c_d^a\langle 0|\bar{d}d|0\rangle + c_s^a\,\langle 0|\bar{s}s|0\rangle) \tag{2.37}$$

with some constants c_i^a which are not all zero at the same time and no sum over a is implied. On the other hand, the conserved vector symmetry $\mathrm{SU}(3)_{\mathrm{V}}$ implies

$$\langle 0|\bar{u}u|0\rangle = \langle 0|\bar{d}d|0\rangle = \langle 0|\bar{s}s|0\rangle = \frac{1}{3}\,\langle 0|\bar{q}q|0\rangle\ . \tag{2.38}$$

This means a non-zero quark condensate is a sufficient condition for chiral symmetry breaking and serves as an order parameter. Starting with [57], lattice simulations have confirmed a non-zero chiral condensate.

The axial charge is given by an integral over the time component of the axial current and has a non-zero overlap with the Goldstone boson states. Making use of Lorentz-invariance, the matrix element is parametrised as

$$\left\langle 0 \middle| A^a_\mu(x) \middle| \pi^b(p) \right\rangle = \delta^{ab} \mathrm{i} f p_\mu e^{-\mathrm{i}px} \,. \tag{2.39}$$

These states are identified with the pions, kaons, and the eta meson of QCD since they are the lightest states of the theory with the correct quantum numbers. The non-zero masses measured in experiments for these particles are due to the non-zero masses of the quarks which break the chiral symmetry explicitly, see Sec. 3.1 for an EFT explanation of the quark mass dependence of the pion masses. The free parameter f in the above equation is the pion decay constant in the chiral limit, i.e. for vanishing quark masses.

The bottom line of the preceding discussion is: for massless quarks, despite the Lagrangian being invariant under the full global symmetry group $\mathrm{SU}(n_f)_\mathrm{L}\times\mathrm{SU}(n_f)_\mathrm{R}$, the ground state is only invariant under the vector group $\mathrm{SU}(n_f)_\mathrm{V}$ for which the transformation matrices of the two groups coincide: $L = R$. On the other hand, one often defines axial transformations as $R = L^\dagger$, but one should keep in mind that these transformations do not form a group since an axial transformation transforms the axial vector current into a vector current:

$$\left[Q^a_\mathrm{A}, A^b_\mu(t,\vec{y}) \right] = \mathrm{i} f^{abc} V^c_\mu(t,\vec{y}) \,. \tag{2.40}$$

This equation is one of the so-called current algebra relations [58, 59] which relate the commutators of the currents with themselves. These relations are important since they fix the renormalisation constants of the currents: as long as the vector current is a conserved current which does not need to be renormalised, the above relation fixes the renormalisation constant of the axial vector current to be also 1. Chiral symmetry also forces the renormalisation constants of the isovector scalar and pseudoscalar density to be the same.

The chiral symmetry of QCD also leads to chiral Ward identities. In general, Ward identities are equations which relate several (not necessarily on-shell) Green's functions. They were first discovered and used in QED [60, 61] to derive the equivalence of the vertex renormalisation factor and the electron wave function renormalisation constant. A generalisation of the identities to non-abelian gauge theories was later given [62–64], these identities are known as Slavnov-Taylor identities. Ward identities can also be derived for global symmetries such as the chiral symmetry of QCD. One way of doing this is to consider the variation of the path integral representation of a correlation function under an infinitesimal *local* symmetry transformation as it is e.g. done in [65]. Infinitesimal isovector transformations can be obtained from the full transformations given in Eqs. (2.26) and (2.27) by a leading order expansion in θ^a_L and θ^a_R:

$$\delta q_\mathrm{L} = -\mathrm{i}\theta^a_\mathrm{L} T^a_\mathrm{L} q_\mathrm{L} \,, \qquad \delta \bar{q}_\mathrm{L} = \mathrm{i}\theta^a_\mathrm{L} \bar{q}_\mathrm{L} T^a_\mathrm{L} \,, \tag{2.41}$$

and likewise for the right-handed quarks. The variation of the path integral vacuum expectation value of an operator $\mathcal{O}$ under an infinitesimal transformation is given by (assuming that the path integral measure is invariant under the transformation)

$$\begin{aligned} 0 &= \frac{1}{\mathcal{Z}} \delta \left[\int \mathcal{D}[F]\, e^{-S_\mathrm{QCD}[F]} \mathcal{O}[F] \right] = \frac{1}{\mathcal{Z}} \int \mathcal{D}[F]\, e^{-S_\mathrm{QCD}[F]} (\delta\mathcal{O}[F] - \mathcal{O}[F]\delta S_\mathrm{QCD}[F]) \,, \\ &\Rightarrow \langle \delta\mathcal{O} \rangle = \langle \mathcal{O}\delta S_\mathrm{QCD} \rangle \,. \end{aligned} \tag{2.42}$$

Here F represents all fields of the QCD action. With this formula, one can for example (in the presence of a quark mass term) derive the so-called partially conserved axial current (PCAC) relation: the starting point is the definition of an infinitesimal local axial transformation

$$\delta q \to \mathrm{i}\theta^a(x)T^a\gamma_5 q\,, \qquad \delta\bar{q} \to \mathrm{i}\theta^a(x)\bar{q}\gamma_5 T^a\,. \tag{2.43}$$

Inserting projectors on left- and right-handed particles shows that this is indeed the infinitesimal form of axial transformations which require $R = L^\dagger$. For this transformation, the variation of the QCD action with mass terms is given by

$$\delta S_{\mathrm{QCD}} = \mathrm{i}\int \mathrm{d}^4x\,\theta^a(x)\left(-\partial_\mu A^a_\mu + \bar{q}\gamma_5[T^a, M_q]_+\,q\right)\,, \tag{2.44}$$

where $[\cdot,\cdot]_+$ denotes the anticommutator. The quark mass matrix M_q is a diagonal matrix in flavour space. So far θ^a is arbitrary, but it is convenient to require that it is non-zero in a fixed region of spacetime and zero outside of it. If at the same time the operator $\mathcal{O}$ is restricted to a second region in spacetime which does not overlap with the region in which θ^a is non-zero, i.e. in which the chiral symmetry transformation is performed, the l.h.s. of Eq. (2.42) vanishes (otherwise contact terms would enter the result). Since θ^a is still arbitrary inside the region in which it is non-zero, one can eliminate it and the integral over x from the equation. Taking a suitable linear combination of the result so that one obtains an axial current of the form $A^{f_1f_2}_\mu = \bar{q}_{f_1}\gamma_\mu\gamma_5 q_{f_2}$, one arrives at the PCAC relation

$$\left\langle \partial_\mu A^{f_1f_2}_\mu(x)\mathcal{O}(y)\right\rangle = (m_{f_1} + m_{f_2})\left\langle P^{f_1f_2}(x)\mathcal{O}(y)\right\rangle\,, \qquad x \neq y\,. \tag{2.45}$$

The current algebra relations mentioned earlier can be derived from integrated chiral Ward identities, see e.g. [66].

There is another way of deriving the chiral Ward identities which was found by Bell [67]: it relies on external fields which have a nontrivial transformation under chiral symmetry and are coupled to the quark fields in the *massless* QCD Lagrangian in such a way that it is invariant under *local* chiral transformations. These fields are $l_\mu = l^a_\mu T^a$, $r_\mu = r^a_\mu T^a$, $s = s^0\mathbb{1} + s^aT^a$, and $p = p^0\mathbb{1} + p^aT^a$, and their chiral transformations are given by

$$r_\mu \to Rr_\mu R^\dagger + \mathrm{i}R\partial_\mu R^\dagger\,, \tag{2.46}$$

$$l_\mu \to Ll_\mu L^\dagger + \mathrm{i}L\partial_\mu L^\dagger\,, \tag{2.47}$$

$$(s + \mathrm{i}p) \to R(s + \mathrm{i}p)L^\dagger\,, \tag{2.48}$$

$$(s - \mathrm{i}p) \to L(s - \mathrm{i}p)R^\dagger\,. \tag{2.49}$$

External isoscalar vector and axial vector currents were dropped here since they do not play a role in the following. It is then easy to show that e.g. the combination

$$\bar{q}_{\mathrm{L}}\gamma_\mu(D_\mu - \mathrm{i}l_\mu)q_{\mathrm{L}} \tag{2.50}$$

is invariant under a local chiral transformation: the covariant derivative (2.3) produces an additional term when the partial derivative hits the spacetime dependent transformation matrix $L(x)$ of the quark field q_{L}, but this contribution is cancelled by the second term on the r.h.s. of Eq. (2.47). It is useful to define the vector $v_\mu = (r_\mu + l_\mu)/2$ and axial vector $a_\mu = (r_\mu - l_\mu)/2$ external fields in order to write the external field part of the Lagrangian as

$$\mathcal{L}_{\mathrm{ext}} = -\mathrm{i}\bar{q}\gamma_\mu\left(v_\mu + \gamma_5 a_\mu\right)q + \bar{q}(s - \mathrm{i}\gamma_5 p)q\,. \tag{2.51}$$

The Lagrangian $\mathcal{L} = \mathcal{L}_{\mathrm{QCD}} + \mathcal{L}_{\mathrm{ext}}$ is then invariant under local chiral transformations. Remember that $\mathcal{L}_{\mathrm{QCD}}$ here and in the following denotes the Lagrangian of massless QCD. Before

turning to the chiral Ward identities, it is useful to consider the generating functional in the presence of external fields,

$$\mathcal{Z}[s,p,v_\mu,a_\mu] = \int \mathcal{D}\left[F\right]\, e^{-S_{\mathrm{QCD}}[F]-S_{\mathrm{ext}}[F,s,p,v_\mu,a_\mu]} = \left\langle e^{-S_{\mathrm{ext}}[F,s,p,v_\mu,a_\mu]} \right\rangle . \tag{2.52}$$

As before F denotes quarks and gluons. As can be shown by an explicit computation, it is possible to derive n-point correlation functions of the currents and densities by taking functional derivatives w.r.t. the appropriate external field and setting them to zero afterwards. The two-point function for e.g. the axial vector current can be obtained by computing

$$\frac{1}{\mathcal{Z}} \frac{\delta^2 \mathcal{Z}[s,p,v_\mu,a_\mu]}{\delta a^a_\mu(x)\, \delta a^b_\nu(y)}\bigg|_{s,p,v_\mu,a_\mu=0} = \left\langle A^a_\mu(x) A^b_\nu(y) \right\rangle . \tag{2.53}$$

It is also easy to incorporate a non-zero quark mass: the scalar density can be thought of to be of the form $s = M_q + \tilde{s}$, where M_q is the quark mass matrix and one only sets $\tilde{s}$ to zero at the end. The mass term must then also be included in the normalisation factor $1/\mathcal{Z}$, which otherwise does not depend on the external fields.

The generating functional with external fields is also the starting point for deriving chiral Ward identities. Computing an infinitesimal isovector chiral transformation of the external fields, one has

$$0 = \frac{1}{\mathcal{Z}}\, \delta \left[\int \mathcal{D}\left[F\right]\, e^{-S_{\mathrm{QCD}}[F]-S_{\mathrm{ext}}[F,s,p,v_\mu,a_\mu]} \right] = - \left\langle e^{-S_{\mathrm{ext}}[F,s,p,v_\mu,a_\mu]} \delta S_{\mathrm{ext}}[F,s,p,v_\mu,a_\mu] \right\rangle . \tag{2.54}$$

Chiral Ward identities follow from the variation of the external fields alone, the quarks are *not* transformed. The reason is the following: it has already been stated above (and shown in one case) that chiral Ward identities can be derived by considering infinitesimal, local chiral transformations of the QCD path integral. This is still true when considering the generating functional which includes the external fields as long as these are *not* transformed and set to zero afterwards (or $s = M_q$ since S_{QCD} is the QCD action for massless quarks). Transforming both, the quark fields and the external fields, leaves the combined action invariant, this means that the transformation of the external fields is the negative of the transformation of the quark fields. As a consequence, transformations of the external fields alone reproduce the chiral Ward identities up to an irrelevant global sign. Note that the above equation still depends on the external fields. Insertion of currents and densities can be obtained by taking derivates w.r.t. these fields and setting them to zero afterwards.

One can easily check that the PCAC relation is reproduced by an axial transformation of the external fields, which is explicitly given by

$$\begin{aligned} \delta v_\mu &= \theta^a(x) f^{abc} a^b_\mu T^c \,, \\ \delta a_\mu &= \theta^a(x) f^{abc} v^b_\mu T^c - \partial_\mu \theta^a(x) T^a \,, \\ \delta(s - \mathrm{i}\gamma_5 p) &= \mathrm{i}\theta^a(x) [s - \mathrm{i}\gamma_5 p, T^a]_+ \gamma_5 \,. \end{aligned} \tag{2.55}$$

With these transformations, δS_{ext} reproduces the r.h.s. of Eq. (2.44) after setting $s = M_q$ and the other external fields to zero.

The external field method is an extremely useful and powerful tool. The invariance of the Lagrangian under local chiral symmetries is enough to derive the correlation functions of the currents and densities as well as the chiral Ward identities. It doesn't make any reference to the degrees of freedom of the theory, it only requires them to have a nontrivial transformation under chiral symmetry in order to couple them to the external fields. This will justify the use of Chiral Perturbation Theory in Ch. 3.

2.2. QCD on a Lattice

Perturbation theory is the best known approach for calculating physical observables in QFTs. The idea is to use the coupling constants g_i as an expansion parameter and compute e.g. cross sections up to a given order in g_i using oftentimes a diagrammatic approach with Feynman diagrams. In the SM, it can be used for QED, electroweak and even to some degree for high-energy QCD processes/corrections. Its validity and accuracy depends on the value of the coupling constants: if they are too large, the higher order corrections can be of the same or even larger size than the Leading Order (LO) result and the convergence of the series is spoiled.[5] Even if the size of consecutive orders in the expansion decreases, the convergence might be too slow to get a reliable result at the order at which a perturbative computation is still feasible. Even more important is that there are inherently non-perturbative observables, such as the mass of the proton. They cannot be computed in perturbation theory and it is thus necessary to take recourse to non-perturbative methods. The most widely used method for QCD is known as lattice QCD and dates back to a publication by Kenneth Wilson [11]. The key idea is the following: instead of considering an infinite volume continuum theory, QCD is evaluated in a finite volume on a Euclidean lattice with spacing a. This lattice spacing serves as an (inverse) cutoff of the theory and thus as an ultraviolet (UV) regulator. On the other hand, an infrared (IR) cutoff is given by the (inverse) length of the finite box in which the simulations are carried out. Correlators can then be computed nonperturbatively in Markov Chain Monte Carlo (MCMC) simulations by solving the path integral as indicated in Eq. (2.22) numerically. In the end, one has to take the infinite volume $L \to \infty$ and continuum limit $a \to 0$ in order to make contact with real world physics. Introductory books on lattice QCD which have been used as a guidance for the following sections are [68–70].

In most lattice simulations one chooses the same number of lattice sites in every of the three spatial dimensions (N_S or N_1, N_2, N_3) and a separate number for the time direction (N_T or N_4). Furthermore, one usually uses hypercubic lattices which means that the spacing a is the same for all directions. The physical spatial (L) and time (T) extent as well as the physical volume are then given by

$$L = aN_\mathrm{S}\,, \tag{2.56}$$

$$T = aN_\mathrm{T}\,, \tag{2.57}$$

$$V = TL^3 = a^4 N_\mathrm{T} N_\mathrm{S}^3\,. \tag{2.58}$$

A point on the lattice is then identified by four numbers (n_1, n_2, n_3, n_4), where n_1, n_2, and n_3 run from 0 to $N_\mathrm{S} - 1$ and n_4 from 0 to $N_\mathrm{T} - 1$. The Fourier space of a finite lattice is itself a finite lattice. Defining $\hat{\mu}$ to be a vector of length a in direction μ, one can impose periodic boundary conditions

$$f(n + N_\mu \hat{\mu}) = f(n)\,. \tag{2.59}$$

The corresponding momenta are then restricted to the first Brillouin zone with smallest momentum $-\pi/a + 2\pi/aN_\mu$ and largest momentum π/a in every direction, and spacing $2\pi/aN_\mu$. There exist other boundary conditions like twisted boundary conditions [71], which would add a complex phase to the left-hand side of the above equation and thus add a constant shift to the momenta. Alternatively one can consider open boundary conditions [72, 73], for which the lattice is not a 4-dimensional torus but has a boundary in the time direction, or the so-called Schrödinger functional [74, 75].

[5] The perturbative series is an asymptotic series and does not converge, but the terminology of 'convergence' is used nonetheless.

A naive discretisation of the free and massless Dirac action amounts to replacing the derivative with a finite difference:

$$\int \mathrm{d}^4x\, \bar{\Psi}(x)\gamma_\mu\partial_\mu\Psi(x) \to a^4 \sum_{n,\mu} \bar{\Psi}(n)\gamma_\mu \frac{\Psi(n+\hat{\mu}) - \Psi(n-\hat{\mu})}{2a} \,. \tag{2.60}$$

This action couples spinors at different points on the lattice, which requires some extra thought if one wants to implement a local symmetry such as the colour symmetry of QCD. A computation of the Dirac propagator in momentum space yields

$$G(p) = -\mathrm{i}a \frac{\sum\limits_\mu \gamma_\mu \sin(p_\mu a)}{\sum\limits_\mu \sin^2(p_\mu a)} \,. \tag{2.61}$$

The propagator has a pole at $p^2 = 0$ as expected for a massless particle, but there are more poles at the edge of the Brillouin zone where at least one of the momentum components has value π/a and the others are 0. There are in total $2^4 = 16$ poles which means there are 16 instead of one propagating fermion. This is known as the *doubling problem* in lattice field theory. There are nowadays several lattice actions for fermions which circumvent this problem. For example Wilson's modification of the quark propagator [76] removes all doublers from the theory. In the Lagrangian framework, this amounts to adding the term

$$\Delta\mathcal{L} = -\frac{a^3}{2} \sum_{n,\mu} \bar{\Psi}(n) \left(\Psi(n+\hat{\mu}) - 2\Psi(n) + \Psi(n-\hat{\mu})\right) \,. \tag{2.62}$$

It is a discretisation of the Euclidean Laplace operator times the lattice spacing a and acts like a mass term of size $m \sim 1/a$ for the unwanted particles. In the continuum limit, these particles therefore decouple from the theory. A drawback of this specific discretisation is that this additional term breaks chiral symmetry explicitly. The chiral Ward identities such as the PCAC relation therefore do not hold and the flavour currents of QCD have to be renormalised. The renormalisation constants will be functions of the lattice spacing, but not of the renormalisation scale which simplifies things a bit. In lattice simulations, their determination has to be carried out nonperturbatively using e.g. the RI/SMOM scheme [77] or a Schrödinger functional renormalisation scheme [78]. It has been shown [79–82] that it is not possible to find a lattice action for fermions without doublers which has a Dirac operator which [83] i) is analytic and periodic in the momenta of the particles, ii) is given by $\mathrm{i}\gamma_\mu p_\mu$ for small momenta, up to discretisation effects, iii) is invertible, and iv) preserves the continuum chiral symmetry. A possible way out is to define actions with a lattice chiral symmetry [84] which is exact on the lattice and reproduces the continuum chiral symmetry in the limit $a \to 0$. Fermions which are invariant under this lattice chiral symmetry are known as Ginsparg-Wilson fermions.

Moving from the free theory to QCD requires the introduction of a local symmetry. Under a gauge transformation, the fermions transform as

$$\Psi(n) \to \Lambda(n)\Psi(n) \,, \qquad \bar{\Psi}(n) \to \bar{\Psi}(n)\Lambda^\dagger(n) \,, \tag{2.63}$$

with spacetime-dependent matrices Λ in the gauge group. This is problematic since the naive kinetic term in Eq. (2.60) couples fermions at different lattice sites. The action would thus not be invariant under a local gauge transformation. The solution is to introduce *group-valued* fields called link variables U_μ which transform as

$$U_\mu(n) \to \Lambda(n)U_\mu(n)\Lambda^\dagger(n+\mu) \,. \tag{2.64}$$

This should be contrasted with the gauge fields of the continuum theory which take values in the *algebra* of the gauge group. With these link variables and their adjoints, the naive fermion action can be made gauge invariant. For example, the Wilson action with a local symmetry reads [11, 76]

$$\begin{aligned}\mathcal{L}_{\mathrm{W}} = a^4 \sum_n \bar{\Psi} \left(\sum_\mu \gamma_\mu \frac{U_\mu(n)\Psi(n+\hat{\mu}) - U_\mu^\dagger(n-\hat{\mu})\Psi(n-\hat{\mu})}{2a} + m\,\Psi(n) \right) \\ - a^5 \sum_{n,\mu} \Psi(n) \frac{U_\mu(n)\Psi(n+\hat{\mu}) - 2\Psi(n) + U_\mu^\dagger(n-\hat{\mu})\Psi(n-\hat{\mu})}{2a^2} \,. \end{aligned} \tag{2.65}$$

The gauge links can be interpreted as parallel transporters of the symmetry group which connect the points n and $n+\hat{\mu}$ on the lattice. In lattice QCD, the gauge links are dynamical objects, so one also needs to construct a kinetic term for the Lagrangian. This can be done using the plaquette variable

$$U_{\mu\nu}(n) = U_\mu(n) U_\nu(n+\hat{\mu}) U_\mu^\dagger(n+\hat{\nu}) U_\nu^\dagger(n) \,. \tag{2.66}$$

It traces the smallest closed curve on the lattice and its trace is gauge invariant. It can be used to define the Wilson gauge action [11, 76]

$$S_{\mathrm{G}}[U] = \frac{2}{g_{\mathrm{s}}^2} \sum_{n,\mu<\nu} \mathfrak{Re} \left\{ \mathrm{Tr}\left[\mathbb{1} - U_{\mu\nu}(n) \right] \right\} \,. \tag{2.67}$$

In lattice field theory, it is common to use $\beta = 6/g_{\mathrm{s}}^2$. As before, g_{s} denotes the bare gauge coupling whereas $\bar{g}_{\mathrm{s}}$ is the renormalised coupling. As one would expect, the bare coupling is a function of the cutoff, i.e. the lattice spacing a, and one can carry out lattice simulations at different spacings by adjusting β. The continuum limit is recovered for $g_{\mathrm{s}} \to 0$ or equivalently $\beta \to \infty$.

Lattice computations of QCD are based on the path integral approach to QFT presented in Sec. 2.1. In QCD, the fields are given by the gauge links U_μ and the quarks q, the latter being treated as Grassmann valued fields in the path integral in order to preserve the anticommutation relations of fermionic operators. Since the action is quadratic in the quark fields, the integration over them can be carried out exactly which amounts to computing Gaussian integrals with Grassmann numbers. A standard result is

$$\int \left(\prod_i \mathrm{d}\bar{\eta}_i \, \mathrm{d}\eta_i \right) \eta_k \bar{\eta}_l e^{-\bar{\eta}_i M_{ij} \eta_j} = M_{kl}^{-1} \det(M) \,. \tag{2.68}$$

There are two noteworthy points: for bosonic Gaussian integrals, the result would include the inverse of the determinant of M, whereas here it is the determinant itself. Furthermore, in QCD the matrix M is the Dirac operator $(D[U] + m)$ and the inverse is the quark propagator. Including more Grassmann fields in the integrand amounts to computing all possible contractions of ηs and $\bar{\eta}$s and including signs if two Grassmann fields are anticommuted. This reproduces exactly Wick's theorem for fermionic particles. In short, in order to compute the path integral over the quark fields in QCD, one only has to apply Wick's theorem and include the fermion determinant which is a function of the gauge links. An evaluation of the path integral over the gauge variables is all that is left to do.

The gauge action on the other hand is not quadratic in the link variables and thus cannot be solved analytically. In addition, the fermion determinant is also a nonlinear function of the link variables and complicates the evaluation of the path integral further. It is thus necessary to resort to numerical techniques. The gauge-invariant integration measure for SU(N) matrices

is given by the Haar measure and since these groups are compact, the domain of integration is finite and gauge fixing is not required. Nonetheless, a direct numerical approach is not feasible: for a lattice of size $N_\mathrm{T} \times N_\mathrm{S}^3$ in four dimensions, one would have to integrate over $4N_\mathrm{T}N_\mathrm{S}^3$ link variables. An alternative strategy is to evaluate the path integral stochastically using a Markov Chain Monte Carlo algorithm. The idea is to evaluate the observables on a subset of gauge field configurations which are sampled according to a probability distribution $p[U]$. This ensures that the observables are mostly evaluated on gauge configurations which give a large contribution to the path integral. MCMC simulations evolve the system from one gauge configuration to another and ensure that after a finite number of updates, the 'thermalisation time', the system evolves with a probability density which is close to the desired density $p[U]$. This density $p[U]$ is chosen to be

$$p[U] = \frac{1}{\mathcal{Z}_\mathrm{G}} e^{-S_\mathrm{G}[U]} \prod_f \det\left(\not{D}[U] + m_f\right) , \tag{2.69}$$

$$\mathcal{Z}_\mathrm{G} = \int \mathcal{D}\left[U\right] \, e^{-S_\mathrm{G}[U]} \prod_f \det\left(\not{D}[U] + m_f\right) , \tag{2.70}$$

with the pure gauge action $S_\mathrm{G}[U]$. The form of $p[U]$ explains why the simulations are carried out in Euclidean space: the Wick rotation turned the complex exponential of the action into a real one and one can interpret $p[U]$ as a probability density as long as it is positive. This identification also depends on the product of fermion determinants. In general, they can be complex, but certain discretisations of the Dirac operator obey γ_5-hermiticity:

$$\gamma_5 D[U] \gamma_5 = D^\dagger[U] \, . \tag{2.71}$$

This relation implies that the determinant is real. This is the case for e.g. Wilson fermions which were introduced above. Furthermore, most QCD simulations are preformed in the isospin symmetric limit in which up- and down-quarks are mass degenerate. The determinant thus enters as a square and ensures that even on gauge configurations for which the determinant is negative the probability density is positive. Setting the quark determinant to 1 by hand is known as the quenched approximation which neglects the effects of sea quarks.

It should be emphasised that it is at the moment not possible to simulate QCD with all six quark masses at their physical value. As mentioned before, the inverse length of the box L and the finite lattice spacing a serve as IR and UV cutoffs, respectively. It follows, that in order to control finite volume and discretisation errors the masses m of all particles should satisfy the bound

$$L^{-1} \ll m \ll a^{-1} \, . \tag{2.72}$$

The mass of the pion, the lightest hadron, dictates the size of L, whereas the value of a depends on the mass of the quark with the largest mass. On the other hand, the number of lattice points in a given direction is given by L/a and cannot be chosen at will but is limited by the computational resources. Including the b quark at its physical mass would put an upper limit on a and thus a lower limit on the number of lattice points which cannot be simulated at the present time. A rough estimate is the following: in order for finite volume effects to be negligible, one should demand $m_\pi L \geq 4$ [85]. On the other hand, one can hope that discretisation effects (i.e. corrections proportional to powers of a) are under control for $am_b \leq 0.5$ if discretisation errors start at order $(am_b)^2$ [86]. This leads to the following estimate for a lower bound of lattice points

$$\frac{L}{a} \geq 8 \frac{m_b}{m_\pi} \approx 8 \frac{4\,\mathrm{GeV}}{0.14\,\mathrm{GeV}} \approx 230 \, . \tag{2.73}$$

For this reason, lattice simulations at the physical point are carried out with two, three, or four flavours. One way to deal with heavy quarks in lattice simulations will be presented in Sec. 2.3.

The lattice computation of a correlation function proceeds as follows: one first defines the operators $\mathcal{O}_i$ in terms of quark fields and gauge links. One then computes all possible Wick contractions of the quarks which will yield traces over products of quark propagators and gamma matrices. In the next step, a set of gauge field configurations is generated using e.g. a hybrid Monte Carlo algorithm or any other suitable MCMC algorithm, or one reuses an older set of configurations. The propagators of the quarks are then computed by solving the gauge-link-dependent Dirac equation on the individual gauge configurations and putting them together accordingly to obtain a result for the correlator one is interested in. From the correlators, physical observables like masses and matrix elements can be extracted. Then, the ensemble mean and the standard error of a quantity X are computed via

$$\hat{X} = \frac{1}{N}\sum_{i=1}^{N} X_i\,, \qquad \sigma^2_{\hat{X}} = \frac{2\tau^X_{\text{int}}}{N(N-1)}\sum_{i=0}^{N}\left(X_i - \hat{X}\right)^2\,. \tag{2.74}$$

In the limit $N \to \infty$ the estimator for the mean tends to the mean of the observable $\langle X \rangle$ and the standard error vanishes. The factor τ^X_{int} in the definition of the error is known as the integrated autocorrelation time which depends on the observable considered. Since in MCMC simulations, the new gauge field configuration is derived from the previous one, the configurations are not independent. To put it crudely, the factor $2\tau^X_{\text{int}}$ in the above formula corrects this and the ratio $N/(2\tau_{\text{int}})$ can be thought of as the number of truly independent configurations. More details and a method for computing it can be found in [87]. It should be noted that the autocorrelation time increases for smaller lattice spacing a as exemplified e.g. in [88]. This phenomenon is known as *critical slowing down*.

Besides statistical errors also systematic errors have to be taken into account in lattice simulations. For one thing, there are finite volume effects which parametrize the difference of the result in a finite and infinite volume. It was shown [89] that for lattices with periodic boundary conditions these fall off exponentially with the mass of the lightest particle, in QCD the pion, and the length of the box. As a rule of thumb, one therefore often demands $m_\pi L \geq 4$ so that finite size effects are negligible. Furthermore, there are discretisation effects, i.e. corrections which scale with powers of the lattice spacing a and fractional powers of logarithms of a. These can be studied analytically in Symanzik's effective theory [90, 91], a theory which can be thought of as an expansion in a, and results are available for several lattice discretisations of QCD [92, 93]. These are especially important when taking the continuum limit: if one wants to make predictions for or compare with experimental results, one wants to take the limit $a \to 0$. This is done by computing the same quantities at fixed physical parameters as well as box length in physical units but several lattice spacings a. The lattice spacing itself is a function of the unrenormalised gauge coupling g_{s} and can thus be controlled by varying it. A numerical extrapolation to $a = 0$ is then carried out. It is even possible to improve the convergence to the continuum limit by *improving* the action and operators used. This means that one adds terms which vanish in the continuum limit, but contribute at finite a and adjusts their Wilson coefficients in such a way that they cancel discretisation effects up to a given order. For example, the Lagrangian of Wilson given in Eq. (2.65) has discretisation errors of order a. Including the Sheikholeslami-Wohlert term [94] which includes the clover discretisation $\hat{F}_{\mu\nu}$ of the continuum field strength tensor,

$$\Delta\mathcal{L} = c_{\text{SW}}\, a^5 \sum_{n,\mu<\nu} \bar{\Psi}(n)\frac{1}{2}\sigma_{\mu\nu}\hat{F}_{\mu\nu}(n)\Psi(n)\,, \tag{2.75}$$

and tuning the free parameter c_{SW} appropriately, the discretisation errors can be elevated to order a^2. This can also be done for the interpolating fields of the lattice correlation functions. Apart from that, the determination of the lattice spacing in physical units also introduces a further error which depends on the specific procedure used to determine a. In general, every quantity which is computed in lattice simulations is dimensionless and every observable with a non-zero mass dimension is given in lattice units. This means that one cannot measure e.g. the mass of a particle directly, but only the product am. The determination of a is known as *scale setting* and there are various ways to do it. In general, one computes a product aX in the lattice simulation and sets it equal to its real world (if applicable) value $\hat{X}$. This means, that one computes the ratio

$$a = \frac{aX}{\hat{X}} \,. \tag{2.76}$$

Some common choices include the pion decay constant f_π, Sommer's scale r_0 [95] and the gradient flow scale t_0 [96].

A further source of systematic errors is the contamination of lattice correlators by excited states. This will be explained in the next section.

2.2.1. Excited States Contamination of Correlation Functions

A drawback of lattice simulations is the fact that only Euclidean correlation functions can be computed. Theoretical predictions for experiments on the other hand require results for matrix elements, which have to be constructed by taking suitable ratios of correlation functions. Another problem is the contamination of the correlators with excited states which comes about as follows: in order to simulate the propagation of a specific particle, say a kaon, one needs to construct an interpolating field with the same quantum numbers as the particle of interest. This interpolating field is then used as a source or sink for the particle in the lattice simulation. In other words, the interpolating field $\mathcal{O}_P$ has a non-zero overlap with the state $|P\rangle$ of the particle in Hilbert space:

$$\langle 0|\mathcal{O}_P|P\rangle \neq 0 \,. \tag{2.77}$$

But in an interacting theory, this is not necessarily the only state which has a non-zero overlap with this operator: as long as they have the same quantum numbers as $|P\rangle$, there are more states that can also be excited from the vacuum by $\mathcal{O}_P$. These other states, called excited states, can be resonances or multi-particle states. Before discussing how they enter the theory, it is helpful to introduce the transfer matrix $\mathbb{T} = e^{-aH}$, where H is the Hamiltonian of the theory. The transfer matrix is the time evolution operator of the theory for time steps of size a. The existence of a transfer matrix for a given lattice theory is far from trivial, but it has been proven for the Wilson formulation in [97]. This matrix can be used to define Euclidean correlation functions, a definition which is equivalent to the path integral definition given before, see e.g. [70] for an introductory treatment. With the transfer matrix, the two-point correlation function of an operator $\mathcal{O}_P$ can be written as

$$C_2^P(t) = \sum_{\vec{x}} \left\langle \mathcal{O}_P(t,\vec{x})\mathcal{O}_P^\dagger(0,\vec{0}) \right\rangle = \sum_{\vec{x}} \lim_{T\to\infty} \frac{\mathrm{Tr}\left[\mathbb{T}^{\frac{T-t}{a}}\mathcal{O}_P(0,\vec{x})\mathbb{T}^{\frac{t}{a}}\mathcal{O}_P^\dagger(0,\vec{0})\right]}{\mathrm{Tr}\left[\mathbb{T}^{\frac{T}{a}}\right]} \,, \tag{2.78}$$

where T is the time extent of the lattice. The sum over the spatial coordinates projects the correlation function to zero spatial momentum. Excited states then enter in the following way:

one inserts complete sets of energy eigenstates $\left|\alpha^i(\vec{p})\right\rangle$[6] in the correlation function and lets the transfer matrix act on them. In the limit $T \to \infty$, this leads to (see [70] for more details)

$$C_2^P(t) = \sum_{\alpha^i} \frac{1}{2E_{\alpha^i}} \left|\left\langle 0 \middle| \mathcal{O}_P \middle| \alpha^i(\vec{0}) \right\rangle\right|^2 e^{-E_{\alpha^i}|t|} \,. \tag{2.79}$$

Here, the normalisation of states in a finite spatial volume is used

$$\left\langle \alpha^i(\vec{p}) \middle| \alpha^j(\vec{p}\,') \right\rangle = 2L^3 E_{\alpha^i}(\vec{p}) \delta_{\vec{p}\vec{p}\,'} \delta_{ij} \,. \tag{2.80}$$

Sometimes a non-relativistic normalisation of states is more convenient, in this case one has

$$\left\langle \alpha^i(\vec{p}) \middle| \alpha^j(\vec{p}\,') \right\rangle = 2L^3 \delta_{\vec{p}\vec{p}\,'} \delta_{ij} \,, \tag{2.81}$$

a choice that will be used later for heavy meson states.

Eq. (2.79) shows that the correlator is a sum of exponentials which fall off in time. States with larger energies are stronger suppressed for the same time t. Most of the time, one is interest in the energy or the matrix element of the ground state, i.e. the state with the lowest energy, and one could hope that for large times it is the dominant contribution to the correlator. This is true in principle if there is a large gap between the energy of the ground state and the first excited state. On the other hand, lattice simulations are MCMC simulations with a statistical error which limits the precision of the results. An important limitation for these simulations is the so-called signal-to-noise ratio which is given by the ratio of the ensemble mean and the standard error of the mean, see Eq. (2.74). It turns out that in general the signal-to-noise ratio decreases exponentially with time [98, 99] and reliable estimates for correlators at large t are most of the time not possible. As a consequence, one has to extract the energy and/or matrix element of the ground state in a time range in which excited states are possibly non-negligible. If they are not adequately treated in the analysis of the correlation functions, the results for the ground state matrix elements can be afflicted by systematic errors which would eventually lead to systematic errors in real world observables, e.g. CKM matrix element. One way to deal with this is to use multi-exponential fits for correlation functions in the hope of capturing the ground state and the most dominant excited states of the correlator. It is also possible to solve a so-called Generalised Eigenvalue Problem [12, 13] of a matrix whose entries are correlators of different interpolating fields. In this work, an alternative approach will be followed: the excited states contamination will be computed analytically using an effective field theory.

The mass of its ground state can be extracted from a two-point function by making use of the *effective mass*

$$m_{P,\text{eff}}(t) = \frac{1}{a} \log\left(\frac{C_2^P(t)}{C_2^P(t+a)}\right) \,, \tag{2.82}$$

which is a discretised version of $-\partial_t \log C_2^P(t)$. For a finite time extent, this formula needs to be adjusted to take the chosen boundary conditions into account.

The above discussion generalises naturally to n-point correlation functions. Of particular interest are three-point functions, since from these one can compute transition matrix elements. With interpolating fields $\mathcal{I}$ and $\mathcal{F}$ for the particles in the initial (I) and final (F) state,

[6] $\left|\alpha^i(\vec{p})\right\rangle$ includes the vacuum, one- and multi-particle states. Multi-particle states with the same particle content can have different internal momentum configurations which lead to the same overall momentum $\vec{p}$, these are distinguished by the index i.

respectively, and the operator $\mathcal{T}$ mediating the transition, one finds the following spectral decomposition

$$\begin{aligned} C_3(t,t') &= \sum_{\vec{x},\vec{y}} \left\langle \mathcal{F}(t,\vec{x})\mathcal{T}(t',\vec{y})\mathcal{I}(0,\vec{0}) \right\rangle \\ &= \frac{1}{4m_I m_F} \langle 0|\mathcal{F}|F\rangle \langle F|\mathcal{T}|I\rangle \langle I|\mathcal{I}|0\rangle \, e^{-m_F(t-t')} e^{-m_I t'} + \dots , \end{aligned} \tag{2.83}$$

where the ellipsis denotes matrix elements with excited states. It is then easy to see that the following three ratios of the above three-point function and the two-point functions of $\mathcal{I}$ and $\mathcal{F}$ are given by the matrix element $\langle F|\mathcal{T}|I\rangle$ up to the excited states contamination which decays exponentially in time [100]:

$$R_1(t,t') = 2\sqrt{m_I m_F} \frac{C_3(t,t')}{\sqrt{C_2^{\mathcal{F}}(2t-2t')C_2^{\mathcal{I}}(2t')}} = \langle F|\mathcal{T}|I\rangle + \dots , \tag{2.84}$$

$$R_2(t,t') = 2\sqrt{m_I m_F} \frac{C_3(t,t')}{\sqrt{C_2^{\mathcal{F}}(t-t')C_2^{\mathcal{I}}(t')}} e^{m_{I,\mathrm{eff}}(t')\frac{t'}{2} + m_{F,\mathrm{eff}}(t-t')\frac{(t-t')}{2}} = \langle F|\mathcal{T}|I\rangle + \dots , \tag{2.85}$$

$$R_3(t,t') = 2\sqrt{m_I m_F} \frac{C_3(t,t')}{\sqrt{C_2^{\mathcal{F}}(t)C_2^{\mathcal{I}}(t)}} e^{(m_{I,\mathrm{eff}}(t) - m_{F,\mathrm{eff}}(t))(t'-\frac{t}{2})} = \langle F|\mathcal{T}|I\rangle + \dots , \tag{2.86}$$

Other ratios are also possible. The size of the excited states contamination is determined by the size of the matrix elements involving excited states, their energy and the time separations t, t', and $t-t'$. It is convenient to define the ground state of the correlator as $C^{\mathrm{g.s.}}$ and the excited states as $C^{\mathrm{e.s.}}$. Then, one can write for an arbitrary n-point correlation function (suppressing all time dependence for the moment)

$$C_n = C_n^{\mathrm{g.s.}} + C_n^{\mathrm{e.s.}} = C_n^{\mathrm{g.s.}} \left(1 + \frac{C_n^{\mathrm{e.s.}}}{C_n^{\mathrm{g.s.}}}\right) \equiv C_n^{\mathrm{g.s.}}(1+\delta C_n) . \tag{2.87}$$

From this equation it is apparent that δC_n is the relative deviation of the full correlator from the ground state. Without excited states, the correlator would be exactly equal to the ground state contribution, but the excited states lead to a non-zero δC_n and thus to an over- or underestimation of the ground state, depending on whether δC_n is positive or negative. For the effective mass, it is more convenient (at least for the following discussion) to define

$$\Delta m_{P,\mathrm{eff}}(t) = m_{P,\mathrm{eff}}(t) - m_P , \tag{2.88}$$

which is the absolute deviation of the effective mass from the true mass. Rewriting the correlators in the ratios defined in Eqs. (2.84)-(2.86) with these definitions, one obtains

$$\begin{aligned} R_1(t,t') &= \langle F|\mathcal{T}|I\rangle \left[1 + \delta C_3(t,t') - \frac{1}{2}\Big(\delta C_2^{\mathcal{F}}(2t-2t') + \delta C_2^{\mathcal{I}}(2t')\Big)\right] \\ &\equiv \langle F|\mathcal{T}|I\rangle \left(1 + \delta R_1(t,t')\right) , \end{aligned} \tag{2.89}$$

$$\begin{aligned} R_2(t,t') &= \langle F|\mathcal{T}|I\rangle \left[1 + \delta C_3(t,t') - \frac{1}{2}\Big(\delta C_2^{\mathcal{F}}(t-t') + \delta C_2^{\mathcal{I}}(t')\Big)\right. \\ &\quad \left. + \Delta m_{I,\mathrm{eff}}(t')\tfrac{t'}{2} + \Delta m_{F,\mathrm{eff}}(t-t')\tfrac{t-t'}{2}\right] \equiv \langle F|\mathcal{T}|I\rangle \left(1 + \delta R_2(t,t')\right) , \end{aligned} \tag{2.90}$$

$$\begin{aligned} R_3(t,t') &= \langle F|\mathcal{T}|I\rangle \left[1 + \delta C_3(t,t') - \frac{1}{2}\Big(\delta C_2^{\mathcal{F}}(t) + \delta C_2^{\mathcal{I}}(t)\Big)\right. \\ &\quad \left. + \left(\Delta m_{I,\mathrm{eff}}(t) - \Delta m_{F,\mathrm{eff}}(t)\right)\left(t' - \tfrac{t}{2}\right)\right] \equiv \langle F|\mathcal{T}|I\rangle \left(1 + \delta R_3(t,t')\right) . \end{aligned} \tag{2.91}$$

Here, it was assumed that the δC_2s and the products $\Delta m_{i,\mathrm{eff}} t_a$ are small so that a Taylor expansion to first order is justified. Two possible procedures to reduce the impact of the excited states will be discussed in the following sections.

2.2.2. Smeared Interpolating Fields

The spectral decomposition of the three-point function in Eq. (2.83) shows that the overlap of the interpolating fields $\mathcal{I}$ and $\mathcal{F}$ with the ground state and excited states determines the size of the excited states contamination. Finding fields which minimise the overlap with the excited states and/or maximises the overlap with the ground state is thus desirable. A first guess for a suitable interpolating field for a meson state is of the form

$$\mathcal{O}_\Gamma = \bar{q}_{f_1} \Gamma q_{f_2} \,, \tag{2.92}$$

where $\bar{q}_{f_1}$ and q_{f_2} are the valence quarks of the meson and Γ is an appropriate gamma matrix. One would for example set $\Gamma = \gamma_5$ for a pseudoscalar and $\Gamma = \gamma_\mu$ for a vector meson. Lattice simulations show that a reduced excited states contamination can be obtained by *smearing* these quark bilinears. This means that the local operators are spread out over neighbouring lattice sites in a gauge-covariant way. Examples include Gaussian and scalar/exponential smearing [101] and Jacobi smearing [102] which is an approximation of the latter. These smearing operations are guided by physical intuition since QCD bound states have a finite spatial extent. It is not clear if these interpolating fields are renormalisable, but this doesn't matter in lattice simulations since their effects drop out in the ratios from which matrix elements are extracted. On the other hand, renormalisability will play a role for the interpolating fields in the effective theory discussed in Sec. 3. Other approaches make use of additional fermion fields [103] or apply the gradient flow [104]. Renormalisability has been proven for these approaches since they are based on local formulations. Whichever smearing procedure is used, it will introduce a finite *smearing radius* $r_{\rm sm}$ over which the quark fields are spread out. Applying different 'levels' of smearing with different smearing radii to the operators and computing a matrix of correlation functions can be even more helpful: it is then possible to solve a Generalised Eigenvalue Problem which finds a linear combination of the operators with the best overlap with the ground state.

2.2.3. Summation Method

In general, the excited states contaminations defined in Eqs. (2.89)-(2.91) are all of the form

$$\delta R_i(t,t') = \sum_j \left(A_{i,j} e^{-\Delta_j (t-t')} + B_{i,j} e^{-\Delta_j t'} + C_{i,j} e^{-\Delta_j t} \right) \,. \tag{2.93}$$

The coefficient functions are ratios of matrix elements of excited states and the ground state, and Δ_j is the corresponding energy difference of the states. If Δ_j and also the individual time separations t' and $t - t'$ are too small, the excited states contamination of the ratio R is large. For the work at hand, mostly matrix elements with pseudoscalar B and vector B^* mesons in the initial and/or final state are relevant. The first excited state of a B meson state is a $B\pi$ state where B is generically used for either B or B^*. To be more specific, for a state $|B\rangle$, the excited states are of the form $|B^*\pi\rangle$, whereas for $|B^*\rangle$ both $|B\pi\rangle$ and $|B^*\pi\rangle$ contributions to the correlation functions are possible. Due to the small mass of the pion and the even smaller mass difference of vector and pseudoscalar B mesons, the energy difference Δ_j can indeed be small and one thus has to expect large excited states contributions.

The summation method [100, 105–107] can help to reduce the excited states contamination of correlation functions. It is based on the idea that by eliminating the intermediate time scale t' from the correlation function, the excited states can only fall off with $\exp(-\Delta_j t)$ where t is the largest time scale of the three-point function. This is implemented by summing over all insertion times of the operator $\mathcal{T}$ in any of the ratios (2.84)-(2.86). This leads to the general

result (it is assumed for simplicity that time is not discretised since this is the setup used in later chapters) [107]

$$\int_0^t \mathrm{d}t'\, R_i(t,t') = \text{const.} + \langle F|\mathcal{T}|I\rangle \left(t + \int_0^t \mathrm{d}t'\, \delta R_i(t,t') \right) . \tag{2.94}$$

Taking then a derivative w.r.t. t, one still recovers the same matrix element as before, but the excited states are then of the form

$$\delta R_i(t) = \frac{\mathrm{d}}{\mathrm{d}t} \int_0^t \mathrm{d}t'\, \delta R_i(t,t') = \sum_j \left[A_{i,j} + B_{i,j} + C_{i,j}(1-\Delta_j t) \right] e^{-\Delta_j t} . \tag{2.95}$$

The potentially large exponentials $\exp(-\Delta_j t')$ and $\exp(-\Delta_j(t-t'))$ have thus been eliminated and one can hope for a reduced excited states contamination.

2.3. Heavy Quark Effective Theory

It was pointed out in the previous section that lattice simulations including a bottom quark at the physical point are not feasible at the moment. The requirement that the masses of the pions as well as of the B mesons should be far away from the IR and UV cutoff necessitates the use of too large lattices. A way to circumvent this problem is to not simulate a relativistic b quark but instead use an effective theory on the lattice. The idea of taking the limit $m_Q \to \infty$ for a heavy quark has been introduced and first used in a series of papers [31–39]. In short, Heavy Quark Effective Theory is an effective theory in which the on-shell momentum $m_Q v^\mu$ is subtracted from the heavy quark momentum and the Lagrangian is given by a power series in $1/m_Q$. A formal way to construct it is by using a functional integral approach [108, 109] or by applying Foldy-Wouthuysen transformations on the QCD Lagrangian [110]. The latter were first used to decouple positive and negative energy solutions in the Dirac equation [111] and also lead to a decoupling of quarks and anti-quarks in HQET. The relevance of this theory to the work at hand is its use in computing matrix elements of heavy-light currents and bound states in lattice simulations. In Sec. 4.1, these are matched to operators in an effective mesonic theory and used for computing the excited states contamination of lattice correlators. For this reason, continuum HQET will be considered in this section if not stated otherwise. This section is based on the discussions in [112, 113].

The HQET Lagrangian is of the form

$$\mathcal{L}^{\mathrm{HQET}} = \mathcal{L}^{(0)} + \sum_n \frac{1}{m_Q^n} \mathcal{L}^{(n)} , \tag{2.96}$$

with a renormalisable Lagrangian $\mathcal{L}^{(0)}$, which contains the QCD Lagrangian of the light flavours and gluons, and the so-called *static* Lagrangian for the heavy quark which will be defined below. The other terms $\mathcal{L}^{(n)}$ are of the form

$$\mathcal{L}^{(n)} = \sum_k C_k^{(n)} \tilde{O}_k^{(n)} , \tag{2.97}$$

with Wilson coefficients $C_k^{(n)}$ and a complete set of local operators $\tilde{O}_k^{(n)}$ of dimension $4+n$ which respect the symmetries of the theory. A similar expansion can be written down for a generic local operator O:

$$O = O^{\mathrm{stat}} + \sum_{n=1}^{\infty} \frac{1}{m_Q^n} O^{(n)} , \qquad O^{(n)} = \sum_k D_k^{(n)} O_k^{(n)} . \tag{2.98}$$

The expansion of correlation functions then proceeds as follows: when expanding the exponential in the path integral, one retains only the m_Q independent parts in the exponent, i.e. the action involving the light flavours and the static Lagrangian. The normalisation factor $\mathcal{Z}$ is thus given by

$$\mathcal{Z} = \int \mathcal{D}[\Phi]\, e^{-S^{(0)}} \left(1 - \frac{1}{m_Q} S^{(1)} + \dots\right) \equiv \mathcal{Z}_0 \left(1 - \frac{1}{m_Q} \left\langle S^{(1)} \right\rangle_0 + \dots\right), \tag{2.99}$$

$$\langle A \rangle_0 = \frac{1}{\mathcal{Z}_0} \int \mathcal{D}[\Phi]\, e^{-S^{(0)}} A\,. \tag{2.100}$$

The definition of correlation functions as given in Eq. (2.22) can then be systematically expanded, e.g. the expansion of a two-point function reads

$$\begin{aligned}\left\langle O_1^{\mathrm{HQET}} O_2^{\mathrm{HQET}} \right\rangle = \left\langle O_1^{\mathrm{stat}} O_2^{\mathrm{stat}} \right\rangle_0 - \frac{1}{m_Q} \Big[&\left\langle O_1^{(1)} O_2^{\mathrm{stat}} \right\rangle_0 \left\langle O_1^{\mathrm{stat}} O_2^{(1)} \right\rangle_0 \\ &- \left\langle O_1^{\mathrm{stat}} O_2^{\mathrm{stat}} S^{(1)} \right\rangle_0 + \left\langle O_1^{\mathrm{stat}} O_2^{\mathrm{stat}} \right\rangle_0 \left\langle S^{(1)} \right\rangle_0 \Big] + \mathcal{O}\left(m_Q^{-2}\right). \end{aligned} \tag{2.101}$$

The theory can then be renormalised at a fixed order in $1/m_Q$ by adjusting (this line of argument follows [113]) i) the Wilson coefficients of the Lagrangian (which includes also the parameters of the LO Lagrangian), and ii) the coefficients of the operators in the expansion of O. When renormalising one of the operators (this applies to $O_k^{(n)}$ and $\tilde{O}_k^{(n)}$), one may have to include operators of lower dimension due to operator mixing. But these terms are already present in the correlation functions and do not lead to new terms, i.e. they only redefine the coefficients $C_k^{(n)}$ and $D_k^{(n)}$. Special care needs to be taken for the correlators which involve the higher order actions: when the distance $|x-y|$ of the operators of the corresponding Lagrangian $\mathcal{L}^{(n)}(x)$ and of one of the operators $O_i(y)$ goes to zero (which it will since the Lagrangian is integrated over all spacetime points), an Operator Product Expansion (OPE) needs to be carried out. The result is a sum of operators with the same quantum numbers as the operator O_i. But all of these operators are already present in the expansion of O_i anyway and the OPE only leads to a redefinition of the coefficients $D_k^{(n)}$. So finally, in order to get a finite result, one has to adjust the multiplicative renormalisation constants Z_k of all operators (of the action and the operator expansion), but these can simply be absorbed in the coefficient functions. This shows that adjusting the coefficients $C_k^{(n)}$ and $D_k^{(n)}$ is enough to renormalise HQET.

The static HQET Lagrangian, i.e. without $1/m_Q$ corrections, in the rest frame of the heavy quark and in Euclidean space reads [34] (the mass term is not included in the reference)

$$\mathcal{L}^{\mathrm{stat}} = Q^\dagger (D_4 + m_Q) Q\,. \tag{2.102}$$

The open index should be thought of as being contracted with the four-velocity $v = (\vec{0}, \mathrm{i})$ of the heavy quark: $D_4 = -\mathrm{i} v_\mu D_\mu$. The appearance of such a term also signals the breaking of Lorentz symmetry, HQET is a nonrelativistic theory. The operator Q destroys a heavy quark but does not create its anti-particle. One can think of Q as a two-component spinor embedded in a four-component spinor which is implemented by the constraint

$$P_+ Q = Q\,, \qquad P_\pm = \frac{1}{2}(\mathbb{1} \pm \gamma_4)\,. \tag{2.103}$$

The field $\tilde{Q}$, the operator destroying a heavy anti-quark, on the other hand satisfies the constraint with P_+ replaced by P_-. The free propagator derived from this Lagrangian is [112]

$$G(x-y) = \theta(x_4 - y_4) e^{-m_Q(x_4 - y_4)} \delta^{(3)}(\vec{x} - \vec{y}) P_+\,. \tag{2.104}$$

All correlation functions of the heavy quark will have this trivial exponential dependence on the heavy quark mass. It is thus convenient to remove the mass term from the Lagrangian (2.102) and add it by hand later if required. This will be assumed in the following. Note that for renormalisation a counter term of the form $\delta m\, Q^\dagger Q$ is still needed [112].

Some comments are in order: choosing the rest frame of the heavy quark is necessary since the energy spectrum is not bounded from below in other frames which leads to inconsistencies [114, 115]. Second, the static Lagrangian is invariant under various symmetry groups (but breaks Lorentz symmetry). For one thing, since there are no gamma matrices inserted between Q and $Q^\dagger$, the static theory is invariant under a Heavy Quark Spin Symmetry (HQSS) transformation [33]

$$Q \to \mathcal{S} Q\,, \qquad\qquad Q^\dagger \to Q^\dagger \mathcal{S}^{-1}\,. \tag{2.105}$$

Furthermore, besides considering only one heavy quark but several different flavours Q_F, the theory would be invariant under global flavour transformations of the form

$$Q_F \to \Lambda_{FF'} Q_{F'}\,, \qquad\qquad Q_F^\dagger \to Q_{F'}^\dagger \Lambda_{FF'}^*\,. \tag{2.106}$$

Here, Λ is a $\mathrm{U}(n_F)$ matrix with n_F being the number of heavy flavours. Finally, promoting this symmetry to a local $\mathrm{U}(n_F)$ transformation which is a function of only the spatial coordinates $\vec{x}$ is also a symmetry. This symmetry follows from the fact that no derivatives D_k are present in the static Lagrangian (2.102). This will become important in Sec. 4.1, when HQET operators are matched to operators in a mesonic theory. For a single heavy quark, one has a local U(1) symmetry which is known as local flavour number (LFN) [112],

$$Q \to e^{\mathrm{i} f(\vec{x})} Q\,. \tag{2.107}$$

For the work at hand, heavy-light currents and densities are of great importance.[7] These are quark bilinears formed of one light quark q (u, d, s) and one heavy quark Q (here: b),

$$V_{f,\mu} = \bar{q}_f \gamma_\mu Q\,, \qquad\qquad A_{f,\mu} = \bar{q}_f \gamma_\mu \gamma_5 Q\,, \tag{2.108}$$

$$S_f = \bar{q}_f \mathbb{1} Q\,, \qquad\qquad P_f = \bar{q}_f \gamma_5 Q\,. \tag{2.109}$$

The index f is a flavour index for the light quarks and will be dropped for convenience where it is not important. The form of the Lagrangian (2.102) shows that (Euclidean) Lorentz symmetry is broken, but it is still convenient to use the notation A_μ and V_μ. As a consequence, the temporal ($\mu = 4$) and spatial ($\mu = 1, 2, 3$) components of the currents are a priori not related by a symmetry transformation. On the other hand, chiral symmetry, heavy quark spin symmetry, and the constraint on the heavy quark spinor lead to nontrivial relations between the currents and densities. Using the constraint in Eq. (2.103) and the fact that γ_μ and γ_5 anticommute, one can show that

$$V_4 = S\,, \qquad\qquad A_4 = -P\,. \tag{2.110}$$

Secondly, one can consider the transformation of the operators under a specific heavy quark spin symmetry transformation. For a rotation about the z-axis by an angle π, the transformation matrix reads ($\sigma_{\mu\nu} = \mathrm{i}/2[\gamma_\mu, \gamma_\nu]$)

$$\mathcal{S}(\theta_z = \pi) = e^{-\frac{\mathrm{i}}{2}\pi\sigma_{12}} = \gamma_1\gamma_2 = \mathrm{i}\begin{pmatrix} \sigma^3 & 0 \\ 0 & \sigma^3 \end{pmatrix}\,, \qquad \mathcal{S}^{-1} = \gamma_4 \mathcal{S}^\dagger \gamma_4 = -\mathcal{S} = \gamma_2\gamma_1\,. \tag{2.111}$$

[7] The following discussion has already been presented in [116].

Applying this transformation to the operators in Eqs. (2.108) and (2.109), one finds (a prime denotes the transformed operators)

$$P' = -\bar{q}\gamma_3 Q = -V_3\,, \qquad V_3' = \bar{q}\gamma_5 Q = P\,, \tag{2.112}$$

$$S' = \bar{q}\gamma_3\gamma_5 Q = A_3\,, \qquad A_3' = -\bar{q}\mathbb{1}Q = -S\,. \tag{2.113}$$

The other two components of the vector current are transformed into each other and the same is true for the axial vector current. One can thus infer that the pseudoscalar density and the vector current transform into each other under Heavy Quark Spin (HQS) transformations and the same is true for the scalar density and the axial vector current. This has some immediate consequences for correlation functions. As an example, the two-point function of the pseudoscalar density can be rewritten as

$$\begin{aligned}\left\langle 0\middle|P(x)P^\dagger(0)\middle|0\right\rangle &= \left\langle 0\middle|U^{-1}(\mathcal{S})\left[U(\mathcal{S})P(x)U^{-1}(\mathcal{S})\right]\left[U(\mathcal{S})P^\dagger(0)U^{-1}(\mathcal{S})\right]U(\mathcal{S})\middle|0\right\rangle \\ &= \left\langle 0\middle|V_3(x)V_3^\dagger(0)\middle|0\right\rangle\,.\end{aligned} \tag{2.114}$$

Here, $U(\mathcal{S})$ is the operator inducing the special spin transformation of Eq. (2.111) and it was used that the vacuum is invariant under it. This result implies that the two-point functions of the pseudoscalar density and the vector current are identical, a direct consequence of HQSS. It also implies that the particles which are interpolated by these operators are mass-degenerate. All of this is only true if HQS transformations are a symmetry of the theory, but this is only true in the static limit of HQET. This symmetry is broken at order $1/m_Q$ by the spin operator

$$\Delta\mathcal{L} = \frac{1}{2m_Q}Q^\dagger\sigma_k B_k Q\,, \tag{2.115}$$

with $\sigma_k = \frac{1}{2}\varepsilon_{ijk}\sigma_{ij}$ and the magnetic field B_k. The gamma matrices between the heavy quark operators do not commute with the spin transformation matrices and thus HQSS is broken.

Another relevant symmetry for the currents and densities is chiral symmetry. The spinors of light quark flavours can be written as the sum of a left- and right-handed light quark by applying the projection operators of Eq. (2.23):

$$A_\mu = (\bar{q}_\mathrm{R} - \bar{q}_\mathrm{L})\gamma_\mu Q\,, \qquad V_\mu = (\bar{q}_\mathrm{R} + \bar{q}_\mathrm{L})\gamma_\mu Q\,. \tag{2.116}$$

This is just a manifestation of the definition of the axial vector and vector current: the axial vector current is the difference of a left- and a right-handed current whereas the vector current is the sum of the two. For the case of isospin symmetry, i.e. for a global $\mathrm{SU}(2)_\mathrm{L}\times\mathrm{SU}(2)_\mathrm{R}$ symmetry, one can even find chiral transformations which take V_μ into A_μ and vice versa. This can be achieved by making use of the fact that a rotation around a fixed axis in isospin space by an angle 2π is represented by $-\mathbb{1}$ in the defining representation of SU(2). The idea is then to use the combination of a vector and an axial transformation about the same axis by an angle π. In formulae, this corresponds to

$$L_1 = e^{\mathrm{i}\pi\frac{\sigma^i}{2}} = \mathrm{i}\sigma^i = R_1\,, \qquad L_2 = L_1 = R_2^\dagger\,, \tag{2.117}$$

$$\Rightarrow L_1 L_2 = -\mathbb{1}\,, \qquad R_1 R_2 = \mathbb{1}\,. \tag{2.118}$$

The left-handed quarks are rotated two times by an angle π, so in total 2π and change sign under this rotation, whereas the right-handed quarks are rotated back to the initial state. This transformation can also be written as

$$\bar{q} \to -\bar{q}\gamma_5\,, \tag{2.119}$$

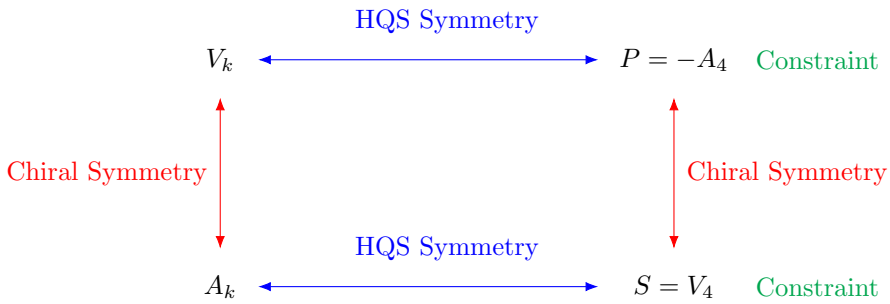

Figure 2.1.: The symmetries relating the heavy-light currents and densities. The constraint refers to Eq. (2.103). Due to the high degree of symmetry, every component of the currents and both densities are related to each other by a symmetry transformation. Recreation of Fig. 1 in [116].

and leads to

$$V_\mu \to -\bar{q}\gamma_5\gamma_\mu Q = \bar{q}\gamma_\mu\gamma_5 Q = A_\mu\,, \qquad A_\mu \to -\bar{q}\gamma_5\gamma_\mu\gamma_5 Q = \bar{q}\gamma_\mu Q = V_\mu\,, \tag{2.120}$$

$$S \to -\bar{q}\gamma_5 Q = -P\,, \qquad P \to -\bar{q}Q = -S\,. \tag{2.121}$$

Combining the various symmetries laid out in this section, one can see that all heavy-light currents and densities can be transformed into each other in HQET. This is shown pictorially in Fig. 2.1.

One last important transformation, which will proof useful in Sec. 4.1 where the analogous interpolating fields are derived in an effective theory, is parity. This symmetry transformation acts by multiplication with the time-like gamma matrix on the quark fields and sending $\vec{x} \to -\vec{x}$. The spatial components of the vector current for example transform as

$$V_k \to \bar{q}\gamma_4\gamma_k\gamma_4 Q = -\bar{q}\gamma_k Q = -V_k\,. \tag{2.122}$$

Besides the operator Q which destroys a heavy quark, there is also an operator $\tilde{Q}$ which destroys the respective heavy anti-quark. This operator satisfies the constraint equation

$$\tilde{Q}P_- = \tilde{Q}\,, \tag{2.123}$$

see Eq. (2.103) for the definition of P_-. Q and $\tilde{Q}$ are a priori independent particles in HQET, but it is convenient to adjust some of the transformations accordingly. Under a heavy quark spin transformation, one has

$$\tilde{Q} \to \tilde{Q}\mathcal{S}^{-1}\,, \qquad \tilde{Q}^\dagger \to \mathcal{S}\tilde{Q}^\dagger\,, \tag{2.124}$$

with the same transformation matrix $\mathcal{S}$ which is used for Q. For the U(1) LFN transformation on the other hand, it is convenient to use a phase transformation which is different from the one used for Q:

$$\tilde{Q} \to e^{-\mathrm{i}f'(\vec{x})}\tilde{Q}\,. \tag{2.125}$$

2.3.1. Matching HQET Currents to QCD

An important step when using effective theories such as HQET is the *matching* to either another effective theory[8] or a fundamental theory, here QCD. Matching describes the process

[8] It is easier to describe particle physics processes at low energies using an effective theory in which the heavy particles were integrated out. This is done consecutively, starting with the top quark. This then means that when integrating out any other particle afterwards, an effective theory with $N-1$ particles is matched to another effective theory with N particles.

of adjusting the parameters of the effective theory so that observables computed in the effective and fundamental theory agree up to higher order corrections. In the case of HQET and QCD, these corrections are given by powers of $1/m$. In the following it is assumed that the heavy quark is a b quark. This section highlights some of the most important points of the discussion given in [112].

As an example, consider the time component of the heavy-light axial vector current in HQET. When computing correlation functions of this current on the lattice, it has to be renormalised in order to have a finite continuum limit. But this doesn't automatically guarantee that e.g. the heavy meson decay constant which can be extracted from its two-point function agrees with the QCD result. Instead, the renormalised currents in QCD and the static limit of HQET have to be related by

$$A_{\mathrm{R},4}^{\mathrm{QCD}} \doteq C_{A_4}(\mu)\, A_{\mathrm{R},4}^{\mathrm{HQET}}(\mu) + \mathcal{O}\left(m_b^{-1}\right) , \tag{2.126}$$

where $C_{A_4}(\mu)$ is a matching constant and $\doteq$ signifies that the operators on the two sides of the equation belong to different theories. The correctly renormalised current in QCD does not depend on the renormalisation scale μ, see the discussion below. If one computes (as an example) the heavy meson decay constant in the static limit of HQET, one needs to adjust this matching constant in such a way that the result reproduces the QCD result up to corrections of order $1/m_b$.

Before discussing the matching constants in more detail, a few words should be said about currents in lattice QCD: most lattice actions, such as Wilson's QCD action, break chiral symmetry and the chiral Ward identities which prevent a renormalisation of the isovector axial vector and vector currents do not hold true. The only exceptions are fermions which satisfy the Ginsparg-Wilson equation [84] which allows for a lattice chiral symmetry and Ward identities. Furthermore, conserved lattice currents are not local operators (in the sense that all particles are located on a single lattice site), but the more convenient use of local operators necessitates the introduction of a renormalisation constant anyway. These renormalisation constants should be chosen in such a way that they enforce the chiral Ward identities, so that in the continuum limit chiral symmetry is restored. For the QCD currents, the renormalisation constants are functions of the lattice spacing a, but not of the scale μ, since chiral symmetry is broken only by the discretisation. For this reason, the renormalised QCD current on the l.h.s. of Eq. (2.126) does not depend on μ. On the other hand, the heavy-light currents of HQET are not protected by chiral Ward identities since the heavy quark does not transform under chiral symmetry, and the renormalisation constants are thus functions of μ. It is then necessary to enforce these Ward identities by hand in order to properly renormalise the theory. Fig. 2.1 shows well that one needs only two different renormalisation constants in HQET if chiral symmetry is broken, e.g. Z_{A} and Z_{V} for the time components of the axial vector and vector currents, respectively. In fact, only one of them and the μ-independent ratio $Z_{\mathrm{A}}/Z_{\mathrm{V}}$ is needed which has been computed e.g. in [117, 118] by enforcing chiral Ward identities. This is enough to renormalise all currents and densities due to the remaining symmetries of HQET.

It was shown in the previous section that all currents and densities transform into each other under the various symmetries of the static theory. This is not true in QCD, since HQS transformations do not leave the QCD Lagrangian invariant and the constraints $P = -A_4$ and $S = V_4$ also only hold true in the static limit of HQET. On the other hand, the chiral symmetry of the light quarks can be used in both theories to relate the matching coefficients:

$$C_P = C_S\,, \qquad C_{A_4} = C_{V_4}\,, \qquad C_{A_k} = C_{V_k}\,. \tag{2.127}$$

It is furthermore possible to relate C_P to C_{A_4} using the PCAC relation. Neglecting the mass of the light quark, which is small compared to the b quark mass, one has

$$\partial_\mu A_{\mathrm{R},\mu}^{\mathrm{QCD}} = \bar{m}_b(\mu) P_{\mathrm{R}}^{\mathrm{QCD}}(\mu)\,. \tag{2.128}$$

One then considers appropriate matrix elements of the operators, e.g. the B to vacuum matrix element. The QCD currents and densities can be replaced by their HQET counterparts using the matching condition. The heavy B meson states in QCD and HQET in the static limit are related by [119]

$$|B\rangle_{\mathrm{QCD}} \to \sqrt{m_B}\,|B\rangle_{\mathrm{HQET}}\,. \tag{2.129}$$

In the rest frame of the heavy meson, the spatial derivatives are zero since the matrix element is proportional to $\exp(\mathrm{i}p_\mu x_\mu) = \exp(-m_B t)$. The derivative w.r.t. time leads to a simple multiplication with $-m_B$. One therefore has

$$-m_B C_{A_4}(\mu)\left\langle 0\middle|A_{\mathrm{R},4}^{\mathrm{HQET}}(\mu)\middle|B\right\rangle = \bar{m}_b(\mu) C_P \left\langle 0\middle|P_{\mathrm{R}}^{\mathrm{HQET}}(\mu)\middle|B\right\rangle\,. \tag{2.130}$$

With the constraint $A_4 = -P$, which also holds true for the renormalised quark bilinears if appropriate renormalisation conditions are used, one arrives at

$$C_P(\mu) = \frac{m_B}{\bar{m}_b(\mu)} C_{A_4}(\mu)\,. \tag{2.131}$$

One thus only needs two matching functions, e.g. C_{A_4} and C_{V_k}.

A drawback of the matching condition in Eq. (2.126) is that the HQET current and the matching constant both depend on the renormalisation scale μ, whereas the QCD current does not. One way to overcome this problem is the use of RGI currents as defined in Eq. (2.18), which additionally do not depend on the chosen renormalisation scheme. To do so, one needs the anomalous dimension of the currents. Due to the various symmetries of HQET in the static limit, all components of the currents and densities can be transformed into each other (assuming that the theory was renormalised in such a way that all symmetries are preserved). As a consequence, in the continuum only a single renormalisation constant needs to be determined and is then valid for all currents and densities:

$$J^\Gamma = Z_J(\mu) J_{\mathrm{R}}^\Gamma(\mu)\,, \qquad J^\Gamma = \bar{q}\,\Gamma Q\,, \qquad \Gamma \in \{\mathbb{1}, \gamma_5, \gamma_\mu, \gamma_\mu\gamma_5\}\,. \tag{2.132}$$

It follows that all heavy-light bilinears have the same anomalous dimension $\gamma(\bar{g}_{\mathrm{s}})$ (see Eq. (2.16) for its definition) with the leading order, scheme-independent coefficient [120, 121]

$$\gamma_J^{(0)} = -\frac{1}{4\pi^2}\,. \tag{2.133}$$

The renormalised currents can then be converted to RGI currents using Eqs. (2.18) and (2.20). These are the currents which will be derived in Heavy Meson ChPT in Sec. 4.1. Switching to the RGI current also leads to a change in the matching coefficient, in this example:

$$C_{A_4}(\mu) \to \frac{C_{A_4}(\mu)}{\varphi_J(\bar{g}_{\mathrm{s}}(\mu))} = C_{\mathrm{PS}}(M_b/\Lambda)\,. \tag{2.134}$$

The ratio is independent of μ and therefore can only depend on the ratio of RGI invariants, here the RGI b quark mass and the QCD lambda parameter [112]. The matching constant C_{PS} as well as the function φ_J which is used to convert to RGI currents need to be evaluated in perturbation theory, i.e. at high enough scales μ so that the truncation errors are small. This means that also a matrix element of the current which one is interested in must be computed at large μ. This can be done using a so-called step-scaling technique in lattice simulations, see [122–124]. From the definition of the following two matrix elements in QCD and HQET

$$\langle 0|A_{\mathrm{R},4}|B\rangle_{\mathrm{QCD}} = -f_B m_B\,, \tag{2.135}$$

$$\langle 0|A_{\mathrm{R},4}|B\rangle_{\mathrm{HQET}} = -\hat{f}\,, \tag{2.136}$$

one can find the relation (remember Eq. (2.129))

$$f_B = C_{\mathrm{PS}} \frac{\hat{f}}{\sqrt{m_B}} + \mathcal{O}\left(m_b^{-1}\right) . \tag{2.137}$$

The second independent matching coefficient is denoted by

$$\frac{C_{V_k}(\mu)}{\varphi_J(\bar{g}_{\mathrm{s}}(\mu))} = C_{\mathrm{V}}(M_b/\Lambda) . \tag{2.138}$$

The strategy for matching QCD and HQET in this section involved the combination of lattice simulations and perturbative computations of matching functions. But it is also possible to match the two theories in a completely non-perturbative approach on the lattice, see [125].

2.4. Flavour Changing Interactions

The QCD Lagrangian (2.1) is diagonal in the quark flavours: the mass matrix is diagonal and the covariant derivative does not contain any interactions which couple different flavours. In the full Standard Model, this is no longer true: the weak interactions allow for so-called flavour changing charged current interactions which induce the transition from an up-type quark to a down-type quark and vice versa,

$$\Delta\mathcal{L} = \frac{g}{\sqrt{2}} \bar{U}_i V_{ij} \gamma^\mu P_{\mathrm{L}} W_\mu^+ D_j + \mathrm{h.c.} , \tag{2.139}$$

with U_i and D_j representing up- and down-type quarks and g is the coupling constant of the $\mathrm{SU}(2)_{\mathrm{L}}$ gauge symmetry of the Standard Model. The matrix V_{ij} is known as the Cabibbo-Kobayashi-Maskawa matrix [7, 8] and describes the probability of a given up- (down-) type quark in generation i (j) to transform into a down- (up-) type quark in generation j (i). The diagonal elements of the CKM matrix are large compared to the off-diagonal elements [6] which shows that decays to quarks of the same generation are more likely. Note the appearance of the projector on left-handed particles in Eq. (2.139) which is a consequence of the chiral structure of the weak interactions.

The CKM matrix is a complex 3×3 matrix because there are three generations of quarks in the SM. It is furthermore unitary since it is defined as the product of two unitary matrices which transform the up- and down-type quark eigenstates of the weak interactions to the mass eigenstates, see any introductory book on particle physics such as [126] for more details. After absorbing some unobservable phases in the quark fields, one is left with four free parameters: three mixing angles and one complex phase. The latter is responsible for CP violation in the Standard Model. The values of these four parameters cannot be deduced from the Standard Model and have to be determined in experiments. At first, this seems to be a nuisance, but at the same time it can also be used as a test of the Standard Model itself and as a probe for new physics: a given CKM matrix element can enter several processes which can be measured in experiments. The value for this matrix element should be the same no matter which process is chosen to extract it from. Assuming that statistical fluctuations as well as systematic errors can be ruled out, a significant tension between two different extracted values can be interpreted as a sign for new physics: hypothetical new particles would contribute stronger to one of the processes used to determine the CKM matrix element than to the other, leading to results which are not compatible.

Another constraint is the unitarity of the CKM matrix. This property leads to constraints between several CKM matrix elements, e.g.

$$V_{ud}V_{ub}^* + V_{cd}V_{cb}^* + V_{td}V_{tb}^* = 0 , \tag{2.140}$$

$$|V_{ud}|^2 + |V_{us}|^2 + |V_{ub}|^2 = 1 . \tag{2.141}$$

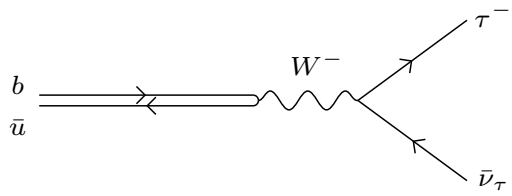

Figure 2.2.: Leading order Feynman diagram for the leptonic decay of a B meson.

The first equation can be interpreted as the sum of three complex numbers which sum to zero. In the complex plane, this looks like a triangle and the relations are thus known as unitarity triangles. A significant deviation from zero would again signal contributions of new particles. The same is true if the second equation does not sum to unity. In fact, as presented in [127], the result shows tensions between $2.8\,\sigma$ and $5.6\,\sigma$ from unity, depending on the method used to extract the CKM matrix elements.

In summary, the CKM matrix can be a window to physics Beyond the Standard Model, but one has to make sure first that all sources of systematic errors are controlled before significant inconsistencies between experimental results and theory predictions can be interpreted as signs for new particles. CKM matrix elements enter in weak decay processes of hadrons which are best computed nonperturbatively in lattice simulations. For reliable results, it is indispensable to estimate the excited states contamination of the lattice correlation functions. The following sections describe how the absolute values of the matrix elements V_{ub} and V_{td} can be extracted from the combination of lattice correlation functions, perturbation theory and experimental input. In Chs. 4 and 5 the computation of the excited states contamination of the relevant correlation functions is presented.

2.4.1. Leptonic B Meson Decays

The matrix element V_{ub} can enter the results of leptonic and semileptonic decays of B mesons. In the leptonic decay channel, a charged B meson decays via the weak interactions into a lepton anti-neutrino pair. At leading order in the Standard Model, the decay rate is given by [6]

$$\Gamma(B^- \to \tau^- \bar{\nu}_\tau) = \frac{G_\mathrm{F}^2 \left|V_{ub}\right|^2}{8\pi} f_B^2 m_B m_\tau^2 \left(1 - \frac{m_\tau^2}{m_B^2}\right) , \tag{2.142}$$

with Fermi's constant $G_\mathrm{F} = 1.166\,\mathrm{GeV}^{-2}$ [6]. The corresponding Feynman diagram can be found in Fig. 2.2. In order to extract V_{ub}, a precise value for the B meson decay constant f_B is needed. It is defined by the QCD matrix element (in Minkowski space)

$$\langle 0|A^\mu|B(p)\rangle = \mathrm{i} f_B p^\mu , \tag{2.143}$$

and its computation in HQET has already been presented in Sec. 2.3.1. On the other hand, also experimental input for the decay rate is needed. So far, measurements have been carried out by Belle [128, 129] and BaBar [130, 131] and evidence for the decay considered here was found. But so far, the results have not reached a significance of $5\,\sigma$ at which a discovery can be claimed. A determination of $|V_{ub}|$ from this process is therefore not reliable at the moment.

2.4.2. Semileptonic B Meson Decays

In the following, the decay $B \to \pi \ell \bar{\nu}_\ell$ is considered with ℓ being a lepton. On the quark level, the valence b quark of the B meson decays via the weak interactions into a u quark which

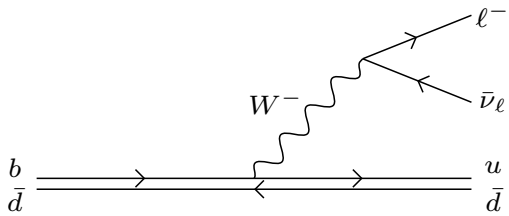

Figure 2.3.: Leading order Feynman diagram for the semileptonic decay of a B meson.

turns the B meson into a pion. In this process, a W boson is emitted which decays into the final state lepton and anti-neutrino. A graphical depiction of this process is given in Fig. 2.3. In the conventions of [127], the differential decay rate for this process is

$$\frac{\mathrm{d}\Gamma(B\to\pi\ell\bar{\nu}_\ell)}{\mathrm{d}q^2} = \frac{G_\mathrm{F}^2\,|V_{ub}|^2}{24\pi^3}\frac{(q^2-m_\ell^2)^2\,|\vec{p}_\pi|}{q^4 m_B^2}\left[\left(1+\frac{m_\ell^2}{2q^2}\right)m_B^2\,\vec{p}_\pi^{\,2}\left|f_+(q^2)\right|^2 + \frac{3m_\ell^2}{8q^2}\left(m_B^2-m_\pi^2\right)^2\left|f_0(q^2)\right|^2\right]. \tag{2.144}$$

The momentum transferred to the final state lepton-neutrino pair is defined as

$$q^\mu = (p_B - p_\pi)^\mu\,. \tag{2.145}$$

If the final state lepton is either an electron or muon, the small lepton mass can be neglected and then only one of the two form factors, f_+, contributes to the decay rate. They are defined via the hadronic matrix element (in Minkowski space) [6]

$$\langle\pi(p_\pi)|V^\mu|B(p_B)\rangle = \left(p_B^\mu + p_\pi^\mu - q^\mu\frac{m_B^2-m_\pi^2}{q^2}\right)f_+(q^2) + q^\mu\frac{m_B^2-m_\pi^2}{q^2}f_0(q^2)\,, \tag{2.146}$$

with the vector current $V^\mu = \bar{u}\gamma^\mu b$. This matrix element arises in the following way: as mentioned above, the initial state B meson decays into a pion by emitting a W boson. This virtual boson couples to the hadronic left-handed current $L^\mu = V^\mu - A^\mu$. Since the matrix element of the axial vector current between the hadronic initial and final state is zero, only the vector current contributes. Another useful decomposition of the matrix element is given by [132]

$$\langle\pi(p_\pi)|V^\mu|B(p_B)\rangle = \sqrt{m_B}\,(p_\pi^\mu - (v\cdot p_\pi)v^\mu)\,h_\perp(v\cdot p_\pi) + v^\mu h_\parallel(v\cdot p_\pi)\,, \tag{2.147}$$

with the velocity of the heavy B meson

$$v^\mu = \frac{p_B^\mu}{m_B}\,. \tag{2.148}$$

The factor $\sqrt{m_B}$ is chosen so that it is absorbed in the definition of the heavy meson state when switching to HQET, cf. Eq. (2.129). Choosing the rest frame of the heavy meson with $\vec{v}=\vec{0}$ in HQET, this simplifies to (only the static theory is considered in the following)

$$\left\langle\pi(p_\pi)\middle|V^k\middle|B\right\rangle_\mathrm{HQET} = p_\pi^k\,h_\perp^\mathrm{HQET}(E_\pi)\,,\qquad \left\langle\pi(p_\pi)\middle|V^0\middle|B\right\rangle_\mathrm{HQET} = h_\parallel^\mathrm{HQET}(E_\pi)\,, \tag{2.149}$$

with the HQET current $V^\mu = \bar{u}\gamma^\mu Q$. If one computes the matrix elements of the RGI vector current, one can use the constants C_PS and C_V of Sec. 2.3.1 to match the HQET to the QCD form factors

$$h_\perp(E_\pi) = C_\mathrm{V}\,h_\perp^\mathrm{HQET}(E_\pi) + \mathcal{O}(m_b^{-1})\,,\qquad h_\parallel(E_\pi) = C_\mathrm{PS}\,h_\parallel^\mathrm{HQET}(E_\pi) + \mathcal{O}(m_b^{-1})\,, \tag{2.150}$$

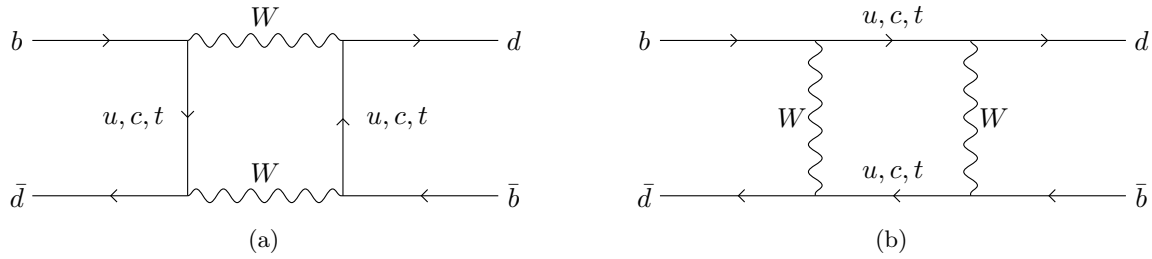

Figure 2.4.: Box diagrams contributing to B^0-$\bar{B}^0$ oscillations in the Standard Model. The dominant contributions stem from the diagrams with two top quarks.

Finally, the relations of these form factors to f_+ and f_0 are given by

$$f_+(q^2) = \frac{\sqrt{m_B}}{2}\left[\left(1 - \frac{E_\pi}{m_B}\right) h_\perp(E_\pi) + \frac{1}{m_B} h_\parallel(E_\pi)\right] , \tag{2.151}$$

$$f_0(q^2) = \frac{m_B^{3/2}}{m_B^2 - m_\pi^2}\left[\left(1 - \frac{E_\pi}{m_\mathrm{B}}\right) h_\parallel(E_\pi) + \frac{E_\pi^2 - m_\pi^2}{m_B} h_\perp(E_\pi)\right] . \tag{2.152}$$

From these equations, it is clear that f_+ is dominated by $h_\perp$ for small pion energies, whereas f_0 is dominated by $h_\parallel$. It is this energy range in which lattice simulations of the form factors can be performed. The Flavour Lattice Averaging Group (FLAG) has carried out a global fit combining three different $n_f = 2 + 1$ lattice results [133–135] for the form factors and experimental results of the BaBar and Belle experiments [136–139] for the differential decay width. The result is given by [127]

$$|V_{ub}| = (3.74 \pm 0.17) \cdot 10^{-3} . \tag{2.153}$$

In contrast to this determination of $|V_{ub}|$ using an exclusive decay (i.e. with a fixed final state hadron), one can also try to extract the value of the CKM matrix element from the inclusive differential decay rate $B \to X_u \ell \nu$, where X_u is any final state hadron with an up quark. The result given by the Particle Data Group is [6]

$$|V_{ub}| = (4.13 \pm 0.12_{\mathrm{exp}} \underset{\mathrm{theo}}{\overset{+0.13}{-0.14}} \pm 0.18_{\Delta\mathrm{model}}) \cdot 10^{-3} . \tag{2.154}$$

This is in a slight $1.3\,\sigma$ tension with the result cited above. It is an open question if this discrepancy is due to underestimated systematic errors or if unknown new particles contribute differently to the exclusive and inclusive decay widths. One of the systematic errors which should be considered is the excited states contamination of lattice correlators introduced in Sec. 2.2.1. An analysis of those will be carried out in Sec. 5.2. A more recent computation [140], which will play a role later on in this work, finds

$$|V_{ub}| = (3.93 \pm 0.41) \cdot 10^{-3} , \tag{2.155}$$

which is in agreement with the result from inclusive decays.

2.4.3. B^0-$\bar{B}^0$ Oscillations

Another class of processes in which CKM matrix elements show up naturally are neutral meson oscillations. This means that a meson of quark content $q_1\bar{q}_2$ transforms into its anti-particle $q_2\bar{q}_1$ and vice versa via the weak interactions. In the following, the mixing of B^0 mesons

with valence quark content $d\bar{b}$ and $\bar{B}^0$ mesons with quark content $b\bar{d}$ will be considered. In the Standard Model, the set of box diagrams shown in Fig. 2.4 mediates this process. It is convenient to consider this process in an effective theory with a 2×2 Hamiltonian [141]. Since B mesons can also decay, this Hamiltonian is not unitary and is written in the generic form

$$H \begin{pmatrix} B^0 \\ \bar{B}^0 \end{pmatrix} = \begin{pmatrix} M - \frac{\mathrm{i}}{2}\Gamma & M_{12} - \frac{\mathrm{i}}{2}\Gamma_{12} \\ M_{12}^* - \frac{\mathrm{i}}{2}\Gamma_{12}^* & M - \frac{\mathrm{i}}{2}\Gamma \end{pmatrix} \begin{pmatrix} B^0 \\ \bar{B}^0 \end{pmatrix} . \tag{2.156}$$

The presence of M_{12} and Γ_{12} signifies the mixing of the two states. The mass and decay width eigenvalues can be found by diagonalising the Hamiltonian and leads to the in general non-degenerate result

$$M_{\mathrm{H,L}} = M \pm \mathfrak{Re} \left\{ \sqrt{\left(M_{12} - \tfrac{\mathrm{i}}{2}\Gamma_{12}\right)\left(M_{12}^* - \tfrac{\mathrm{i}}{2}\Gamma_{12}^*\right)} \right\} , \tag{2.157}$$

$$\Gamma_{\mathrm{H,L}} = \Gamma \mp 2\mathfrak{Im} \left\{ \sqrt{\left(M_{12} - \tfrac{\mathrm{i}}{2}\Gamma_{12}\right)\left(M_{12}^* - \tfrac{\mathrm{i}}{2}\Gamma_{12}^*\right)} \right\} . \tag{2.158}$$

The mass difference ΔM is then evidently two times the real part of the square root. As it turns out, one has the following approximations in the B system [141]

$$\Delta\Gamma \ll \Delta M , \qquad \Delta M \approx 2\,|M_{12}| . \tag{2.159}$$

The mass difference can be measured in experiments: neglecting CP violating effects, the probability for an initially pure B^0 state for staying in this state (index $+$) or for oscillating into a $\bar{B}^0$ state (index $-$) as a function of time t is given by [6]

$$|g_\pm(t)|^2 = \frac{e^{-\Gamma t}}{2} \left[\cosh\left(\frac{\Delta\Gamma}{2} t\right) \pm \cos\left(\Delta M t\right) \right] . \tag{2.160}$$

The oscillation due to the cosine can be measured in experiments and today's best value is [6]

$$\Delta M = (0.5065 \pm 0.0019)\,\mathrm{ps}^{-1} . \tag{2.161}$$

On the theory side, it is useful to apply an effective theory. For energies below the top quark and W boson mass, the box diagrams can be replaced by an effective four fermion coupling. The effective Hamiltonian, which can be identified with the off-diagonal entries of the matrix in Eq. (2.156), is of the form [142, 143]

$$H^{|\Delta B=2|} = \frac{G_{\mathrm{F}}^2 m_W^2}{16\pi^2} C(m_c, m_t, m_W)\, \mathcal{O} + \text{h.c.} , \tag{2.162}$$

$$\mathcal{O} = [\bar{b}\gamma^\mu(\mathbb{1} - \gamma_5)d][\bar{b}\gamma_\mu(\mathbb{1} - \gamma_5)d] , \tag{2.163}$$

where C is a Wilson coefficient which is a function of the masses of the particles which can propagate in the box diagrams (the up quark is taken massless), and also depends on CKM matrix elements. It turns out that only the contribution from the top quark is relevant, and to a very good approximation one finds for the mass difference

$$\Delta M = \frac{G_{\mathrm{F}}^2 m_W^2 m_B \eta_B f_B^2 \hat{B}_d}{6\pi^2} S_0\left(\frac{m_t^2}{m_W^2}\right) |V_{td}V_{tb}|^2 . \tag{2.164}$$

$m_W = 80.377(12)\,\mathrm{GeV}$ [6] is the mass of the W boson. The function $S_0(x)$ is one of the Inami-Lim functions [144] (in the conventions of [145])

$$S_0(x) = x\left[\frac{1}{4} + \frac{9}{4}\frac{1}{1-x} - \frac{3}{2}\frac{1}{(1-x)^2}\right] + \frac{3}{2}\frac{x^3}{(x-1)^3}\log x . \tag{2.165}$$

These functions account for purely electroweak loop corrections. On the other hand, η_B represents QCD corrections which were computed in [142]. Finally, $\hat{B}_d$ is the RGI bag parameter defined in terms of the matrix element

$$\left\langle \bar{B}^0 \middle| \mathcal{O} \middle| B^0 \right\rangle = \frac{8}{3} f_B^2 m_B^2 B_d \,, \tag{2.166}$$

and the RGI parameter can be obtained by multiplying by a function φ_{B_d} which is of the same form as the one defined in Eq. (2.20) for RGI currents. This parameter has been computed in four-flavour QCD with result [146]

$$\hat{B}_d = 1.222 \pm 0.061 \,. \tag{2.167}$$

In the same reference, this value was used to determine $|V_{td}|$ by using $|V_{tb}| = 0.999$ from a previous fit result:

$$|V_{td}| = 0.00867 \pm 0.00023 \,. \tag{2.168}$$

The matrix element in Eq. (2.166) can be computed in HQET by matching the operator (2.163) to operators involving heavy quarks. At leading order in the $1/m_b$ expansion, one finds the two operators

$$\mathcal{O}_{\mathrm{L}} = [Q^\dagger \gamma^\mu (\mathbb{1} - \gamma_5) d][\tilde{Q} \gamma_\mu (\mathbb{1} - \gamma_5) d] \,, \tag{2.169}$$

$$\mathcal{O}_{\mathrm{S}} = [Q^\dagger (\mathbb{1} - \gamma_5) d][\tilde{Q} (\mathbb{1} - \gamma_5) d] \,. \tag{2.170}$$

As a reminder, $\tilde{Q} = -\tilde{Q}\gamma_4$ is the operator creating a heavy anti-quark. The matching is performed at the scale $\mu = m_b$ and reads schematically

$$\mathcal{O}(m_b) = C_{\mathrm{L}}(\alpha_s(m_b))\, \mathcal{O}_{\mathrm{L}}(m_b) + C_{\mathrm{S}}(\alpha_s(m_b))\, \mathcal{O}_{\mathrm{S}}(m_b) + \dots \,, \tag{2.171}$$

with the matching coefficient C_{L} starting at order 1, whereas C_{S} starts at order α_s. A NNLO computation of them can be found in [147, 148].

In [149], it was first shown systematically using symmetry arguments that in the static limit $\mathcal{O}_{\mathrm{L}}$ and $\mathcal{O}_{\mathrm{S}}$ are the only operators contributing to the B^0-$\bar{B}^0$ matrix elements as long as chiral symmetry is respected. Furthermore, they mix under renormalisation. In Sec. 5.3, the B^0-$\bar{B}^0$ oscillation matrix elements and their excited states contamination will be computed in HM ChPT using RGI invariant operators, and it is therefore necessary to find operators which renormalise independently. In the continuum and for lattice regularisations which preserve chiral symmetry, the operators

$$O_{\mathrm{L}} = \mathcal{O}_{\mathrm{L}} \,, \tag{2.172}$$

$$O_{\mathrm{M}} = \mathcal{O}_{\mathrm{L}} + 4\mathcal{O}_{\mathrm{S}} \,, \tag{2.173}$$

renormalise multiplicatively. Their anomalous dimension, which is required for constructing the RGI operators, read at LO [149–151]

$$\gamma_{\mathrm{L}}^{(0)} = -\frac{8}{(4\pi)^2} \,, \tag{2.174}$$

$$\gamma_{\mathrm{M}}^{(0)} = -\frac{8}{3(4\pi)^2} \,. \tag{2.175}$$

3. Chiral Perturbation Theory

The large coupling of QCD at low energies prevents the computation of soft processes in perturbation theory. As an alternative, an effective field theory can be used which describes the interactions of the low energy degrees of freedom. In QCD, these particles are the pions and the effective field theory put forward by Weinberg, Gasser, and Leutwyler is known as Chiral Perturbation Theory [14–16]. As the name suggests, it is based on the chiral symmetry discussed in Sec. 2.1.1. This chapter will give an overview of the most important concepts of ChPT and will also consider generalisations to theories involving heavy mesons. A comprehensive book on ChPT is [49] which was used as a guidance for the following section.

3.1. Basics of Chiral Perturbation Theory

It has already been discussed in Sec. 2.1.1 that the global chiral symmetry $\mathrm{SU}(n_f)_\mathrm{L}\times\mathrm{SU}(n_f)_\mathrm{R}$ of massless QCD with n_f flavours is broken spontaneously by a non-zero quark condensate $\langle\bar{q}q\rangle$. Goldstone's theorem then implies that n_f^2-1 massless spin 0 particles appear in the spectrum of the theory. In reality, the non-zero quark masses break chiral symmetry explicitly, and the Goldstone bosons acquire a non-zero mass. Nonetheless, the pions (and to a certain degree the kaons and the eta meson) are considerably lighter than other hadronic particles. This mass gap justifies the assumption that low energetic QCD processes are dominated by pion physics. Chiral Perturbation Theory is the low energy effective theory of QCD which describes the interactions of these particles. Like many other effective theories, it has an infinite number of interaction terms, which are arranged according to the number of derivatives and, as will be shown later, powers of the particle masses. This entails an expansion of physical observables in powers of the small dimensionless ratios p^2/Λ_χ^2 and m_π^2/Λ_χ^2 with the chiral symmetry breaking scale Λ_χ which will be defined below. Weinberg conjectured [14] that in order to derive the Lagrangian of an EFT one has to write down all possible terms built out of the low energy degrees of freedom which respect the symmetries of the UV theory in order to obtain the most general result for any physical observable from it. The symmetries do not include the $\mathrm{SU}(3)_\mathrm{C}$ gauge group, since pions are colour neutral bound states. The relevant symmetry is, as the name of the theory suggests, the chiral symmetry group. Leutwyler later argued [152] that the relation

$$\frac{1}{\mathcal{Z}_\mathrm{QCD}[0]}\mathcal{Z}_\mathrm{QCD}[s,p,v_\mu,a_\mu]=\left\langle 0\middle|e^{-S_\mathrm{ext}[s,p,v_\mu,a_\mu]}\middle|0\right\rangle \doteq \frac{1}{\mathcal{Z}_\mathrm{ChPT}[0]}\mathcal{Z}_\mathrm{ChPT}[s,p,v_\mu,a_\mu] \tag{3.1}$$

between the generating functionals of QCD and ChPT in the presence of external fields holds true at low energies. The external fields s, p, v_μ, and a_μ were introduced in Sec. 2.1.1 and are the same in QCD and ChPT. This in turn automatically guarantees that the chiral Ward identities are also satisfied in the effective theory due to the external field method described at the end of Sec. 2.1.1.

As a first step in constructing the effective theory, one has to establish the transformation of the particles under the chiral symmetry group, the full group and the subgroup which is left unbroken after spontaneous symmetry breaking. A key aspect of ChPT is the non-linear realisation of the chiral symmetry group $\mathrm{SU}(n_f)_\mathrm{L}\times\mathrm{SU}(n_f)_\mathrm{R}$ (the U(1) symmetries will be of no interest here). In the framework of Coleman, Callan, Wess, and Zumino (CCWZ) [153, 154],

the Goldstone bosons of a symmetry breaking scheme G $\to$ H are interpreted as coordinates along the direction of the broken generators on the group manifold. A broken generator is defined to be an element of the full group G (here the chiral group), but not the unbroken subgroup H ($\mathrm{SU}(n_f)_\mathrm{V}$). These particles transform non-linearly under the full symmetry group but linearly under the unbroken subgroup and are given by an exponential

$$U(x) = e^{\frac{2\mathrm{i}}{f}\pi(x)}\,, \qquad \pi(x) = \pi^a(x)T^a\,, \tag{3.2}$$

where in the case of chiral symmetry the T^as are generators of $\mathrm{SU}(n_f)$ and f is the chiral limit of the pion decay constant. Eqs. (A.2) and (A.36) in App. A show the pion matrix for the cases $n_f = 2$ and $n_f = 3$. U is thus an element of the coset space $\mathrm{SU}(n_f)_\mathrm{L}\times\mathrm{SU}(n_f)_\mathrm{R}/\mathrm{SU}(n_f)_\mathrm{V}$. In this work, the particles π^a will be generically called pions ($a = 1, 2, 3$), but could in principle also include the kaons ($a = 4, 5, 6, 7$) and the eta meson ($a = 8$ if the mixing with π^0 is neglected). Under the full chiral symmetry group, U transforms as

$$U(x) \to LU(x)R^\dagger\,, \tag{3.3}$$

where L and R are $\mathrm{SU}(n_f)_\mathrm{L}$ and $\mathrm{SU}(n_f)_\mathrm{R}$ matrices, respectively. The unbroken subgroup consists of the elements $L = R = V$ and the transformation law of the pions under vector transformations is therefore given by

$$\pi \to V\pi V^\dagger\,. \tag{3.4}$$

Chiral symmetry is a global symmetry, so the matrices L and R are not functions of x. It is however convenient to construct a Lagrangian which is invariant under local chiral symmetry transformations since, as was shown in Sec. 2.1.1, the external fields, which then have to be introduced, can act as sources for the conserved global currents and can be used for reproducing the chiral Ward identities of QCD. The transformation of the external particles were given in Eqs. (2.46)–(2.49) and these transformations determine how the fields can be coupled to U. The external vector fields l_μ and r_μ are needed for a covariant transformation of derivatives of the pions. Using their explicit transformation behaviour, one can check that the following expressions are indeed covariant derivatives:

$$D_\mu U(x) \equiv \partial_\mu U(x) - \mathrm{i}l_\mu U(x) + \mathrm{i}U(x)r_\mu \to L(x)D_\mu U(x)R^\dagger(x)\,, \tag{3.5}$$

$$D_\mu U^\dagger(x) \equiv \partial_\mu U^\dagger(x) - \mathrm{i}r_\mu U^\dagger(x) + \mathrm{i}U^\dagger(x)l_\mu \to R(x)D_\mu U^\dagger(x)L^\dagger(x)\,. \tag{3.6}$$

Since ChPT is an expansion in p^2/Λ_χ^2 and D_μ turns into the particle's momentum after transforming to Fourier space, the number of derivatives can be used to order the terms in the Lagrangian according to their chiral dimension, i.e. powers of p/Λ_χ. Using the covariant derivative as well as the external scalar and pseudoscalar field, one can write down the most general Lagrangian at order $\mathcal{O}(p^2)$ in the chiral expansion (for higher orders, one also needs the field strength tensor of the external vector fields) which is invariant under local symmetry transformations [15, 16]:

$$\mathcal{L}_\pi^{(2)} = \frac{f^2}{4}\mathrm{Tr}\left[D_\mu U D_\mu U^\dagger\right] - \frac{Bf^2}{2}\mathrm{Tr}\left[U(s+\mathrm{i}p) + (s-\mathrm{i}p)U^\dagger\right]\,. \tag{3.7}$$

The relative sign in the second term is chosen so that the term is invariant under parity. Its inclusion in the order p^2 Lagrangian will be explained below. Expanding the first term in powers of π^a and evaluating the trace over the flavour indices, one arrives at

$$\mathcal{L}_\mathrm{kin} = \frac{1}{2}\partial_\mu\pi^a\partial_\mu\pi^a + \dots\,, \tag{3.8}$$

which is the canonically normalised kinetic term of the pions and justifies the prefactor of the term. Expanding U to higher powers in the pion fields will yield interaction vertices with an arbitrary but even number of fields.

The significance of the second term in the Lagrangian is the following: in QCD, one can set the external scalar field s equal to the quark mass matrix which introduces an explicit breaking of chiral symmetry. Since the external fields are the same in the generating functionals of QCD and ChPT, see Eq. (3.1), one can also set $s = M_q$ in ChPT to obtain massive quarks and an explicit breaking of chiral symmetry. Indeed, expanding U to second order in the pion fields, one obtains

$$\mathcal{L}_m = \text{const.} + 2B\pi^a\pi^b \text{Tr}\left[M_q T^a T^b\right] + \dots \,, \tag{3.9}$$

where the ellipsis denote interaction vertices for the pions. This leads to the following pseudo-Goldstone boson masses in the case of isospin symmetry, i.e. $m_u = m_d \equiv m_l$:

$$m_\pi^2 = 2Bm_l \,, \tag{3.10}$$

$$m_K^2 = B(m_l + m_s) \,, \tag{3.11}$$

$$m_\eta^2 = \frac{2}{3}B(m_l + 2m_s) \,. \tag{3.12}$$

This also justifies the inclusion of this term in the order p^2 Lagrangian: the relativistic energy momentum relation puts m_π on an equal footing with p and they therefore should be treated as terms of the same order in the chiral expansion. The above result for the pseudo-Goldstone boson masses shows that their square is a linear function of the quark masses, and one can therefore infer that s and thus also the quark mass matrix is of order p^2.

The second term in the Lagrangian comes with a new low energy constant, B. Its physical interpretation can be deduced by making use of the generating functional with only s non-zero: taking the derivative of the QCD functional w.r.t. s^0 and setting $s = 0$ afterwards leads to

$$\frac{1}{\mathcal{Z}_{\text{QCD}}[0]} \frac{\delta \mathcal{Z}_{\text{QCD}}[s]}{\delta s^0}\bigg|_{s=0} = -\langle 0|\bar{q}q|0\rangle \,. \tag{3.13}$$

For a regularisation which preserves chiral symmetry, the condensate only needs a multiplicative renormalisation constant. This calculation can be repeated in the effective theory and the result reads

$$\frac{1}{\mathcal{Z}_{\text{ChPT}}[0]} \frac{\delta \mathcal{Z}_{\text{ChPT}}[s]}{\delta s^0}\bigg|_{s=0} = n_f B f^2 \,, \tag{3.14}$$

where again only a multiplicative renormalisation constant is needed. It is therefore evident that $\langle 0|\bar{q}q|0\rangle$ is proportional to B for massless quarks. For non-zero quark masses, one needs to take into account an additive renormalisation and the result in the effective theory is augmented by higher order mass corrections.

Combining the result for the kinetic and mass term of the pions shows that they satisfy the Klein Gordon equation. The propagator of the free theory can therefore be obtained by the usual methods of QFTs. For later convenience, the result is presented in a finite spatial volume of size L^3 and an infinite time extent:

$$\left\langle \pi^a(\vec{x},t)\pi^b(\vec{y},t')\right\rangle = \delta^{ab} \sum_{\vec{p}} \frac{e^{\mathrm{i}\vec{p}(\vec{x}-\vec{y})}}{2E_{\pi,\vec{p}}} e^{-E_{\pi,\vec{p}}|t-t'|} \,. \tag{3.15}$$

The energy is given by the relativistic expression

$$E_{\pi,\vec{p}} = \sqrt{\vec{p}^{\,2} + m_\pi^2} \,. \tag{3.16}$$

A significant feature of effective field theories is so-called power counting: the results are given by a power series in a small, dimensionless parameter δ. Chiral Perturbation Theory is no exception to this. Computing S matrix elements or correlation functions in ChPT, one finds that the results are given by a power series in the external momenta p and the particle masses m_i divided by $4\pi f \equiv \Lambda_\chi \sim 1\,\mathrm{GeV}$. This series can of course only be computed to a given order in the expansion parameter, and this order determines the accuracy of the resulting predictions. Weinberg's power counting scheme [155] can be used to figure out which Feynman diagrams contribute to a given order in the chiral expansion:

$$D = 2 + \sum_d N_d(d-2) + 2N_\mathrm{L}\,. \tag{3.17}$$

Here, D is the chiral dimension of the diagram which will then be of order $(p/\Lambda_\chi)^D$, N_L is the number of loops in the diagram, and N_d the number of interaction vertices stemming from the Lagrangian of order p^d. D can thus be used to estimate the importance of individual diagrams: diagrams with lower D will be dominant whereas those with larger D will be suppressed.

This is also tightly connected with renormalisability: ChPT is a theory with an infinite number of terms in the Lagrangian (one can write down terms with any even number of derivatives and any number of quark mass insertions) and consequently infinitely many low energy constants which have to be renormalised. For example the NLO ChPT Lagrangian by Gasser and Leutwyler [16], which is of order $\mathcal{O}(p^4)$, introduces ten new LECs L_i (and two H_i which multiply only external fields) for $n_f = 3$, and the number increases dramatically at higher orders. On the other hand, if e.g. a matrix element is computed to only a fixed order in the expansion parameter, only a finite number of interaction terms of the Lagrangian and thus a finite number N of LECs will contribute to it. This finite number of LECs can be renormalised by matching N conveniently chosen observables calculated in ChPT to experimental or lattice results. If this can be carried out for all low energy constants of the Lagrangian up to a fixed order in p^2, one has renormalised the theory to that given order and can then compute any other observable to that order in ChPT. The power counting formula in Eq. (3.17) can be used to establish which diagrams have to be computed to do this.

So far, only the effective theory for the lightest bound states of QCD has been considered. The interactions of these particles with the lightest nucleons can also be described in ChPT [17, 18]. The applications of this theory in lattice field theory are numerous. For one thing, lattice simulations are oftentimes not performed with physical quark masses, but one instead inter- and extrapolates the results of several simulations with different m_qs to the physical point. The inter-/extrapolation formulae are derived in ChPT. Furthermore, in the spirit of Symanzik's effective theory one can include a non-zero lattice spacing in the ChPT Lagrangian [156–158] and examine how lattice results are affected by discretisation effects. A rather recent development is the computation of the excited states contamination of lattice correlation functions. This has been applied to several Nucleon observables in [19–26]. The aim of this thesis is to transfer this idea to the excited states contamination of heavy meson correlation functions. In order to do this, one first needs an effective theory which also includes mesons with a heavy quark. This will be presented in the next section.

3.2. Heavy Meson Chiral Perturbation Theory

It was pointed out in the previous section that the mesons of chiral perturbation theory are treated as the pseudo-Goldstone bosons of the spontaneous breaking of the approximate chiral symmetry of QCD. This demands that the quark masses need to be, in some sense, small which translated to dimensionless small parameters m_i/Λ_χ where the m_is are the pion masses.

If one wants to describe interactions between these pions and heavy mesons, like D or B mesons, which contain a charm or bottom quark, respectively, ChPT has to be modified to accommodate for the new heavy particles. The simple reason is that the charm and bottom quark masses are in a certain sense to large to be treated as a small perturbation to a massless theory with a global chiral symmetry. In ChPT, this amounts to the fact that the dimensionless parameters m_B/Λ_χ and m_D/Λ_χ are not smaller than 1 and can thus not be used as expansion parameters. This poses a problem, since theoretical predictions for processes like semileptonic decays of B mesons ($B \to \pi \ell \bar{\nu}_l$) at low energies are then not possible in ChPT.

This problem is reminiscent of lattice simulations with a bottom quark: the physical mass of the bottom quark is too large to be simulated with computer clusters in use today, see the discussion below Eq. (2.72). A possible way out is to use an effective theory in which the inverse bottom quark mass is used as an expansion parameter. Heavy Meson Chiral Perturbation Theory [27–30] takes a similar route: it is an effective theory for heavy mesons in which, besides the momentum and small pion masses, the inverse of the heavy meson mass is used as an expansion parameter. There is even more to be learned from HQET: in the static limit, i.e. in the theory without heavy quark mass corrections, the HQET Lagrangian is invariant under local flavour number and heavy quark spin transformations. Since the heavy meson is a bound state of a heavy and a light quark, $Q\bar{q}$, HM ChPT must also respect these symmetries when all meson mass corrections are neglected. The consequences of the latter of the two symmetries have already been worked out in Sec. 2.3: the pseudoscalar and the vector meson transform into each other under HQS transformations. It is thus necessary to introduce fields $P^{(Q)}$ and $P_\mu^{(Q)*}$ which destroy heavy pseudoscalars and vector mesons with a heavy quark Q. They do not create the respective anti-particles for the same reason that the field Q in HQET does not create a heavy anti-quark. It is then convenient to introduce a superfield $H^{(Q)}$ which incorporates the two fields and also has an easy transformation behaviour under the various symmetries of the theory. This makes it easier to construct the Lagrangian of the theory, in which the heavy mesons interact with the light pseudo-Goldstone bosons of chiral symmetry breaking.

The field $H^{(Q)}$ is defined as [159] (the overall phase of the field differs in the reference, but it has no physical significance)

$$H_f^{(Q)} = P_+ \left[\mathrm{i}\gamma_\mu P_{f,\mu}^{(Q)*} + \mathrm{i}\gamma_5 P_f^{(Q)} \right] , \tag{3.18}$$

$$\bar{H}_f^{(Q)} = \gamma_4 H_f^{(Q)\dagger} \gamma_4 = \left[\mathrm{i}\gamma_\mu P_{f,\mu}^{(Q)*\dagger} + \mathrm{i}\gamma_5 P_f^{(Q)\dagger} \right] P_+ . \tag{3.19}$$

In the following, $H^{(Q)}$ is assumed to be a row vector in flavour space and the light flavour index f will be suppressed. Furthermore, as long as no anti-particles $H^{(\bar{Q})}$ are considered, it is convenient to set $H^{(Q)} \equiv H$. The theory here is defined in the rest frame of the heavy meson. The projector P_+ was defined in Eq. (2.103) in the rest frame of the heavy quark. Its presence is required by the constraint $\gamma_4 Q = Q$ and the interpretation of the heavy meson as a bound state of the form $Q\bar{q}$. An explicit calculation shows that

$$H = \gamma_4 H = -H\gamma_4 . \tag{3.20}$$

In the static theory, the heavy vector meson furthermore satisfies the constraint

$$P_4^* = 0 \tag{3.21}$$

in the rest frame of the heavy particles [160, 161]. The fields for the pseudoscalar and vector meson can be recovered by computing the trace of H with an appropriate gamma matrix insertion:

$$\mathrm{Tr}\left[H\gamma_5\right] = 2\mathrm{i}P , \qquad \mathrm{Tr}\left[H\gamma_k\right] = 2\mathrm{i}P_k^* . \tag{3.22}$$

But it is often more convenient to use H because it has an easy transformation behaviour under a general HQS transformation $\mathcal{S}$:

$$H \to \mathcal{S}H\,, \qquad \bar{H} \to \bar{H}\mathcal{S}^{-1}\,. \tag{3.23}$$

The construction of the Lagrangian in the static limit in which HQS is a good symmetry is then simplified by using H instead of P and P_k^*.

The heavy quarks in static HQET are moreover equipped with LFN symmetry, see Eq. (2.107). The pseduoscalar and vector mesons of HQET are bound states of a heavy quark and a light anti-quark, $Q\bar{q}$, and one therefore has

$$H \to e^{\mathrm{i}f(\vec{x})}H\,. \tag{3.24}$$

The last relevant symmetry under which the heavy mesons transform is chiral symmetry. The light anti-quark $\bar{q}$ contains both a left- and a right-handed piece and a straightforward transformation using the matrices L and R of $\mathrm{SU}(n_f)_\mathrm{L}$ and $\mathrm{SU}(n_f)_\mathrm{R}$ is not possible. Instead, it is convenient to use the so called *compensator field* $h[\pi(x)]$ of the CCWZ construction which is a function of the pseudo-Goldstone bosons and thus also of the spacetime coordinates. It naturally shows up in the transformation of the matrix square root of the pion field U:

$$\sqrt{U} \equiv u = e^{\mathrm{i}\frac{\pi}{f}} \to Luh^\dagger = huR^\dagger\,. \tag{3.25}$$

One then defines the transformation of the heavy fields under a chiral symmetry as

$$H \to Hh^\dagger, \qquad \bar{H} \to h\bar{H}\,, \tag{3.26}$$

which also holds for the operators P and P_k^* and their adjoints. The introduction of h complicates things a bit: since it depends on the spacetime coordinates, one needs to define a connection so that derivatives transform covariantly under chiral transformations. It will be useful to also include the external fields l_μ and r_μ which were already encountered in Sec. 2.1.1:

$$\Gamma_\mu = \frac{\mathrm{i}}{2}\left(u^\dagger(\partial_\mu - \mathrm{i}l_\mu)u + u(\partial_\mu - \mathrm{i}r_\mu)u^\dagger\right)\,. \tag{3.27}$$

The covariant derivative of H and $\bar{H}$ is then given by

$$D_\mu H = \partial_\mu H + \mathrm{i}H\Gamma_\mu\,, \qquad D_\mu\bar{H} = \partial_\mu\bar{H} - \mathrm{i}\Gamma_\mu\bar{H}\,. \tag{3.28}$$

Note that Γ_μ is a matrix in flavour space and the above equations should be interpreted as vector matrix multiplications. Besides the symmetric combination of derivatives of u, there also exists the antisymmetric combination which has the simple transformation behaviour

$$u_\mu = \frac{\mathrm{i}}{2}\left(u^\dagger(\partial_\mu - \mathrm{i}l_\mu)u - u(\partial_\mu - \mathrm{i}r_\mu)u^\dagger\right) \to hu_\mu h^\dagger\,. \tag{3.29}$$

With these building blocks, it is possible to write down the leading order Lagrangian for HM ChPT in the rest frame of the heavy mesons and in the static limit:

$$\begin{aligned}\mathcal{L}_H^{(1)} &= -\mathrm{Tr}\left[D_4 H\bar{H}\right] - \mathrm{i}g\mathrm{Tr}\left[H\gamma_5\gamma_\mu u_\mu\bar{H}\right]\\ &= 2D_4PP^\dagger + 2D_4P_k^*P_k^{*\dagger} + 2\mathrm{i}gPu_kP_k^{*\dagger} - 2\mathrm{i}gP_k^*u_kP^\dagger - 2\mathrm{i}g\,\varepsilon_{klm}P_k^*u_lP_m^{*\dagger}\,,\end{aligned} \tag{3.30}$$

where the shorthand notation $\varepsilon_{klm} \equiv \varepsilon_{klm4}$ with $\varepsilon_{1234} = +1$ is used. Some more comments are in order: for one thing the kinetic term looks the same as the one for the heavy quarks in HQET, i.e. the mesons have the unusual mass dimension 3/2. As shown in [29], this can be

traced back to the relation of the operators in the effective theory and relativistic operators describing heavy mesons. The relativistic operators are multiplied by a factor $\sqrt{m_B}$ and this also explains the factor of $\sqrt{m_B}$ in the definition of HQET/HM ChPT states in Eq. (2.129). For another thing, local flavour number conservation forbids any derivative with spatial indices, D_k, acting on the heavy meson fields. Furthermore, one could have added a mass term, but it can be neglected for the same reason as for the heavy quarks: it always leads to a trivial exponential dependence of the correlation functions on the heavy meson mass, so it will be neglected in this work (in general, a mass counterterm is still needed). Additionally, from the Lagrangian involving H and $\bar{H}$ it is clear that it is invariant under HQS transformations, this is not so easy to see from the terms with P and P_k^*. The implicit contraction of the flavour indices as well as the use of covariant derivatives ensures the invariance under chiral symmetry transformations. Finally, in contrast to the ChPT Lagrangian presented in Eq. (3.7), the above Lagrangian is of order p. The reason is that, since also a vector meson and implicitly the four-velocity v of the heavy mesons can enter, one can contract derivatives with other open indices.

The Lagrangian contains only one low energy constant: g. Its physical interpretation is the following: the so-called $B^*B\pi$ coupling is defined by

$$\langle B|A_k|B^*\rangle = g_{B^*B\pi} = g + \dots\,, \tag{3.31}$$

where the ellipsis stand for higher order chiral and $1/m_B$ corrections and A_k is the light axial vector current. g is therefore the chiral and static limit value of the $B^*B\pi$ coupling constant. A preliminary result of an ongoing computation in $2+1$-flavour HQET sets its value at approximately $g = 0.49(1)$ [162]. The value and error estimate have been taken from Fig. 3 in the reference.

The propagators which are derived from the kinetic term of the Lagrangian read

$$\left\langle P(\vec{x},t)P^\dagger(\vec{y},t')\right\rangle = \frac{1}{2}\theta(t-t')\delta^{(3)}(\vec{x}-\vec{y})\,, \tag{3.32}$$

$$\left\langle P_k^*(\vec{x},t)P_l^{*\dagger}(\vec{y},t')\right\rangle = \frac{\delta_{kl}}{2}\theta(t-t')\delta^{(3)}(\vec{x}-\vec{y})\,. \tag{3.33}$$

The interpretation of this result is the following: the Dirac delta function fixes the heavy mesons to stay at the same point in space, hence the name static limit. The Heaviside function ensures that the particles propagate only forward in time, the reason being that the operators do not create/destroy the respective anti-particles.

The connection Γ_μ as well as the field u_μ can be expanded in powers of the pion field π and thus lead to interaction vertices of two heavy mesons and any number of pions. It turns out that Γ_μ contains only an even number of pions whereas u_μ only odd powers. The interaction terms stemming from the latter term are furthermore proportional to g. One has

$$\begin{aligned}\Gamma_\mu &= \frac{\mathrm{i}}{2f^2}[\pi,\partial_\mu\pi] + \mathcal{O}(\pi^4)\,,\\ u_\mu &= -\frac{\partial_\mu\pi}{f} + \mathcal{O}(\pi^3)\,.\end{aligned} \tag{3.34}$$

For reasons which will become apparent later, it is also convenient to define the sum and difference of u and its adjoint,

$$u^\pm = (u \pm u^\dagger)\,. \tag{3.35}$$

The NLO Lagrangian is of order p^2 and thus of the same order in the chiral expansion as the LO ChPT Lagrangian of the previous section. Considering only two light flavours, the NLO

Lagrangian is given by [163]

$$\mathcal{L}_H^{(2)} = d_1 \mathrm{Tr}\left[H u_\mu u_\mu \bar{H}\right] + d_2 \mathrm{Tr}\left[H u_4 u_4 \bar{H}\right] + \mathrm{i} d_3 \mathrm{Tr}\left[H u_\mu u_\nu \sigma_{\mu\nu} \bar{H}\right] + d_4 \mathrm{Tr}\left[H f^+_{\mu\nu} \sigma_{\mu\nu} \bar{H}\right]$$
$$+ d_5 \mathrm{Tr}\left[H \sigma_{\mu\nu} \bar{H}\right] \mathrm{Tr}\left[f^+_{\mu\nu}\right] + d_6 \mathrm{Tr}\left[H \chi_+ \bar{H}\right] + d_7 \mathrm{Tr}\left[H \bar{H}\right] \mathrm{Tr}\left[\chi_+\right] , \tag{3.36}$$

where the traces over $f^+_{\mu\nu}$ and χ_+ are over flavour indices only. The two are proportional to the external fields defined in Sec. 2.1.1,

$$f^+_{\mu\nu} = u^\dagger \left(\partial_\mu l_\nu - \partial_\nu l_\mu - \mathrm{i}[l_\mu, l_\nu]\right) u + u \left(\partial_\mu r_\nu - \partial_\nu r_\mu - \mathrm{i}[r_\mu, r_\nu]\right) u^\dagger ,$$
$$\chi_+ = 2B \left[u(s + \mathrm{i}p)u + u^\dagger (s - \mathrm{i}p) u^\dagger\right] . \tag{3.37}$$

It is then easy to see that, after setting $s = M_q$ and the other external fields to zero, the interaction vertices of the NLO Lagrangian couple two heavy mesons to an even number of pions only.

It is sometimes necessary to consider processes involving heavy mesons and their anti-particles, e.g. for B^0-$\bar{B}^0$ mixing introduced in Sec. 2.4.3. These are the heavy-light bound states of the heavy anti-quark $\tilde{Q}$ defined in Sec. 2.3 and a light quark field. In [164], it was outlined how to obtain the superfield $H^{(\bar{Q})}$ from $H^{(Q)}$ using charge conjugation. With the conventions used there, one has

$$H^{(\bar{Q})} = C(\mathcal{C} H^{(Q)} \mathcal{C}^{-1})^T C^{-1} = \left[\mathrm{i}\gamma_k P_k^{(\bar{Q})*} + \mathrm{i}\gamma_5 P^{(\bar{Q})}\right] P_- , \tag{3.38}$$

$$\bar{H}^{(\bar{Q})} = \gamma_4 H^{(\bar{Q})\dagger} \gamma_4 = P_- \left[\mathrm{i}\gamma_k P_k^{(\bar{Q})*\dagger} + \mathrm{i}\gamma_5 P^{(\bar{Q})\dagger}\right] , \tag{3.39}$$

with the charge conjugation operator $\mathcal{C}$ acting on the fields as

$$\mathcal{C} u \mathcal{C}^{-1} = u^T , \qquad \mathcal{C} P^{(Q)} \mathcal{C}^{-1} = P^{(\bar{Q})} , \qquad \mathcal{C} P_k^{(Q)*} \mathcal{C}^{-1} = -P_k^{(\bar{Q})*} , \tag{3.40}$$

and the charge conjugation matrix in the Dirac representation

$$C = \mathrm{i}\gamma_2 \gamma_4 . \tag{3.41}$$

The gamma matrices satisfy

$$C \gamma_\mu C^{-1} = -\gamma_\mu^{\mathrm{T}} \qquad C \gamma_5 C^{-1} = \gamma_5^{\mathrm{T}} . \tag{3.42}$$

The projector P_- was defined in Eq. (2.103). The transpose acts on the Dirac indices but also on the flavour indices, so $H^{(\bar{Q})}$ is a column vector in flavour space and an explicit flavour index f is suppressed. Under chiral and HQS transformations, the superfield transforms as

$$H^{(\bar{Q})} \to h H^{(\bar{Q})} \mathcal{S}^{-1} , \qquad \bar{H}^{(\bar{Q})} \to \mathcal{S} \bar{H}^{(\bar{Q})} h^\dagger , \tag{3.43}$$

whereas under LFN transformations one has

$$H^{(\bar{Q})} \to e^{-\mathrm{i} f'(\vec{x})} H^{(\bar{Q})} . \tag{3.44}$$

The HQS and LFN transformations follow from Eqs. (2.124) and (2.125). Applying charge conjugation to the LO Lagrangian of the field $H^{(Q)}$ in Eq. (3.30), one finds

$$\mathcal{L} = 2P^{(\bar{Q})\dagger} D_4 P^{(\bar{Q})} + 2P_k^{(\bar{Q})*\dagger} D_4 P_k^{(\bar{Q})*} - 2\mathrm{i}g P_k^{(\bar{Q})*\dagger} u_k P^{(\bar{Q})} + 2\mathrm{i}g P^{(\bar{Q})\dagger} u_k P_k^{(\bar{Q})*}$$
$$- 2\mathrm{i}g \varepsilon_{klm} P_m^{(\bar{Q})*\dagger} u_l P_k^{(\bar{Q})*} . \tag{3.45}$$

The propagators for the anti-mesons which follow from this Lagrangian are the same as the ones found for the mesons in Eqs. (3.32) and (3.33). Taking a closer look at the interaction vertices reveals that the terms coupling a pseudoscalar, a vector and an odd number of pions have changed signs. This implies that e.g. the $B^* B \pi$ coupling has the opposite sign of the $\bar{B}^* \bar{B} \pi$ coupling if one sets $Q = b$.

4. Excited States Contamination of Light and Heavy Meson Two-Point Functions

The two-point function of an interpolating field $\mathcal{O}_P$ contains important information of the states it interpolates. Most of the time, one is only interested in the ground state for which the energy (or mass for vanishing momentum) as well as the overlap of this state with the interpolating field can be extracted. In lattice QCD, one often uses quark bilinears as interpolators for mesonic states, e.g. $\bar{q}_1\gamma_5 q_2$ for pseudoscalars like pions. Two-point functions are also needed for the extraction of matrix elements, these can be obtained by taking suitable ratios of three-point functions with the two-point functions of the interpolating fields of the initial and final state particles, see Sec. 2.2.1.

In the notation of Eq. (2.79), the spectral decomposition of a two-point function is given by ($t > 0$)

$$C_2^P(t) = \sum_{\vec{x}} \left\langle \mathcal{O}_P(t,\vec{x})\mathcal{O}_P^\dagger(0,\vec{0})\right\rangle = \frac{\left|\left\langle 0\middle|\mathcal{O}_P\middle|P(\vec{0})\right\rangle\right|^2}{2m_P} e^{-m_P t} + \sum_{\alpha^i \neq P} \frac{1}{2E_{\alpha^i}} \left|\left\langle 0\middle|\mathcal{O}_P\middle|\alpha^i(\vec{0})\right\rangle\right|^2 e^{-E_{\alpha^i} t} \,. \tag{4.1}$$

As already explained in Sec. 2.2.1, it is then possible to define the so-called effective mass

$$m_{P,\mathrm{eff}}(t) = -\partial_t \log\left(C_2^P(t)\right) \approx m_P + \sum_i A_i e^{-\Delta E_i t} \,, \tag{4.2}$$

with the energy differences $\Delta E_i > 0$ of the ground state energy and the excited states energies, and the coefficients A_i are proportional to ratios of matrix elements. For large t, the contribution of the excited states becomes negligibly small, but on the other hand the signal-to-noise ratio in a lattice simulation decreases exponentially in time [98, 99]. At intermediate times, the excited states might give a non-negligible but hard to detect contribution, which can lead to a systematic error in the result for m_P. Computing the excited states contamination in ChPT can thus help to obtain reliable results for the masses of particles.

The effective mass can then be used to extract the matrix element Γ of the interpolating field between the ground state and the vacuum:

$$\Gamma^2(t) = 2m_{P,\mathrm{eff}}(t) C_2^P(t) e^{m_{P,\mathrm{eff}}(t)t} = |\langle 0|\mathcal{O}_P|P\rangle|^2 + \dots \,. \tag{4.3}$$

For local interpolating fields of the form $\bar{q}_1\gamma_5 q_2$, this matrix element is proportional to the decay constant of the meson that is interpolated by the field.

The next section lays out how the analogues of the heavy-light quark bilinears $\bar{q}\,\Gamma Q$, which were discussed in Sec. 2.3, can be constructed in HM ChPT. These will be used as interpolating fields for B mesons. Afterwards, the excited states contamination of the B meson two-point function will be computed in HM ChPT, and it will be investigated how it enters in the B meson effective mass and decay constant. Some of these results have already been presented in [116, 165]. Finally, the excited states contamination of the pion and kaon two-point functions will be discussed.

4.1. Heavy-Light Currents and Densities

The pseudoscalar density and axial vector current have the correct quantum numbers to excite pseudoscalar mesons from the vacuum. For the pions, they can be obtained directly from the ChPT Lagrangian by taking derivatives with respect to the external fields p^a and a^a_μ, respectively. For the heavy B mesons, this is not possible and one has to construct them 'by hand'. This is not so much of a problem in HM ChPT, since the high degree of symmetry of the theory in the static limit restricts the number of terms and also relates the LECs of the currents and densities. From the discussion in Sec. 2.3 it follows that it is sufficient to construct one of the six fields V_k, V_4, A_k, A_4, P, or S and the others are obtained by applying chiral and HQS transformations.

In ChPT, the currents and densities are given as a sum of terms which can be grouped according to their chiral dimension. In principle, HM ChPT also includes an expansion in inverse powers of the heavy meson mass, but these corrections will be neglected in this thesis. The main reason is the large energy difference of the chiral symmetry breaking scale $\Lambda_\chi \approx 1.2\,\text{GeV}$ and the B meson mass $m_B \approx 5\,\text{GeV}$. One can thus expect that the leading chiral corrections are way larger than the $1/m_B$ corrections. As an example, the heavy-light vector current V_k can therefore be written in the form

$$V_k = \sum_{i=0} V_k^{(i)}\,, \qquad\qquad V_k^{(i)} = \sum_j c_j^{(i)} V_k^{(i),j}\,, \tag{4.4}$$

where i is the chiral dimension of the terms. The $c_j^{(i)}$ are low energy constants which by naive power counting should scale like $1/\Lambda_\chi^i$ since they multiply terms of chiral dimension i. The individual terms $V_k^{(i),j}$ are products of the fields of HM ChPT which are coupled in such a way that they have the quantum numbers of the vector current $\bar{q}\gamma_k Q$. The chiral dimension of a term is given by the number of derivatives (order p) and insertions of the quark mass matrix (order p^2).

It has already been shown in Eq. (3.22) that computing the trace of H with either γ_5 or γ_k will result in the field of the pseudoscalar or vector meson, respectively. In complete analogy, the individual terms of the heavy-light vector current are of the form

$$V_k^{(i),j} = \text{Tr}\left[\mathcal{O}^{(i),j}\gamma_k\right]\,. \tag{4.5}$$

The task is then to find all possible, independent product of fields $\mathcal{O}^{(i),j}$ at a given order in the chiral expansion.

Terms without any derivatives or insertions of the quark mass matrix are of lowest order in the expansion and will be constructed here first. The starting point is the field H containing the fields for both pseudoscalar and vector mesons. This field has inherited the symmetry properties of the heavy quark, namely the transformation under HQS symmetry and LFN symmetry. But H does not transform in the same way as the HQET bilinears $\bar{q}\gamma_5 Q$ and $\bar{q}\gamma_k Q$ under chiral symmetry. The heavy-light currents are given by the sum or difference of a left- and right-handed piece, see Eq. (2.116). The field H and thus P and P_k^*, on the other hand, have a complicated transformation under chiral symmetry as it was shown in Eq. (3.26), and thus cannot by themself serve as the vector current or pseudoscalar density at LO. But the transformation of u in Eq. (3.25) shows that it and its adjoint can be coupled to H to give appropriate building blocks which transform as left- and right-handed fields:

$$Hu \to HuR^\dagger\,, \qquad\qquad Hu^\dagger \to Hu^\dagger L^\dagger\,. \tag{4.6}$$

One can then construct the interpolating fields by using linear combinations of the two terms above. But only the sum u^+ and difference u^- of u and $u^\dagger$, see Eq. (3.35) for their definition,

are parity eigenstates[1], a requirement that will be needed later on. Hu^- and Hu^+ are the only allowed products of fields at LO, insertions of u_μ, covariant derivatives or the quark mass matrix would increase the chiral dimension by at least one.

With these ingredients, the vector current V_k can be constructed at LO in the chiral expansion. The $\mathcal{O}^{(i),j}$s can also contain insertions of elements of the Clifford algebra, namely $\mathbb{1}$, γ_μ, γ_5, $\gamma_\mu\gamma_5$, and $\sigma_{\mu\nu}$. But it should be remembered at this point that HM ChPT is a non-relativistic theory, and Lorentz symmetry is broken. The three spatial coordinates are still connected by rotational symmetry, but the time direction should be treated separately. For this reason, the index μ should be broken up into the spatial components $k = 1, 2, 3$ and the time direction 4. Spatial indices k need to contracted, whereas the 4-index can appear without any restrictions in the formulae.[2] Due to Eq. (3.20), insertions of γ_4 are redundant and can be neglected. Taking these considerations into account, one is left with four candidate terms

$$\mathcal{O}^{(0),1} = Hu^+ \,, \qquad \mathcal{O}^{(0),2} = Hu^- \,, \tag{4.7}$$

$$\mathcal{O}^{(0),3} = Hu^+\gamma_5 \,, \qquad \mathcal{O}^{(0),4} = Hu^-\gamma_5 \,. \tag{4.8}$$

But the third and fourth term vanish identically when the projection of Eq. (4.5) is carried out. Of the first two, the second term has an incorrect transformation under parity transformations: the field u transforms into its adjoint and vice versa, so that $u^+ \to u^+$ and $u^- \to -u^-$, whereas H transforms as [119]

$$H \to \gamma_4 H \gamma_4 \,. \tag{4.9}$$

This means that the second term transforms as

$$V_k^{(0),2} \to \mathrm{Tr}\left[H(-u^-)\gamma_4\gamma_k\gamma_4\right] = \mathrm{Tr}\left[Hu^-\gamma_k\right] = V_k^{(0),2} \,, \tag{4.10}$$

which is incorrect for a spatial component of a vector, see Eq. (2.122). As one can check, $V_k^{(0),1}$ has the correct transformation behaviour. The vector current at leading order is then given by this term which needs to be multiplied by an at first unknown LEC α

$$V_k^{\mathrm{LO}} = \frac{-\mathrm{i}\alpha}{4}\mathrm{Tr}\left[Hu^+\gamma_k\right] = \frac{\alpha}{2}P_k^* u^+ = \alpha P_k^* + \dots \,. \tag{4.11}$$

For convenience, the superscript '(0)' was replaced by 'LO'. For the last part of the equation, u^+ was expanded to leading order in the pion fields, see Eq. (A.13).

In HQET, the interpolating field for the pseudoscalar density can be obtained by applying the HQS transformation defined in Eq. (2.111) on the $k = 3$ component, see Eq. (2.112). This must also be true in HM ChPT, and one can derive P in this way. Furthermore, the relation $A_4 = -P$ of HQET must also hold in the effective theory, and is now used to avoid confusing the pseudoscalar density with the field which destroys a heavy pseudoscalar meson. One finds

$$A_4^{\mathrm{LO}} = -U(\mathcal{S})V_3^{\mathrm{LO}}U^{-1}(\mathcal{S}) = \frac{\mathrm{i}\alpha}{4}\mathrm{Tr}\left[\mathcal{S}Hu^+\gamma_3\right] = \frac{\mathrm{i}\alpha}{4}\mathrm{Tr}\left[Hu^+\gamma_5\right] = -\frac{\alpha}{2}Pu^+ = -\alpha P + \dots \,. \tag{4.12}$$

Here, cyclicity of the trace was used to explicitly calculate the product $\gamma_3\mathcal{S}P_+ = \gamma_5 P_+$, where P_+ is the projector in the definition of the field H, see Eqs. (2.103) and (3.18).

[1] Parity transformations of the light mesons are given by $u \to u^\dagger$. This can be seen from the fact that the pions are pseudoscalars which transform as $\pi \to -\pi$ and the definition of u in Eq. (3.25).

[2] Using the 4-velocity $v = (\vec{0}, \mathrm{i})$ of the heavy meson in its rest frame, one can interpret these open indices as the contraction $f_4 = -\mathrm{i}f_\mu v_\mu$. Terms of the form $a_k b_k$ can then be interpreted as being projected on the subspace perpendicular to v_μ.

It is now possible to give a physical interpretation for the LEC α: in Eq. (2.136), the HQET decay constant $\hat{f}$ was defined. Computing the same matrix element in HM ChPT leads to

$$\left\langle 0 \middle| A_4^{\mathrm{LO}} \middle| B \right\rangle = -\alpha \,, \tag{4.13}$$

and one can identify α with the chiral limit value of the heavy meson decay constant in the static limit,

$$\alpha = \hat{f} \,. \tag{4.14}$$

In ChPT with two light flavours, $V_4 = S$ and A_k can be obtained by applying the special chiral transformation defined in Eq. (2.117). This transformation replaces Hu^+ with Hu^- and vice versa, so the result at leading order is

$$V_4^{\mathrm{LO}} = S = -\frac{\alpha}{2} P u^- = -\mathrm{i}\alpha P \frac{\pi}{f} + \dots \,, \qquad A_k^{\mathrm{LO}} = \frac{\alpha}{2} P_k^* u^- = \mathrm{i}\alpha P_k^* \frac{\pi}{f} + \dots \,. \tag{4.15}$$

At next-to-leading order in the chiral expansion, one has to add a term of order $\mathcal{O}(p)$. Some terms have been considered in [166], but a full derivation of the fields has not been given there. Since the quark mass matrix is already of order $\mathcal{O}(p^2)$, only terms with a single derivative can contribute at this order. In principle, there are three different classes of terms: terms which contain i) $D_\mu H$, ii) $D_\mu u$ or $D_\mu u^\dagger$, or iii) u_μ. But not all of them are allowed by the symmetries of the theory, others are redundant. For one thing, derivatives of the heavy meson can be neglected for the following two reasons: on the one hand, LFN conservation forbids derivatives of the heavy meson fields w.r.t. a spatial coordinate k. On the other hand, terms proportional to $D_4 H$ can be rewritten using the (matrix-valued) equation of motion following from the LO Lagrangian in Eq. (3.30)

$$D_4 H + \mathrm{i} g H u_\mu \gamma_5 \gamma_\mu = 0 \,. \tag{4.16}$$

This means one has effectively traded $D_4 H$ for a term proportional to u_μ which is of the same order in the chiral expansion. Contributions from the NLO Lagrangian in the equation of motion would yield terms with a larger chiral dimension and are thus dropped.

Another class of redundant terms are those with derivatives of the pion field, $D_\mu u$, since an explicit calculation reveals that

$$D_\mu u = -\mathrm{i} u_\mu u \,, \qquad D_\mu u^\dagger = \mathrm{i} u_\mu u^\dagger \,. \tag{4.17}$$

It is therefore only necessary to find all possible terms involving u_μ to get the NLO expression for the heavy-light currents. Since the trace over the flavour indices vanishes, $\mathrm{Tr}\,[u_\mu] = 0$, only terms of the form $H u_\mu u^\pm$ can enter the result. Demanding again the correct transformation under parity and neglecting terms which vanish after evaluating the trace over the Dirac matrices, one finds exactly two terms,

$$\begin{aligned} V_k^{\mathrm{NLO}} &= -\frac{\alpha\beta_1}{4} \mathrm{Tr}\left[H u_m u^+ \gamma_m \gamma_5 \gamma_k \right] + \frac{\alpha\beta_2}{4} \mathrm{Tr}\left[H u_4 u^- \gamma_k \right] \\ &= \frac{\mathrm{i}\alpha\beta_1}{2} (P u_k - \varepsilon_{klm} P_l^* u_m) u^+ + \frac{\mathrm{i}\alpha\beta_2}{2} P_k^* u_4 u^- \,. \end{aligned} \tag{4.18}$$

The LECs are written as a product of the LO LEC α and a pair of NLO LECs β_i which are of mass dimension -1. The terms proportional to β_1 couple an odd number of pions to the heavy mesons, whereas the term multiplied by β_2 contains an even number of pions, starting with two pions.

The NLO terms for the time component of the axial vector current can be obtained in the same way as for the LO term. The result reads

$$\begin{aligned} A_4^{\mathrm{NLO}} &= \frac{\alpha\beta_1}{4}\mathrm{Tr}\left[Hu_m u^+\gamma_m\right] - \frac{\alpha\beta_2}{4}\mathrm{Tr}\left[Hu_4u^-\gamma_5\right] \\ &= \frac{\mathrm{i}\alpha\beta_1}{2}P_m^* u_m u^+ - \frac{\mathrm{i}\alpha\beta_2}{2}Pu_4u^- \,. \end{aligned} \tag{4.19}$$

The expressions for all densities and currents are compiled in App. A.

The aim of this thesis is to quantify the excited states contamination of matrix elements and other physical observables. To do so, one needs an estimate for the numerical values of the NLO coefficients β_i. These can be extracted from lattice results of the $B \to \pi$ vector form factors by comparing them with the HM ChPT expressions. The form factors in the effective theory will be computed in Sec. 5.2 and a comparison with the lattice results of [140] will also be given there. For now it is enough to cite the values found there:

$$\beta_1 = 0.14(5)\,\mathrm{GeV}^{-1}\,, \tag{4.20}$$

$$\beta_2 = 1.2(3)\,\mathrm{GeV}^{-1}\,. \tag{4.21}$$

Comments on the size of the error can also be found in the aforementioned section.

4.1.1. Matching Smeared Interpolating Fields to Chiral Perturbation Theory

It was pointed out in Sec. 2.2.2 that smearing the interpolating field of a particle can help to reduce the excited states contamination of lattice correlation functions. This also implies the appearance of a new scale in the theory, the smearing radius r_{sm}. In the effective theory, the effect of smearing is incorporated by a different set of LECs for the interpolating fields [19, 167, 168]. The smeared versions of the pseudoscalar density P and the vector current V_k, which will be used as interpolating fields for the pseudoscalar and vector B mesons, will be denoted $\mathcal{B}$ and $\mathcal{B}_k$ (the asterisk of the vector meson is suppressed for notational convenience). Starting from the general form given in Eq. (4.4), but with a set of new LECs $\tilde{c}_j^{(i)}$, one can repeat the steps undertaken for V_k in order to derive $\mathcal{B}_k$. In the end, one can redefine the LECs to $\tilde{\alpha}$ and $\tilde{\beta}_i$ which are the analogues of α and β_i, compare Eqs. (A.21) and (A.24) in App. A. The LECs of $\mathcal{B}$ and $\mathcal{B}_k$ are related by HQSS, so even if chiral symmetry is broken by the lattice discretisation, the LECs will be the same as long as one applies the same smearing method.

In Sec. 5.2.4, a method is presented which can be used to extract the smeared LEC $\tilde{\beta}_1$ from a ratio of correlation functions. Determining $\tilde{\beta}_1$ for several smearing techniques and levels and using the numerical values in the analytic expressions which will be computed in the following sections, one can study the effect of smearing on the excited states contamination of different observables.

The LECs are not only functions of the smearing method, but also of the chosen lattice discretisation. For renormalisable smearings, the dependence on the bare coupling g_{s}, which is a function of the lattice spacing a, can be factored,

$$\tilde{c}_j^{(i)}(g_{\mathrm{s}}) = \zeta(g_{\mathrm{s}})\bar{c}_j^{(i)}(r_{\mathrm{sm}})\,. \tag{4.22}$$

In ratios of correlation functions, such as Eqs. (2.84)-(2.86), this overall factor drops out and only a dependence on the smearing radius remains, up to discretisation errors which are not considered in this thesis. One further complication arises from the smearing radius r_{sm}: the extended operators of the lattice simulations are mapped to the particles of (HM) ChPT, which are point-like particles. It is expected that ChPT is nevertheless a good approximation if the smearing radius is much smaller than the pion wavelength $m_\pi^{-1} \approx 1.4\,\mathrm{fm}$.

4.2. B Meson Two-Point Function

The two-point function of the B mesons has two uses: it is needed for the extraction of matrix elements with a B meson in the initial or final state, but it can also be used to compute the mass and decay constant of the B meson. As any other correlation function, it is affected by excited states and therefore can introduce a systematic error in any of those quantities. Estimating the excited states contamination is therefore of utmost importance. For the decay constant, one has to compute the two-point function with at least one local field, otherwise it is possible to use smeared interpolating fields at source and sink.

Some preliminary remarks are in order: the following computations are intended to be applied to the results of lattice simulations and are therefore carried out in a finite spatial volume of size L^3. Choosing periodic boundary conditions, this implies that the momenta are given by $\vec{p} = 2\pi/L\,\vec{n}$, where the components of $\vec{n}$ are integers. Since the time extent in lattice simulations is usually taken larger than the spatial extent, it will be assumed for simplicity to be infinite in the following. The computations will also be carried out in the continuum limit since lattice spacing effects are not expected to play a central role in the following discussions. The spectral decomposition of the B meson two-point function in static HQET/HM ChPT then reads

$$\int\limits_{L^3} \mathrm{d}^3\vec{x}\, \left\langle \mathcal{B}(\vec{x},t)\mathcal{B}^\dagger(\vec{0},0)\right\rangle = \frac{|\langle 0|\mathcal{B}|B\rangle|^2}{2} + \sum_{\vec{p}} \frac{|\langle 0|\mathcal{B}|B^*(-\vec{p})\pi(\vec{p})\rangle|^2}{4L^3 E_{\pi,\vec{p}}} e^{-E_{B^*\pi,\vec{p}}t} + \dots\,. \tag{4.23}$$

At low energies, the matrix elements can be computed in ChPT. For the B meson states, the non-relativistic normalisation of Eq. (2.81) was used. The first thing to notice here is that the first term is a constant. For one thing, HQET/HM ChPT without a bare mass term is considered in the following, and this mass thus cannot appear in an exponential of the form $\exp(-m_B t)$. Secondly, quantum effects generate a divergent self-energy for the B meson, also known as the static energy E_{stat} in static HQET. But this energy drops out in the ratios of correlation functions from which matrix elements will be extracted in the following sections. For this reason it is simply dropped in the spectral decomposition of the correlation functions in this work. In HM ChPT, it also only enters at a higher order in the chiral expansion than considered here. The second term in the above formula also does not fit the general form given in Eq. (2.79). The reason is the following: the interaction vertices of HM ChPT involve derivatives of the pions and their mass. Since the pion mass is comparatively small and ChPT is a low energy effective theory, the coupling between the pion and the heavy meson is weak. For convenience, the $|B^*\pi\rangle$ state was therefore normalised in the same way as the state in the non-interacting theory, in which it decomposes into the product state $|B^*\rangle \otimes |\pi\rangle$. This goes hand in hand with the approximation

$$E_{B^*\pi} \approx E_B + E_\pi\,, \tag{4.24}$$

which is exact in the non-interacting theory. In the static approximation the B meson energy is neglected for the reasons given above. Since the pion is the particle with the smallest mass in QCD, the $B\pi$ states[3] yield the dominant contribution to the excited states contamination of the two-point function.

In HM ChPT, the computation of the $B\pi$ excited states contamination proceeds by evaluating the Feynman diagrams shown in Fig. 4.1. The aim is to compute the excited states

[3] In the following, correlation functions will be considered which contain both $B\pi$ and $B^*\pi$ excited states. For convenience, both of them will be generically denoted as $B\pi$ states since the vector and pseudoscalar B mesons transform into each other under HQSS.

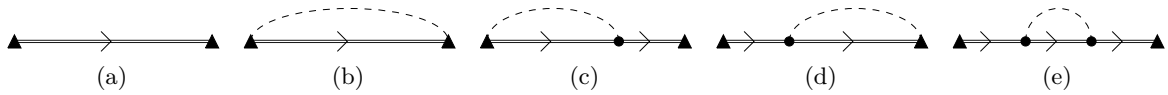

Figure 4.1.: Diagrams contributing to the B meson two-point function ground state and $B\pi$ excited states. The filled black triangle represents the pseudoscalar density creating and destroying a B meson whereas filled circles stand for interaction vertices. Pion propagators are given by dashed lines, the solid double line is a B or B^* meson propagator.

contamination to NLO in the chiral expansion. It does not matter if one computes the two-point function of B^- or $\bar{B}^0$, the results agree due to isospin symmetry which will be assumed throughout this thesis. The expression for the interpolating field is given in Eq. (A.20) and for the interaction vertices of the LO HM ChPT Lagrangian in Eq. (A.9). Using those, the Feynman diagrams can be computed in perturbation theory. Diagram (a) is identified with the ground state, since only a single B meson propagates, whereas the other diagrams are all possible Feynman diagrams with an additional propagating pion and therefore correspond to the second term in the spectral decomposition given in Eq. (4.23).

The result for the single B meson diagram is obtained by using those terms in the interpolating field, which involve one heavy meson field and no pions. Only the LO term gives rise to such a term, and one therefore has ($t > 0$)

$$C_2^{B,\text{g.s.}}(t) = \int\limits_{L^3} \mathrm{d}^3\vec{x} \left\langle \tilde{\alpha} P(t,\vec{x}) \tilde{\alpha} P^\dagger(0,\vec{0}) \right\rangle = \frac{\tilde{\alpha}^2}{2} \,. \tag{4.25}$$

Comparing with Eq. (4.23), one sees that this term is a contribution to $|\langle 0|\mathcal{B}|B\rangle|^2$.

For diagrams (b), (c), and (d), one needs those terms of the interpolating fields which couple one heavy meson and one pion. These are the NLO parts of the interpolating field which are proportional to $\tilde{\beta}_1$. Diagrams with n interaction vertices, on the other hand, include insertions of $(-S_{\text{int}})^n/n!$ in the correlation function, with S_{int} being in this case the part of the HM ChPT action which couples two heavy mesons to one pion. Since it is the action, this automatically implies that one has to integrate over the spacetime point at which the vertex is inserted. Evaluating the diagrams, one does not only find terms proportional to $\exp(-E_{\pi,\vec{p}}t)$, terms which constitute contributions to $B\pi$ excited states as can be seen from the spectral decomposition in Eq. (4.23). For example, the result for diagram (e) is given by

$$\text{(e)} = \frac{3\tilde{\alpha}^2 g^2}{16 f^2 L^3} \left[\sum_{\vec{p}} \frac{\vec{p}^{\,2} e^{-E_{\pi,\vec{p}}t}}{E^3_{\pi,\vec{p}}} - \sum_{\vec{p}} \frac{\vec{p}^{\,2}}{E^3_{\pi,\vec{p}}} + t \sum_{\vec{p}} \frac{\vec{p}^{\,2}}{E^2_{\pi,\vec{p}}} \right] . \tag{4.26}$$

The second and third term are not multiplied by an exponential, just like the LO result for the ground state in Eq. (4.25). In App. B, it will be shown that these terms are indeed higher order corrections to the single B state matrix element and the self-energy E_{stat}. The second term in Eq. (4.26) produces a higher order correction to the LEC $\tilde{\alpha}$ when evaluated in the infinite volume limit using dimensional regularisation. The same is true for some terms in diagrams (c) and (d). The third term in Eq. (4.26) gives a contribution to the static energy E_{stat}, see App. B for more details. It has already been pointed out in [169] that terms proportional to t yield corrections to the energy of the propagating particle.

That these are indeed higher order corrections can be seen from the fact that e.g. the result for diagram (e) is proportional to $1/f^2 \sim 1/\Lambda_\chi^2$, i.e. it is of order p^2. The reason is easy to see

from the Feynman diagrams: they contain a pion line which corresponds to a propagator of the pion fields in the analytic expression. A propagator is given by the contraction of two pion fields π, but those only enter the theory via $u = \exp(\mathrm{i}\pi/f)$, so every pion field is accompanied by a factor $1/f$. From this is discussion, it is clear that the $B\pi$ excited states contamination, which necessarily involves a pion line, starts at order p^2. Diagram (e) is of this order since only the LO term of the B meson interpolating field with the LEC α, which is of order p^0, enters, and also the LEC g from the interaction vertices is of this order. Diagrams (c) and (d) are of order p^3 since, besides the pion line, they also need one insertion of the NLO B meson interpolating field, which is proportional to $\tilde{\beta}_1$. This NLO LEC is expected to scale like $1/\Lambda_\chi$. Diagram (b) can then be identified to be of order p^4, which is of NNLO and thus of a higher order than initial sought after, but it will be included nevertheless for the reasons given below. All in all, the result for the $B\pi$ excited states contamination starts at order p^2, whereas the single B ground state is of order p^0. Naively, one would therefore expect the $B\pi$ state contribution to be small, since it is suppressed by a factor $\exp(-E_{\pi,\vec{p}}t)/f^2$. But one should keep in mind that, as shown in the spectral decomposition (4.23) and also in the result for diagram (e) (4.26), there is not a single $B\pi$ state, but a tower of states given by the sum over the momentum $\vec{p}$ of the pion. Even if an individual state gives only a small contribution, the effect of the sum might still be sizeable.

In this discussion, the factor $1/L^3$ was left out for the following reason: It is true that for large L, this factor suppresses the individual states. But at the same time, the density of states in momentum space increases because the distance between two consecutive momenta of the Brillouin zone are separated by a distance $\Delta p = 2\pi/L$ along all three dimensions. This distance decreases for increasing L, so that one has in the continuum limit

$$\frac{1}{L^3}\sum_{\vec{p}} \to \int \frac{\mathrm{d}^3\vec{p}}{(2\pi)^3}\,. \tag{4.27}$$

The factor $1/L^3$ therefore just signals that one is working in a finite volume.

For completeness, it should be mentioned that there are more Feynman diagrams which can contribute to the $B\pi$ excited states contamination, which are not considered because they contribute at a higher order in the chiral expansion. Consider e.g. diagram (c), and add a second pion line which connects the interaction vertex (the black filled circle) with the B meson interpolating field on the right (black triangle). Evaluating this diagram would also yield terms which fall off with a single exponential $\exp(-E_{\pi,\vec{p}}t)$. But since this diagram has two pion lines, it is at least of order p^4 and not of interest for the following discussion.

With these considerations out of the way, it is time to form the ratio δC_2^B, the ratio of the excited states (here only the $B\pi$ contribution has been computed and can be included) to the ground state. The result reads to the order it has been computed here

$$\delta C_2^B(t) = \sum_{\vec{p}} \frac{3}{8(fL)^2(E_{\pi,\vec{p}}L)}\frac{\vec{p}^{\,2}}{E_{\pi,\vec{p}}^2}(g+\tilde{\beta}_1 E_{\pi,\vec{p}})^2 e^{-E_{\pi,\vec{p}}t} = \sum_{\vec{p}} \xi(\vec{p})c_{2\mathrm{pt}}(\vec{p})e^{-E_{\pi,\vec{p}}t}\,, \tag{4.28}$$

$$\xi(\vec{p}) = \frac{1}{3(fL)^2(E_{\pi,\vec{p}}L)}\frac{\vec{p}^{\,2}}{E_{\pi,\vec{p}}^2}\,, \qquad c_{2\mathrm{pt}}(\vec{p}) = \frac{9}{8}(g+\tilde{\beta}_1 E_{\pi,\vec{p}})^2\,. \tag{4.29}$$

The coefficients ξ and $c_{2\mathrm{pt}}$ are defined for later convenience. As was shown in Sec. 2.3, the result for the vector meson two-point function is the same.

In order to arrive at the above result, it was assumed that the same smearing procedure (or non at all) has been applied to the source and sink operator. The result is then strictly positive. In reality, one is not restricted to do this but instead can apply different methods on

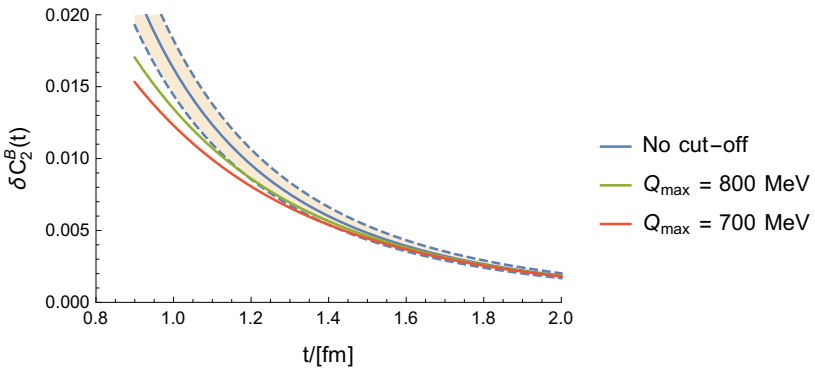

Figure 4.2.: The relative deviation δC_2^B of the B meson two-point function from its ground state as a function of time t and for two momentum cut-offs $Q_{\max}$ of the integral (4.31).

the two operators. In fact, it will be useful to define the local-smeared two-point function

$$\begin{aligned} C_2^{B,\mathrm{LS}}(t) &= \int\limits_{L^3} \mathrm{d}^3\vec{x}\, \left\langle P(t,\vec{x})\mathcal{B}(0,\vec{0})\right\rangle \\ &= \frac{\alpha\tilde{\alpha}}{2}\left(1+\sum_{\vec{p}} \frac{3}{8(fL)^2(E_{\pi,\vec{p}}L)}\frac{\vec{p}^{\,2}}{E_{\pi,\vec{p}}^2}(g+\beta_1 E_{\pi,\vec{p}})(g+\tilde{\beta}_1 E_{\pi,\vec{p}})e^{-E_{\pi,\vec{p}}t}+\dots\right) . \end{aligned} \tag{4.30}$$

This correlator with a local field at the sink and a smeared field at the source will become relevant when the excited states contamination of the B meson decay constant is derived in Sec. 4.2.2.

For now, it is beneficial to consider Eq. (4.28) in order to investigate how sizeable the excited states contamination is. To do so, one has to fix values for the different parameters of the result. In the following, the pion mass is considered in the isospin limit and set to its (nearly) physical value $m_\pi = 140\,\mathrm{MeV}$. As mentioned in Sec. 2.2, finite size effects are negligible for $m_\pi L \geq 4$, so for the moment the lower bound $m_\pi L = 4$ is used for fixing the value of L. The constant f, the chiral limit value of the pion decay constant, is set to the physical value $f = f_\pi \approx 93\,\mathrm{MeV}$. The origin of the value $g = 0.49(1)$ has already been presented in Sec. 3.2. These parameters will be used for all the plots of this thesis if not stated otherwise. For the LEC $\tilde{\beta}_1$, it is not possible to give a specific value because it will depend on the smearing procedure applied. So far, its value is only known for local interpolating fields, see Eq. (4.20). But this value can be considered as an upper bound on $\tilde{\beta}_1$: lattice results show that applying a smearing technique reduces the excited states contamination. Since, as long as the same smearing procedure is applied to the source and the sink, the two-point function is strictly positive, this would imply $\tilde{\beta}_1 < \beta_1$. This should be taken with a grain of salt since $\tilde{\beta}_1$ was never extracted from such a correlation function. The result presented in Eq. (4.28) is assumed to be reliable for large time separations t so that ChPT applies. On the other hand, smearing in lattice simulations is used to minimise the excited states contamination also for smaller values of t at which not only $B\pi$ states give a sizeable contribution. It is possible that these additional states are minimised at the cost of increasing $\tilde{\beta}_1$ so that the overall excited states contamination is reduced. Nevertheless, in the following it is assumed that the inequality $\tilde{\beta}_1 < \beta_1$ holds.

Before discussing the size of the excited states contamination of the two-point function, it is important to remember that ChPT is a low energy effective theory. But the sum in Eq. (4.28) runs over all momenta and therefore also includes states with energies which cannot be reliably described in ChPT. This problem can be circumvented by choosing the time separation t in

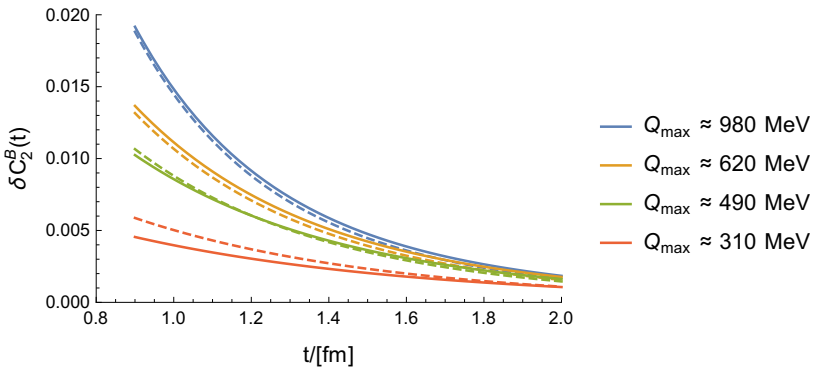

Figure 4.3.: Comparison of finite (dashed lines) and infinite volume (solid lines) results for δC_2^B for the same cut-offs in momentum space.

the two-point function large enough, so that the high energy states are negligibly small due to the exponential suppression. Finding the numerical value for the minimum of t, for which the ChPT results can be trusted, is best done in the infinite volume limit (finite size effects will be studied below). For clarity, the formula that will be evaluated numerically is given by

$$\delta C_2^{B,\mathrm{IVL}}(t) = \int_0^\infty \mathrm{d}p \, \frac{3}{16\pi^2 (fL)^2 (E_{\pi,p} L)} \frac{p^4}{E_{\pi,p}^2} (g + \tilde{\beta}_1 E_{\pi,p})^2 e^{-E_{\pi,p} t} \,, \tag{4.31}$$

which can be obtained by using Eq. (4.27) and switching to spherical coordinates so that $p = |\vec{p}|$. These integrals can be expressed in terms of Bessel and Struve functions, see App. B in [116]. In order to gauge the applicability of ChPT, Fig. 4.2 shows how much the result deviates from the full integral if one imposes a cut-off $Q_{\max}$ on the integral. The NLO LEC $\tilde{\beta}_1$ of the interpolating field was set to $\tilde{\beta}_1 = \beta_1 = 0.14\,\mathrm{GeV}^{-1}$. For the line without cut-off, also the errors of the LECs are taken into account by the band. A look at the plots suggests that around $t \sim 1.3\,\mathrm{fm}$ the line with the larger cut-off is within this band. Including error bands for both cut-offs would show that they all overlap with the band for no cut-off for this value of t. It is therefore reasonable to assume that the deviation due to the contribution of high energy pions is small compared to the uncertainty of the low energy constants for $t \geq 1.3\,\mathrm{fm}$. For smaller t, the result might still be a good first approximation, but one should be careful when applying it in that range. This limit on t also applies to all other correlation functions presented in this work, although the explicit checks will not be presented here. For some of them, only the bands of the results without cut-off and with cut-off $Q_{\max} = 800\,\mathrm{MeV}$ overlap at $t = 1.3\,\mathrm{fm}$, whereas there is still a tiny gap when comparing with the cut-off $Q_{\max} = 700\,\mathrm{MeV}$. But to a first approximation, $t \geq 1.3\,\mathrm{fm}$ seems to be a reasonable choice for the range of applicability of the results presented in this thesis.

As stated before, one should also check whether finite volume effects are large before presenting the results in the infinite volume limit. This is done in Fig. 4.3 which shows δC_2^B in a finite box of size $m_\pi L = 4$, the bound at which finite size effects are believed to be small, and the infinite volume limit for several cut-offs in momentum space. For $t \geq 1.3\,\mathrm{fm}$, the finite volume effects, i.e. the difference between the solid and dashed lines, are tiny and can be neglected. For this reason, plots of B meson correlation functions and observables will be presented in the infinite volume limit in the following.

After this discussion on the applicability of the result, it is now possible to give an estimate for the excited states contamination of the B meson two-point function. In Fig. 4.4, plots for δC_2^B as a function of time t can be found. The band enclosed by the dashed blue lines

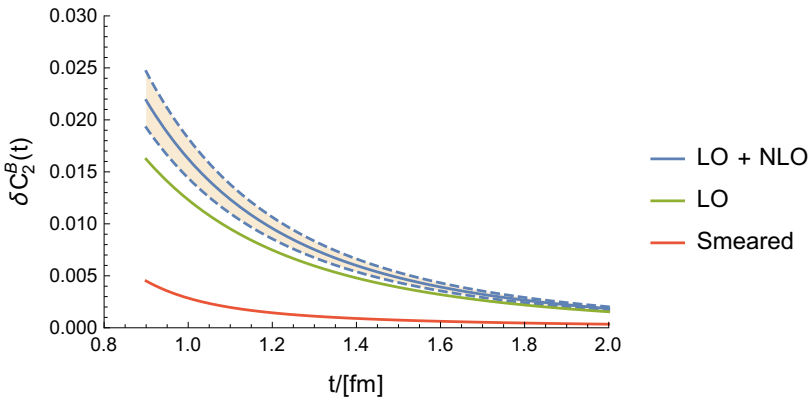

Figure 4.4.: δC_2^B as a function of time. For the green line, the NLO LEC $\tilde{\beta}_1$ was set to zero. The solid blue line includes this LEC by setting $\tilde{\beta}_1 = \beta_1$. The band enclosed by the dashed blue lines signifies the uncertainty due to the error estimates for g and β_1. Finally, for the red line $\tilde{\beta}_1 = -\Lambda_\chi^{-1}$ was used in order to exemplify how much smearing could reduce the excited states contamination.

is the main result, it is obtained by setting $\tilde{\beta}_1 = \beta_1$ and including its error as well as the error for g. As discussed earlier, this should be seen as an upper bound for the excited states contamination, applying a smearing procedure to the interpolating fields should reduce δC_2^B. Remember that δC_2^B is given by the ratio of the excited states and the ground state contributions to the two-point function, it therefore describes the relative deviation of the correlator from its ground state as a function of time. This means that the approximate value of 0.01 which is found at $t = 1.3\,\text{fm}$ implies an overestimation of the ground state by 1%. This is comparatively small, but can spoil sub-percent level accuracy of lattice results if not taken into account properly. Compared to the LO result, given by the green line, the NLO correction due to β_1 is comparatively small. This can be explained by the small value for β_1: since it is an NLO LEC of the chiral expansion, it should scale like Λ_χ^{-1}. Factoring out this scale results in a dimensionless number which should be of order 1. This leads to $\beta_1 \Lambda_\chi \approx 0.16$ which is comparatively small and explains the minor NLO correction.

The last question which will be addressed here is the influence of smearing on the excited states contamination. So far, there is no estimate for realistic values of $\tilde{\beta}_1$ which can be achieved in a lattice simulation, so for the moment it must suffice to discuss what can happen in a best case scenario. First notice that the two-point function is strictly positive as long as the same smearing procedure is applied to both interpolating fields, see the spectral decomposition in Eq. (4.23). It is therefore possible to find a minimum for δC_2^B as a function of $\tilde{\beta}_1$ for a fixed value of t. At $t = 1.3\,\text{fm}$ this yields the approximate value $\tilde{\beta}_1^{\text{min}} \approx -\Lambda_\chi^{-1}$. The corresponding result for the excited states contamination is given by the red line in Fig. 4.4. It can easily be seen that the excited states are strongly suppressed and δC_2^B is around 0.1%, one order of magnitude smaller compared to the result for local interpolating fields. It is on the other hand not clear if this can be achieved in an actual lattice simulation and how to reliably extract $\tilde{\beta}_1$. One possibility is to use correlation functions which are also needed for the computation of the $B \to \pi$ vector form factors. This will be discussed in Sec. 5.2.

A general strategy for minimising the excited states contamination which can be pursued not only for correlation functions but also ratios is the following: the result for the correlation function or ratio in HM ChPT is a function of the LEC $\tilde{\beta}_1$ (and possibly also $\tilde{\beta}_2$, but this will not be discussed here). This result can be minimised as a function of $\tilde{\beta}_1$ for fixed time intervals of the operators. In the above example, the two-point function was minimised at

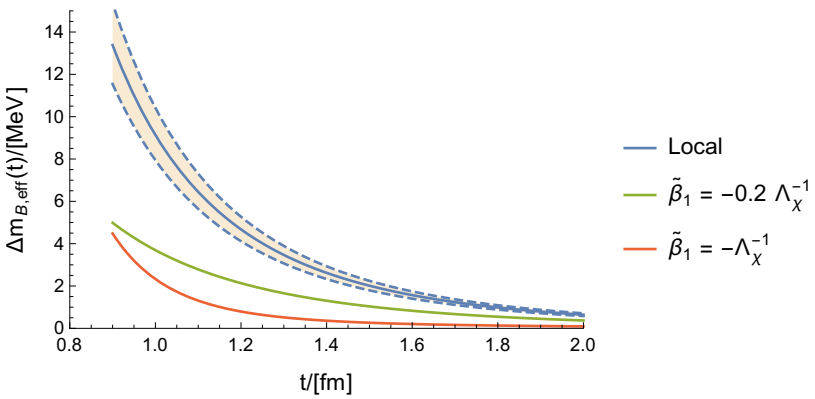

Figure 4.5.: The excited states contamination of the B meson mass. The 'local' result corresponds to the choice $\tilde{\beta}_1 = \beta_1$.

$t = 1.3\,\mathrm{fm}$ which resulted in $\tilde{\beta}_1^{\mathrm{min}} \approx -\Lambda_\chi^{-1}$. One can then use the method described in Sec. 5.2 to determine the value of $\tilde{\beta}_1$ for several smearing techniques and smearing levels. The method which yields a value closest to $\tilde{\beta}_1^{\mathrm{min}}$ which was deduced from the analytic expression should then be used in the lattice computation of the (ratio of) correlation functions.

4.2.1. Effective Mass

The general decomposition of a two-point function in Eq. (4.1) shows that one can extract two physical observables from it: the mass of the ground state and the matrix element $\langle 0|\mathcal{O}_P|P\rangle$. The computation and the excited states contamination of the latter will be presented in the next section. In this section, the focus is on the mass. In general, one can get a suitable estimate for m_P by defining the *effective mass* as it was done in Eq. (4.2). This quantity is directly derived from the two-point function and inherits its excited states contamination.

In HM ChPT without an explicit mass term, only the excited states contribute to the effective mass at the order of the chiral expansion considered here. Computing the effective mass therefore yields $\Delta m_{B,\mathrm{eff}}$ which was defined in Eq. (2.88). The result reads

$$\begin{aligned}\Delta m_{B,\mathrm{eff}}(t) &= -\partial_t \log\left(C_2^{B,\mathrm{g.s.}}[1+\delta C_2^B(t)]\right) = -\frac{\partial_t \delta C_2^B(t)}{1+\delta C_2^B(t)} = -\partial_t \delta C_2^B(t) + \dots \\ &= \sum_{\vec{p}} \frac{3}{8(fL)^2(E_{\pi,\vec{p}}L)} \frac{\vec{p}^{\,2}}{E_{\pi,\vec{p}}} (g+\tilde{\beta}_1 E_{\pi,\vec{p}})^2 e^{-E_{\pi,\vec{p}}t} + \dots\,, \end{aligned} \tag{4.32}$$

with $C_2^{B,\mathrm{g.s.}}$ defined in Eq. (4.25). The dots represent higher order terms from expanding the denominator, i.e. terms of order $(\delta C_2)^2$ and higher which will not be considered in the following. A numerical evaluation of this formula can be found in Fig. 4.5. At the physical point and for $\tilde{\beta}_1 = \beta_1$, one finds $\Delta m_{B,\mathrm{eff}} \approx 4\,\mathrm{MeV}$ at $t = 1.3\,\mathrm{fm}$. Smearing on the other hand helps to reduce the excited states contamination, as exemplified by the green and red line in the plot. It is especially interesting to see that the excited states are considerably suppressed before coming close to the value of $\tilde{\beta}_1$ which minimises the two-point function. For $\tilde{\beta}_1 = -0.2\Lambda_\chi^{-1}$, the value for $\Delta m_{B,\mathrm{eff}}$ at $t = 1.3\,\mathrm{fm}$ is nearly reduced by a factor two.

4.2.2. Effective Decay Constant

The importance of the B meson decay constant f_B for the computation of CKM matrix elements has already been pointed out in Sec. 2.4.1: it enters in leptonic decays of the B

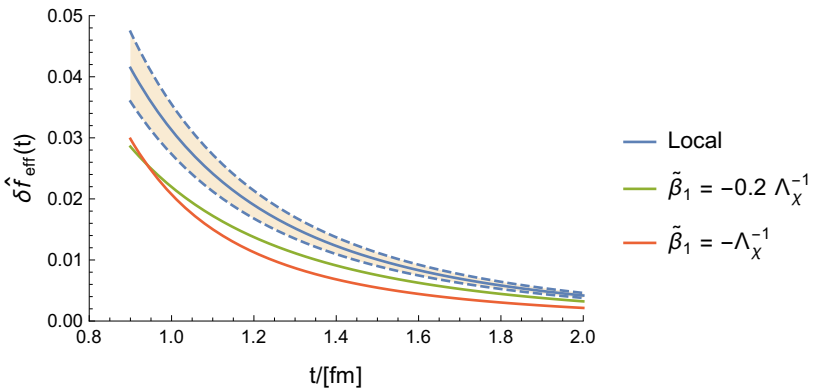

Figure 4.6.: The excited states contamination of the B meson decay constant. The 'local' result corresponds to the choice $\tilde{\beta}_1 = \beta_1$.

meson which can be used to probe the CKM matrix element V_{ub}. The matching of the QCD decay constant to the constant $\hat{f}$ in the effective theory was given in Eq. (2.137), and it was furthermore possible to identify $\hat{f}$ with the LO LEC α of the B meson axial vector current in HM ChPT, see Eq. (4.13). A ratio of correlation functions which converges to $\hat{f}$ for large t is given by

$$\hat{f}_{\rm eff}(t) = \sqrt{2}\frac{C_2^{B,\rm LS}(t)}{\sqrt{C_2^{B,\rm SS}(t)}}e^{m_{B,\rm eff}(t)\frac{t}{2}}\,. \tag{4.33}$$

From the discussion of the previous section, it is clear that in the following $m_{B,\rm eff} = \Delta m_{B,\rm eff}$ is used. $C_2^{B,\rm LS}$ was defined in Eq. (4.30), it is the B meson two-point function with one local and one smeared interpolating field. On the other hand, in the correlator $C_2^{B,\rm SS}$ both interpolating fields are smeared with the same method and smearing level as the one in the local-smeared correlator. It is furthermore assumed that $\Delta m_{B,\rm eff}$ was also obtained from the smeared-smeared correlation function. Rewriting the correlation functions in terms of their ground states and excited states, one finds

$$\begin{aligned}\hat{f}_{\rm eff}(t) = \hat{f}\left(1+\delta\hat{f}_{\rm eff}(t)\right) &= \alpha\frac{1+\delta C_2^{B,\rm LS}(t)}{\sqrt{1+\delta C_2^{B,\rm SS}(t)}}e^{\Delta m_{B,\rm eff}(t)\frac{t}{2}}\\ &= \alpha\left(1+\delta C_2^{B,\rm LS}(t)\right)\left(1-\frac{1}{2}\delta C_2^{B,\rm SS}(t)+\dots\right)\left(1+\Delta m_{B,\rm eff}(t)\frac{t}{2}+\dots\right)\\ &= \alpha\left(1+\delta C_2^{B,\rm LS}(t)-\frac{1}{2}\delta C_2^{B,\rm SS}(t)+\Delta m_{B,\rm eff}(t)\frac{t}{2}+\dots\right)\,.\end{aligned} \tag{4.34}$$

As always, higher orders of the series expansions, which were used to go from the first to the second line, are neglected since the excited states are small. A numerical evaluation of the excited states contamination can be found in Fig. 4.6. The band enclosed by the blue dashed lines shows the result for $\tilde{\beta}_1 = \beta_1$ including its error and the one of g. It has already been discussed in a previous section that this should be considered as an upper limit for the excited states contribution and that smearing is expected to improve this result. At $t = 1.3\,\rm fm$, $\delta\hat{f}_{\rm eff}$ is around 1.5%, and it is decreasing further for larger t. On the other hand, using $\tilde{\beta}_1 = -\Lambda_\chi^{-1}$ which minimised the two-point function at $t = 1.3\,\rm fm$ does not have a strong effect on the exited states of the decay constant. For the same time, it is still around 1% as can be seen from the red line in the plot.

In conclusion, one can say that the excited states contamination is about 1% for $t = 1.3\,\rm fm$ and is expected to be larger for smaller time separations t. This can have a non-negligible

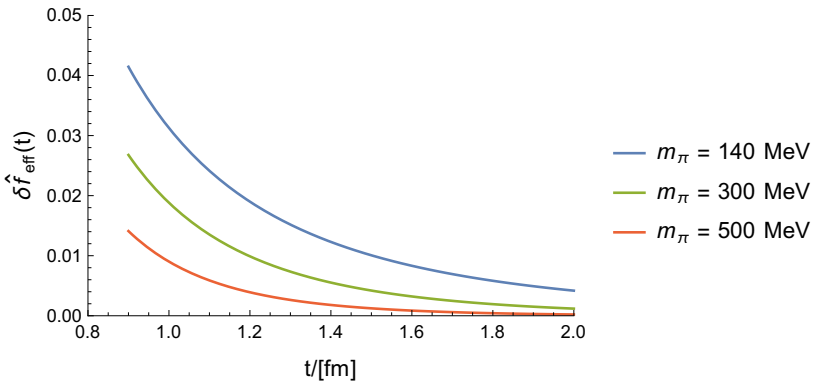

Figure 4.7.: The excited states contamination of the B meson decay constant for three different values of the pion mass.

effect on the extraction of $\hat{f}$ from the correlation functions. This would imply a systematic error for f_B and would affect the extraction of V_{ub} from leptonic decays of B mesons as laid out in Sec. 2.4.1. For a reliable determination of the CKM matrix element with subpercent level accuracy a careful analysis of the lattice correlation functions for excited states needs to be carried out.

Before turning to the two-point functions of the light mesons, there is another point that should be investigated. The plots shown so far were compiled for a pion mass of $m_\pi = 140\,\text{MeV}$, but some lattice simulations are carried out at various values of m_π and then extrapolated to the physical point using ChPT. The $B\pi$ excited states contamination of the two-point function δC_2^B as well as the effective mass $m_{B,\text{eff}}$ are given by sums of terms which are multiplied by exponentials of the form $\exp(-E_{\pi,\vec{p}}t)$. Increasing the pion mass therefore leads to a suppression of the excited states, their effect is diminished. This can be seen in Fig. 4.7, in which $\delta\hat{f}_{\text{eff}}$ is plotted for three different values of the pion mass and $\tilde{\beta}_1 = \beta_1$. At $t = 1.3\,\text{fm}$, the excited states lead to an overestimation of $\hat{f}$ by 1.5% for $m_\pi = 140\,\text{MeV}$, whereas for $m_\pi = 300\,\text{MeV}$ it is about 0.7% and for $m_\pi = 500\,\text{MeV}$ below 0.3%.

4.3. Pion and Kaon Two-Point Functions

The two-point functions of pions and kaons are relevant in this work for the following reason: in Sec. 5.2, the excited states contamination of the $B \to \pi$ vector form factors are computed in HM ChPT from two- and three-point correlation functions. The extraction of the matrix elements requires the pion two-point function, and its multi-particle states will contribute to the excited states contamination of the form factors. The same calculation can be carried out for $B_s \to K$ form factors for which the kaon two-point function is needed.

In QCD, there are two interpolating fields which can be used for exciting a pion or kaon from the vacuum: the axial vector A_μ^a and the pseudoscalar density P^a. The two are related by the PCAC relation and the correlation functions are thus not independent. For $a = 1, 2, 3$ the fields interpolate a pion, for $a = 4, 5, 6, 7$ a kaon. The following computations are carried out in the isospin limit, i.e. for mass degenerate up and down quarks. This means that all pions are mass degenerate with mass m_π, and also all kaons have the same mass m_K. As a further consequence, the results for all three pion two-point functions coincide, and the same is true for the kaon two-point functions. For the computations, it is convenient to not work in the physical basis, but consider only $a = 1$ and $a = 4$.

The spectral decomposition of the P^a two-point function reads (no sum over a and assuming

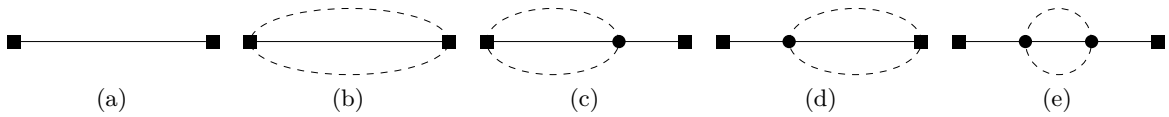

Figure 4.8.: Diagrams contributing to the pion and kaon two-point function and its excited states contamination. The filled black box represents the pseudoscalar density creating and destroying pions and kaons whereas filled circles stand for interaction vertices. Pion propagators are given by dashed lines, the solid line is a propagating kaon in case of the kaon two-point function or a pion for the pion two-point function.

$t > 0$)

$$\int_{L^3} \mathrm{d}^3\vec{x} \left\langle P^a(t,\vec{x})P^a(0,\vec{0})\right\rangle \sim \frac{\left|\left\langle 0\middle|P^a\middle|\pi^a(\vec{0})\right\rangle\right|^2}{2m_{\pi^a}} e^{-m_{\pi^a}t} + \sum_{\vec{p},\vec{q}} \frac{1}{8L^6 E_{\pi,\vec{p}} E_{\pi,\vec{q}} E_{\pi^a,\vec{p}+\vec{q}}} \times \left|\langle 0|P^a|\pi^a(-\vec{p}-\vec{q})\pi(\vec{p})\pi(\vec{q})\rangle\right|^2 e^{-E_{\mathrm{tot},\vec{p},\vec{q}}t} + \dots \,. \tag{4.35}$$

where already the normalisation of non-interacting multi-particle states was used. The total energy of the $|\pi^a\pi\pi\rangle$ state is approximated by

$$E_{\mathrm{tot},\vec{p},\vec{q}} \approx E_{\pi^a,\vec{p}+\vec{q}} + E_{\pi,\vec{p}} + E_{\pi,\vec{q}} \,. \tag{4.36}$$

All of this is in complete analogy to the B meson two-point function, see the beginning of Sec. 4.2 for more information. π^a can be either a pion ($a = 1,2,3$) or a kaon ($a = 4,5,6,7$), but the other πs in the multi-particle states are pions. Additional excited states are states with two kaons instead of pions, states with five pions and so on. All of these states are stronger suppressed for a fixed time t due to their larger total energies. It can thus be expected that these states play a subdominant role in the excited states contamination of lattice correlators, at least for large enough t. The aim of this section is to explicitly compute the matrix elements of the spectral decomposition to leading order in ChPT and estimate the size of the excited states contamination. The matrix elements can be computed order by order in the chiral expansion, in the following only the LO result is of interest.

In ChPT, the light axial vector current and the pseudoscalar density can be obtained by taking a derivative of the Lagrangian w.r.t. the external axial vector field a^a_μ and the pseudoscalar density p^a. Since this is a computation at leading order in the chiral expansion, only the LO Lagrangian of Eq. (3.7) is needed. The interpolating fields which follow from it are

$$A^a_\mu = -\frac{\mathrm{i}f^2}{2}\mathrm{Tr}\left[T^a\left(\partial_\mu U^\dagger U - \partial_\mu U U^\dagger\right)\right] = f\partial_\mu\pi^a + \mathcal{O}(\pi^3)\,, \tag{4.37}$$

$$P^a = -\frac{\mathrm{i}Bf^2}{2}\mathrm{Tr}\left[T^a\left(U - U^\dagger\right)\right] = Bf\pi^a + \mathcal{O}(\pi^a)\,. \tag{4.38}$$

Here, the identity

$$\partial_\mu U U^\dagger = -U\partial_\mu U^\dagger \tag{4.39}$$

was used. Expanding U yields terms with only odd powers of pion fields which is required by the parity quantum numbers of A_μ and P. Terms with more than one pion field can be found in Eqs. (A.37) and (A.38) in App. A. Besides the interpolating fields, one also needs the interaction vertices of ChPT. For the computation at hand, it is sufficient to consider

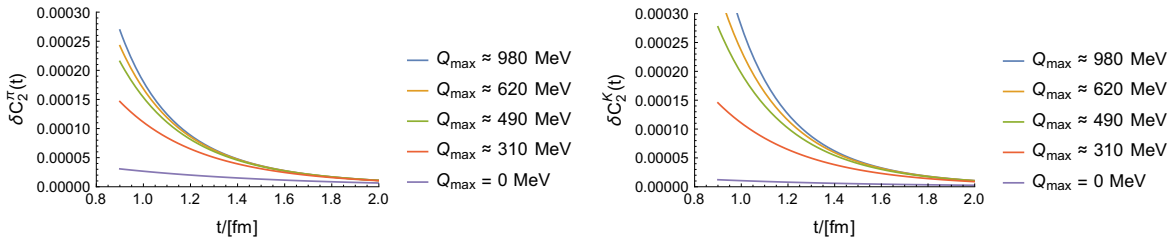

Figure 4.9.: The relative deviation δC_2^π of the pion (left) and δC_2^K of the kaon (right) two-point function from their respective ground state as a function of time t and for several momentum cut-offs $Q_{\max}$ of the sums in Eq. (4.44).

interaction vertices with four pion fields or two pions and two kaons. They follow from the Lagrangian (3.7) and stem from both, the mass term and the kinetic term. They can be found in Eqs. (A.39) and (A.40).

The Feynman diagrams needed for the computation of the two-point functions can be found in Fig. 4.8. The result for the leading order diagram (a) is obtained by inserting the one-pion parts of the pseudoscalar density defined in Eq. (4.38) in the definition of the two-point function, Eq. (4.35). The result reads

$$C_2^{\pi^a,\text{g.s.}}(t) = B^2 f^2 \int\limits_{L^3} \mathrm{d}^3\vec{x}\, \left\langle \pi^a(t,\vec{x})\pi^a(0,\vec{0})\right\rangle = \frac{B^2 f^2}{2m_{\pi^a}} e^{-m_{\pi^a} t}\,. \tag{4.40}$$

It involves the two LO low energy constants B and f of $\mathcal{L}_\pi^{(2)}$ and is evidently positive.

For diagrams (b)-(e), one also neds the terms of the interpolating fields with three pions. The result for these diagrams will in general also include terms which fall of with $\exp(-m_{\pi^a} t)$ and $t\exp(-m_{\pi^a} t)$ instead of the total energy $E_{\text{tot},\vec{p},\vec{q}}$ after the integration over the interaction vertices is carried out. These yield corrections to the decay constant and energy of the single pion or kaon state. Those terms are not of interest for the following discussion and are therefore dropped.

For the contribution of the $|\pi\pi\pi\rangle$ and $|K\pi\pi\rangle$ multi-particle states one finds

$$C_2^{\pi^a,\text{e.s.}}(t) = \sum_{\vec{p},\vec{q}} \frac{B^2 b_{\pi^a}(\vec{p},\vec{q})}{48 E_{\pi,\vec{p}} E_{\pi,\vec{q}} E_{\pi^a,\vec{p}+\vec{q}} f^2 L^6} e^{-E_{\text{tot},\vec{p},\vec{q}} t}\,, \tag{4.41}$$

$$b_\pi(\vec{p},\vec{q}) = \frac{E_{\text{tot},\vec{p},\vec{q}}^4 + 6((E_{\pi,\vec{p}} + E_{\pi,\vec{q}})^2 - E_{\pi,\vec{p}+\vec{q}}^2)^2}{(E_{\text{tot},\vec{p},\vec{q}}^2 - m_\pi^2)^2}\,, \tag{4.42}$$

$$b_K(\vec{p},\vec{q}) = \frac{9}{4}\frac{E_{\text{tot},\vec{p},\vec{q}}^2[(E_{\pi,\vec{p}} + E_{\pi,\vec{q}})^2 + 2(E_{\pi,\vec{p}} - E_{\pi,\vec{q}})^2]}{(E_{\text{tot},\vec{p},\vec{q}}^2 - m_K^2)^2}\,. \tag{4.43}$$

These results are again positive, in agreement with the form of Eq. (4.35) which is a sum of squares. The total energy $E_{\text{tot},\vec{p},\vec{q}}$ was defined in Eq. (4.36). Following Eq. (2.87), one defines the ratio of the excited states to the single pion state as the relative deviation of the correlator from its ground state:

$$\delta C_2^{\pi^a}(t) = \sum_{\vec{p},\vec{q}} \frac{b_{\pi^a}(\vec{p},\vec{q})}{24(fL)^4 (E_{\pi,\vec{p}}L)(E_{\pi,\vec{q}}L)} \frac{m_{\pi^a}}{E_{\pi^a,\vec{p}+\vec{q}}} e^{-(E_{\text{tot},\vec{p},\vec{q}} - m_{\pi^a})t}\,. \tag{4.44}$$

A closer look reveals that the excited states are suppressed by a factor $1/f^4 \sim 1/\Lambda_\chi^4$ relative to the ground state. Furthermore, every single excited state, i.e. every momentum configuration,

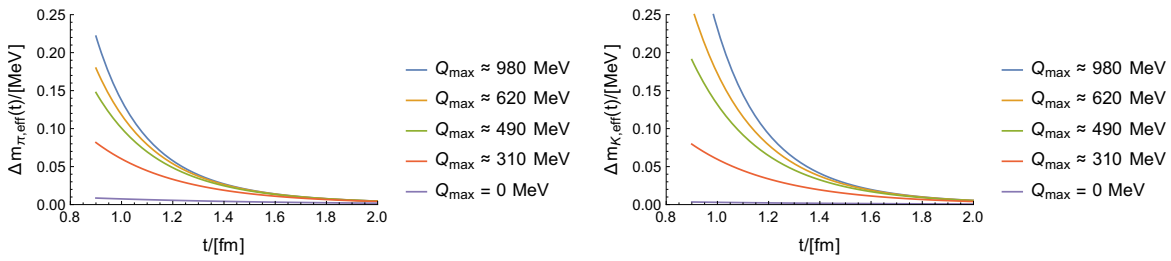

Figure 4.10.: Δm_{eff} of the pion (left) and kaon (right) for several cut-offs of the sums in Eq. (4.45).

is suppressed by $1/V_{\text{s}}^2$ where $V_{\text{s}} = L^3$ is the spatial volume of the lattice. For the $B\pi$ excited states, only a factor $1/f^2$ and $1/V_{\text{s}}$ is present. The reason is that here two additional pions enter the excited states, both of which introduce a factor $\exp(-E_\pi t)/f^2$ and a sum over an internal momentum which is accompanied by a factor $1/V_{\text{s}}$.

In Fig. 4.9, the relative deviations δC_2^π and δC_2^K are plotted as functions of time for several cut-offs of the sums in Eq. (4.44), i.e. $|\vec{p}| \leq Q_{\max}$ and $|\vec{q}| \leq Q_{\max}$. The parameters for the plot are the same as the ones used for the B meson two-point function, for example $m_\pi L = 4$ is used to fix the size of the spatial box. The kaon mass is set to $m_K = 500\,\text{MeV}$ which is close to its physical mass. It is first necessary to make sure that the ChPT results are applied for values of t for which the high energy pions are sufficiently suppressed by the exponentials in Eq. (4.44). From the plots, it seems reasonable that this is the case for $t \geq 1\,\text{fm}$ for the pions and $t \geq 1.2\,\text{fm}$ for the kaons. Considering now the overall scale of the plots, one sees that the excited states lead to an overestimation of the ground state by less than 0.1%. This is two orders of magnitude smaller than the result for δC_2^B, cf. Fig. 4.4. For this reason, their contribution to the excited states contamination of the ratio used for the extraction of $B \to \pi$ and $B_s \to K$ form factors will be ignored in Sec. 5.2.

But not only δC_2^π enters in the ratios, but also the effective mass. The deviation of the effective mass from the true mass of the pions and kaons is given by

$$\Delta m_{\pi^a,\text{eff}}(t) = m_{\pi^a,\text{eff}}(t) - m_{\pi^a} = \sum_{\vec{p},\vec{q}} \frac{b_{\pi^a}(\vec{p},\vec{q})(E_{\text{tot},\vec{p},\vec{q}} - m_{\pi^a})}{24(fL)^4(E_{\pi,\vec{p}}L)(E_{\pi,\vec{q}}L)} \frac{m_{\pi^a}}{E_{\pi^a,\vec{p}+\vec{q}}} e^{-(E_{\text{tot},\vec{p},\vec{q}} - m_{\pi^a})t} \,. \quad (4.45)$$

Plots of this function can be found in Fig. 4.10. One sees that Δm_{eff} is far below 1 MeV for the pion as well as the kaon. Compared to $\Delta m_{B,\text{eff}}$, which is approximately 4 MeV at $t = 1.3\,\text{fm}$ (see Fig. 4.5), this is again negligibly small.

5. Excited States Contamination of Hadronic B Meson Matrix Elements

The preceding chapter covered the computation of the B meson two-point function, the extraction of $\hat{f}$ and $\Delta m_{B,\text{eff}}$, and the computation of the excited states contamination that can be expected for these parameters when computed in a lattice simulation. The latter will also enter the contamination of hadronic S matrix elements involving heavy mesons which can affect the determination of CKM matrix elements, see Sec. 2.4. In Sec. 5.1, the excited states contamination of the only LO HM ChPT LEC g will be presented. The following two sections deal with the $B \to \pi$ vector form factors relevant for semileptonic decays of B mesons, and the B^0-$\bar{B}^0$ mixing amplitude.

5.1. $B^*B\pi$ Coupling Constant

The LEC g is the only LO constant of the HM ChPT Lagrangian and couples an odd number of light mesons to two heavy mesons. It is the LO result in the chiral and $1/m_B$ expansion of the hadronic matrix element of the light axial vector current between a pseudoscalar and vector B meson state:

$$\langle B|A_k|B^*\rangle = g_{B^*B\pi} = g + \dots \,. \tag{5.1}$$

As it turns out, it enters every result of this thesis, so a precise knowledge of its value is desirable. This means that also the excited states contamination of the above hadronic matrix element should be investigated in order to rule out a possible source of systematic errors. Results of this section have already been presented in [116, 165].

The above matrix element can be extracted from the ground state of the following three-point function (no sum over k and $t > t' > 0$)

$$C_3(t,t') = \int\limits_{L^3} \mathrm{d}^3\vec{x}\,\mathrm{d}^3\vec{y}\,\left\langle \bar{\mathcal{B}}^0(t,\vec{x})A_k^-(t',\vec{y})\mathcal{B}_k^{-\dagger}(0,\vec{0})\right\rangle \,, \tag{5.2}$$

where the light axial vector current is related to the basis currents by $A_k^- = A_k^1 + \mathrm{i}A_k^2$. A suitable ratio for extracting $g_{B^*B\pi}$ is given by

$$g_{B^*B\pi} = \lim_{t',(t-t')\to\infty} -\mathrm{i}\frac{C_3(t,t')}{C_2(t)} \,. \tag{5.3}$$

This result makes use of HQSS symmetry which guarantees the equivalence of the pseudoscalar and vector B meson two-point function as long as the same smearing is used in both. Otherwise, one would have to divide by the square root of the vector and pseudscalar two-point functions. For finite t and $t - t'$, also excited states matrix elements of the two- and three-point function enter the ratio. Note that for the three-point function, there are $B\pi$ states in the initial state such as $\langle B|A_k|B\pi\rangle$, in the final state, $\langle B^*\pi|A_k|B^*\rangle$, and in the initial and final state at the same time such as $\langle B^*\pi|A_k|B\pi\rangle$. The contribution of all of these states to the ratio will be computed in HM ChPT below. In the effective theory and for finite time separations, the

excited states contamination can be parametrised as

$$g_{B^*B\pi,\mathrm{eff}}(t,t') = -\mathrm{i}\frac{C_3(t,t')}{C_2(t)} = g_{B^*B\pi}\left(1+\delta C_3(t,t') - \delta C_2(t) + \ldots\right)$$
$$= g_{B^*B\pi}\left(1+\delta g_{B^*B\pi}(t,t')\right)\,, \tag{5.4}$$
$$\delta g_{B^*B\pi}(t,t') = \sum_{\vec{p}}\left(b_1(\vec{p})e^{-E_{\pi,\vec{p}}t'} + b_2(\vec{p})e^{-E_{\pi,\vec{p}}(t-t')} + c(\vec{p})e^{-E_{\pi,\vec{p}}t}\right)\,. \tag{5.5}$$

For the second equation, only the excited states contamination with one additional pion in the initial and/or final state was kept. The function $c(\vec{p})$ gets contributions from the three- and two-point function and is defined by

$$c(\vec{p}) = c_{3\mathrm{pt}}(\vec{p}) - c_{2\mathrm{pt}}(\vec{p})\,, \tag{5.6}$$

whereas $b_1(\vec{p})$ and $b_2(\vec{p})$ are due to the three-point function alone. The coefficient $c_{2\mathrm{pt}}$ has been defined in Eq. (4.29). As pointed out in Sec. 2.2.3, it is beneficial to use the summation method in order to reduce the excited states contamination since it eliminates the smaller time intervals t' and $t-t'$ in favour of t. Applying this procedure to $g_{B^*B\pi,\mathrm{eff}}$, one has

$$g^{\mathrm{sum}}_{B^*B\pi,\mathrm{eff}}(t) = \frac{\mathrm{d}}{\mathrm{d}t}\int_0^t \mathrm{d}t'\, g_{B^*B\pi,\mathrm{eff}}(t,t') = g_{B^*B\pi}\left(1+\delta g^{\mathrm{sum}}_{B^*B\pi}(t)\right)\,, \tag{5.7}$$
$$\delta g^{\mathrm{sum}}_{B^*B\pi}(t) = \sum_{\vec{p}}\Big(b_1(\vec{p}) + b_2(\vec{p}) + c(\vec{p})(1-E_{\pi,\vec{p}}t)\Big)e^{-E_{\pi,\vec{p}}t}\,. \tag{5.8}$$

For the computation of the excited states, the expression of $A^a_\mu = \bar{q}\gamma_\mu\gamma_5 T^a q$ in the effective theory is needed. Just like in QCD, it can be obtained by taking a functional derivative of the action w.r.t. the external axial field a^a_μ:

$$A^a_\mu(x) = \left.\frac{\delta S_{\mathrm{eff}}\left[a_\nu\right]}{\delta a^a_\mu(x)}\right|_{a^a_\mu=0}\,. \tag{5.9}$$

The action here is the sum of the ChPT action of the light mesons and the HM ChPT action. The contribution of the former has already been presented in Eq. (4.37). From the leading order HM ChPT Lagrangian given in Eq. (3.30), one has

$$A^a_k = -2\mathrm{i}g(PT^aP^{*\dagger}_k - P^*_kT^aP^\dagger + \varepsilon_{klm}P^*_lT^aP^{*\dagger}_m) + \mathcal{O}(\pi^2)\,. \tag{5.10}$$

From this form, it is evident that the LO result for $g_{B^*B\pi}$ is proportional to g. The NLO Lagrangian in Eq. (3.36) gives also a non-zero contribution to the axial vector current, see Eq. (A.31), but it only contributes to the excited states contamination to the order in the chiral expansion that is considered here.

The relevant Feynman diagrams for the computation of the $B\pi$ excited states contamination of the three-point function can be found in Fig. 5.1. The ground state of the correlator gets a contribution from diagram (a) which reads

$$C_3^{\mathrm{g.s.}} = \mathrm{i}g\frac{\tilde{\alpha}^2}{2}\,. \tag{5.11}$$

This assumes that the same smearing was applied to the interpolating field of the pseudoscalar and vector B meson. Dividing by the B meson two-point function given in Eq. (4.25), one finds to leading order for the ratio (5.3)

$$g_{B^*B\pi} = g\,. \tag{5.12}$$

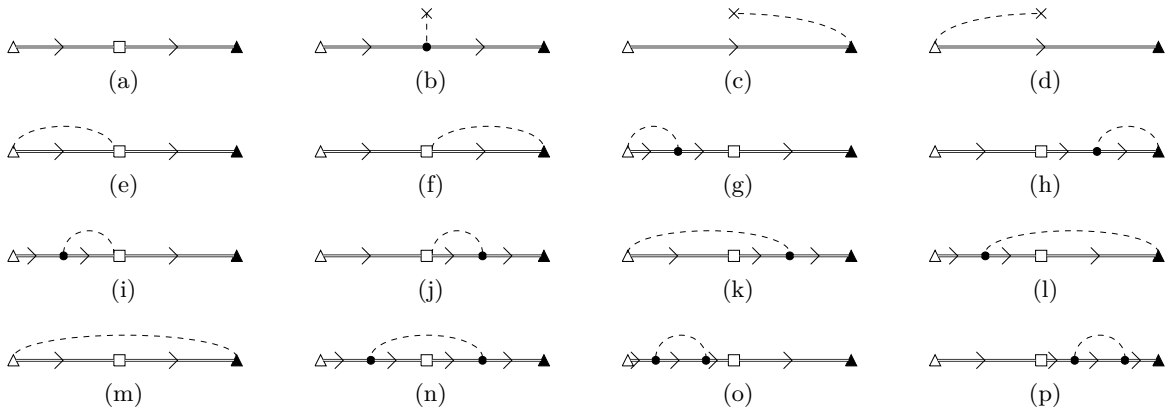

Figure 5.1.: Feynman diagrams contributing to $g_{B^*B\pi}$ and its excited states contamination. The empty and filled triangle represent the interpolating field of the vector and pseudoscalar B meson, respectively. The axial vector current from the HM ChPT Lagrangian is given by the empty box, whereas A_k from the ChPT Lagrangian is denoted by the cross. Interaction vertices are represented by filled circles.

Diagrams (b) (which would also contribute to the ground state of the correlation function), (c), and (d) include the light axial current in the form $A_k^a = f\partial_k\pi^a$. They vanish since the axial vector current is projected to zero momentum in the correlation function. The remaining diagrams contribute to the $B\pi$ excited states contamination and to higher order corrections of $g_{B^*B\pi}$ which will be neglected here. The excited states start at order p^2, the p^3 terms can also be consistently computed, but not the higher order ones since this would require the order p^2 terms of the B meson interpolating fields. This on the other hand means that also some of the diagrams in Fig. 5.2 can be neglected: diagrams (e) and (f) only contribute at order p^4. The terms in the axial vector current which couple two heavy mesons and one pion start at order p, and the term which couples one heavy meson and one pion in the interpolating fields is also of that order in the chiral expansion. Diagram (m) is of order p^4 too, but its contribution is kept in the result since it will partially cancel the p^4 terms of δC_2^B in the coefficient c.

The computation of the diagrams proceeds as usual, the results can be simplified by making use of the identity (no sum over k)

$$\sum_{\vec{p}} f(\vec{p}^{\,2})p_k^2 = \frac{1}{3}\sum_{\vec{p}} f(\vec{p}^{\,2})\vec{p}^{\,2}\,, \tag{5.13}$$

which holds as long as the sum runs over a symmetric domain. Computing the individual diagrams and forming the ratio (5.4), one finds for the coefficients

$$b_1(\vec{p}) = b_2(\vec{p}) = \xi(\vec{p})\left(g^2 + (g\tilde{\beta}_1 + \gamma)E_{\pi,\vec{p}}\right)\,, \tag{5.14}$$

$$c_{3\mathrm{pt}}(\vec{p}) = \frac{1}{8}\xi(\vec{p})\left(g + \tilde{\beta}_1 E_{\pi,\vec{p}}\right)^2\,, \tag{5.15}$$

$$c(\vec{p}) = c_{3\mathrm{pt}}(\vec{p}) - c_{2\mathrm{pt}}(\vec{p}) = -\xi(\vec{p})\left(g + \tilde{\beta}_1 E_{\pi,\vec{p}}\right)^2\,, \tag{5.16}$$

with the functions $c_{2\mathrm{pt}}$ and ξ defined in Eq. (4.29), and the linear combination of NLO LECs

$$\gamma = d_3 - \frac{d_1}{4}\,. \tag{5.17}$$

These are the LECs of the NLO HM ChPT Lagrangian (3.36) which enter the expression for the axial vector current through Eq. (5.9). Values for these LECs do not exist in the literature,

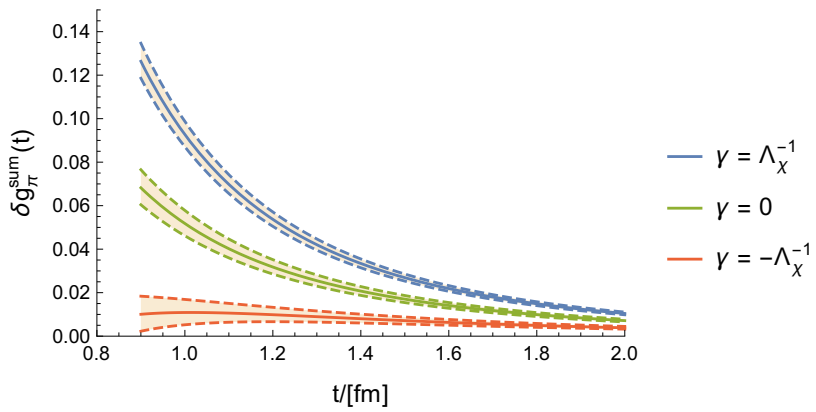

Figure 5.2.: Excited states contamination of the summed ratio defined in Eq. (5.7) for three different values of γ. The bands signify the uncertainty due to the errors of g and β_1.

so it is necessary to find correlation functions from which they can be obtained. This will be done in Sec. 5.1.1. For the moment, one has to take recourse to dimensional analysis in order to estimate the size of γ: it is a combination of NLO LECs of chiral perturbation theory, so it should scale like $\gamma \sim \Lambda_\chi^{-1}$. The numerical constant which multiplies this scale should then be of order $\mathcal{O}(1)$, so that a naive estimate is given by $-1 < \gamma\Lambda_\chi < 1$. This is of course not a hard limit on the value of γ, it is only used as a first estimate for evaluating $\delta g^{\rm sum}_{B^*B\pi}$ numerically.

Fig. 5.2 shows a plot of $\delta g^{\rm sum}_{B^*B\pi}$ as a function of time t, for $\tilde{\beta}_1 = \beta_1$, and for three values of γ. The bands enclosed by the dashed lines capture the errors of g and β_1. It is evident that a larger value for γ increases the excited states contamination. This can be seen quite easily from Eqs. (5.8) and (5.14): $\delta g^{\rm sum}_{B^*B\pi}$ is a linear function of γ, so for larger values it will also increase the excited states contamination. Without a specific value for γ, no clear prediction can be made, but one can infer from the plot that the excited states contamination could be as large as 5% at $t = 1.3\,\text{fm}$, but also nearly zero depending on the value chosen for γ.

The influence of smearing on the excited states contamination by adjusting $\tilde{\beta}_1$ can also be investigated here. For simplicity, γ was set to zero. Fig. 5.3 shows $\delta g^{\rm sum}_{B^*B\pi}$ for three different values of the smeared LEC and without including the errors of the LECs. One can see that for $\tilde{\beta}_1 = -\Lambda_\chi^{-1}$, the excited states contamination is below 1% for times at which ChPT is applicable, whereas for the local LEC it is around 3% at $t = 1.3\,\text{fm}$. One should be careful here, because if γ were not zero but a large negative number, this would imply that $\tilde{\beta}_1 = -\Lambda_\chi^{-1}$ would lead to a negative excited states contamination instead of driving it to zero. It is therefore necessary to take the interplay of smearing and the LEC γ into account when trying to minimise the excited states contamination.

5.1.1. Correlation Functions for the Determination of the NLO LEC γ

The LEC γ, defined in Eq. (5.17), is a linear combination of two NLO LECs d_1 and d_3 of the HM ChPT Lagrangian (3.36). For this reason, an explicit determination of the individual LECs is not only desirable for a better estimate of $\delta g^{\rm sum}_{B^*B\pi}$, but can also be used in the future for other heavy meson observables which are computed to NLO in the chiral expansion. The

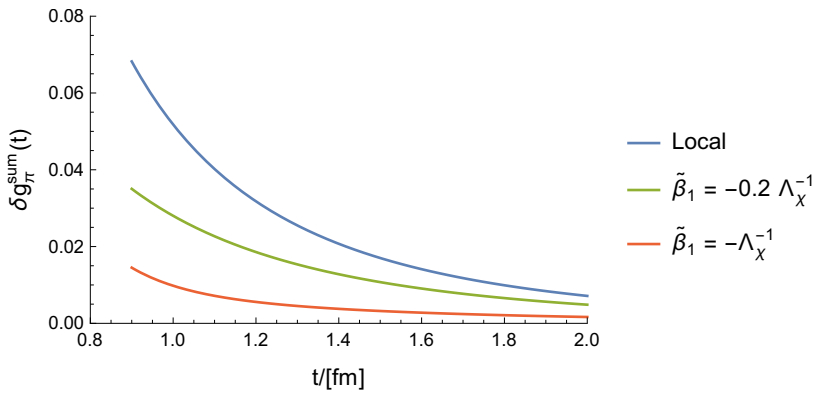

Figure 5.3.: Excited states contamination of the summed ratio defined in Eq. (5.7) for varying $\tilde{\beta}_1$. The 'local' line refers to the special case $\tilde{\beta}_1 = \beta_1$, and γ was set to zero throughout.

explicit form of the NLO light axial vector current,

$$A_k^{\mathrm{NLO}} = -d_1 \frac{\partial_k \pi^a}{f} \left(P P^\dagger + P_l^* P_k^{*\dagger} \right) + 2\mathrm{i} d_3 \varepsilon^{abc} \frac{\partial_l \pi^b}{f} \left(P_k^* T^c P_l^{*\dagger} - P_l^* T^c P_k^{*\dagger} + \varepsilon_{klm} \left[P T^c P_m^{*\dagger} - P_m^* T^c P^\dagger \right] \right) , \tag{5.18}$$

shows that the terms which multiply d_1 and d_3 couple two heavy mesons and at least one pion. This suggests that one needs to compute a four-point function in order to extract the LECs from a lattice simulation, at least no three-point function was found so far which could be used to do that. Attaining a satisfactory signal from a four-point function is quite demanding, so it is not clear if the method described here can in practice be used to extract d_1 and d_3, but there are at the moment no better alternatives. It is best to use a correlation function with two vector B mesons since, as can be seen from Eq. (5.18), it is then possible to extract both LECs.

The first correlator which will be considered here is (assuming $t_x > t_y > t_z > 0$)

$$C_4^{(1)}(\vec{q}, t_x, t_y, t_z) = \int_{L^3} \mathrm{d}^3\vec{x}\, \mathrm{d}^3\vec{y}\, \mathrm{d}^3\vec{z}\, e^{\mathrm{i}\vec{q}\vec{x}} \left\langle A_a^+(x) \bar{\mathcal{B}}_b^{*0}(y) A_c^-(z) \bar{\mathcal{B}}_d^{*0\dagger}(0) \right\rangle . \tag{5.19}$$

All four indices a, b, c, and d are spatial indices and A^+ and A^- are the light axial vector currents creating and destroying charged pions. All possible leading order HM ChPT Feynman diagrams for this correlator can be found in Fig. 5.4. Diagram (a) is a disconnected diagram which could be avoided by changing the flavour content of the four-point function. As an example consider $\langle A^0 \mathcal{B}^{*-} A^+ \bar{\mathcal{B}}^{*0\dagger} \rangle$, in which a charged and neutral light current enter and also the B meson interpolating fields are charged differently. The two axial currents cannot be Wick contracted and diagram (a) would thus be zero. But a closer look at the term proportional to d_1 in Eq. (5.18) reveals that it will not contribute to this type of correlation function because the two interpolating fields of the B mesons have to be their own antiparticles in order to yield a non-zero Wick contraction. The conclusion of this discussion is that one cannot circumvent correlation functions which include Feynman diagram (a) in Fig. 5.4 if one wants to extract d_1.

Computing diagram (a) for the flavour content presented in Eq. (5.19) results in

$$(\mathrm{a}) = \frac{\tilde{\alpha}^2 f^2 L^3}{2E_{\pi,\vec{q}}} e^{-E_{\pi,\vec{q}}(t_x - t_z)} \delta_{\vec{q},\vec{0}}\, q_a q_c , \tag{5.20}$$

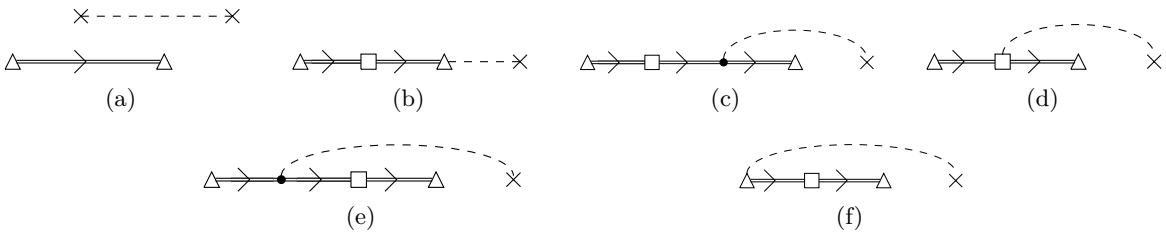

Figure 5.4.: HM ChPT Feynman diagrams for the four-point correlation functions from which d_1 and d_3 can be extracted. The double lines denotes a heavy meson propagator, whereas a dashed line is a pion propagator. The empty box represents the light axial vector current obtained from HM ChPT and the cross the ChPT analogue. The heavy vector meson interpolating fields are given by the triangles.

At first sight, it seems like the contribution of this diagram diverges in the infinite volume limit and one can in fact identify the factor L^3 with the three-dimensional Dirac delta function $\delta^{(3)}(\vec{0})$ which one obtains when performing the computation in momentum space. But a closer look reveals that the result is proportional to both the external momentum $\vec{q}$ and a Kronecker delta which forces this momentum to vanish. So no matter what external momentum $\vec{q}$ is chosen, this diagram will not contribute to the correlation function.

Computing the other Feynman diagrams in Fig. 5.4, one finds that diagrams (b) and (c) are zero due to the flavour content of the correlation function (5.19). The result for the remaining diagrams reads

$$\begin{aligned} C_4^{(1)}(\vec{q}, t_x, t_y, t_z) = \frac{\tilde{\alpha}^2}{4E_{\pi,\vec{q}}^2} e^{-E_{\pi,\vec{q}}\, t_x} \big[&- g(g + \tilde{\beta}_1 E_{\pi,\vec{q}})(\delta_{cd} q_b - \delta_{bd} q_c - \delta_{bc} q_d) \\ &+ e^{E_{\pi,\vec{q}}\, t_z} \{ g^2 (\delta_{cd} q_b - \delta_{bd} q_c - \delta_{bc} q_d) \\ &- E_{\pi,\vec{q}} (d_3 \delta_{cd} q_b + d_1 \delta_{bd} q_c - d_3 \delta_{bc} q_d) \} \big] q_a \,. \end{aligned} \tag{5.21}$$

Higher order corrections and further contributions in the spectral decomposition of the correlation functions are neglected since they are expected to be small. As pointed out earlier, the signal of a four-point correlation function obtained from a lattice simulation is potentially not good enough to yield a reliable result. In order to improve it, one can use the summation method by summing over the insertion time t_z of the axial vector current. The terms linear in t_y which then appear in the result, can be eliminated by taking a derivative

$$\begin{aligned} \frac{\mathrm{d}}{\mathrm{d}t_y} \int \mathrm{d}t_z \, C_4^{(1)}(\vec{q}, t_x, t_y, t_z) = \frac{\tilde{\alpha}^2}{4E_{\pi,\vec{q}}^2} e^{-E_{\pi,\vec{q}}\, t_x} \big[&- g(g + \tilde{\beta}_1 E_{\pi,\vec{q}})(\delta_{cd} q_b - \delta_{bd} q_c - \delta_{bc} q_d) \\ &+ e^{E_{\pi,\vec{q}}\, t_y} \{ g^2 (\delta_{cd} q_b - \delta_{bd} q_c - \delta_{bc} q_d) \\ &- E_{\pi,\vec{q}} (d_3 \delta_{cd} q_b + d_1 \delta_{bd} q_c - d_3 \delta_{bc} q_d) \} \big] q_a \,. \end{aligned} \tag{5.22}$$

This result has two nice features: for one thing, the NLO LECs d_1 and d_3 are multiplied with an additional exponential compared to the other NLO LEC $\tilde{\beta}_1$. This means that if one can discern the two exponentials in the result of the correlation function from a lattice simulation, one has disentangled the NLO corrections due to the B meson interpolating fields and the axial vector current. For another thing, the LECs d_1 and d_3 can be determined individually by choosing the indices of the currents and interpolating fields appropriately. Choosing for example $c = d \neq b$, only the first term in the last line, which is proportional to d_3 will be non-zero. On the other hand, for $b = d \neq c$ only the term proportional to d_1 will survive.

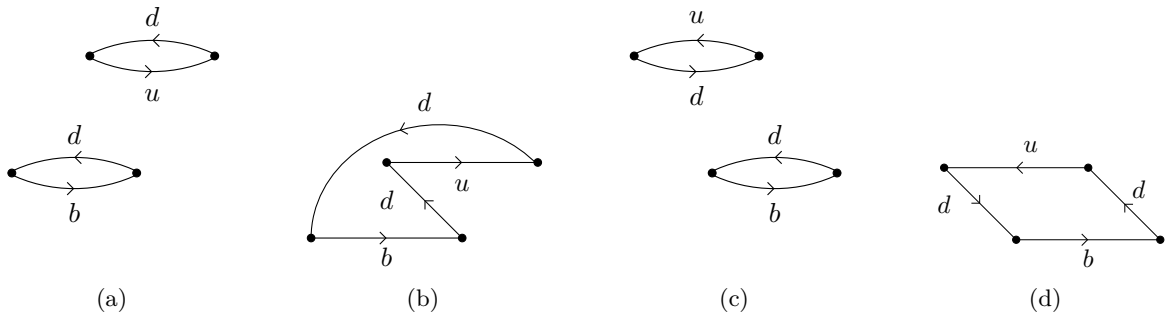

Figure 5.5.: Quark lines diagrams of the four-point functions considered in the text. Diagrams (a) and (b) correspond to the correlator of Eq. (5.19) with $t_x > t_y$, and (c) and (d) to the same correlator for $0 > t_x$.

A problem remains: there is still a leading order term which is proportional to g^2 and falls off in time with the same exponential as the d_i terms. It would have been better if this term was absent since now the d_i terms are potentially small corrections to the LO result and thus harder to extract. But so far, no correlation function has been found for which the LO terms are absent. It is thus necessary to compute the above four-point function for at least two different values of $\vec{q}$, so that one can disentangle the NLO terms, which are proportional to an additional factor $E_{\pi,\vec{q}}$, from the leading order term.

It is also instructive to consider the quark line diagrams which correspond to the correlation function (5.19). These are diagrams (a) and (b) in Fig. 5.5. Diagram (a) is a disconnected diagram. These kind of diagrams are noisy and additional effort will be necessary to get a reliable result. Compared with the disconnected diagram in HM ChPT, one can also not expect it to vanish in a lattice simulation after setting $\vec{q} \neq \vec{0}$, since virtual particles can be exchanged and thus transferring momentum between the two pieces. Since this is due to short-range interactions, one can hope that this diagram does not scale with a factor L^3 like diagram (a) in HM ChPT, but it could still yield a dominant contribution to the correlation function.

One can also consider another time ordering of the fields in the correlator. As an example, consider the correlator with the axial vector current $A_a^+(x)$ inserted on a time slice $t_x < 0$. The summation estimate for Eq. (5.19) with the time ordering $t_y > t_z > 0 > t_x$ and without the disconnected piece reads

$$\begin{aligned}\frac{\mathrm{d}}{\mathrm{d}t_y}\int \mathrm{d}t_z\, C_4^{(1)}(\vec{q},t_x,t_y,t_z) = \frac{\tilde{\alpha}^2}{4E_{\pi,\vec{q}}^2} e^{-E_{\pi,\vec{q}}|t_x|}\big[g(g+\tilde{\beta}_1 E_{\pi,\vec{q}})(\delta_{cd}q_b - \delta_{bd}q_c - \delta_{bc}q_d) \\ + e^{-E_{\pi,\vec{q}}\,t_y}\{-g^2(\delta_{cd}q_b - \delta_{bd}q_c - \delta_{bc}q_d) \\ - E_{\pi,\vec{q}}(d_3\delta_{cd}q_b + d_1\delta_{bd}q_c - d_3\delta_{bc}q_d)\}\big]q_a\,. \end{aligned} \tag{5.23}$$

This result comes with the drawback, that the coefficients d_i are multiplied by the subleading exponential $\exp(-E_{\pi,\vec{q}}(t_y + |t_x|))$, compared to the other terms which fall of with the larger exponential $\exp(-E_{\pi,\vec{q}}\,|t_x|)$. This might hinder a reliable extraction of the NLO LECs d_i.

Finally, one can consider a correlation function with A^+ and A^- interchanged. It is given by

$$C_4^{(2)}(\vec{q},t_x,t_y,t_z) = \int\limits_{L^3} \mathrm{d}^3\vec{x}\,\mathrm{d}^3\vec{y}\,\mathrm{d}^3\vec{z}\,e^{\mathrm{i}\vec{q}\vec{x}}\left\langle A_a^-(x)\bar{\mathcal{B}}_b^{*0}(y)A_c^+(z)\bar{\mathcal{B}}_d^{*0\dagger}(0)\right\rangle\,. \tag{5.24}$$

Computing the correlator in HM ChPT reveals that there is again a disconnected piece, which is of the same form as the one found for $C^{(1)}$. For the connected piece and the time ordering $t_x > t_y > t_z > 0$, the result reads

$$\begin{aligned} C_4^{(2)}(\vec{q}, t_x, t_y, t_z) = \frac{\tilde{\alpha}^2}{4E_{\pi,\vec{q}}^2} e^{-E_{\pi,\vec{q}}\, t_x} \Big[& e^{-E_{\pi,\vec{q}}\, t_z} \{\delta_{cd} q_b (g^2 + d_3 E_{\pi,\vec{q}}) + \delta_{bd} q_c (g^2 - d_1 E_{\pi,\vec{q}}) \\ & - \delta_{bc} q_d (g^2 + d_2 E_{\pi,\vec{q}})\} + e^{-E_{\pi,\vec{q}}\, t_y} \{\delta_{cd} q_b (\tilde{\beta}_1 E_{\pi,\vec{q}} - g^2) \\ & + \delta_{bd} q_c (\tilde{\beta}_1 E_{\pi,\vec{q}} - g^2) + \delta_{bc} q_d (-\tilde{\beta}_1 E_{\pi,\vec{q}} + g^2)\} \Big] q_a \end{aligned} \tag{5.25}$$

Using the summation method, one finds

$$\begin{aligned} \frac{\mathrm{d}}{\mathrm{d}t_y} \int \mathrm{d}t_z\, C_4^{(2)}(\vec{q}, t_x, t_y, t_z) = \frac{\tilde{\alpha}^2}{4E_{\pi,\vec{q}}^2} e^{-(t_x - t_y) E_{\pi,\vec{q}}} [& \delta_{cd} q_b \{g(\tilde{\beta}_1 E_{\pi,\vec{q}} - g E_{\pi,\vec{q}} t_y + \tilde{\beta}_1 E_{\pi,\vec{q}}^2 t_y) + d_3 E_{\pi,\vec{q}}\} \\ & - \delta_{bc} q_d \{g(\tilde{\beta}_1 E_{\pi,\vec{q}} - g E_{\pi,\vec{q}} t_y + \tilde{\beta}_1 E_{\pi,\vec{q}}^2 t_y) + d_3 E_{\pi,\vec{q}}\} \\ & + \delta_{bd} q_c \{g(\tilde{\beta}_1 E_{\pi,\vec{q}} - g E_{\pi,\vec{q}} t_y + \tilde{\beta}_1 E_{\pi,\vec{q}}^2 t_y) - d_1 E_{\pi,\vec{q}}\}] q_a \,. \end{aligned} \tag{5.26}$$

The result given here has the disadvantage that there is only a single exponential, and the NLO LECs d_i and $\tilde{\beta}_1$ are therefore harder to disentangle. One therefore needs an estimate $\tilde{\beta}_1$ for extracting the LECs d_i, a strategy for extracting them is given in Sec. 5.2.4. Additionally, there are also terms which are multiplied by t_y.

As one can see, there are several correlation functions from which the LECs d_1 and d_3 can be evaluated, but all of them come with a drawback. Only computing the different correlation functions presented here in a lattice simulation will show which of them is suitable for extracting the LECs.

5.2. $B \to \pi$ Vector Form Factors

The significance of the $B \to \pi$ vector form factors for the extraction of the CKM matrix element V_{ub} has already been stated in Sec. 2.4.2. The following section describes the computation of the excited states contamination of the HQET matrix elements defined in Eq. (2.149) in HM ChPT up to NLO in the chiral expansion. Some preliminary results were already presented in [170].

The form factors can be extracted from the three-point function

$$C_{3,\mu}(\vec{q}, t, t_\mathrm{v}) = \int_{L^3} \mathrm{d}^3\vec{x}\, \mathrm{d}^3\vec{y}\, e^{\mathrm{i}\vec{q}(\vec{x}-\vec{y})} \left\langle \Pi^+(t, \vec{x}) V_\mu^-(t_\mathrm{v}, \vec{y}) \bar{\mathcal{B}}^{0\dagger}(0, \vec{0}) \right\rangle \,, \tag{5.27}$$

with pseudoscalar interpolating fields Π^+ and $\bar{\mathcal{B}}^0$ for a pion and a heavy meson, respectively, and the heavy-light vector current V_μ. The momentum $\vec{q}$ in the correlation function is the momentum of the pion in the final state. The matrix elements which define the HQET form factors $h_\parallel$ and $h_\perp$ can be extracted from the following ratio of correlation functions

$$\left\langle \pi^+(\vec{q}) \middle| V_\mu^- \middle| \bar{B}^0(\vec{0}) \right\rangle = \lim_{t_\mathrm{v}, (t-t_\mathrm{v}) \to \infty} \frac{2\sqrt{E_{\pi,\vec{q}}}\, C_{3,\mu}(\vec{q}, t, t_\mathrm{v})}{\sqrt{C_2^B(t_\mathrm{v}) C_2^\pi(t - t_\mathrm{v})}} e^{m_{B,\mathrm{eff}}(t_\mathrm{v}) \frac{t_\mathrm{v}}{2}} e^{E_{\pi,\vec{q}}^{\mathrm{eff}}(t - t_\mathrm{v}) \frac{t - t_\mathrm{v}}{2}} \,. \tag{5.28}$$

For finite t and t_v, one has to take the excited states into account. The discussion in Sec. 4.3 makes it clear that the excited states contamination of the pion two-point function and the pion mass is small. It will therefore be neglected in the following. On the other hand, the excited states of the B meson two-point function δC_2^B as well as the B meson mass $\Delta m_{B,\mathrm{eff}}$

cannot be neglected. Additionally, there are also contributions from the three-point function. Assuming that the multi-particle states are weakly coupled, the spectral decomposition reads

$$\begin{aligned} C_{3,\mu}(\vec{q},t,t_\mathrm{v}) = &\frac{1}{4E_{\pi,\vec{q}}}\langle 0|\Pi^+|\pi(\vec{q})\rangle\langle\pi(\vec{q})|V_\mu^-|B(\vec{0})\rangle\langle B(\vec{0})|\bar{\mathcal{B}}^{0\dagger}|0\rangle e^{-E_{\pi,\vec{p}}(t-t_\mathrm{v})} \\ &+ \frac{1}{L^3}\sum_{\vec{p}}\frac{1}{8E_{\pi,\vec{p}}E_{\pi,\vec{q}}}\langle 0|\Pi^+|\pi(\vec{q})\rangle\langle\pi(\vec{q})|V_\mu^-|B^*(-\vec{p})\pi(\vec{p})\rangle \\ &\times \langle B^*(-\vec{p})\pi(\vec{p})|\bar{\mathcal{B}}^{0\dagger}|0\rangle e^{-E_{\pi,\vec{p}}t_\mathrm{v}}e^{-E_{\pi,\vec{q}}(t-t_\mathrm{v})} + \dots\,. \end{aligned} \tag{5.29}$$

One can see that there are $B\pi$ excited states propagating from 0 to t_v with energy $E_{B^*\pi} \approx E_{\pi,\vec{p}}$ (remember that the static limit of HQET/HM ChPT with no mass term is considered). On the other hand, there are only $\pi\pi\pi$ states (not shown in the formula) propagating from t_v to t which are suppressed by an additional exponential function $\exp(-E_\pi t)$ and a factor $1/f^2 \sim 1/\Lambda_\chi^2$. One can expect that these lead to an excited states contamination which is of the same size as the contamination of the pion two-point function and they are therefore also neglected in the following. Only the contribution of the $B\pi$ states will be computed.

With these considerations in mind, one can define effective form factors as (no sum over k)

$$\begin{aligned} h_{\perp,\mathrm{eff}}(\vec{q},t,t_\mathrm{v}) &= \frac{1}{q_k}\frac{2\sqrt{E_{\pi,\vec{q}}}\,C_{3,k}(\vec{q},t,t_\mathrm{v})}{\sqrt{C_2^B(t_\mathrm{v})C_2^\pi(t-t_\mathrm{v})}}e^{m_{B,\mathrm{eff}}(t_\mathrm{v})\frac{t_\mathrm{v}}{2}}e^{E^\mathrm{eff}_{\pi,\vec{q}}(t-t_\mathrm{v})\frac{t-t_\mathrm{v}}{2}} = h_\perp(\vec{q})(1+\delta h_\perp(\vec{q},t,t_\mathrm{v})) \\ &= h_\perp(\vec{q})\left(1+\delta C_{3,k}(\vec{q},t,t_\mathrm{v}) - \frac{1}{2}\delta C_2^B(t_\mathrm{v}) + \frac{1}{2}\Delta m_{B,\mathrm{eff}}(t_\mathrm{v})t_\mathrm{v}\right)\,, \end{aligned} \tag{5.30}$$

$$\begin{aligned} h_{\parallel,\mathrm{eff}}(\vec{q},t,t_\mathrm{v}) &= \frac{2\sqrt{E_{\pi,\vec{q}}}\,C_{3,4}(\vec{q},t,t_\mathrm{v})}{\sqrt{C_2^B(t_\mathrm{v})C_2^\pi(t-t_\mathrm{v})}}e^{m_{B,\mathrm{eff}}(t_\mathrm{v})\frac{t_\mathrm{v}}{2}}e^{E^\mathrm{eff}_{\pi,\vec{q}}(t-t_\mathrm{v})\frac{t-t_\mathrm{v}}{2}} = h_\parallel(\vec{q})(1+\delta h_\parallel(\vec{q},t,t_\mathrm{v})) \\ &= h_\parallel(\vec{q})\left(1+\delta C_{3,4}(\vec{q},t,t_\mathrm{v}) - \frac{1}{2}\delta C_2^B(t_\mathrm{v}) + \frac{1}{2}\Delta m_{B,\mathrm{eff}}(t_\mathrm{v})t_\mathrm{v}\right)\,. \end{aligned} \tag{5.31}$$

The first equation is of course only defined for $q_k \neq 0$. As discussed in Sec. 2.2.1, there are several ratios from which the form factors can be extracted. A comparison between the excited states contaminations of different ratios is presented in Sec. 5.2.3.

The computation of δC_2^B and $\Delta m_{B,\mathrm{eff}}$ has been presented in Sec. 4.2. The computation of $C_{3,\mu}$ and its $B\pi$ state contamination in HM ChPT can be carried out in the usual way: the interpolating field for the B meson has already been introduced before and is given explicitly in Eq. (A.20) in App. A. For the pseudoscalar density which excites a pion from the vacuum, one has

$$\Pi^+ = \tilde{c}\pi^+ + \dots\,, \tag{5.32}$$

with an LEC $\tilde{c}$ which drops out at the order in the chiral expansion that is considered in the following. The heavy-light vector current, the analogue of $\bar{q}\gamma_\mu Q$ in HQET, is also given in the appendix, see Eqs. (A.24) and (A.25). So far, it has been used as an interpolating field for the vector meson in the computation of $g_{B^*B\pi}$ and its excited states contamination. There, it was also possible to use a smeared operator since the matrix elements of the interpolating field do not contribute to $g_{B^*B\pi}$, only to the excited states contamination. Here, one is interested in the matrix element of the physical heavy-light vector current between a B and a pion state, and applying a smearing procedure is therefore prohibited.

Diagrams which can in principle contribute to $h_\perp$, $h_\parallel$, and their respective $B\pi$ excited states contamination can be found in Fig. 5.6.[1] These diagrams show two features which have not been encountered in this work so far: i) diagrams (d), (e), (h), and (g) need interaction

[1] Diagrams (n) and (o) are missing in [170].

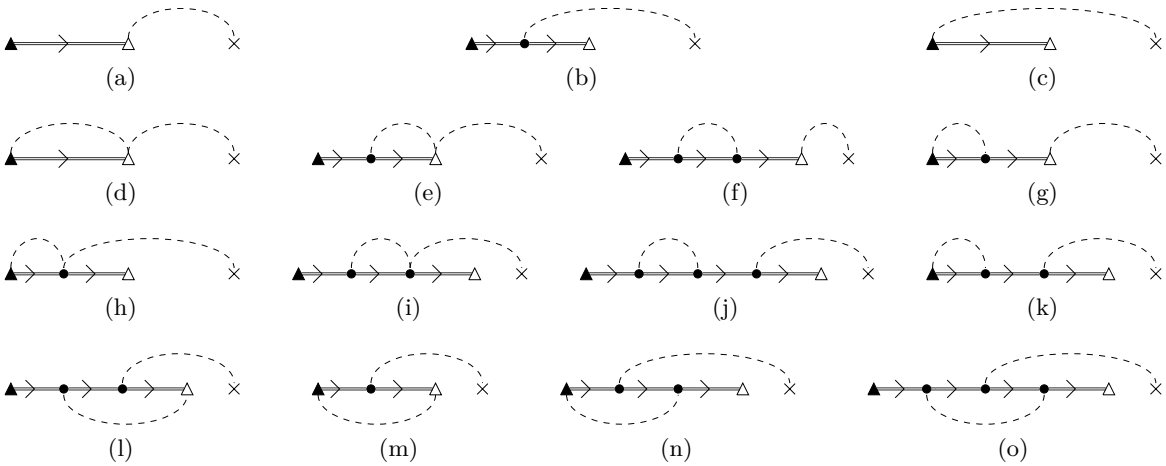

Figure 5.6.: A subset of Feynman diagrams contributing to $h_\perp$, $h_\parallel$, and the $B\pi$ excited states contamination of these form factors. See the caption of Fig. 5.1 for an explanation of the symbols.

vertices coupling two pions to two heavy mesons and the vector current expanded to up to two pion fields; and ii) whereas diagrams (a)-(c) have only a single propagating pion line, the others have two. This means that the latter diagrams are suppressed by a relative factor of $1/f^2$ compared to the former.

5.2.1. $h_\perp$

For the form factor $h_\perp$, the three-point function (5.27) with $\mu = k$ needs to be computed. Computing diagrams (a) and (b) in Fig. 5.6 shows that they yield terms with the same time dependence as the first term in the spectral decomposition (5.29). They therefore contribute to the HM ChPT result for $h_\perp$. Some of the diagrams (e)-(o) also show the same time dependence, but these terms are of NNLO in the chiral expansion, an order which is not computed in full here. These terms will therefore be neglected as before.

Using the results from diagrams (a) and (b) and computing the ratio (5.28), one finds

$$h_\perp(\vec{q}) = \frac{\alpha g}{\sqrt{2} f E_{\pi,\vec{q}}} \left(1 - \frac{\beta_1 E_{\pi,\vec{q}}}{g}\right) + \dots . \tag{5.33}$$

The LO result was first presented in [171], and reproduced and extended to one-loop corrections of order p^2 in [132]. These results also include the mass splitting $\Delta = m_{B^*} - m_B$ which is zero in the static limit of HQET and therefore neglected here. The references do not include the order p correction presented here since they do not consider the order p term of the vector current. In [172] on the other hand, the NLO term is included without relating the coefficient explicitly to the LECs of the vector current. Note that all three publications mentioned here use a different normalisation for f which explains the additional factor $1/\sqrt{2}$ in the above equation.

For the $B\pi$ excited states contamination, all terms which show the same time dependence as the second term in Eq. (5.29) need to be considered. Forming the ratio (5.30), one finds for the excited states of $h_\perp$

$$\delta h_\perp(t, t_\mathrm{v}, \vec{q}) = -\frac{1 + \tilde{\beta}_1 E_{\pi,\vec{q}}/g}{1 - \beta_1 E_{\pi,\vec{q}}/g} e^{-E_{\pi,\vec{q}}\, t_\mathrm{v}} + \delta C^{\mathrm{SL}}_{3,k}(\vec{q}, t, t_\mathrm{v}) - \frac{1}{2}\delta C^B_2(t_\mathrm{v}) + \frac{1}{2}\Delta m_{B,\mathrm{eff}}(t_\mathrm{v}) t_\mathrm{v} . \tag{5.34}$$

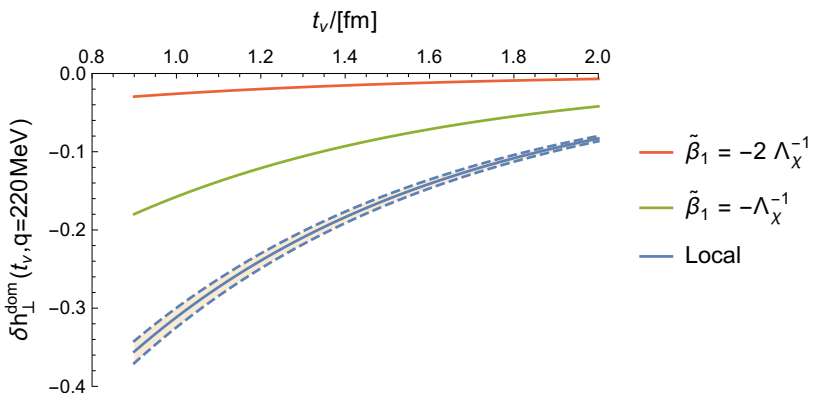

Figure 5.7.: Plot of $\delta h_\perp^{\rm dom}$, see Eq. (5.36), as a function of $t_{\rm v}$. The momentum of the pion in the final state is chosen to be $|\vec{q}| = 220\,{\rm MeV}$.

where the subleading contribution to the three-point function, $\delta C_{3,k}^{\rm SL}(\vec{q}, t, t_{\rm v})$, will be discussed in App. C. The most outstanding feature of this result is the first term which is due to diagrams (a)-(c): compared to the other three terms (and also all other results presented so far) it is not suppressed by a factor $1/f^2$ and it is also not a tower of excited states since no sum over a free internal momentum $\vec{p}$ is present. This means that the leading excited state is of the same order in the chiral expansion as the LO result for the form factor $h_\perp$ itself. Even more striking is that at LO, i.e. for $\beta_1 = \tilde{\beta}_1 = 0$, the coefficient of the exponential is -1. One can therefore expect that this term will give a large, negative contribution to the excited states contamination. This term can be traced back to the result for diagram (b):

$$(\text{b}) = \frac{\tilde{\alpha}\tilde{c}q_k e^{-E_{\pi,\vec{q}}(t-t_{\rm v})}}{4E_{\pi,\vec{q}}} \frac{\alpha g}{\sqrt{2} f E_{\pi,\vec{q}}} (1 - e^{-E_{\pi,\vec{q}}\, t_{\rm v}})\,. \tag{5.35}$$

The first factor drops out in the ratio (5.30), whereas the second term is the LO result for $h_\perp$ which is factored out in Eq. (5.30). The factor 1 in the brackets is the contribution to the form factor whereas the exponential contributes to the excited states contamination. It is the latter term which is responsible for the large excited state. Computing all three diagrams shows that the term proportional to β_1 in the denominator is due to diagram (a), whereas the $\tilde{\beta}_1$ term stems from diagram (c). The three diagrams which show only a single propagating pion line therefore yield the dominant contribution to both the form factor and the excited states contamination.

Since δC_2^B and $\Delta m_{B,\rm eff}$ start at order p^2, whereas the result presented above is of order p^0 and p^1, the dominant excited states contamination of the form factor $h_\perp$ is given by

$$\delta h_\perp^{\rm dom}(t_{\rm v}, \vec{q}) = -\frac{1 + \tilde{\beta}_1 E_{\pi,\vec{q}}/g}{1 - \beta_1 E_{\pi,\vec{q}}/g} e^{-E_{\pi,\vec{q}}\, t_{\rm v}}\,. \tag{5.36}$$

Fig. 5.7 shows a plot of this term and also investigates the effect of smearing. Since the matrix element is proportional to the momentum q_k of the final state pion, see Eq. (2.149), one has to chose a non-zero value for it. Here, the momentum was set to $|\vec{q}| = 220\,{\rm MeV}$ which corresponds to the smallest non-zero momentum $2\pi/L$ on a lattice of size $L = 4/m_\pi$ at the physical point. It is evident that the excited states contamination is indeed large and negative when one sets $\tilde{\beta}_1 = \beta_1$, i.e. without any smearing. At $t_{\rm v} = 1.3\,{\rm fm}$, $\delta h_\perp^{\rm dom}$ is around -20% and rather slowly increasing for larger $t_{\rm v}$. Even at $t_{\rm v} = 2.0\,{\rm fm}$, it is still at around -10%. The green and red lines in the plot show how smearing can affect the excited states. The green line, which corresponds to the value of $\tilde{\beta}_1$ at which the excited states contamination of the B

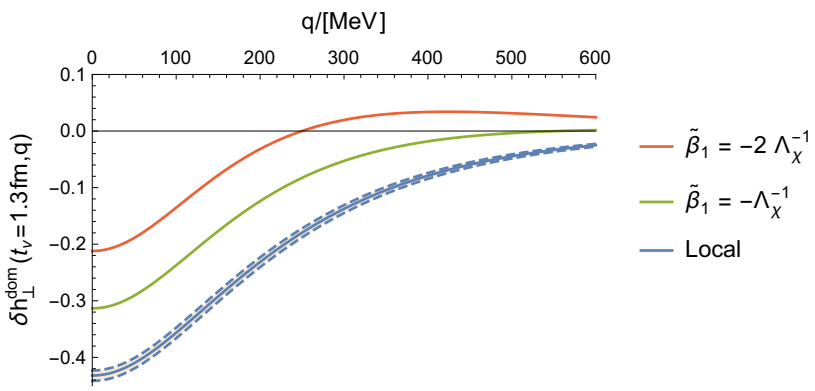

Figure 5.8.: Plot of $\delta h_\perp^{\rm dom}$ as a function of the final state pion momentum $|\vec{q}|$. The insertion time of the vector current was set to $t_{\rm v} = 1.3\,{\rm fm}$.

meson two-point function was minimised at $t = 1.3\,{\rm fm}$, shows a significant reduction of the excited states, but they are still at roughly -10% at $t_{\rm v} = 1.3\,{\rm fm}$. Setting $\tilde\beta_1 = -2\Lambda_\chi^{-1}$ on the other hand eliminates the excited states nearly completely, $\delta h_\perp^{\rm dom}$ is around -2% at most.

This large excited state is not only present in the correlation function for the $B \to \pi$ form factor, but also its $B_s \to K$ analogue. The result is mostly the same, only the energy of the final state pion $E_{\pi,\vec{q}}$ has to be replaced by the energy of the kaon $E_{K,\vec{q}}$. For this reason, the excited state is stronger suppressed, at least as long as the simulation is carried out with $m_\pi < m_K$. Since the LECs β_1 and $\tilde\beta_1$ are LECs in the chiral (and static) limit, they are also the same in both cases as long as one is comparing simulations with the same number of sea quarks.

Another interesting point to consider is the dependence of the excited states contamination on the external momentum $\vec{q}$. This is shown in Fig. 5.8 for a fixed vector current insertion time of $t_{\rm v} = 1.3\,{\rm fm}$. For larger $t_{\rm v}$, the excited states will be smaller due to the exponential suppression. As one can see from the figure, $\delta h_\perp^{\rm dom}$ is larger for smaller pion momentum $|\vec{q}|$. This is not surprising, since the exponential $\exp(-E_{\pi,\vec{q}}\,t_{\rm v})$ is suppressed for larger values of the energy $E_{\pi,\vec{q}}$. For $\tilde\beta_1 = \beta_1$, $\delta h_\perp^{\rm dom}$ can be about -40% for very small momenta and is still around -10% for $|\vec{q}| = 400\,{\rm MeV}$. It is clear that the excited states are large for most of the energy range in which chiral perturbation theory is applicable. The red and green lines show how smearing can help to reduce the excited states contamination. But as can be inferred form the figure, this strongly depends on the pion momentum chosen. The red line minimises the excited states at around $|\vec{q}| = 220\,{\rm MeV}$, but for larger momentum it 'overshoots' and leads to a positive contamination (not shown in the plot). This is then the region in which the green line leads to a significant reduction of $\delta h_\perp^{\rm dom}$. The lesson that can be learned from this plot is that for smaller final state pion momentum, more smearing is needed (assuming as always that smearing decreases the value of $\tilde\beta_1$).

This concludes the discussion of the leading excited states contamination of $h_\perp$, i.e. terms of order 1 and p. On the other hand, the results for $\delta\hat{f}_{\rm eff}$ and $\delta g_{B^*B\pi}^{\rm sum}$ presented in the preceding sections show that p^2 and p^3 terms can still yield a contamination of over 1%, and including those terms also in the discussion of $\delta h_\perp$ is therefore desirable if one aims for a high precision for the form factors. This requires the order p^2 and p^3 pieces of the interpolating fields and the vector current, since these pieces contribute to diagrams (a)-(c) in Fig. 5.6 at that order. But these terms have not been derived so far and the values of the new LECs which accompany them are also not known. This prohibits an accurate prediction of the size of the excited states contamination at order p^2 and higher at the moment. Furthermore, some of the remaining

diagrams in Fig. 5.6, which contribute at the same order in the chiral expansion, are UV divergent and the aforementioned LECs also need to be adjusted to serve as counterterms. In App. C, the computation of these diagrams is discussed.

5.2.2. $h_\parallel$

The second form factor $h_\parallel$ is defined via the matrix element of the time component of the vector current: $\langle\pi|V_4|B\rangle$. Its determination requires the computation of the three-point function $C_{3,\mu}$ (5.27) for $\mu = 4$, and the excited states contamination of the ratio of correlation functions (5.28) has already been defined in Eq. (5.31). The excited states contamination of the two-point function and B meson effective mass is the same as before, the computation of $\delta C_{3,4}$ in the effective theory proceeds along the same lines as the one for $\delta C_{3,k}$. This means that the same Feynman diagrams, see Fig. 5.6, have to be computed in the effective theory, and one would expect that diagrams (b) and (c) in Fig. 5.6 would contribute $\mathcal{O}(p^0)$ and $\mathcal{O}(p^1)$ terms to $\delta C_{3,4}$. But the form of V_4 in the effective theory, see Eq. (A.25) in App. A, does not allow for such diagrams: for these diagrams, one needs terms in V_4 with exactly one heavy meson and zero pions. The only heavy mesons in the theory are the pseudoscalar P and the vector P_k^* fields (P_4^* is zero due to the constraint (3.21)), but these do not have the same quantum numbers as V_4. The time component of a vector transforms as a scalar under parity transformations, but P and P_k^* both change sign under this transformation. For this reason, all terms of V_4 in the effective theory couple a heavy meson to at least one pion. This implies that diagrams (b), (c), (h), (i), (j), (k), (n), and (o) in Fig. 5.6 do not contribute to the correlation function $C_{3,4}$. This reduces the number of diagrams which need to be computed considerably, and also prevents the appearance of large excited states. Furthermore, Fig. C.2 in App. C presents another set of diagrams which contribute to the order p^2 and p^3 excited states contamination of $h_\perp$, and one might expect that they also contribute to $\delta h_\parallel$. These diagrams are higher order corrections to the large excited state which falls of with the energy of the final state pion, $\exp(-E_{\pi,\vec{q}}\, t)$. But this large excited state is absent in $\delta h_\parallel$ and it is therefore not surprising that all of these diagrams vanish for the three-point function $C_{3,4}$ from which $h_\parallel$ is extracted.

The result for the form factor up to order p^1 is completely given by diagram (a) in Fig. 5.6. It receives contributions from the LO and NLO terms of V_4:

$$h_\parallel(\vec{q}) = -\mathrm{i}\frac{\alpha}{\sqrt{2}f}\left(1 - \beta_2 E_{\pi,\vec{q}}\right) + \dots\,. \tag{5.37}$$

Up to a phase, the LO result again agrees with [132, 171, 172] if one neglects the B-B^* mass splitting and adjusts the normalisation of f. At NLO, the LEC β_2 enters whose value has been given in Eq. (4.21) and will be derived in Sec. 5.2.4.

The excited states contamination of the three-point function only receives contributions from diagrams (e), (f), and (g) in Fig. 5.6, all other diagrams either vanish or are of a higher order in the chiral expansion. The result can be written in the compact form

$$\delta C_{3,4}(\vec{q}, t_\mathrm{v}, t) = \frac{1}{1 - \beta_2 E_{\pi,\vec{q}}} \sum_{\vec{p}} \frac{3\vec{p}^{\,2}}{8f^2L^3E_{\pi,\vec{p}}^3}\left[g^2(1 - \beta_2 E_{\pi,\vec{q}}) + g(\beta_1 + \tilde{\beta}_1)E_{\pi,\vec{p}}\right] e^{-E_{\pi,\vec{p}}t_\mathrm{v}}\,. \tag{5.38}$$

This result can be inserted in Eq. (5.31), the result for the excited states contamination of the form factor. Fig. 5.9 shows the result as i) a function of time for $|\vec{q}| = 0\,\mathrm{MeV}$, and ii) a function of $|\vec{q}|$ for $t_\mathrm{v} = 1.3\,\mathrm{fm}$. The plots show that $\delta h_\parallel$ is positive and about an order of magnitude smaller than $\delta h_\perp$. This can be traced back to the absence of the large excited state due to diagrams (b) and (c) in Fig. 5.6. For this reason, one finds at $t_\mathrm{v} = 1.3\,\mathrm{fm}$ and vanishing pion

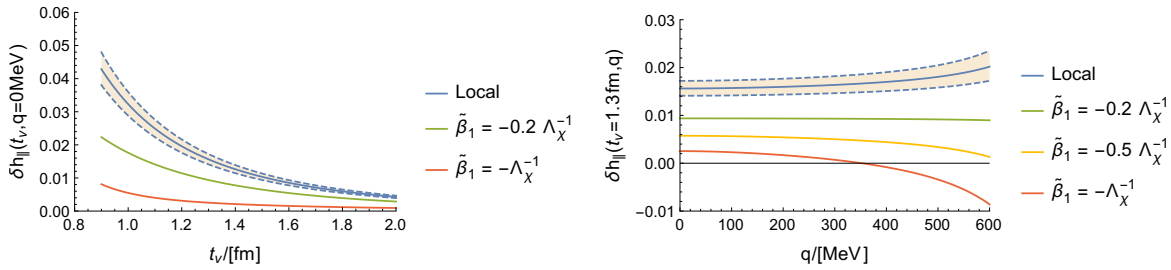

Figure 5.9.: The excited states contamination $\delta h_{\|}$ as a function of time (left) and of the final state pion momentum (right).

momentum an excited states contamination of about 2%. This result, which was obtained by setting $\tilde{\beta}_1 = \beta_1$, can be improved by applying smearing as exemplified by the green and red lines in the left plot. If $\tilde{\beta}_1 = -\Lambda_\chi^{-1}$ can be reached by a smearing procedure, one can consistently drive the excited states contamination to values smaller than 1% for time scales at which ChPT is applicable. The plot on the r.h.s. in Fig. 5.9 shows that the dependence on the pion momentum is mild. Only for larger $|\vec{q}|$, it increases due to the overall factor of $1/(1-\beta_2 E_{\pi,\vec{q}})$ in Eq. (5.38). This is just a sign that the form factor (5.37) is getting closer to zero in this range of pion momenta. The green, red, and yellow lines show that applying smearing to the interpolating fields can help to reduce the excited states contamination even more. It can even lead to negative values of $\delta h_{\|}$, e.g. the yellow band with $\tilde{\beta}_1 = -\Lambda_\chi^{-1}$ is about -0.009 for $|\vec{q}| = 600\,\text{MeV}$.

In order to get $\delta h_{\|}$ for the process $B_s \to K$, one has to make only minor modifications: the results for $\delta C_2^{B_s}$, $\Delta m_{B_s,\text{eff}}$, and $\delta C_{3,4}^{B_s}$ are larger by a factor 4/3 compared to the $\bar{B}^0$ and B^- results, which means that also $\delta h_{\|}$ is rescaled by this factor, see Eq. (5.31). Furthermore, the pion energies $E_{\pi,\vec{p}}$ and $E_{\pi,\vec{q}}$ need to be replaced by the kaon energies $E_{K,\vec{p}}$ and $E_{K,\vec{q}}$.

It is also worthwhile to investigate which momentum configurations in the sum (5.38) give the dominant contribution to $\delta h_{\|}$. In the analysis of lattice results, one often uses a fit ansatz with a few exponentials which are supposed to capture the ground state and lowest lying excited states contributions to a given correlation function. In order to see if this is indeed enough or reliable, $\delta h_{\|}$ will be evaluated in a finite volume with spatial extent $L = 4/m_\pi$ and for several cut-offs of the momentum sum in (5.38). In a finite volume, the momenta are quantised and of the generic form

$$\vec{p} = \frac{2\pi}{L}\vec{n}\,, \qquad\qquad |\vec{p}| = \frac{2\pi}{L}\sqrt{n}, \tag{5.39}$$

with $\vec{n}$ a vector whose components are integers, and n is also an integer. In Fig. 5.10, $\delta h_{\|}$ is plotted for vanishing external momentum $\vec{q}$, $\tilde{\beta}_1 = \beta_1$, and for several cut-off values for n. They correspond approximately to the values 220 MeV, 310 MeV, 380 MeV, 440 MeV, 490 MeV, 700 MeV, 910 MeV, and 980 MeV. It is clear from the plot that at $t_\text{v} = 1.3\,\text{fm}$ the lowest two or three momentum configurations constitute only a fraction of the total excited states contamination. Even when including the five $B\pi$ excited states with the lowest energies, there is still a considerable gap to the results which include the lowest 17 or 20 states, the states at which the sum in Eq. (5.38) is apparently saturated. In other words, the excited states with momentum larger than $|\vec{p}| = \sqrt{5}\,2\pi/L$ still give a non-negligible contribution to the correlation function and it therefore seems unlikely that a fit with only a few exponentials will yield a reliable result.

To sum up, fits which try to capture only the lowest few excited states might not be sufficient for disentangling the ground state from the excited states contributions to correlation functions.

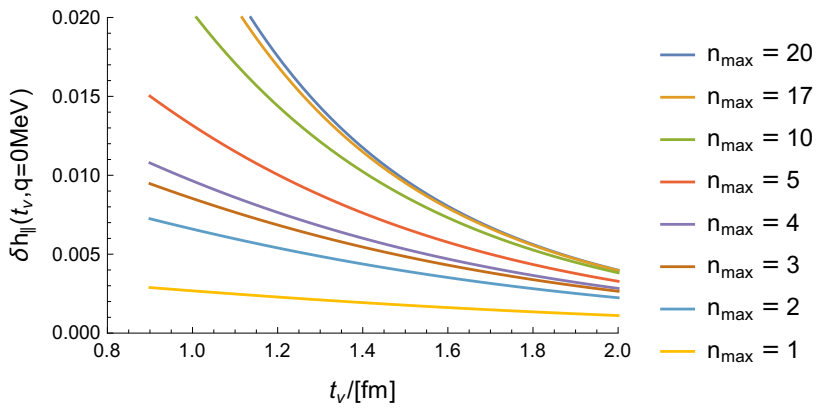

Figure 5.10.: The excited states contamination $\delta h_{\parallel}$ in a finite volume for several cut-offs in momentum space.

All in all, the excited states contamination of $\delta h_{\parallel}$ is small compared to $\delta h_{\perp}$, and positive. It also does not show a significant dependence on the momentum of the final state pion over the range considered here. The following section discusses how the choice of ratio from which the form factor is extracted influences the size of the excited states contamination.

5.2.3. Comparing the Excited States Contamination of Different Ratios

In Sec. 2.2.1 several ratios for extracting matrix elements from three-point functions have been presented. In Eqs. (2.89)-(2.91), it was explicitly spelled out how the excited states contamination of the three- and two-point functions as well as the effective masses combine to the contamination of the ratios. This section studies how the choice of ratio influences the overall excited states contamination of the $B \to \pi$ form factors. As discussed before, the contributions of the pion two-point function and effective mass are so small that they can be neglected. $\delta C_{3,\mu}$ on the other hand is the same for all ratios, so it is enough to study the effect of δC_2^B and $\Delta m_{B,\text{eff}}$, see Eqs. (4.28) and (4.32) for the respective leading results in HM ChPT. This also has the advantage that the discussion is independent of the three-point function and the particle in the final state. The results presented here are therefore applicable to any ratio involving a heavy B meson in the initial state and can be combined with the excited states contamination of the three-point function and the final state particle to arrive at the full excited states contamination of a matrix element. Collecting the terms proportional to δC_2^B and $\Delta m_{B,\text{eff}}$ in the δR_is, one has

$$\delta R_1^B(t_\text{v}) = -\frac{1}{2}\delta C_2^B(2t_\text{v})\,, \tag{5.40}$$

$$\delta R_2^B(t_\text{v}) = -\frac{1}{2}\delta C_2^B(t_\text{v}) + \Delta m_{B,\text{eff}}(t_\text{v})\tfrac{t_\text{v}}{2}\,, \tag{5.41}$$

$$\delta R_3^B(t_\text{v}, t) = -\frac{1}{2}\delta C_2^B(t) + \Delta m_{B,\text{eff}}(t)\left(t_\text{v} - \tfrac{t}{2}\right)\,. \tag{5.42}$$

As a reminder, the B interpolating field is inserted on time slice 0, the vector current at t_v, and the pion interpolating field on time slice t. The latter time slice only enters in the third equation. In Ch. 4, it has been argued that the ChPT results for B mesons are reliable, as long as the time separation between the operators interpolating them is larger than 1.3 fm, whereas for pions it should be larger than 1 fm. From the form of the three-point function (5.27) from which the form factors are extracted, it is therefore clear that one is restricted to $t_\text{v} \geq 1.3\,\text{fm}$ and $t - t_\text{v} \geq 1\,\text{fm}$. For δR_1^B and δR_3^B, one would therefore have to compute the B meson

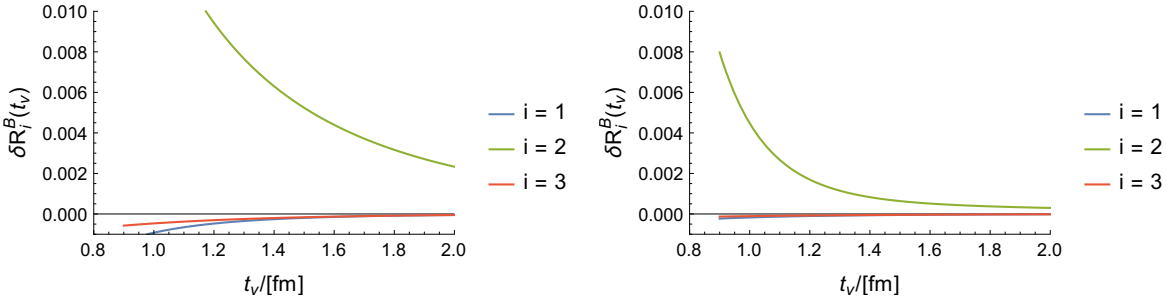

Figure 5.11.: The contribution of δC_2^B and $\Delta m_{B,\text{eff}}$ to the excited states contamination of the three ratios defined in Eq. (2.84)-(2.86). The NLO LEC of the B meson interpolating field was set to its local value $\tilde{\beta}_1 = \beta_1$ for the plot on the left, and $\tilde{\beta}_1 = -\Lambda_\chi^{-1}$ on the right.

two-point function for time intervals larger than 2.6 fm and 2.3 fm, respectively. At the moment, the signal-to-noise ratio becomes too large for time separations above approximately 1.2 fm (compare the plots in [173]), but one can hope that the discussion presented here carries over to the contamination due to interpolating fields of other particles. The reason is that the effective mass is derived from the two-point function, and the above δR_i^Bs should show the same qualitative behaviour irrespective of the chosen particle. On the other hand, there is also the chance that improvements in algorithms will help to tame the signal-to-noise problem in HQET, and one will one day reach time separations for which the results of this section are applicable.

Numerical evaluations of the individual δR_i^Bs can be found in Fig. 5.11. The plot on the l.h.s. was compiled for $\tilde{\beta}_1 = \beta_1$, whereas for the second plot $\tilde{\beta}_1 = -\Lambda_\chi^{-1}$ was used. The δR_i^Bs are plotted as a function of t_v, the time interval over which the B meson propagates. For δR_3^B also t needs to be fixed, and $t = t_\text{v} + 1.5\,\text{fm}$ was chosen. The main reason for this choice is that for smaller values of $t - t_\text{v}$ the results for δR_1^B and δR_3^B become more and more degenerate. As can be seen from the plots, they both lead to a negative and tiny contribution to the excited states contamination of the form factors. For times larger than 1.3 fm, one finds an underestimation of at most 0.05%. The effect of δR_2^B on the other hand is more pronounced, and one finds a positive result of size 0.7% for local interpolating fields and 0.1% for the smeared fields at $t_\text{v} = 1.3\,\text{fm}$. The reason for this larger contribution to the excited states contamination can be easily explained: from Eqs. (4.28) and (4.32), it is clear that the δR_i^Bs are given by sums of exponentials of the form $\exp(-E_{\pi,\vec{p}}\, t')$. Whereas for $i = 2$, one has to set $t = t_\text{v}$, the other two have $t' = 2t_\text{v}$ and $t' = t_\text{v} + 1.5\,\text{fm}$ and are thus stronger suppressed.

With these results at hand, one can study their influence on the excited states contamination of the $B \to \pi$ form factors. Since $\delta h_\perp$ is dominated by the large excited states in the three-point function, it will not be discussed here. From the plot of $\delta h_\parallel$ for fixed $|\vec{q}| = 0$ in Fig. 5.9, one can read off an excited states contamination of approximately 2% at $t_\text{v} = 1.3\,\text{fm}$ and for local interpolating fields. This plot shows the excited states contamination of the ratio R_2 defined in Eq. (2.85). In this section, it was found that $\delta R_2^B(1.3\,\text{fm}) \approx 0.7\%$, which is about one third of the total contamination of the ratio. If it would be possible in the future to use ratio R_1 (Eq. (2.84)) or R_3 (Eq. (2.85)) for extracting the form factor $h_\parallel$, the effects of excited states would be dramatically smaller. The same conclusion can be deduced for the ratios with smeared interpolating fields.

On the other hand, it seems plausible that if one can one day simulate the B meson two-point function with a time separation of 2.6 fm, one can also simulate three-point functions with a

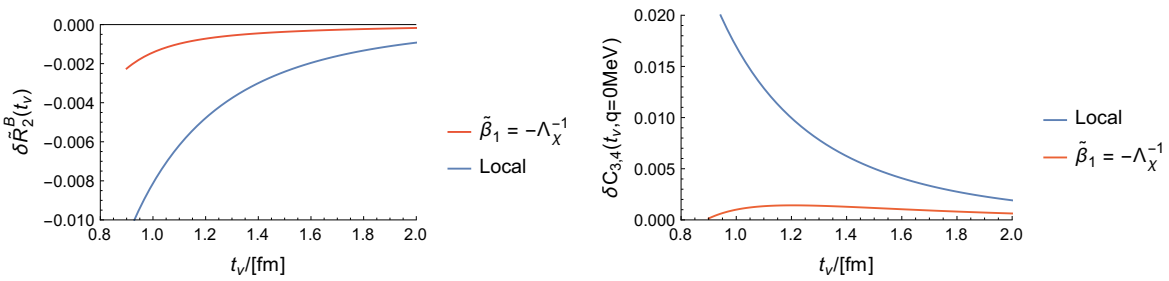

Figure 5.12.: On the l.h.s. the contribution of δC_2^B to the excited states contamination of the ratio $\tilde{R}_2$ is shown for $\tilde{\beta}_1 = \beta_1$. On the right, the $B\pi$ excited states contamination of $C_{3,4}$, the three-point function from which $h_\parallel$ is extracted (see Eq. (5.38) for the result in HM ChPT) is shown.

B meson propagating over a time interval of similar size. For this reason, it makes sense to compare the ratios $R_1(t, 1.3\,\text{fm})$ and $R_2(t, 2.6\,\text{fm})$ for the extraction of $h_\parallel$. Since the effects of the pion two-point function and effective mass are not considered, and the $B\pi$ states in the three-point function propagate from 0 to t_v, the result for the excited states contamination of the two ratios does not depend on t to the order it has been computed in this thesis. Computing it explicitly, one finds

$$\delta R_1(t, 1.3\,\text{fm}) = \delta C_{3,4}(t, 1.3\,\text{fm}) - \frac{1}{2}\delta C_2^B(2.6\,\text{fm}) = 0.7\%\,, \tag{5.43}$$

$$\delta R_2(t, 2.6\,\text{fm}) = \delta C_{3,4}(t, 2.6\,\text{fm}) - \frac{1}{2}\delta C_2^B(2.6\,\text{fm}) + \Delta m_{B,\text{eff}}(2.6\,\text{fm}) \times 1.3\,\text{fm} = 0.2\%\,. \tag{5.44}$$

The contamination of R_2 is smaller, a result that can be traced back to $\delta C_{3,4}$ whose explicit form is given in Eq. (5.38) and plotted in Fig. 5.12. For R_1, it is evaluated at 1.3 fm, whereas for R_2 at 2.6 fm. The exponentials $\exp(-E_{\pi,\vec{p}}\, t_\text{v})$ lead to a stronger suppression for R_2 which explains the smaller value for δR_2^B.

There is another point which should be discussed: having a closer look at Eq. (5.41), one sees that δC_2^B, which is strictly positive if the same smearing is used for the operators at source and sink, enters with a negative sign, whereas $\Delta m_{B,\text{eff}}$, which is also strictly positive under the same assumptions, enters with a positive sign. From the plot in Fig. 5.11 one can infer that the contribution of the latter must therefore be larger. On the other hand, one does not have to use the effective mass in the definition of the ratios, but can instead extract the B meson mass beforehand and use it in the exponentials. If one can be sure that the excited states have been eliminated consistently, only the contribution of the two-point function enters in Eqs. (5.40)-(5.42). Since δR_1^B does not depend on the effective mass and δR_3^B is small anyway, only δR_2^B will be considered in the following. First, for completeness and in full generality, the ratio considered in the following is given by

$$\begin{aligned}\tilde{R}_2(t,t') = 2\sqrt{m_I m_F}\frac{C_3(t,t')}{\sqrt{C_2^{\mathcal{F}}(t-t')C_2^{\mathcal{I}}(t')}}e^{m_I\frac{t'}{2}+m_F\frac{(t-t')}{2}} &= \langle F|\mathcal{T}|I\rangle\left[1+\delta C_3(t,t')\right.\\ \left.-\frac{1}{2}\left(\delta C_2^{\mathcal{F}}(t-t')+\delta C_2^{\mathcal{I}}(t')\right)\right] &\equiv \langle F|\mathcal{T}|I\rangle\left(1+\delta\tilde{R}_2(t,t')\right),\end{aligned} \tag{5.45}$$

with arbitrary particles in the initial and final state, see Eq. (2.83) for the definition of the three-point function. In the following however, $B \to \pi$ matrix elements are of interest. The contribution of the initial state B meson interpolating field to the excited states contamination

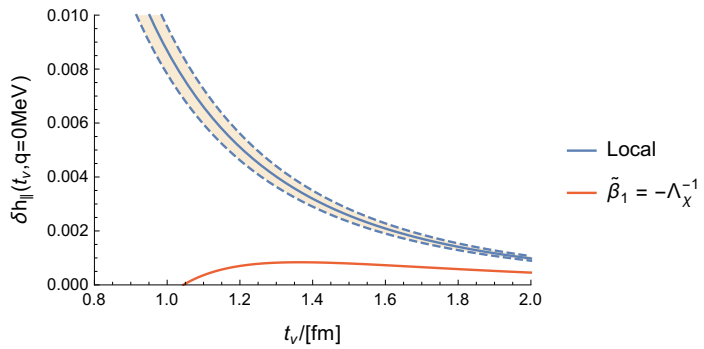

Figure 5.13.: The excited states contamination of $h_{\|}$ when extracted from the ratio $\tilde{R}_2$ defined in Eq. (5.45).

of the ratio therefore reads

$$\delta\tilde{R}_2^B(t_\mathrm{v}) = -\frac{1}{2}\delta C_2^B(t_\mathrm{v})\,. \tag{5.46}$$

The l.h.s. plot in Fig. 5.12 shows $\delta\tilde{R}_2^B$ as a function of t_v, it is negative and approximately -0.4% at $t_\mathrm{v} = 1.3\,\mathrm{fm}$. The other plot in the figure shows $\delta C_{3,4}$, the excited states contamination of the three-point function from which $h_{\|}$ is extracted. Neglecting the excited states contamination of the pion two-point function, $\delta h_{\|}$ is given by the sum of $\delta C_{3,4}$ and $\delta\tilde{R}_2^B$. Since $\delta C_{3,4}$ is positive, a cancellation between the two contributions takes place. The result is plotted in Fig. 5.13. Comparing it with the plot in Fig. 5.9, which shows the excited states contamination of the ratio given in Eq. (5.31), it is clear that the ratio considered here is superior since $\delta h_{\|}$ is below the 1% level. At $t_\mathrm{v} = 1.3\,\mathrm{fm}$, the excited states are reduced by a factor 5 for local interpolating fields. With a suitable smearing procedure, it seems even possible to consistently reach a 0.1% level. One therefore has to conclude that, at least for $h_{\|}$, ratios involving the effective B meson mass lead to a larger excited states contamination and should therefore be avoided by extracting the B meson mass beforehand.

5.2.4. Extracting β_1 and β_2 from the Form Factors

The high degree of symmetry of static HQET made it possible to significantly reduce the number of LECs of the local heavy-light currents and densities. There is only one constant at leading order in the chiral expansion, α, which is related to the heavy meson decay constant. At NLO, there are two LECs, β_1 and β_2, which couple at least one pion to a heavy meson. As can be seen from Eqs. (5.33) and (5.37), they enter the results for the $B \to \pi$ vector form factors. Comparing the analytic results found in HM ChPT to lattice determinations of the form factors is therefore a promising procedure for extracting the NLO LECs. A similar discussion has already been presented in [116].

A recent lattice computation of the form factors using relativistic heavy quarks was carried out by the JLQCD collaboration [140]. In the publication, they also give an explicit expression for the fit to the numerical results of the two form factors. From the results for the fit parameters, it is possible to deduce numerical values for the two LECs β_1 and β_2. The relevant terms of the fit read

$$f_2(E_\pi) = D_0 \frac{E_\pi}{E_\pi + \Delta_B}(1 + D_E N_E E_\pi)\cdots\,, \tag{5.47}$$

$$f_1(E_\pi) + f_2(E_\pi) = C_0\left(1 + \sum_{n=1}^{3} C_{E^n} N_E^n E_\pi^n\right)\cdots\,. \tag{5.48}$$

The dots represent additional terms of the fit which include chiral logarithms, $1/m_b$ corrections, and discretisation effects. Δ_B is the mass difference of the vector and pseudoscalar B meson and $N_E = 1/(0.3\,\text{GeV})$ is a normalisation constant. The constants D_i and C_i are the free parameters of the fit. The two form factors f_1 and f_2 are related to the form factors $h_\perp$ and $h_\parallel$ defined in Eq. (2.147) via the equations

$$h_\perp(E_\pi) = 2\frac{f_2(E_\pi)}{E_\pi}\,, \tag{5.49}$$

$$h_\parallel(E_\pi) = 2[f_1(E_\pi) + f_2(E_\pi)]\,. \tag{5.50}$$

Note that these are the form factors for relativistic b quarks, the matching to the form factors in static HQET is given by the relations in Eq. (2.150). Equating then the HM ChPT results with the NLO results of the fit function, one has

$$C_\text{V}\frac{\alpha g}{\sqrt{2}fE_\pi}\left(1 - \frac{\beta_1 E_\pi}{g}\right) = 2\frac{D_0}{E_\pi}\frac{E_\pi}{E_\pi + \Delta_B}(1 + D_E N_E E_\pi)\,, \tag{5.51}$$

$$C_\text{PS}\frac{\alpha}{\sqrt{2}f}(1 - \beta_2 E_\pi) = 2C_0(1 + C_E N_E E_\pi)\,. \tag{5.52}$$

If one neglects the $B - B^*$ mass splitting, which is zero in the static limit of HQET, the LECs β_1 and β_2 can be inferred from the above equation,

$$\beta_1 = -gD_E N_E\,, \tag{5.53}$$

$$\beta_2 = -C_E N_E\,. \tag{5.54}$$

The numerical results for the fit parameters are given as $C_E = -0.37(1)$ and $D_E = -0.086(14)$. From these, the best values and the errors for the NLO LECs can be computed. For β_1, also $g = 0.49(1)$ is needed. The errors which are obtained from these inputs might in fact be too small: the lattice computation was carried out for relativistic quarks whereas the β_is are LECs of static HM ChPT/HQET. To be sure that the systematic errors which arise due to the difference between the two theories are captured, the resulting errors for β_1 and β_2 are doubled. This leads to the results already presented in Eqs. (4.20) and (4.21):

$$\beta_1 = 0.14(5)\,\text{GeV}^{-1}\,, \tag{5.55}$$

$$\beta_2 = 1.2(3)\,\text{GeV}^{-1}\,. \tag{5.56}$$

These are the results for the LECs of the local heavy-light currents and densities. The results for the excited states contamination presented in this work on the other hand also depend on the LEC $\tilde{\beta}_1$ of the smeared interpolating fields. Since the value for this LEC is not universal but depends on the applied smearing, it is desirable to find a procedure from which it can be extracted. A straightforward, but tedious strategy would be to compute the matrix element $\langle\pi|\mathcal{B}_k|B\rangle$ where $\mathcal{B}_k$ is the smeared interpolating field of the vector B meson. An easier approach consists in computing the three-point function $C_{3,k}$ (5.27) for local and smeared heavy-light vector currents, and taking their ratio. These correlation functions will be denoted by $C_{3,k}^\text{loc}$ and $C_{3,k}^\text{sm}$, respectively. The dominant contributions to these correlators stem from diagrams (a)-(c) in Fig. 5.6, and the result for the correlator with the local vector current reads

$$C_{3,k}^\text{dom,loc}(\vec{q}, t, t_\text{v}) = \frac{\alpha\hat{\alpha}\hat{c}g}{4\sqrt{2}fE_{\pi,\vec{q}}^2}q_k e^{-E_{\pi,\vec{q}}(t-t_\text{v})}\left[1 - \frac{\beta_1 E_{\pi,\vec{q}}}{g} - e^{-E_{\pi,\vec{q}}\,t_\text{v}} - \frac{\hat{\beta}_1 E_{\pi,\vec{q}}}{g}e^{-E_{\pi,\vec{q}}\,t_\text{v}}\right]. \tag{5.57}$$

For the smeared vector current, one has to make the replacements $\alpha \to \tilde{\alpha}$ and $\beta_1 \to \tilde{\beta}_1$. The constants $\hat{\alpha}$, $\hat{\beta}_1$, and $\hat{c}$ are the LECs of the interpolating fields for the initial state B meson

and the final state pion. One should use the same smearing for them in both correlation functions. Taking the ratio mentioned before and expanding the denominator, one finds

$$\frac{C_{3,k}^{\mathrm{dom,sm}}(\vec{q},t,t_{\mathrm{v}})}{C_{3,k}^{\mathrm{dom,loc}}(\vec{q},t,t_{\mathrm{v}})} = \frac{\tilde{\alpha}}{\alpha}\left[1 - \frac{\beta_1 - \tilde{\beta}_1}{g}E_{\pi,\vec{q}} - \frac{\beta_1 + \tilde{\beta}_1}{g}E_{\pi,\vec{q}}\, e^{-E_{\pi,\vec{q}}\, t_{\mathrm{v}}} + \mathcal{O}(E_{\pi,\vec{q}}^2)\right] . \tag{5.58}$$

The LEC $\hat{\beta}_1$ drops out to this order in the expansion. The expansion itself on the other hand is only justified as long as

$$\left|\frac{\beta_1 E_{\pi,\vec{q}}}{g} + e^{-E_{\pi,\vec{q}}\, t_{\mathrm{v}}} + \frac{\hat{\beta}_1 E_{\pi,\vec{q}}}{g} e^{-E_{\pi,\vec{q}}\, t_{\mathrm{v}}}\right| \ll 1 \tag{5.59}$$

holds true. This requirement might be spoiled by the second term, the single exponential without prefactor, if the pion energy is small. Since the size of the time interval t_{v} is limited by the signal-to-noise ratio of the heavy meson, a moderately large pion energy $E_{\pi,\vec{q}}$ might be necessary. On the other hand, the energy cannot be too large, otherwise higher order terms in the chiral expansion cannot be neglected or the chiral expansion breaks down completely. It is therefore advisable to compute the ratio (5.58) for more than one pion momentum in order to check if the results reasonably follow the analytic form presented here. If the expansion is justified, Eq. (5.58) can be used to extract $\tilde{\beta}_1$. The overall constant $\tilde{\alpha}/\alpha$ can be extracted from a ratio of B meson two-point functions, e.g.

$$\frac{C_2^{B,\mathrm{LS}}(t)}{C_2^{B,\mathrm{SS}}(t)} = \frac{\tilde{\alpha}}{\alpha} + \cdots , \tag{5.60}$$

where the dots stand for higher order corrections and the excited states contamination of the correlators. $C_2^{B,\mathrm{LS}}$ is the B meson two-point function with one local and one smeared interpolating field, whereas $C_2^{B,\mathrm{SS}}$ uses the same smearing at both source and sink. After dividing the ratio (5.58) by this factor, $\tilde{\beta}_1$ is the only unknown parameter of the result. It is nevertheless necessary to compute the ratio for at least two values of t_{v} so that the second and third term in Eq. (5.58) can be reliably disentangled. Computing the ratio for at least two pion momenta of different magnitude is needed for distinguishing the constant and $\mathcal{O}(p^1)$ terms.

The result for the ratios (5.58) and (5.60) only considered the leading contributions to the correlation functions and neglected all higher order corrections and the subleading excited states contamination. This can introduce systematic errors in the determination of $\tilde{\beta}_1$, but they are only of a higher order in the chiral expansion. Since $\tilde{\beta}_1$ is an NLO LEC, it is not necessary to determine it at the subpercent-level anyway.

5.3. B^0-$\bar{B}^0$ Oscillations

This section lays out the computation of the $B\pi$ excited states contamination of the B^0-$\bar{B}^0$ mixing amplitude in HM ChPT. The relevance of this oscillation process and how the CKM matrix element V_{td} can be extracted from it has already been presented in Sec. 2.4.3. The very nature of this process, in which a particle is converted into its anti-particle, makes it necessary to consider correlation functions which do not only include the interpolating fields for heavy mesons with a b quark, but also with a $\bar{b}$ quark. Besides the interpolating field $\mathcal{B}^{(b)}$, which interpolates a $\bar{B}$ meson and was denoted by $\mathcal{B}$ so far, one also needs an interpolating field for its anti-particle, the B. This field will be denoted by $\mathcal{B}^{(\bar{b})}$ and can be obtained by charge

conjugation. The two fields are needed for computing the three point function ($t > t_\mathrm{I} > 0$ is assumed throughout)

$$C_{3,i}(t,t_\mathrm{I}) = \int\limits_{L^3} \mathrm{d}^3\vec{x}\,\mathrm{d}^3\vec{y}\,\left\langle \bar{\mathcal{B}}^0(t,\vec{x})O_i(t_\mathrm{I},\vec{y})\mathcal{B}^{0\dagger}(0,\vec{0})\right\rangle\,, \tag{5.61}$$

where O_i, $i = \mathrm{L},\mathrm{M}$, are the two operators which mediate the neutral B meson oscillation in HQET/HM ChPT, see Sec. 2.4.3. The ground state contribution to this correlation function is proportional to the matrix element $\langle \bar{B}^0|O_i|B^0\rangle$ and it can be extracted from a suitable ratio of the above three-point function with the B and $\bar{B}$ meson two-point functions. Since the interpolating fields for a B and $\bar{B}$ meson are related by charge conjugation it follows that the two-point functions are identical:

$$\begin{aligned}\left\langle 0\middle|\mathcal{B}^{(b)}(x)\mathcal{B}^{(b)\dagger}(0)\middle|0\right\rangle &= \left\langle 0\middle|\mathcal{C}^{-1}\left[\mathcal{C}\mathcal{B}^{(b)}(x)\mathcal{C}^{-1}\right]\left[\mathcal{C}\mathcal{B}^{(b)\dagger}(0)\mathcal{C}^{-1}\right]\mathcal{C}\middle|0\right\rangle \\ &= \left\langle 0\middle|\mathcal{B}^{(\bar{b})}(x)\mathcal{B}^{(\bar{b})\dagger}(0)\middle|0\right\rangle\,.\end{aligned} \tag{5.62}$$

A suitable ratio for extracting the B^0-$\bar{B}^0$ mixing matrix elements is therefore given by

$$\left\langle \bar{B}^0\middle|O_i\middle|B^0\right\rangle = \lim_{t_\mathrm{I},(t-t_\mathrm{I})\to\infty} 2\frac{C_{3,i}(t,t_\mathrm{I})}{C_2^B(t)}\,. \tag{5.63}$$

For finite time intervals t_I and $t - t_\mathrm{I}$, excited states will also contribute to the ratio. It is therefore convenient to define

$$\begin{aligned}R_i(t,t_\mathrm{I}) = 2\frac{C_{3,i}(t,t_\mathrm{I})}{C_2^B(t)} &= \left\langle \bar{B}^0\middle|O_i\middle|B^0\right\rangle\left(1+\delta C_{3,i}(t,t_\mathrm{I}) - \delta C_2^B(t)\right) \\ &= \left\langle \bar{B}^0\middle|O_i\middle|B^0\right\rangle\left(1+\delta R_i(t,t_\mathrm{I})\right)\,, \end{aligned} \tag{5.64}$$

$$\delta R_i(t,t_\mathrm{I}) = \sum_{\vec{p}}\left(b_{1,i}(\vec{p})e^{-E_{\pi,\vec{p}}t_\mathrm{I}} + b_{2,i}(\vec{p})e^{-E_{\pi,\vec{p}}(t-t_\mathrm{I})} + c_i(\vec{p})e^{-E_{\pi,\vec{p}}t}\right)\,. \tag{5.65}$$

δR_i captures the effects of the excited states. As before, only the dominant $B\pi$ excited states contamination is considered which leads to the above form for δR_i. The coefficient $b_{1,i}$ gets contributions from the matrix element $\langle \bar{B}|O_i|B^*\pi\rangle$, whereas $\langle \bar{B}^*\pi|O_i|B\rangle$ contributes to $b_{2,i}$. The coefficient c_i receives contributions from the matrix element $\langle \bar{B}^*\pi|O_i|B^*\pi\rangle$, but also from the excited states of the two-point function and is given by

$$c_i(\vec{p}) = c_{3\mathrm{pt},i}(\vec{p}) - c_{2\mathrm{pt}}(\vec{p})\,. \tag{5.66}$$

The coefficient $c_{2\mathrm{pt}}$ of the B meson two-point function has been defined in Eq. (4.29). The result in Eq. (5.65) is of the same form as what has been found for the excited states contamination of $g_{B^*B\pi}$ in Sec. 5.1. There, it was argued that the summation method is a suitable tool for reducing the effects of excited states. For this reason, it will also be applied here and one defines

$$R_i^\mathrm{sum}(t) = \frac{\mathrm{d}}{\mathrm{d}t}\int\limits_0^t \mathrm{d}t_\mathrm{I}\,R_i(t,t_\mathrm{I}) = \left\langle \bar{B}^0\middle|O_i\middle|B^0\right\rangle\left(1+\delta R_i^\mathrm{sum}(t)\right)\,, \tag{5.67}$$

$$\delta R_i^\mathrm{sum}(t) = \sum_{\vec{p}}\left(b_{1,i}(\vec{p}) + b_{2,i}(\vec{p}) + c_i(\vec{p})(1-E_{\pi,\vec{p}}t)\right)e^{-E_{\pi,\vec{p}}t}\,. \tag{5.68}$$

In the following, the computation of the three-point function (5.61) in HM ChPT is presented, from which the coefficients b_i and $c_{3\mathrm{pt}}$ can be obtained. To do so, one first needs to derive

the interpolating field $\mathcal{B}^{(\bar{b})}$ for a B meson with a $\bar{b}$ quark, and also the analogues of the HQET operators O_{L} and O_{M} in HM ChPT. The former can be obtained by applying charge conjugation to the interpolating field $\mathcal{B}^{(b)}$. The transformations of the fields $H^{(b)}$ and u under charge conjugation have already been given in Eqs. (3.38) and (3.40), and the action of the charge conjugation matrix C on the gamma matrices was presented in Eq. (3.42). Applying this to the interpolating field derived in Sec. 4.1, one finds

$$\begin{aligned}\mathcal{B}^{(\bar{b})} = \mathcal{C}\mathcal{B}^{(b)}\mathcal{C}^{-1} &= -\frac{\mathrm{i}\tilde{\alpha}}{4}\mathrm{Tr}\left[\gamma_5 u^+ H^{(\bar{b})}\right] + \frac{\tilde{\alpha}\tilde{\beta}_1}{4}\mathrm{Tr}\left[\gamma_m u^+ u_m H^{(\bar{b})}\right] + \frac{\tilde{\alpha}\tilde{\beta}_2}{4}\mathrm{Tr}\left[\gamma_5 u^- u_4 H^{(\bar{b})}\right] \\ &= \frac{\tilde{\alpha}}{2}u^+ P^{(\bar{b})} + \frac{\mathrm{i}\tilde{\alpha}\tilde{\beta}_1}{2}u^+ u_k P_k^{(\bar{b})*} + \frac{\mathrm{i}\tilde{\alpha}\tilde{\beta}_2}{2}u^- u_4 P^{(\bar{b})}\,. \end{aligned} \tag{5.69}$$

An explicit calculation shows that the two-point functions of the fields $\mathcal{B}^{(b)}$ and $\mathcal{B}^{(\bar{b})}$ do indeed agree. The interpolating field for a vector meson with a $\bar{b}$ quark will be needed in Sec. 5.3.3, so it is convenient to present it here

$$\begin{aligned}\mathcal{B}_k^{(\bar{b})} = -\mathcal{C}\mathcal{B}_k^{(b)}\mathcal{C}^{-1} &= -\frac{\mathrm{i}\tilde{\alpha}}{4}\mathrm{Tr}\left[\gamma_k u^+ H^{(\bar{b})}\right] + \frac{\tilde{\alpha}\tilde{\beta}_1}{4}\mathrm{Tr}\left[\gamma_k\gamma_5\gamma_m u^+ u_m H^{(\bar{b})}\right] + \frac{\tilde{\alpha}\tilde{\beta}_2}{4}\mathrm{Tr}\left[\gamma_k u^- u_4 H^{(\bar{b})}\right] \\ &= \frac{\tilde{\alpha}}{2}u^+ P_k^{(\bar{b})*} - \frac{\mathrm{i}\tilde{\alpha}\tilde{\beta}_1}{2}u^+\left(\varepsilon_{klm}u_m P_l^{(\bar{b})*} + u_k P^{(\bar{b})}\right) + \frac{\mathrm{i}\tilde{\alpha}\tilde{\beta}_2}{2}u^- u_4 P_k^{(\bar{b})*}\,. \end{aligned} \tag{5.70}$$

The minus sign in the definition of $\mathcal{B}_k^{(\bar{b})}$ is due to the convention for charge conjugation of vector mesons, see the definition in Eq. (3.40) which carries over to the interpolating field of a vector particle.

5.3.1. O_{L} and O_{M} in HM ChPT

The derivation of the operators O_{L} and O_{M} in HM ChPT is more involved. The LO results for O_{L} [164] and $\mathcal{O}_{\mathrm{S}}$ [174], which enters in O_{M}, can be found in the literature, but expressions for the NLO terms do not exist. Before starting with the derivation, it is useful to present two symmetries which will reduce the number of independent LECs of the operators in HM ChPT. On the one hand, one can show that the operator $\mathcal{O}$ defined in Eq. (2.163), which mediates the neutral meson oscillation in QCD, transforms into its adjoint under a CP transformation:

$$(\mathcal{CP})\,\mathcal{O}(t,\vec{x})\,(\mathcal{CP})^{-1} = \mathcal{O}^\dagger(t,-\vec{x})\,. \tag{5.71}$$

This can be checked explicitly by using the following transformation laws of spinors [70] (the action of the matrix C on the gamma matrices has been defined in Eq. (3.42))

$$\mathcal{P}\psi(t,\vec{x})\mathcal{P}^{-1} = \gamma_4\psi(t,-\vec{x})\,, \qquad \mathcal{P}\bar{\psi}(t,\vec{x})\mathcal{P}^{-1} = \bar{\psi}(t,-\vec{x})\gamma_4\,, \tag{5.72}$$

$$\mathcal{C}\psi(t,\vec{x})\mathcal{C}^{-1} = C^{-1}\bar{\psi}(t,\vec{x})^{\mathrm{T}}\,, \qquad \mathcal{C}\bar{\psi}(t,\vec{x})\mathcal{C}^{-1} = -\psi(t,\vec{x})^{\mathrm{T}}C\,. \tag{5.73}$$

This property of $\mathcal{O}$ descends to the operators in the effective theory if one demands that the independent HQET operators Q and $\tilde{Q}$ transform into each other under charge conjugation. It should therefore also be implemented for the analogues of O_{L} and O_{M} in HM ChPT.

Secondly, the operator O_{L} is invariant under a special HQS transformation, a rotation of the heavy quark spin around the z-axis by an angle π. It is the same spin rotation which has already been used in Sec. 2.3 to relate the heavy-light pseudoscalar density and the vector current in HQET, see Eq. (2.111) for its matrix representation $\mathcal{S}$. Using the transformation laws given in Eqs. (2.105) and (2.124), O_{L} transforms under this specific transformation as

$$O_{\mathrm{L}} = [Q^\dagger\gamma_\mu(\mathbb{1}-\gamma_5)d][\tilde{Q}\gamma_\mu(\mathbb{1}-\gamma_5)d] \to [Q^\dagger\mathcal{S}^{-1}\gamma_\mu(\mathbb{1}-\gamma_5)d][\tilde{Q}\mathcal{S}^{-1}\gamma_\mu(\mathbb{1}-\gamma_5)d]\,. \tag{5.74}$$

In order to prove the invariance of O_{L}, it is enough to compute the product of matrices directly. One finds

$$\mathcal{S}^{-1}\gamma_1(\mathbb{1}-\gamma_5) = \gamma_2(\mathbb{1}-\gamma_5)\,, \tag{5.75}$$
$$\mathcal{S}^{-1}\gamma_2(\mathbb{1}-\gamma_5) = -\gamma_1(\mathbb{1}-\gamma_5)\,, \tag{5.76}$$
$$\mathcal{S}^{-1}\gamma_3(\mathbb{1}-\gamma_5) = -\gamma_4(\mathbb{1}-\gamma_5)\,, \tag{5.77}$$
$$\mathcal{S}^{-1}\gamma_4(\mathbb{1}-\gamma_5) = \gamma_3(\mathbb{1}-\gamma_5)\,. \tag{5.78}$$

Plugging these results into Eq. (5.74), one sees that O_{L} is indeed invariant under this spin rotation. This fact will be used when deriving O_{L} in HM ChPT.

This invariance also leads to a non-trivial relation between correlation functions: Apply the same transformation to all fields in the three-point function (5.61), which is used to extract the B^0-$\bar{B}^0$ mixing matrix elements. In HQET, the interpolating fields transform as

$$\bar{q}\gamma_5 Q \to \bar{q}\gamma_5\mathcal{S}Q = -\bar{q}\gamma_3 Q\,, \tag{5.79}$$
$$\bar{q}\gamma_5\tilde{Q}^\dagger \to \bar{q}\gamma_5\mathcal{S}\tilde{Q}^\dagger = \bar{q}\gamma_3\tilde{Q}^\dagger\,. \tag{5.80}$$

Note the sign in the first equation which is absent in the second. The same is true in the effective theory. This then implies

$$\begin{aligned}
&\left\langle 0\middle|\mathcal{B}^{(b)}O_{\mathrm{L}}\mathcal{B}^{(\bar{b})\dagger}\middle|0\right\rangle \\
&\quad= \left\langle 0\middle|U^{-1}(\mathcal{S})\left[U(\mathcal{S})\mathcal{B}^{(b)}U^{-1}(\mathcal{S})\right]\left[U(\mathcal{S})O_{\mathrm{L}}U^{-1}(\mathcal{S})\right]\left[U(\mathcal{S})\mathcal{B}^{(\bar{b})\dagger}U^{-1}(\mathcal{S})\right]U(\mathcal{S})\middle|0\right\rangle \\
&\quad= -\left\langle 0\middle|\mathcal{B}_k^{(b)}O_{\mathrm{L}}\mathcal{B}_k^{(\bar{b})\dagger}\middle|0\right\rangle\,.
\end{aligned} \tag{5.81}$$

The matrix elements for pseudoscalar and vector meson oscillations which can be extracted from the ground states of these three-point functions thus satisfy

$$\left\langle \bar{B}^0\middle|O_{\mathrm{L}}\middle|B^0\right\rangle = -\left\langle \bar{B}^{*0}\middle|O_{\mathrm{L}}\middle|B^{*0}\right\rangle\,, \tag{5.82}$$

a result that has already been noted in [164, 174].

With these considerations in mind, one can start deriving O_{L} and O_{M} in HM ChPT. The procedure will be similar to the derivation of the B meson interpolating fields in Sec. 4.1. It is useful to start by stating the transformation laws of the operators under LFN, HQS, and chiral transformations. For the first two, one has

$$O_{i,\alpha\beta} \to e^{-\mathrm{i}f(\vec{x})}e^{-\mathrm{i}f'(\vec{x})}O_{i,\gamma\delta}\mathcal{S}^{-1}_{\gamma\alpha}\mathcal{S}^{-1}_{\delta\beta}\,, \tag{5.83}$$

with an arbitrary HQS transformation matrix $\mathcal{S}$ and the phase factors which are due to the U(1) LFN conservation. The indices α and β are the spinor indices of the two heavy quarks. Since Q and $\tilde{Q}$ are a priori independent fields in HQET, they transform with different phases under LFN transformations. From this, it is clear that the operators contain one $\bar{H}^{(b)}$ and one $H^{(\bar{b})}$ field.

For the chiral transformations, it is convenient to keep the flavour of the two light quarks of the operators arbitrary but identical. Setting the flavour index f to $f=2$, one recovers the operators for B^0-$\bar{B}^0$ mixing, whereas for $f=3$ one obtains the B_s^0-$\bar{B}_s^0$ mixing operators if one studies three-flavour ChPT. Under an arbitrary chiral rotation, one has the transformation law (no sum over f)

$$O_{i,ff} \to L_{ff_1}L_{ff_2}O_{i,f_1f_2}\,, \tag{5.84}$$

where L is a transformation matrix of $\mathrm{SU}(2)_\mathrm{L}$. In the effective theory, the fields $\bar{H}^{(b)}$ and $H^{(\bar{b})}$ transform with the compensator field h under chiral transformations, but coupling them to the Goldstone bosons u one finds the correct transformation behaviour

$$u\bar{H}^{(b)} \to Lu\bar{H}^{(b)}\,, \qquad\qquad uH^{(\bar{b})} \to LuH^{(\bar{b})}\,. \tag{5.85}$$

At leading order in the chiral expansion, these are the only building blocks. Following [174], the most general form for the two operators is then given by

$$\begin{aligned} O^{\mathrm{LO}}_{i,ff} = &\sum_j \alpha^{(0)}_{i,j}\,\mathrm{Tr}\left[\Gamma^1_j\left(u\bar{H}^{(b)}\right)_f\right]\mathrm{Tr}\left[\Gamma^2_j\left(uH^{(\bar{b})}\right)_f\right] \\ &+\sum_k \beta^{(0)}_{i,k}\,\mathrm{Tr}\left[\tilde{\Gamma}^1_k\left(u\bar{H}^{(b)}\right)_f\tilde{\Gamma}^2_k\left(uH^{(\bar{b})}\right)_f\right] \end{aligned} \tag{5.86}$$

where the Γ_js and $\tilde{\Gamma}_k$s represent any combination of Clifford algebra elements as long as all spatial indices are contracted. As noted before, terms with γ_4 are redundant due to the constraints

$$\bar{H}^{(b)}\gamma_4 = \bar{H}^{(b)} = -\gamma_4\bar{H}^{(b)}\,, \tag{5.87}$$

$$H^{(\bar{b})}\gamma_4 = -H^{(\bar{b})} = -\gamma_4 H^{(\bar{b})}\,. \tag{5.88}$$

But even then Eq. (5.86) is redundant: the terms with two traces and one trace are related by the identity [175]

$$\begin{aligned} 4\mathrm{Tr}\left[AB\right] = &\,\mathrm{Tr}\left[A\right]\mathrm{Tr}\left[B\right] + \mathrm{Tr}\left[A\gamma_5\right]\mathrm{Tr}\left[\gamma_5 B\right] + \mathrm{Tr}\left[A\gamma_\mu\right]\mathrm{Tr}\left[\gamma_\mu B\right] \\ &+\mathrm{Tr}\left[A\gamma_\mu\gamma_5\right]\mathrm{Tr}\left[\gamma_5\gamma_\mu B\right] + \frac{1}{2}\mathrm{Tr}\left[A\sigma_{\mu\nu}\right]\mathrm{Tr}\left[\sigma_{\mu\nu}B\right]\,. \end{aligned} \tag{5.89}$$

It is therefore possible to drop the terms proportional to $\beta^{(0)}_{i,k}$. The terms proportional to $\alpha^{(0)}_{i,j}$ on the other hand are similar to the terms encountered in the interpolating fields of the B mesons. It is therefore not surprising that the only non-zero contributions to the operators stem from the terms

$$O^{\mathrm{LO}}_i = \alpha^{(0)}_{i,1}\,\mathrm{Tr}\left[\gamma_5 u\bar{H}^{(b)}\right]\mathrm{Tr}\left[\gamma_5 uH^{(\bar{b})}\right] + \alpha^{(0)}_{i,2}\,\mathrm{Tr}\left[\gamma_k u\bar{H}^{(b)}\right]\mathrm{Tr}\left[\gamma_k uH^{(\bar{b})}\right]\,. \tag{5.90}$$

All other insertions of gamma matrices either vanish or are proportional to the terms presented here. For convenience, the flavour index f was dropped, but one should keep in mind in the following that there are two open indices. For O_M, it is convenient to evaluate the trace over the Dirac indices and redefine the LECs so that

$$O^{\mathrm{LO}}_\mathrm{M} = \eta_1\left(uP^{(b)\dagger}\right)\left(uP^{(\bar{b})}\right) + \eta_2\left(uP^{(b)*\dagger}_k\right)\left(uP^{(\bar{b})*}_k\right)\,. \tag{5.91}$$

This is the final result for O_M at leading order, using CP transformations does not lead to a relation between the two independent LECs. The same result has already been presented in [174]. It will be shown later that η_1 is the LO result for the matrix element $\langle\bar{B}^0|O_\mathrm{M}|B^0\rangle$.

For O_L on the other hand, one can use that the operator is invariant under the specific HQS rotation introduced before. The transformation of O_L under this rotation is most easily carried out using Eq. (5.90). Inserting the definition of the rotation matrix, see Eq. (2.111), in the individual terms and computing the products $P_\pm\mathcal{S}^{-1}\gamma_i$ explicitly ($P_\pm$ are the projectors

in the definition of the H fields, see Eqs. (3.19) and (3.38)), one finds

$$\mathrm{Tr}\left[\gamma_1 u H^{(\bar{b})}\mathcal{S}^{-1}\right] = \mathrm{Tr}\left[\gamma_2 u H^{(\bar{b})}\right], \qquad \mathrm{Tr}\left[\gamma_1 u \bar{H}^{(b)}\mathcal{S}^{-1}\right] = \mathrm{Tr}\left[\gamma_2 u \bar{H}^{(b)}\right], \tag{5.92}$$

$$\mathrm{Tr}\left[\gamma_2 u H^{(\bar{b})}\mathcal{S}^{-1}\right] = -\mathrm{Tr}\left[\gamma_1 u H^{(\bar{b})}\right], \qquad \mathrm{Tr}\left[\gamma_2 u \bar{H}^{(b)}\mathcal{S}^{-1}\right] = -\mathrm{Tr}\left[\gamma_1 u \bar{H}^{(b)}\right], \tag{5.93}$$

$$\mathrm{Tr}\left[\gamma_3 u H^{(\bar{b})}\mathcal{S}^{-1}\right] = -\mathrm{Tr}\left[\gamma_5 u H^{(\bar{b})}\right], \qquad \mathrm{Tr}\left[\gamma_3 u \bar{H}^{(b)}\mathcal{S}^{-1}\right] = \mathrm{Tr}\left[\gamma_5 u \bar{H}^{(b)}\right], \tag{5.94}$$

$$\mathrm{Tr}\left[\gamma_5 u H^{(\bar{b})}\mathcal{S}^{-1}\right] = \mathrm{Tr}\left[\gamma_3 u H^{(\bar{b})}\right], \qquad \mathrm{Tr}\left[\gamma_5 u \bar{H}^{(b)}\mathcal{S}^{-1}\right] = -\mathrm{Tr}\left[\gamma_3 u \bar{H}^{(b)}\right]. \tag{5.95}$$

This leads to the following transformation of O_{L} under the HQS transformation

$$\begin{aligned} O_{\mathrm{L}}^{\mathrm{LO}} &= \alpha_{\mathrm{L},1}^{(0)}\,\mathrm{Tr}\left[\gamma_5 u \bar{H}^{(b)}\right]\mathrm{Tr}\left[\gamma_5 u H^{(\bar{b})}\right] + \alpha_{\mathrm{L},2}^{(0)}\,\mathrm{Tr}\left[\gamma_k u \bar{H}^{(b)}\right]\mathrm{Tr}\left[\gamma_k u H^{(\bar{b})}\right] \\ &\to -\alpha_{\mathrm{L},1}^{(0)}\,\mathrm{Tr}\left[\gamma_k u \bar{H}^{(b)}\right]\mathrm{Tr}\left[\gamma_k u H^{(\bar{b})}\right] - \alpha_{\mathrm{L},2}^{(0)}\,\mathrm{Tr}\left[\gamma_5 u \bar{H}^{(b)}\right]\mathrm{Tr}\left[\gamma_5 u H^{(\bar{b})}\right]. \end{aligned} \tag{5.96}$$

Requiring that the operator is invariant leads to $\alpha_{\mathrm{L},1}^{(0)} = -\alpha_{\mathrm{L},2}^{(0)}$, and after evaluating the trace over the Dirac indices and redefining the LEC, one arrives at

$$O_{\mathrm{L}}^{\mathrm{LO}} = \rho\left[\left(uP^{(b)\dagger}\right)\left(uP^{(\bar{b})}\right) - \left(uP_k^{(b)*\dagger}\right)\left(uP_k^{(\bar{b})*}\right)\right]. \tag{5.97}$$

The Minkowski space version of this result has already been derived in [164, 174].

At NLO in the chiral expansion, no results for the operators exist in the literature and one therefore has to work them out first. The discussion in Sec. 4.1 for the B meson interpolating fields shows that it is enough to consider inclusions of the field u_μ, the reader is referred to this section for more information. Due to its transformation behaviour under chiral symmetry, this field can only be inserted between the H fields and u, and the most general expression for the operators thus reads

$$\begin{aligned} O_i^{\mathrm{NLO}} = {} & \alpha_{i,1}^{(1)}\mathrm{Tr}\left[\gamma_5 u u_k \bar{H}^{(b)}\right]\mathrm{Tr}\left[\gamma_k u H^{(\bar{b})}\right] + \alpha_{i,2}^{(1)}\mathrm{Tr}\left[\gamma_k u u_k \bar{H}^{(b)}\right]\mathrm{Tr}\left[\gamma_5 u H^{(\bar{b})}\right] \\ & + \alpha_{i,3}^{(1)}\,\varepsilon_{klm}\mathrm{Tr}\left[\gamma_l u u_k \bar{H}^{(b)}\right]\mathrm{Tr}\left[\gamma_m u H^{(\bar{b})}\right] + \alpha_{i,4}^{(1)}\mathrm{Tr}\left[\gamma_5 u \bar{H}^{(b)}\right]\mathrm{Tr}\left[\gamma_k u u_k H^{(\bar{b})}\right] \\ & + \alpha_{i,5}^{(1)}\mathrm{Tr}\left[\gamma_k u \bar{H}^{(b)}\right]\mathrm{Tr}\left[\gamma_5 u u_k H^{(\bar{b})}\right] + \alpha_{i,6}^{(1)}\,\varepsilon_{klm}\mathrm{Tr}\left[\gamma_l u \bar{H}^{(b)}\right]\mathrm{Tr}\left[\gamma_m u u_k H^{(\bar{b})}\right] \\ & + \alpha_{i,7}^{(1)}\mathrm{Tr}\left[\gamma_5 u u_4 \bar{H}^{(b)}\right]\mathrm{Tr}\left[\gamma_5 u H^{(\bar{b})}\right] + \alpha_{i,8}^{(1)}\mathrm{Tr}\left[\gamma_k u u_4 \bar{H}^{(b)}\right]\mathrm{Tr}\left[\gamma_k u H^{(\bar{b})}\right] \\ & + \alpha_{i,9}^{(1)}\mathrm{Tr}\left[\gamma_5 u \bar{H}^{(b)}\right]\mathrm{Tr}\left[\gamma_5 u u_4 H^{(\bar{b})}\right] + \alpha_{i,10}^{(1)}\mathrm{Tr}\left[\gamma_k u \bar{H}^{(b)}\right]\mathrm{Tr}\left[\gamma_k u u_4 H^{(\bar{b})}\right]. \end{aligned} \tag{5.98}$$

Again, these terms include all possible non-vanishing and non-redundant insertions of gamma matrices. Evaluating the traces, one finds for the operator O_{M}

$$\begin{aligned} O_{\mathrm{M}}^{\mathrm{NLO}} = \eta_1\Big[& \mathrm{i}\phi_1\left(uu_kP^{(b)\dagger}\right)\left(uP_k^{(\bar{b})*}\right) + \mathrm{i}\phi_2\left(uu_kP_k^{(b)*\dagger}\right)\left(uP^{(\bar{b})}\right) + \mathrm{i}\phi_3\varepsilon_{klm}\left(uu_kP_l^{(b)*\dagger}\right)\left(uP_m^{(\bar{b})*}\right) \\ & + \mathrm{i}\phi_4\left(uP^{(b)\dagger}\right)\left(uu_kP_k^{(\bar{b})*}\right) + \mathrm{i}\phi_5\left(uP_k^{(b)*\dagger}\right)\left(uu_kP^{(\bar{b})}\right) + \mathrm{i}\phi_6\varepsilon_{klm}\left(uP_l^{(b)*\dagger}\right)\left(uu_kP_m^{(\bar{b})*}\right) \\ & + \phi_7\left(uu_4P^{(b)\dagger}\right)\left(uP^{(\bar{b})}\right) + \phi_8\left(uu_4P_k^{(b)*\dagger}\right)\left(uP_k^{(\bar{b})*}\right) \\ & + \phi_9\left(uP^{(b)\dagger}\right)\left(uu_4P^{(\bar{b})}\right) + \phi_{10}\left(uP_k^{(b)*\dagger}\right)\left(uu_4P_k^{(\bar{b})*}\right)\Big]. \end{aligned} \tag{5.99}$$

The LECs have been redefined for later convenience. This result can now be simplified by applying a CP transformation. As explained earlier, the operator must transform into its adjoint under this transformation, which leads to non-trivial relations between the LECs ϕ_i. In order to see how this works, consider the terms proportional to ϕ_1 and ϕ_5:

$$\Delta O_{\mathrm{M}}^{\mathrm{NLO}} = \eta_1\left[\mathrm{i}\phi_1\left(uu_kP^{(b)\dagger}\right)\left(uP_k^{(\bar{b})*}\right) + \mathrm{i}\phi_5\left(uP_k^{(b)*\dagger}\right)\left(uu_kP^{(\bar{b})}\right)\right]. \tag{5.100}$$

	P	P_k^*	u	u_k	u_4
$\mathcal{C}$	$\bar{P}$	$-\bar{P}_k^*$	u^T	u_k^T	u_4^T
$\mathcal{P}$	$-P$	$-P_k^*$	$u^\dagger$	u_k	$-u_4$

Table 5.1.: Transformation of the various fields under C and P transformations. The notation $\bar{P}$ denotes the transformation into the respective anti-particle.

By using the transformation rules of the fields given in Tab. 5.1, it is possible to compute the CP transformed of these terms

$$(\mathcal{CP})\,\Delta O_{\mathrm{M}}^{\mathrm{NLO}}\,(\mathcal{CP})^{-1} = \eta_1\left[-\mathrm{i}\phi_1\Big(P^{(\bar{b})\dagger}u_k u^\dagger\Big)\Big(P_k^{(b)*}u^\dagger\Big) - \mathrm{i}\phi_5\Big(P_k^{(\bar{b})*\dagger}u^\dagger\Big)\Big(P^{(b)}u_k u^\dagger\Big)\right]. \tag{5.101}$$

The adjoint of $\Delta O_{\mathrm{M}}^{\mathrm{NLO}}$ on the other hand is given by

$$\Delta O_{\mathrm{M}}^{\mathrm{NLO}\dagger} = \eta_1\left[-\mathrm{i}\phi_5^*\Big(P^{(\bar{b})\dagger}u_k u^\dagger\Big)\Big(P_k^{(b)*}u^\dagger\Big) - \mathrm{i}\phi_1^*\Big(P_k^{(\bar{b})*\dagger}u^\dagger\Big)\Big(P^{(b)}u_k u^\dagger\Big)\right]. \tag{5.102}$$

Comparing the two results, one finds $\phi_1 = \phi_5^*$. This procedure can be repeated for the other terms, and one finds $\phi_2 = \phi_4^*$, $\phi_3 = \phi_6^*$, $\phi_7 = -\phi_9^*$, and $\phi_8 = -\phi_{10}^*$. Here, it was already used that η_1 is real which follows from the fact that

$$\begin{aligned}\eta_1 &= \left\langle \bar{B}^0\middle|O_{\mathrm{M}}\middle|B^0\right\rangle = \left\langle \bar{B}^0\middle|(\mathcal{CP})^{-1}(\mathcal{CP})O_{\mathrm{M}}(\mathcal{CP})^{-1}(\mathcal{CP})\middle|B^0\right\rangle = (-1)^2\left\langle B^0\middle|O_{\mathrm{M}}^\dagger\middle|\bar{B}^0\right\rangle \\ &= \left\langle \bar{B}^0\middle|O_{\mathrm{M}}\middle|B^0\right\rangle^* = \eta_1^*\,,\end{aligned} \tag{5.103}$$

which is just a manifestation of CP invariance of QCD which is inherited by HQET. It is expected that also the excited states of this matrix element are then purely real. From the computation of the excited states contamination, which will be presented in Sec. 5.3.2, one can infer that ϕ_1, ϕ_2, and ϕ_3 have to be real valued for this to be true. For the LECs ϕ_7 and ϕ_8, no such statement can be made since they do not enter the result for the excited states of this matrix element. The final result for the NLO terms of O_{M} therefore reads

$$\begin{aligned}O_{\mathrm{M}}^{\mathrm{NLO}} = \eta_1\Big[&\mathrm{i}\phi_1\Big(uu_kP^{(b)\dagger}\Big)\Big(uP_k^{(\bar{b})*}\Big) + \mathrm{i}\phi_2\Big(uu_kP_k^{(b)*\dagger}\Big)\Big(uP^{(\bar{b})}\Big) + \mathrm{i}\phi_3\varepsilon_{klm}\Big(uu_kP_l^{(b)*\dagger}\Big)\Big(uP_m^{(\bar{b})*}\Big) \\ &+ \mathrm{i}\phi_2\Big(uP^{(b)\dagger}\Big)\Big(uu_kP_k^{(\bar{b})*}\Big) + \mathrm{i}\phi_1\Big(uP_k^{(b)*\dagger}\Big)\Big(uu_kP^{(\bar{b})}\Big) + \mathrm{i}\phi_3\varepsilon_{klm}\Big(uP_l^{(b)*\dagger}\Big)\Big(uu_kP_m^{(\bar{b})*}\Big) \\ &+ \phi_7\Big(uu_4P^{(b)\dagger}\Big)\Big(uP^{(\bar{b})}\Big) + \phi_8\Big(uu_4P_k^{(b)*\dagger}\Big)\Big(uP_k^{(\bar{b})*}\Big) \\ &- \phi_7^*\Big(uP^{(b)\dagger}\Big)\Big(uu_4P^{(\bar{b})}\Big) - \phi_8^*\Big(uP_k^{(b)*\dagger}\Big)\Big(uu_4P_k^{(\bar{b})*}\Big)\Big].\end{aligned} \tag{5.104}$$

The invariance under the special HQS rotation given in Eq. (2.111) reduces the number of independent LECs of O_{L} even further. The effect of this transformation is best studied in Eq. (5.98). For starters, one can notice that the terms proportional to $\alpha_{\mathrm{L},7}^{(1)}$, $\alpha_{\mathrm{L},8}^{(1)}$, $\alpha_{\mathrm{L},9}^{(1)}$, and $\alpha_{\mathrm{L},10}^{(1)}$ have the same Dirac structure as the LO terms presented in Eq. (5.90). Using the relations (5.92)-(5.95), one can infer that the equalities $\alpha_{\mathrm{L},7}^{(1)} = -\alpha_{\mathrm{L},8}^{(1)}$ and $\alpha_{\mathrm{L},9}^{(1)} = -\alpha_{\mathrm{L},10}^{(1)}$ follow from the invariance of O_{L} under this spin rotation. Furthermore, considering the $\alpha_{\mathrm{L},1}^{(1)}$, $\alpha_{\mathrm{L},2}^{(1)}$, $\alpha_{\mathrm{L},4}^{(1)}$, and $\alpha_{\mathrm{L},5}^{(1)}$ terms with index $k = 3$ for u_k and γ_k, one can derive from the same relations that $\alpha_{\mathrm{L},1}^{(1)} = \alpha_{\mathrm{L},2}^{(1)}$ and $\alpha_{\mathrm{L},4}^{(1)} = \alpha_{\mathrm{L},5}^{(1)}$. The terms with $k = 1, 2$ relate these coefficients to $\alpha_{\mathrm{L},3}^{(1)}$ and

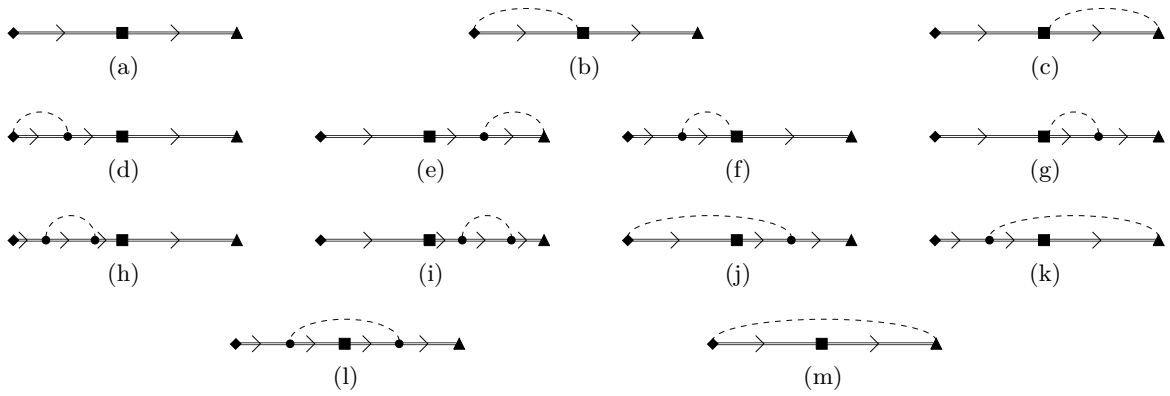

Figure 5.14.: Feynman diagrams contributing to the matrix elements $\langle \bar{B}^0 | O_{\mathrm{L}} | B^0 \rangle$, $\langle \bar{B}^0 | O_{\mathrm{M}} | B^0 \rangle$, and their respective excited states contamination. The filled square represents the operators O_{L} and O_{M}, the diamond the interpolating field of a B meson and the triangle of a $\bar{B}$ meson. The other symbols have the same meaning as before, see the caption of Fig. 5.1.

$\alpha^{(1)}_{\mathrm{L},6}$. For example, one finds that

$$\begin{aligned}\alpha^{(1)}_{\mathrm{L},1} \mathrm{Tr}\left[\gamma_5 \xi \xi_1 \bar{H}^{(b)} \mathcal{S}^{-1}\right] \mathrm{Tr}\left[\gamma_1 \xi H^{(\bar{b})} \mathcal{S}^{-1}\right] &= -\alpha^{(1)}_{\mathrm{L},1} \mathrm{Tr}\left[\gamma_3 \xi \xi_1 \bar{H}^{(b)}\right] \mathrm{Tr}\left[\gamma_2 \xi H^{(\bar{b})}\right] \\ &= \alpha^{(1)}_{\mathrm{L},1} \varepsilon_{132} \mathrm{Tr}\left[\gamma_3 \xi \xi_1 \bar{H}^{(b)}\right] \mathrm{Tr}\left[\gamma_2 \xi H^{(\bar{b})}\right] , \end{aligned} \tag{5.105}$$

from which it follows that $\alpha^{(1)}_{\mathrm{L},1} = \alpha^{(1)}_{\mathrm{L},3}$, and from a similar relation one can infer that $\alpha^{(1)}_{\mathrm{L},4} = \alpha^{(1)}_{\mathrm{L},6}$. All in all, the invariance of O_{L} under the special HQS transformation has already brought down the number of independent LECs to four. From here, one can use the same steps which were already undertaken for the NLO terms of O_{M}: one evaluates the traces over the Dirac indices, performs a CP transformation and demands that the result is the adjoint of O_{L}. This reduces the number of independent LECs by another factor of two. After redefining the LECs, one can write the final result in the form

$$\begin{aligned} O_{\mathrm{L}}^{\mathrm{NLO}} = \rho \Big[& \mathrm{i}\omega_1 \left(u u_k P^{(b)\dagger}\right) \left(u P_k^{(\bar{b})*}\right) + \mathrm{i}\omega_1 \left(u u_k P_k^{(b)*\dagger}\right) \left(u P^{(\bar{b})}\right) + \mathrm{i}\omega_1 \varepsilon_{klm} \left(u u_k P_l^{(b)*\dagger}\right) \left(u P_m^{(\bar{b})*}\right) \\ & + \mathrm{i}\omega_1 \left(u P^{(b)\dagger}\right) \left(u u_k P_k^{(\bar{b})*}\right) + \mathrm{i}\omega_1 \left(u P_k^{(b)*\dagger}\right) \left(u u_k P^{(\bar{b})}\right) + \mathrm{i}\omega_1 \varepsilon_{klm} \left(u P_l^{(b)*\dagger}\right) \left(u u_k P_m^{(\bar{b})*}\right) \\ & + \omega_2 \left(u u_4 P^{(b)\dagger}\right) \left(u P^{(\bar{b})}\right) - \omega_2 \left(u u_4 P_k^{(b)*\dagger}\right) \left(u P_k^{(\bar{b})*}\right) \\ & - \omega_2^* \left(u P^{(b)\dagger}\right) \left(u u_4 P^{(\bar{b})}\right) + \omega_2^* \left(u P_k^{(b)*\dagger}\right) \left(u u_4 P_k^{(\bar{b})*}\right) \Big] . \end{aligned} \tag{5.106}$$

This concludes the derivation of the operators O_{L} and O_{M} to NLO in the chiral expansion in HM ChPT.

5.3.2. Excited States Contamination of B^0-$\bar{B}^0$ Mixing Matrix Elements

The computation of the three-point function defined in Eq. (5.61) requires to evaluate the diagrams shown in Fig. 5.14. The explicit expressions for the interpolating fields are given in Eqs. (A.20) and (A.22), whereas the expansions of the operators O_{L} and O_{M} to first order in the pion field are given in Eqs. (A.33) and (A.34). The interaction vertices coupling two heavy mesons to a single pion can be found in Eqs. (A.9) and (A.35). In the following, the excited states contamination up to NLO in the chiral expansion will be presented. Diagrams

(b) and (c) only start to contribute at NNLO and are therefore neglected in the following. Diagram (m) is also of order p^4, but it will be kept in the results since it partially cancels a contribution of the two-point function in the ratios.

The LO results for the three-point functions receive contributions from diagram (a) and read

$$C_{3,\mathrm{L}}(t,t_\mathrm{I}) = \frac{\tilde{\alpha}^2\rho}{4}\,, \tag{5.107}$$

$$C_{3,\mathrm{M}}(t,t_\mathrm{I}) = \frac{\tilde{\alpha}^2\eta_1}{4} \tag{5.108}$$

from which the LO result for the matrix elements can be extracted from ratio (5.63):

$$\left\langle \bar{B}^0 \middle| O_\mathrm{L} \middle| B^0 \right\rangle = \rho + \dots\,, \tag{5.109}$$

$$\left\langle \bar{B}^0 \middle| O_\mathrm{M} \middle| B^0 \right\rangle = \eta_1 + \dots\,. \tag{5.110}$$

The ellipsis stand for higher order corrections in the chiral expansion and $1/m_B$.

The excited states contamination of the ratio was defined in Eq. (5.65). First, the excited states contamination of the ratio used for extracting the matrix element $\langle \bar{B}^0|O_\mathrm{L}|B^0\rangle$ will be investigated. The explicit results for the coefficients in Eq. (5.65) read

$$b_{1,\mathrm{L}}(\vec{p}) = b_{2,\mathrm{L}}(\vec{p}) = \frac{3}{4}\xi(\vec{p})g(g+\tilde{\beta}_1 E_{\pi,\vec{p}} + 2\omega_1 E_{\pi,\vec{p}})\,, \tag{5.111}$$

$$c_{3\mathrm{pt},\mathrm{L}}(\vec{p}) = \frac{3}{8}\xi(\vec{p})(g+\tilde{\beta}_1 E_{\pi,\vec{p}})^2\,, \tag{5.112}$$

$$c_\mathrm{L}(\vec{p}) = c_{3\mathrm{pt},\mathrm{L}}(\vec{p}) - c_{2\mathrm{pt}}(\vec{p}) = -\frac{3}{4}\xi(\vec{p})(g+\tilde{\beta}_1 E_{\pi,\vec{p}})^2\,. \tag{5.113}$$

The coefficient $c_{2\mathrm{pt}}$ and the function ξ have been defined in Eq. (4.29).

The unknown LEC ω_1 of the operator O_L is also present in the result, a suitable correlation function from which it might be determined in a lattice simulation is presented in Sec. 5.3.3. For the following numerical evaluation of $\delta R_\mathrm{L}^\mathrm{sum}$, one has to take recourse to dimensional analysis in order to estimate its impact. In analogy to the estimate of the NLO LEC γ in Sec. 5.1, it will be assumed that $-\Lambda_\chi^{-1} < \omega_1 < \Lambda_\chi^{-1}$ is a reasonable guess for the value of ω_1. In Fig. 5.15, a plot of $\delta R_\mathrm{L}^\mathrm{sum}(t)$ can be found for three different values of ω_1 and $\tilde{\beta}_1 = \beta_1$. Since the excited states contribution is a linear function of ω_1 (to NLO in the chiral expansion), it is clear that larger values also lead to a larger value of $\delta R_\mathrm{L}^\mathrm{sum}$. In the worst case scenario considered, which is $\omega_1 = \Lambda_\chi^{-1}$, the excited states contamination is roughly 4% at $t = 1.3\,\mathrm{fm}$. On the other hand, for $\omega_1 = -\Lambda_\chi^{-1}$ it is around 1%.

In Fig. 5.16, the dependence of $\delta R_\mathrm{L}^\mathrm{sum}$ on the smeared LEC $\tilde{\beta}_1$ for $\omega_1 = 0$ is presented. It is clear from that plot that smearing can indeed help in reducing the excited states contamination. For $\tilde{\beta}_1 = -\Lambda_\chi^{-1}$, the contribution of the excited states is more than halved. But even for $\tilde{\beta}_1 = -0.2\Lambda_\chi^{-1}$, the excited states are already notably suppressed.

Next up is the discussion of the excited states contamination of the ratio involving O_M, $\delta R_\mathrm{M}^\mathrm{sum}$. The result for the coefficients in Eq. (5.65) reads

$$b_{1,\mathrm{M}}(\vec{p}) = b_{2,\mathrm{M}}(\vec{p}) = \frac{3}{8}\xi(\vec{p})g(g(3+\hat{\eta}) + (3+\hat{\eta})\tilde{\beta}_1 E_{\pi,\vec{p}} + 4\hat{\phi}E_{\pi,\vec{p}})\,, \tag{5.114}$$

$$c_{3pt,\mathrm{M}}(\vec{p}) = -\frac{\hat{\eta}}{8}\xi(\vec{p})(g+\tilde{\beta}_1 E_{\pi,\vec{p}})^2\,, \tag{5.115}$$

$$c_\mathrm{M}(\vec{p}) = c_{3\mathrm{pt},\mathrm{M}}(\vec{p}) - c_{2\mathrm{pt}}(\vec{p}) = -\frac{(3+\hat{\eta})}{8}\xi(\vec{p})(g+\tilde{\beta}_1 E_{\pi,\vec{p}})^2\,. \tag{5.116}$$

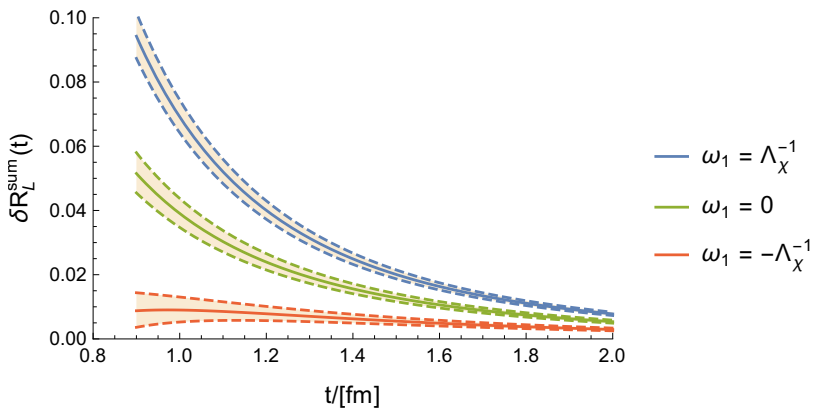

Figure 5.15.: The excited states contamination of the ratio $R_{\mathrm{L}}^{\mathrm{sum}}$ defined in Eq. (5.67) as a function of time t for three values of the unknown NLO LEC ω_1 and $\tilde{\beta}_1 = \beta_1$.

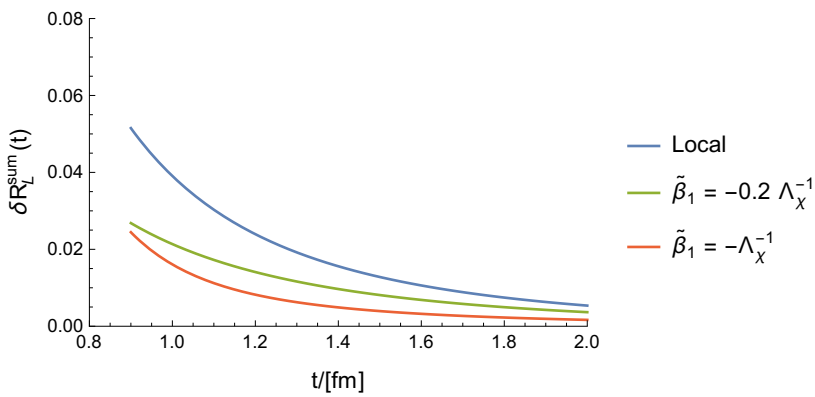

Figure 5.16.: The excited states contamination of the ratio $R_{\mathrm{L}}^{\mathrm{sum}}$ defined in Eq. (5.67) as a function of time t for $\omega_1 = 0$ and three different values of $\tilde{\beta}_1$.

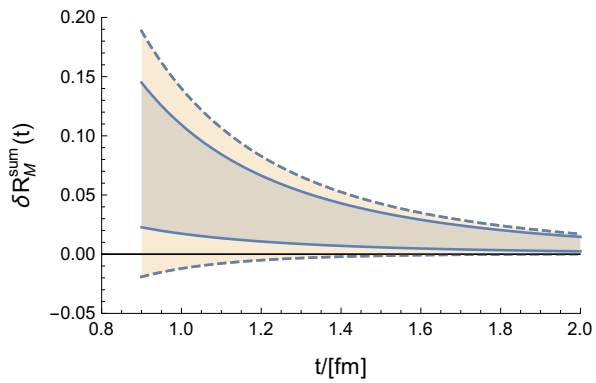

Figure 5.17.: The excited states contamination of $R_{\mathrm{M}}^{\mathrm{sum}}$ as a function of time t and for $\tilde{\beta}_1 = \beta_1$. The band enclosed by the solid lines includes only the uncertainty due to $\hat{\eta}$, $\hat{\phi}$ is set to zero. For the dashed lines, also the uncertainty due to $\hat{\phi}$ is taken into account.

This result depends on two unknown LECs. At LO, the ratio $\hat{\eta} = \eta_2/\eta_1$ enters. The LEC η_1 has already been identified with the LO result for the matrix element $\langle \bar{B}^0 | O_{\mathrm{M}} | B^0 \rangle$. A straightforward computation reveals that η_2 is the LO result for $\langle \bar{B}^{*0} | O_{\mathrm{M}} | B^{*0} \rangle$. It is not clear which of the two matrix elements is larger, so varying $\hat{\eta}$ in the range $-2 < \hat{\eta} < 2$ seems reasonable and has already been used in [174]. For the sum of NLO LECs $\hat{\phi} = (\phi_1 + 3\phi_2)/4$, the same estimate will be used as for ω_1: $-\Lambda_\chi^{-1} < \hat{\phi} < \Lambda_\chi^{-1}$. Since there are two unknown LECs, one of which is a ratio of LO LECs which is naively expected to be large, the result for $\delta R_{\mathrm{M}}^{\mathrm{sum}}$ is associated with large uncertainties. Fig. 5.17 shows a plot of the excited states contamination which confirms this. The band enclosed by the solid lines is due to the uncertainty of $\hat{\eta}$ alone, $\hat{\phi}$ is set to zero. The NLO LEC of the interpolating field was set to $\tilde{\beta}_1 = \beta_1$. The plot shows that the uncertainty due to the LO LEC is larger than the uncertainty due to ω_1 in $\delta R_{\mathrm{L}}^{\mathrm{sum}}$, compare with Fig. 5.15. At $t = 1.3\,\mathrm{fm}$, $\delta R_{\mathrm{M}}^{\mathrm{sum}}$ can be as large as 5%. Including the effect of $\hat{\phi}$, which is illustrated by the dashed lines, it can be larger than 6%. On the other hand, values close to zero are possible as well, depending on the values of $\hat{\eta}$ and $\hat{\phi}$. A meaningful evaluation of the excited states contamination is only possible after determining the two LECs in a lattice simulation. In the next section, a strategy is outlined to extract them from correlation functions.

5.3.3. Correlation Functions for the Determination of the LECs ω_1, $\hat{\eta}$, and $\hat{\phi}$

The results for the excited states contamination of the matrix elements $\langle \bar{B}^0 | O_{\mathrm{L}} | B^0 \rangle$ and $\langle \bar{B}^0 | O_{\mathrm{M}} | B^0 \rangle$ depend on LECs which are at present unknown. For the matrix element involving O_{L}, one has to determine only a single NLO LEC, ω_1. For the other matrix element, one needs to determine a ratio of LO LECs, $\hat{\eta} = \eta_2/\eta_1$, and a linear combination of two NLO LECs, $\hat{\phi} = (\phi_1 + 3\phi_2)/4$.

Computing the ratio of LO LECs seems to be the easiest task. To leading order in the chiral and $1/m_B$ expansion, it is given by the ratio of matrix elements

$$\frac{\left\langle \bar{B}^{*0} \middle| O_{\mathrm{M}} \middle| B^{*0} \right\rangle}{\left\langle \bar{B}^{0} \middle| O_{\mathrm{M}} \middle| B^{0} \right\rangle} = \frac{\eta_2}{\eta_1} + \dots . \tag{5.117}$$

Due to heavy quark spin symmetry, this can also be written as the ratio of the three-point functions from which the matrix elements are extracted since the two-point functions drop

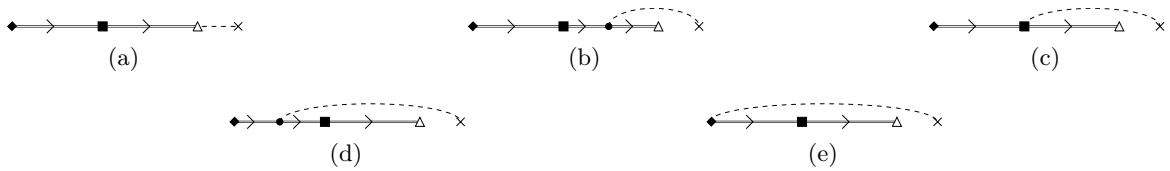

Figure 5.18.: Feynman diagrams for the correlators (5.120) and (5.122). For the correlator considered in Eq. (5.123), the interpolating fields need to be adjusted accordingly.

out (no sum over the spatial index k)

$$\frac{\int \mathrm{d}^3\vec{x}\,\mathrm{d}^3\vec{y}\,\left\langle \bar{\mathcal{B}}^0_k(t,\vec{x})O_\mathrm{M}(t_\mathrm{I},\vec{y})\mathcal{B}^{0\dagger}_k(0,\vec{0})\right\rangle}{\int \mathrm{d}^3\vec{x}\,\mathrm{d}^3\vec{y}\,\left\langle \bar{\mathcal{B}}^0(t,\vec{x})O_\mathrm{M}(t_\mathrm{I},\vec{y})\mathcal{B}^{0\dagger}(0,\vec{0})\right\rangle} = \frac{\eta_2}{\eta_1} + \dots\,. \tag{5.118}$$

Here, the ellipsis do not only stand for the higher order corrections, but also include the excited states contamination of the correlation functions. One could also use the summation method by integrating over the insertion time t_I of the operator O_M, and then taking the derivative w.r.t. t. If possible, computing the three-point functions for different values of t and t_I can also help to estimate the effect of excited states.

For the NLO LECs, things are more complicated. All the NLO terms of O_L and O_M in Eqs. (5.104) and (5.106) are proportional to $u_\mu = -\partial_\mu\pi/f$, and therefore contain an additional pion. Extracting the NLO LECs from a correlation function therefore necessitates the inclusion of another pion interpolating field. In the following, the light axial vector current

$$A^+_\mu(x) = \sqrt{2}f\partial_\mu\pi^+(x) \tag{5.119}$$

is used. The LEC ω_1 of O_L can then be obtained from the following four-point function with a vector and pseudoscalar B meson interpolating field

$$\begin{aligned} C_4^{\omega_1}(t_x,t_y,t_z,\vec{q}) &= \int\limits_{L^3} \mathrm{d}^3\vec{x}\,\mathrm{d}^3\vec{y}\,\mathrm{d}^3\vec{z}\,e^{\mathrm{i}\vec{q}\cdot\vec{x}}\left\langle A^+_k(x)\mathcal{B}^-_l(y)O_\mathrm{L}(z)\mathcal{B}^{0\dagger}(0)\right\rangle \\ &= -\mathrm{i}\frac{\tilde{\alpha}^2\rho q_k q_l e^{-E_{\pi,\vec{q}}\,t_x}}{8E^2_{\pi,\vec{q}}}\left(e^{E_{\pi,\vec{q}}\,t_z}(g+\omega_1 E_{\pi,\vec{q}}) - e^{E_{\pi,\vec{q}}\,t_y}(g-\tilde{\beta}_1 E_{\pi,\vec{q}})\right)\,. \end{aligned} \tag{5.120}$$

The indices k and l are spatial indices, and the Feynman diagrams, which need to be computed, can be found in Fig. 5.18. The contributions of further states in the spectral decomposition of the correlator as well as higher order corrections have been neglected, it is expected that they are small compared to the result presented above. The result is the sum of two exponentials, ω_1 is multiplied by the sub-leading one. As before, it is assumed that the HM ChPT result is applicable if the time separations between all operators is at least 1.3 fm. This might be difficult to achieve in an actual lattice simulation, so it is useful to consider the summation estimate of the correlation function which eliminates one time interval. In order to do this, one integrates over the insertion time of the operator O_L and then takes a derivative w.r.t. t_y. This leads to

$$\begin{aligned} &\frac{\mathrm{d}}{\mathrm{d}t_y}\int\limits_0^{t_y}\mathrm{d}t_z\,C_4^{\omega_1}(t_x,t_y,t_z,\vec{q}) \\ &\quad= -\mathrm{i}\frac{\tilde{\alpha}^2\rho q_k q_l e^{-E_{\pi,\vec{q}}(t_x-t_y)}}{8E^2_{\pi,\vec{q}}}\left((\omega_1+\tilde{\beta}_1)E_{\pi,\vec{q}} + (\tilde{\beta}_1 E_{\pi,\vec{q}} - g)E_{\pi,\vec{q}}\,t_y\right)\,. \end{aligned} \tag{5.121}$$

The prefactor $\tilde{\alpha}^2\rho$ can be eliminated by dividing by the LO result of the three-point function from which the matrix element $\langle \bar{B}^0|O_{\mathrm{L}}|B^0\rangle$ is extracted, see Eq. (5.107). Evaluating the correlation function for at least two values of t_y and/or $E_{\pi,\vec{q}}$, it is possible to extract the sum $\omega_1 + \tilde{\beta}_1$ from a fit to the above analytic expression. After determining $\tilde{\beta}_1$ and plugging it in the result, one then has a prediction for ω_1. For the same reasoning as before, the excited states contamination of the three-point and four-point functions are neglected.

The LECs ϕ_1 and ϕ_2 of O_{M} can be extracted in a similar fashion. Using the same correlation as before, but replacing O_{L} with O_{M}, one has

$$\begin{aligned}
&\frac{\mathrm{d}}{\mathrm{d}t_y}\int\limits_0^{t_y}\mathrm{d}t_z\int\limits_{L^3}\mathrm{d}^3\vec{x}\,\mathrm{d}^3\vec{y}\,\mathrm{d}^3\vec{z}\,e^{\mathrm{i}\vec{q}\cdot\vec{x}}\left\langle A_k^+(x)\mathcal{B}_l^-(y)O_{\mathrm{M}}(z)\mathcal{B}^{0\dagger}(0)\right\rangle \\
&\quad = -\mathrm{i}\frac{\tilde{\alpha}^2\eta_1 q_k q_l e^{-E_{\pi,\vec{q}}(t_x-t_y)}}{8E_{\pi,\vec{q}}^2}\left((\phi_2+\tilde{\beta}_1)E_{\pi,\vec{q}} + (\tilde{\beta}_1 E_{\pi,\vec{q}} - g)E_{\pi,\vec{q}}\,t_y\right)\,. \qquad (5.122)
\end{aligned}$$

The prefactor $\tilde{\alpha}^2\eta_1$ can be removed by dividing by the three-point function from which the matrix element $\langle \bar{B}^0|O_{\mathrm{M}}|B^0\rangle$ is extracted. The LEC ϕ_2 can then be extracted in the same way as ω_1.

For ϕ_1, a similar correlation function can be used. Instead of inserting a pseudoscalar at $t=0$ and a vector B meson at t_y, one can insert a vector at $t=0$ and a pseudoscalar at t_y. The summation estimate for this correlation function yields

$$\begin{aligned}
&\frac{\mathrm{d}}{\mathrm{d}t_y}\int\limits_0^{t_y}\mathrm{d}t_z\int\limits_{L^3}\mathrm{d}^3\vec{x}\,\mathrm{d}^3\vec{y}\,\mathrm{d}^3\vec{z}\,e^{\mathrm{i}\vec{q}\cdot\vec{x}}\left\langle A_k^+(x)\mathcal{B}^-(y)O_{\mathrm{M}}(z)\mathcal{B}_l^{0\dagger}(0)\right\rangle \\
&\quad = -\mathrm{i}\frac{\tilde{\alpha}^2\eta_1 q_k q_l e^{-E_{\pi,\vec{q}}(t_x-t_y)}}{8E_{\pi,\vec{q}}^2}\left((\phi_1-\hat{\eta}\tilde{\beta}_1)E_{\pi,\vec{q}} + \hat{\eta}(g-\tilde{\beta}_1 E_{\pi,\vec{q}})E_{\pi,\vec{q}}\,t_y\right)\,. \qquad (5.123)
\end{aligned}$$

In order to extract ϕ_1, one needs to determine the ratio $\hat{\eta} = \eta_2/\eta_1$ first. Only then one can apply the same strategy which has been suggested for the other correlation functions.

6. Conclusions and Outlook

Indirect searches for BSM physics require increasing precision from experiment and theory alike. This also requires control over systematic errors, such as the excited states contamination of QCD correlation functions in lattice simulations. In the past, ChPT has already been successfully applied to this problem, and analytic results for the dominant excited states contamination of observables of the nucleon sector [19–26] have been obtained. Based on this, this thesis presented a similar approach in the B meson sector, and presented the study of matrix elements relevant for weak interaction processes.

The computations were carried out in Heavy Meson Chiral Perturbation Theory, an effective theory which is defined by a double expansion in small particle energies and inverse powers of the heavy meson mass, here m_B. The high degree of symmetry of the static limit of this theory, which is defined by neglecting all $1/m_B$ corrections, dramatically reduces the number of low energy constants of the heavy-light currents and densities. As a result, there is only one LEC at LO and two at NLO. This is also true for the smeared interpolating fields of the pseudoscalar and vector meson. Whereas the relevant LECs of the local fields were extracted from numerical results for the $B \to \pi$ vector form factors found in the literature, no results exist for the LECs of the smeared bilinears so far. But they can in principle be obtained from suitable lattice correlation functions which were identified in HM ChPT. This means that HM ChPT allows for a systematic study of smearing in lattice simulations by determining the LECs of the smeared interpolating fields. In the future, it would be desirable to transfer this approach to other hadronic interpolating fields in order to allow for a better understanding of how smearing affects the excited states contamination of correlation functions in lattice QCD.

From the correlation functions considered in this thesis, several relevant quantities can be extracted. From the two-point function, one can determine the effective mass of the B meson, a quantity that can enter in ratios from which matrix elements are determined, see Eqs. (2.85) and (2.86). It therefore is not only relevant for the excited states contamination of the $B \to \pi$ vector form factors which were considered in this work, but also plays a role for other B meson matrix elements. Another in some sense 'universal' quantity is the LEC g, the chiral and static limit value of the $B^*B\pi$ coupling constant. It is the only LEC of the LO HM ChPT Lagrangian and its importance can be seen from the fact that it enters every result presented in this thesis. Detecting any systematic errors due to excited states is therefore essential.

The other matrix elements considered are relevant for processes of the weak interactions. They are needed for extracting CKM matrix elements by combining non-perturbative lattice results, perturbative electroweak calculations, and experimental input. As discussed in the introduction, CKM matrix elements are relevant for indirect searches of BSM physics, and it is thus desirable to achieve a sub-percent level accuracy for them. Eliminating systematic errors stemming from the excited states contamination of lattice correlators is imperative in this endeavour. With one exception, the excited states lead to an overestimation of the true matrix elements by a few percent, but some results depend on some yet undetermined LECs. Suitable correlation functions from which they can in principle be extracted have been identified in HM ChPT, but it remains to be seen if the proposed approach is useful in practice. The smallness of the excited states contamination can be best understood in the form of Feynman diagrams: the non-zero diagrams which contribute to $B\pi$ states contain an additional internal pion line. But from the Feynman rules of ChPT, it follows that every additional pion line increases the

chiral dimension by two. Compared to the matrix elements themselves, they are of a higher order and one can naively expect them to be small.

The excited states contamination of $h_\perp$ is quite different, it leads to a large underestimation of the form factor. This can be traced back to the fact that an interpolating field of a pion is needed in the three-point function from which $h_\perp$ is extracted. This implies that Feynman diagrams therefore naturally have a pion line which connects the pion interpolating field to the rest of the diagram. In the case of $h_\perp$, there are diagrams which contribute to the $B\pi$ states, but do not contain an additional pion line compared to the diagrams which contribute to the form factor itself. These are diagrams (b) and (c) in Fig. 5.6. These diagrams are therefore of the same chiral order as the form factor itself, which means that the leading order in $\delta h_\perp$, the ratio of the $B\pi$ state contamination and the form factor, starts at order p^0, and therefore is large in comparison to the order p^2 results for the other matrix elements. This should be taken as a warning: whenever there is a pion interpolating field in a correlation function, large excited states can arise in the same way as for $h_\perp$. That this is not always the case can be seen from the example of $h_\parallel$: naively, one would expect that the same Feynman diagrams need to be computed as for $h_\perp$. But the form of the time-component of the heavy-light vector current V_4 is quite different from V_k and simply does not allow for these kind of diagrams. Kinematics can also play a role as can be seen from the example of g: it is extracted from the three-point function given in Eq. (5.2), with the light axial vector current projected to zero momentum. It turns out that for non-zero momentum, there would also be large excited states, the same that have been found for the axial form factors of the nucleon [23]. All these considerations should be kept in mind when lattice correlation functions with pion interpolating fields are analysed.

The most pressing task for the future is the determination of the yet unknown LECs which appear in the results presented in this thesis. These are two LECs of the NLO HM ChPT Lagrangian which enter in γ, the (ratios of) LECs ω_1, $\hat{\phi}$, and $\hat{\eta}$ encountered in the correlation functions of B^0-$\bar{B}^0$ mixing, and the LECs of smeared B meson interpolating fields as discussed above. Only with them, concrete NLO predictions for the excited states contamination of the correlation functions can be made. The question which arises then is: do the formulae describe the lattice data well enough, or are higher order terms of the double expansion in small particle energies and $1/m_B$ required? A naive estimate for a pion with energy $E_\pi = 800\,\text{MeV}$ suggests that the first term in the inverse mass expansion $p/m_B \approx 0.16$, with $m_B = 5\,\text{GeV}$ for simplicity, is still smaller than the size of the fourth order in the chiral expansion, $(p/\Lambda_\chi)^4 \approx 0.20$ with $\Lambda_\chi = 1.2\,\text{GeV}$. It therefore seems reasonable to concentrate on higher orders in the chiral expansion before turning to $1/m_B$ corrections. On the other hand, the number of LECs in the higher order Lagrangian and interpolating fields are expected to increase dramatically and it remains to be seen if this is feasible. Besides computing higher order corrections in p and $1/m_B$, one can also use ChPT to study discretisation effects. These would also be associated with additional LECs and would moreover depend on the chosen discretisation (Wilson fermions, staggered fermions, etc.).

Another future research direction is to study the excited states contamination of D meson correlation functions. The results in the static limit of HM ChPT are the same as the ones for B mesons presented in this thesis, but the $1/m_D$ corrections are expected to be larger. From the size of the D meson mass, $m_D \approx 2\,\text{GeV}$, one can expect them to be only slightly smaller than the leading chiral corrections and one should include them for a reliable estimate. Another process which has already been studied a long time ago in HM ChPT [33, 176, 177] is the semileptonic decay $B \to D\ell\bar{\nu}_\ell$. In light of the $2.5\,\sigma$ tension between inclusive and exclusive determinations of $|V_{cb}|$ [6], it is desirable to get an estimate for the excited states contamination of the relevant three-point function in order to exclude this source of systematic errors as the cause of the discrepancy. This would in general require to work with HQET at finite velocity. On the other hand, the zero-recoil limit, in which both the B and D meson are

at rest might already give some valuable input when combined with experimental results.

The ability to compute the excited states contamination of correlation functions in an effective theory constitutes a powerful tool for lattice QCD. The additional effort needed to extract LECs from suitable correlation functions is offset by having a reusable and analytic expression which makes predictions for the size of excited states. It is therefore desirable that this approach is taken up by more researchers in the future and is also extended to other sectors of QCD.

Acknowledgements

I want to thank my supervisor Rainer Sommer for proposing the project and his supervision; Oliver Bär for teaching me Chiral Perturbation Theory, his encouragement, many long and fruitful discussions, and his feedback; Agostino Patella for his input in the CDP meetings; Lorenzo Barca, Julien Frison, and Andreas Risch for helpful discussions and their efforts on computing some of the unknown NLO LECs; Stefan Schaefer for helping with numerical simulations which did not make it into this thesis; the members of the RTG 'Rethinking Quantum Field Theory' as well as the members of the lattice groups at HU Berlin and Desy Zeuthen; Felipe for sharing an office and stories of Colombia and Bamberg; and my family and friends for their support.

This work is funded by the Deutsche Forschungsgemeinschaft (DFG, German Research Foundation) - Projektnummer 417533893/GRK2575 "Rethinking Quantum Field Theory".

Appendices

A. Feynman Rules

In this appendix, the explicit form of the interpolating fields and interaction vertices is presented. The pions enter the theory via

$$u = e^{\frac{\mathrm{i}}{f}\pi}\,, \tag{A.1}$$

where the pion matrix for a theory with two light quark flavours is given by

$$\pi = \pi^a T^a = \frac{1}{\sqrt{2}} \begin{pmatrix} \frac{\pi^0}{\sqrt{2}} & \pi^+ \\ \pi^- & -\frac{\pi^0}{\sqrt{2}} \end{pmatrix}\,. \tag{A.2}$$

The traceless generators T^a of SU(2) are related to the Pauli matrices σ^a via $T^a = \sigma^a/2$, and satisfy the relation

$$T^a T^b = \frac{\delta^{ab}}{4}\mathbb{1}_2 + \frac{\mathrm{i}}{2}\varepsilon^{abc}T^c\,. \tag{A.3}$$

The propagators of the light and heavy mesons are given by

$$\left\langle \pi^a(\vec{x},t)\pi^b(\vec{y},t')\right\rangle = \delta^{ab}\sum_{\vec{p}} \frac{e^{\mathrm{i}\vec{p}(\vec{x}-\vec{y})}}{2E_{\pi,\vec{p}}} e^{-E_{\pi,\vec{p}}|t-t'|}\,, \tag{A.4}$$

$$\left\langle P(\vec{x},t)P^\dagger(\vec{y},t')\right\rangle = \frac{1}{2}\theta(t-t')\delta^{(3)}(\vec{x}-\vec{y})\,, \tag{A.5}$$

$$\left\langle P_k^*(\vec{x},t)P_l^{*\dagger}(\vec{y},t')\right\rangle = \frac{\delta_{kl}}{2}\theta(t-t')\delta^{(3)}(\vec{x}-\vec{y})\,. \tag{A.6}$$

In the HM ChPT Lagrangian, the pions enter in the combinations u_μ and Γ_μ. Expanding them to up to two pion fields, one finds

$$u_\mu = \frac{\mathrm{i}}{2}\left(u^\dagger\partial_\mu u - u\partial_\mu u^\dagger\right) = -\frac{\partial_\mu \pi}{f} + \dots\,, \tag{A.7}$$

$$\Gamma_\mu = \frac{\mathrm{i}}{2}\left(u^\dagger\partial_\mu u + u\partial_\mu u^\dagger\right) = -\frac{1}{2f^2}\varepsilon^{abc}\pi^a\partial_\mu\pi^b T^c + \dots\,. \tag{A.8}$$

Inserting these results in the LO HM ChPT Lagrangian (3.30), one finds for the interaction terms of two heavy mesons and up to two pions

$$\begin{aligned}\Delta\mathcal{L}_H^{(1)} = &\frac{2\mathrm{i}g}{f}\left(P_k^*\partial_k\pi P^\dagger - P\partial_k\pi P_k^{*\dagger} + \varepsilon_{klm}P_k^*\partial_l\pi P_m^{*\dagger}\right)\\ &- \frac{\mathrm{i}}{f^2}\varepsilon^{abc}\pi^a\partial_4\pi^b\left(PT^cP^\dagger + P_k^*T^cP_k^{*\dagger}\right)\,.\end{aligned} \tag{A.9}$$

In the NLO Lagrangian, also the combination of fields χ_+ defined in Eq. (3.37) enters. Setting the external pseudoscalar field to zero and the scalar field equal to the quark mass matrix M_q, one finds

$$\chi_+ = 2B\left(uM_qu + u^\dagger M_q u^\dagger\right) = 4B\left(M_q - \frac{\pi^2}{f^2}M_q - \frac{\pi}{f}M_q\frac{\pi}{f} - M_q\frac{\pi^2}{f^2} + \dots\right)\,. \tag{A.10}$$

The explicit expansion of the NLO Lagrangian (3.36) in powers of the pion fields shows that it does not contain any terms with a single pion. The terms which couple two pions to two heavy meson fields are given by

$$\begin{aligned}\Delta\mathcal{L}_H^{(2)} = &-2d_1\left(P\frac{\partial_\mu\pi}{f}\frac{\partial_\mu\pi}{f}P^\dagger + P_k^*\frac{\partial_\mu\pi}{f}\frac{\partial_\mu\pi}{f}P_k^{*\dagger}\right) - 2d_2\left(P\frac{\partial_4\pi}{f}\frac{\partial_4\pi}{f}P^\dagger + P_k^*\frac{\partial_4\pi}{f}\frac{\partial_4\pi}{f}P_k^{*\dagger}\right)\\ &- 2d_3\left(\mathrm{i}\varepsilon^{abc}\partial_\nu\pi^a\partial_\mu\pi^b P_\mu^* T^c P_\nu^{*\dagger} + \varepsilon_{klm}\left(P_l^*\frac{\partial_m\pi}{f}\frac{\partial_n\pi}{f}P^\dagger - P\frac{\partial_m\pi}{f}\frac{\partial_n\pi}{f}P_l^{*\dagger}\right)\right)\\ &+ 4Bd_6\left(P\left[\frac{\pi^2}{f^2}M_q + M_q\frac{\pi^2}{f^2} + 2\frac{\pi}{f}M_q\frac{\pi}{f}\right]P^\dagger + P_k^*\left[\frac{\pi^2}{f^2}M_q + M_q\frac{\pi^2}{f^2} + 2\frac{\pi}{f}M_q\frac{\pi}{f}\right]P_k^{*\dagger}\right)\\ &+ 16Bd_7\left(PP^\dagger + P_k^*P_k^{*\dagger}\right)\mathrm{Tr}\left[M_q\frac{\pi^2}{f^2}\right]. \end{aligned} \tag{A.11}$$

For the case of mass-degenerate quarks, i.e. $M_q = m_l\mathbb{1}_2$, the last two terms can be simplified by using $m_\pi^2 = 2Bm_l$:

$$\Delta\mathcal{L}_{H,M}^{(2)} = 2m_\pi^2(d_6 + 2d_7)\pi^a\pi^a\left(PP^\dagger + P_k^*P_k^{*\dagger}\right). \tag{A.12}$$

For the heavy-light currents and densities, $\bar{q}\,\Gamma Q$, one also needs the linear combinations

$$u_+ = u + u^\dagger = 2 - \frac{\pi^2}{f^2} + \dots, \tag{A.13}$$

$$u_- = u - u^\dagger = 2\mathrm{i}\frac{\pi}{f} + \dots. \tag{A.14}$$

The results for the currents at LO and NLO order in the chiral expansion and in the static limit read

$$V_k = \frac{\alpha}{2}P_k^*u_+ + \frac{\mathrm{i}\alpha\beta_1}{2}(Pu_k - \varepsilon_{klm}P_l^*u_m)u_+ + \frac{\mathrm{i}\alpha\beta_2}{2}P_k^*u_4u_-, \tag{A.15}$$

$$V_4 = -\frac{\alpha}{2}Pu_- + \frac{\mathrm{i}\alpha\beta_1}{2}P_k^*u_ku_- - \frac{\mathrm{i}\alpha\beta_2}{2}Pu_4u_+, \tag{A.16}$$

$$A_k = \frac{\alpha}{2}P_k^*u_- + \frac{\mathrm{i}\alpha\beta_1}{2}(Pu_k - \varepsilon_{klm}P_l^*u_m)u_- + \frac{\mathrm{i}\alpha\beta_2}{2}P_k^*u_4u_+, \tag{A.17}$$

$$A_4 = -\frac{\alpha}{2}Pu_+ + \frac{\mathrm{i}\alpha\beta_1}{2}P_k^*u_ku_+ - \frac{\mathrm{i}\alpha\beta_2}{2}Pu_4u_-, \tag{A.18}$$

and the pseudoscalar and scalar density are related to the time components of the vector and axial vector currents via (here, P denotes the heavy-light pseudoscalar density and not the heavy meson field)

$$P = -A_4, \qquad S = V_4. \tag{A.19}$$

The currents and densities can be expanded in powers of the pion fields using Eqs. (A.7), (A.13), and (A.14). For the smeared interpolating fields of the B and B^* meson, the result with up to two pions reads

$$\mathcal{B} = \tilde{\alpha}P\left(1 - \frac{\pi^2}{2f^2}\right) + \frac{\mathrm{i}\tilde{\alpha}\tilde{\beta}_1}{f}P_k^*\partial_k\pi + \frac{\tilde{\alpha}\tilde{\beta}_2}{f^2}P\partial_4\pi\pi + \dots, \tag{A.20}$$

$$\mathcal{B}_k = \tilde{\alpha}P_k^*\left(1 - \frac{\pi^2}{2f^2}\right) + \frac{\mathrm{i}\tilde{\alpha}\tilde{\beta}_1}{f}\left(\varepsilon_{klm}P_l^*\partial_m\pi - P\partial_k\pi\right) + \frac{\tilde{\alpha}\tilde{\beta}_2}{f^2}P_k^*\partial_4\pi\pi + \dots. \tag{A.21}$$

These are the interpolating fields for heavy mesons with a b quark, sometimes also denoted by $\mathcal{B}^{(b)}$. For the charge conjugated fields, one finds

$$\mathcal{B}^{(\bar{b})} = \tilde{\alpha}\left(1-\frac{\pi^2}{2f^2}\right)P^{(\bar{b})} - \frac{\mathrm{i}\tilde{\alpha}\tilde{\beta}_1}{f}\partial_k\pi P_k^{(\bar{b})*} + \frac{\tilde{\alpha}\tilde{\beta}_2}{f^2}\pi\,\partial_4\pi P^{(\bar{b})} + \dots\,, \tag{A.22}$$

$$\mathcal{B}_k^{(\bar{b})} = \tilde{\alpha}\left(1-\frac{\pi^2}{2f^2}\right)P_k^{(\bar{b})*} + \frac{\mathrm{i}\tilde{\alpha}\tilde{\beta}_1}{f}\left(\varepsilon_{klm}\,\partial_m\pi\,P_l^{(\bar{b})*} + \partial_k\pi P^{(\bar{b})}\right) + \frac{\tilde{\alpha}\tilde{\beta}_2}{f^2}\pi\,\partial_4\pi P_k^{(\bar{b})*} + \dots\,, \tag{A.23}$$

For the computation of the $B\to\pi$ form factors, the local vector current is needed. It is given by

$$V_k = \alpha P_k^*\left(1-\frac{\pi^2}{2f^2}\right) + \frac{\mathrm{i}\alpha\beta_1}{f}\left(\varepsilon_{klm}P_l^*\partial_m\pi - P\partial_k\pi\right) + \frac{\alpha\beta_2}{f^2}P_k^*\partial_4\pi\pi + \dots\,, \tag{A.24}$$

$$V_4 = -\frac{\mathrm{i}\alpha}{f}P\pi + \frac{\alpha\beta_1}{f^2}P_k^*\partial_k\pi\pi + \frac{\mathrm{i}\alpha\beta_2}{f}P\partial_4\pi + \dots\,. \tag{A.25}$$

For the determination of $g_{B^*B\pi}$ and the $B\to\pi$ vector form factors, also the light axial vector current A_μ^a and pseudoscalar density P^a, which are given by $\bar{q}\gamma_\mu T^a q$ and $\bar{q}\gamma_5 T^a q$ in QCD, are needed. These can be obtained by taking a functional derivative of the action wr.r.t. the external fields a_μ^a and p^a, respectively, and setting the external fields to zero (or $s=M_q$ if needed) afterwards. A_μ^a and P^a get contributions from the HM ChPT Lagrangian, but also the ChPT Lagrangian (3.7) which only involves the light meson fields. Using the relation

$$0 = \partial_\mu\mathbb{1} = \partial_\mu(UU^\dagger) = \partial_\mu UU^\dagger + U\partial_\mu U^\dagger\,, \tag{A.26}$$

$$\Rightarrow \partial_\mu UU^\dagger = -U\partial_\mu U^\dagger\,, \tag{A.27}$$

one can derive from this Lagrangian the expressions

$$A_\mu^a = -\frac{\mathrm{i}f^2}{2}\mathrm{Tr}\left[T^a\left(\partial_\mu UU^\dagger - \partial_\mu U^\dagger U\right)\right] = f\partial_\mu\pi^a + \dots\,, \tag{A.28}$$

$$P^a = -\frac{\mathrm{i}Bf^2}{2}\mathrm{Tr}\left[T^a\left(U-U^\dagger\right)\right] = Bf\pi^a + \dots\,. \tag{A.29}$$

This is the only term which is needed for the pseudoscalar density P^a in the computation of the $B\to\pi$ form factors, the contributions from the HM ChPT Lagrangian are irrelevant. For the determination of $g_{B^*B\pi}$ on the other hand, one needs the spatial components of the axial vector current. From the LO Lagrangian (3.30), one can derive

$$A_k^a = -2\mathrm{i}g\left(PT^aP_k^{*\dagger} - P_k^*T^aP^\dagger + \varepsilon_{klm}P_l^*T^aP_m^{*\dagger}\right)\,, \tag{A.30}$$

and from the NLO Lagrangian (3.36)

$$\begin{aligned} A_k^a = &-d_1\frac{\partial_k\pi^a}{f}\left(PP^\dagger + P_l^*P_l^{*\dagger}\right) \\ &+ 2\mathrm{i}d_3\varepsilon^{abc}\frac{\partial_l\pi^b}{f}\left(P_k^*T^cP_l^{*\dagger} - P_l^*T^cP_k^{*\dagger} + \varepsilon_{klm}\left[PT^cP_m^{*\dagger} - P_m^*T^cP^\dagger\right]\right)\,. \end{aligned} \tag{A.31}$$

The charged currents are defined by the linear combinations

$$A_\mu^\pm = A_\mu^1 \mp \mathrm{i}A_\mu^2 = \sqrt{2}f\partial_\mu\pi^\pm + \dots\,. \tag{A.32}$$

In Sec. 5.3.1, the explicit form of the two operators O_{L} and O_{M}, which are needed in the computation of B^0-$\bar{B}^0$ amplitudes, was derived in HM ChPT. The LO part of O_{M} has terms both with zero and one pion field:

$$\begin{aligned} O_{\mathrm{M}}^{\mathrm{LO}} = \eta_1 &\left[\left(P^{(b)\dagger}\right)\left(P^{(\bar{b})}\right) + \frac{\mathrm{i}}{f}\left(\pi P^{(b)\dagger}\right)\left(P^{(\bar{b})}\right) + \frac{\mathrm{i}}{f}\left(P^{(b)\dagger}\right)\left(\pi P^{(\bar{b})}\right)\right] \\ &+ \eta_2 \left[\left(P_k^{(b)*\dagger}\right)\left(P_k^{(\bar{b})*}\right) + \frac{\mathrm{i}}{f}\left(\pi P_k^{(b)*\dagger}\right)\left(P_k^{(\bar{b})*}\right) + \frac{\mathrm{i}}{f}\left(P_k^{(b)*\dagger}\right)\left(\pi P_k^{(\bar{b})*}\right)\right] . \end{aligned} \tag{A.33}$$

The result for $O_{\mathrm{L}}^{\mathrm{LO}}$ can be obtained by setting $\rho = \eta_1 = -\eta_2$. At NLO, only terms with one pion enter, and one finds for O_{M}

$$\begin{aligned} O_{\mathrm{M}}^{\mathrm{NLO}} = -\frac{\eta_1}{f} \Big[&\mathrm{i}\phi_1\left(\partial_k \pi P^{(b)\dagger}\right)\left(P_k^{(\bar{b})*}\right) + \mathrm{i}\phi_2\left(\partial_k \pi P_k^{(b)*\dagger}\right)\left(P^{(\bar{b})}\right) + \mathrm{i}\phi_3 \varepsilon_{klm}\left(\partial_k \pi P_l^{(b)*\dagger}\right)\left(P_m^{(\bar{b})*}\right) \\ &+ \mathrm{i}\phi_2\left(P^{(b)\dagger}\right)\left(\partial_k \pi P_k^{(\bar{b})*}\right) + \mathrm{i}\phi_1\left(P_k^{(b)*\dagger}\right)\left(\partial_k \pi P^{(\bar{b})}\right) + \mathrm{i}\phi_3 \varepsilon_{klm}\left(P_l^{(b)*\dagger}\right)\left(\partial_k \pi P_m^{(\bar{b})*}\right) \\ &+ \phi_7\left(\partial_4 \pi P^{(b)\dagger}\right)\left(P^{(\bar{b})}\right) + \phi_8\left(\partial_4 \pi P_k^{(b)*\dagger}\right)\left(P_k^{(\bar{b})*}\right) \\ &- \phi_7^*\left(P^{(b)\dagger}\right)\left(\partial_4 \pi P^{(\bar{b})}\right) - \phi_8^*\left(P_k^{(b)*\dagger}\right)\left(\partial_4 \pi P_k^{(\bar{b})*}\right)\Big] . \end{aligned} \tag{A.34}$$

Setting $\rho = \eta_1$, $\omega_1 = \phi_1 = \phi_2 = \phi_3$, and $\omega_2 = \phi_7 = -\phi_8$, one recovers the result for $O_{\mathrm{L}}^{\mathrm{NLO}}$.

Applying charge conjugation to the first line in Eq. (A.9), one finds the interaction vertices coupling two heavy mesons with heavy anti-quarks to one pion field:

$$\Delta\mathcal{L}_{H^{(\bar{b})}}^{(1)} = \frac{2\mathrm{i}g}{f}\left(P_k^{(\bar{b})*\dagger}\partial_k \pi P^{(\bar{b})} - P^{(\bar{b})\dagger}\partial_k \pi P_k^{(\bar{b})*} + \varepsilon_{klm} P_m^{(\bar{b})*\dagger}\partial_l \pi P_k^{(\bar{b})*}\right) . \tag{A.35}$$

The discussion of the excited states contamination of the pion and kaon two-point function in Sec. 4.3 requires additional interaction vertices, and also terms with three pions for the light pseudoscalar density. More importantly, one has to use ChPT with three light quark flavours in order to include the kaons. In this case, the pion matrix reads

$$\pi = \pi^a T^a = \frac{1}{\sqrt{2}}\begin{pmatrix} \frac{\pi^0}{\sqrt{2}} + \frac{\eta}{\sqrt{6}} & \pi^+ & K^+ \\ \pi^- & -\frac{\pi^0}{\sqrt{2}} + \frac{\eta}{\sqrt{6}} & K^0 \\ K^- & \bar{K}^0 & -\sqrt{\frac{2}{3}}\eta \end{pmatrix} , \tag{A.36}$$

but it is in fact more convenient to not use the physical basis, but the fields π^1, π^2, et cetera. In the following, the isospin limit is taken in which the up and down quark are mass degenerate with mass m_l, which means that the fields π^1, π^2, and π^3 all have the same mass $m_\pi^2 = 2Bm_l$. These are the three fields from which the physical fields are formed. On the other hand, the four fields π^4, π^5, π^6, and π^7, which are linear combinations of the physical kaons, are also mass degenerate with mass $m_K = B(m_l + m_s)$. In the isospin limit, the correlation functions of the three pions are identical, and the same is true for the four kaons. It is therefore enough to specialise to the two-point functions of π^1 and π^4.

In order to compute the excited states of the two-point functions, one also needs the three-particle pieces of the pseudoscalar density (A.29). For $\pi\pi\pi$ and $K\pi\pi$ excited states, only the following terms are needed:

$$P^1 = Bf\pi^1 - \frac{B}{6f}\pi^1\left((\pi^1)^2 + (\pi^2)^2 + (\pi^3)^2\right) + \dots , \tag{A.37}$$

$$P^4 = Bf\pi^4 - \frac{B}{6f}\pi^4\left((\pi^1)^2 + (\pi^2)^2 + (\pi^3)^2\right) \dots . \tag{A.38}$$

The relevant interaction vertices couple four fields. For the π^1 correlation functions, only π^1, π^2, and π^3 are relevant, all other terms contribute to excited states which are stronger suppressed. The vertices must also contain at least one π^1 field so that they can be contracted with the π^1 field in P^1. The result reads

$$\begin{aligned}\Delta\mathcal{L}_\pi^{(2)} = &-\frac{(\pi^1)^2}{6f^2}\left(\partial_\mu\pi^2\partial_\mu\pi^2 + \partial_\mu\pi^3\partial_\mu\pi^3\right) - \frac{\partial_\mu\pi^1\partial_\mu\pi^1}{6f^2}\left((\pi^2)^2 + (\pi^3)^2\right) \\ &+ \frac{\pi^1\partial_\mu\pi^1}{3f^2}\left(\pi^2\partial_\mu\pi^2 + \pi^3\partial_\mu\pi^3\right) - \frac{m_\pi^2}{24f^2}\left((\pi^1)^4 + 2(\pi^1)^2(\pi^2)^2 + 2(\pi^1)^2(\pi^3)^2\right) .\end{aligned} \tag{A.39}$$

For the π^4 correlation function, one needs at least one π^4 field in the interaction vertices in order to have non-zero Wick contractions with P^4. Since one is interested in $K\pi\pi$ states, the vertices should also couple two of the light pions, i.e. π^1, π^2, and π^3 to two kaons. One finds

$$\begin{aligned}\Delta\mathcal{L}_\pi^{(2)} = &-\frac{1}{24f^2}\sum_{a=1}^{3}\Big[(\pi^4)^2\partial_\mu\pi^a\partial_\mu\pi^a - 2\pi^4\partial_\mu\pi^4\pi^a\partial_\mu\pi^a + \partial_\mu\pi^4\partial_\mu\pi^4(\pi^a)^2 \\ &+(m_\pi^2 + m_K^2)(\pi^4)^2(\pi^a)^2\Big] - \frac{\pi^4}{4f^2}\Big[\partial_\mu\pi^5(\pi^1\partial_\mu\pi^2 - \pi^2\partial_\mu\pi^1) \\ &+\partial_\mu\pi^6(\pi^3\partial_\mu\pi^1 - \pi^1\partial_\mu\pi^3) + \partial_\mu\pi^7(\pi^2\partial_\mu\pi^3 - \pi^3\partial_\mu\pi^2)\Big] \\ &- \frac{\partial_\mu\pi^4}{4f^2}\Big[\pi^5(\pi^2\partial_\mu\pi^1 - \pi^1\partial_\mu\pi^2) + \pi^6(\pi^1\partial_\mu\pi^3 - \pi^3\partial_\mu\pi^1) \\ &+\pi^7(\pi^3\partial_\mu\pi^2 - \pi^2\partial_\mu\pi^3)\Big] .\end{aligned} \tag{A.40}$$

B. Higher Order Corrections of the B Meson Two-Point Function

In Sec. 4.2, the computation of the excited states contamination of the B meson two-point function was presented. This section summarises the results for the terms which are higher order corrections to the single B contribution to the correlator. Some of the terms diverge when the sum over internal momenta is performed, and one first has to introduce a regularisation for them. This is most easily done after taking the continuum limit, because then the application of dimensional regularisation is straightforward. In general, sums of the following form are replaced by integrals in $d = 3 - 2\varepsilon$ dimensions

$$\frac{1}{L^3}\sum_{\vec{p}} \frac{\vec{p}^{\,2a}}{(m_\pi^2 + \vec{p}^{\,2})^{\frac{b}{2}}} \to \mathcal{I}(a,b) = \frac{\mu^{2\varepsilon}}{(2\pi)^d}\int \mathrm{d}^d\vec{p}\,\frac{\vec{p}^{\,2a}}{(m_\pi^2 + \vec{p}^{\,2})^{\frac{b}{2}}}\,. \tag{B.1}$$

μ is an energy scale which can be identified with the renormalisation scale. These integrals can be solved analytically by first transforming to spherical coordinates, performing the spherical integration using the result [178]

$$\int \mathrm{d}\Omega_d = \frac{2\pi^{\frac{d}{2}}}{\Gamma\left(\frac{d}{2}\right)}\,, \tag{B.2}$$

where $\Gamma(x)$ is Euler's gamma function, and using the variable transformation $x = |\vec{p}\,|^2/m_\pi^2$, to arrive at

$$\mathcal{I}(a,b) = \frac{\mu^{2\varepsilon}\pi^{-\frac{d}{2}}}{2^d\Gamma\left(\frac{d}{2}\right)} m_\pi^{d+2a-b}\int_0^\infty \mathrm{d}x\,\frac{x^{\frac{d}{2}-1+a}}{(1+x)^{\frac{b}{2}}}\,. \tag{B.3}$$

This integral is of the the same form as an integral representation of Euler's beta function [179]

$$B(y,z) = \int_0^\infty \mathrm{d}t\,\frac{t^{y-1}}{(1+t)^{y+z}} = \frac{\Gamma(y)\Gamma(z)}{\Gamma(y+z)}\,, \tag{B.4}$$

and one finally arrives at

$$\mathcal{I}(a,b) = \frac{\mu^{2\varepsilon}\pi^{-\frac{d}{2}}}{2^d\Gamma\left(\frac{d}{2}\right)} m_\pi^{d+2a-b}\frac{\Gamma\left(\frac{d}{2}+a\right)\Gamma\left(\frac{b}{2}-\frac{d}{2}-a\right)}{\Gamma\left(\frac{b}{2}\right)}\,. \tag{B.5}$$

For fixed values of a and b, the result can then be expanded in powers of $\varepsilon = (3-d)/2$, see [178] for more details. For this appendix, the following results are needed:

$$\mathcal{I}(0,1) = \frac{m_\pi^2}{8\pi^2}\left(-\frac{1}{\varepsilon} - 1 + \gamma_\mathrm{E} - \log(4\pi) + \log\left(\frac{m_\pi^2}{\mu^2}\right)\right) + \mathcal{O}(\varepsilon)\,, \tag{B.6}$$

$$\mathcal{I}(1,2) = \frac{m_\pi^3}{4\pi} + \mathcal{O}(\varepsilon)\,, \tag{B.7}$$

$$\mathcal{I}(1,3) = \frac{3m_\pi^2}{8\pi^2}\left(-\frac{1}{\varepsilon} - \frac{1}{3} + \gamma_\mathrm{E} - \log(4\pi) + \log\left(\frac{m_\pi^2}{\mu^2}\right)\right) + \mathcal{O}(\varepsilon)\,. \tag{B.8}$$

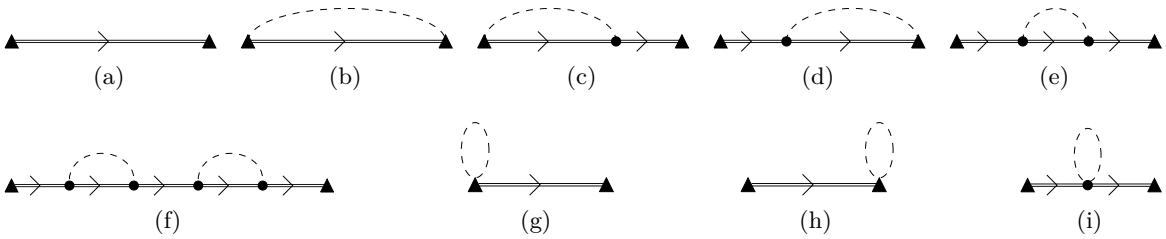

Figure B.1.: Diagrams contributing to the B meson two-point function.

With these considerations out of the way, one can turn to the diagrams in Fig. B.1. For starters, consider the full result for diagram (e) for local interpolating fields:

$$(\mathrm{e}) = \frac{3\alpha^2 g^2}{16 f^2 L^3}\left[\sum_{\vec{p}} \frac{\vec{p}^{\,2} e^{-E_{\pi,\vec{q}}\,t}}{E^3_{\pi,\vec{p}}} - \sum_{\vec{p}} \frac{\vec{p}^{\,2}}{E^3_{\pi,\vec{p}}} + t \sum_{\vec{p}} \frac{\vec{p}^{\,2}}{E^2_{\pi,\vec{p}}}\right] \tag{B.9}$$

The first term has already been identified as a contribution to the $B\pi$ excited states contamination in Sec. 4.2. As will be shown now the third term gives a correction to the energy of the B meson. This is not surprising since the diagram has the usual form of a one-particle irreducible (1PI) one-loop self-energy diagram after cutting of the external interpolating fields. In the infinite volume limit, one has

$$\frac{3\alpha^2 g^2}{16 f^2} t\, \mathcal{I}(1,2) = \frac{3\alpha^2 g^2 m_\pi^3}{64\pi f^2} t + \mathcal{O}(\varepsilon)\,. \tag{B.10}$$

As explained in [126], for the computation of the self-energy one has to sum up all diagrams with any number of insertions of the 1PI diagram. In momentum space, this sum has the form of a geometric series. In position space, the terms of the sum should rearrange themselves into the series expansion of an exponential, since the correlation functions fall of with the energy of the particles, $\exp(-Et)$. Indeed, the result for two insertions of the 1PI diagram, diagram (f) in Fig. B.1, has been checked explicitly to confirm this pattern, and one therefore finds (including diagram (a) with no insertions)

$$\frac{\alpha^2}{2}\left(1 + \frac{3g^2 m_\pi^3}{32\pi f^2} t + \frac{1}{2!}\left(\frac{3g^2 m_\pi^3}{32\pi f^2}\right)^2 t^2 + \ldots\right) = \frac{\alpha^2}{2} e^{\frac{3g^2 m_\pi^3}{32\pi f^2} t}\,. \tag{B.11}$$

This yields a mass shift for the B meson

$$\Delta m_B = -\frac{3g^2 m_\pi^3}{32\pi f^2}\,, \tag{B.12}$$

a result that has already been derived in [164] in momentum space.

The second term in Eq. (B.9) yields a correction to α^2, the square of the B meson decay constant. Evaluating the contribution in the infinite volume limit and in dimensional regularisation, one finds

$$-\frac{3\alpha^2 g^2}{16 f^2}\mathcal{I}(1,3) = -\frac{9\alpha^2 g^2 m_\pi^2}{128\pi^2 f^2}\left(-\frac{1}{\varepsilon} - \frac{1}{3} + \gamma_{\mathrm{E}} - \log(4\pi) + \log\left(\frac{m_\pi^2}{\mu^2}\right)\right) + \mathcal{O}(\varepsilon)\,. \tag{B.13}$$

This diagram therefore leads to a logarithmic correction of the B meson decay constant $\hat{f}$. The $1/\varepsilon$ pole needs to be cancelled by a suitable counterterm. These would arise from the

$\mathcal{O}(p^2)$ interpolating fields of the B meson as discussed in [29]. Two such terms can be obtained by using χ_+ which has been defined in Eq. (A.10),

$$O_1 = \delta_1 P \chi_+ u_+ = \delta_1 4BPM_q + \ldots = \delta_1 2m_\pi^2 P + \ldots\,, \tag{B.14}$$

$$O_2 = \delta_2 \mathrm{Tr}\left[\chi_+\right] P u_+ = \delta_2 4B\,\mathrm{Tr}\left[M_q\right] P + \ldots = \delta_2 4m_\pi^2 P + \ldots\,. \tag{B.15}$$

It was assumed that $M_q = m_l \mathbb{1}_2$. The LECs δ_i are then split into two parts,

$$\delta_i = \delta_i^{\mathrm{R}}(\mu) + \bar{\delta}_i(\mu)\,, \tag{B.16}$$

where $\delta_i^{\mathrm{R}}(\mu)$ is the finite, renormalised LEC and $\bar{\delta}_i(\mu)$ a counterterm. The values of $\delta_i^{\mathrm{R}}(\mu)$ need to be determined from experiments or lattice simulations to make a prediction for the order p^2 corrections of the B meson decay constant.

It turns out that there are two more diagrams which yield logarithmic corrections to $\hat{f}$. These are given by diagrams (g) and (h) in Fig. B.1. Using only the LO terms of the interpolating field, one finds for the sum of the two diagrams

$$\begin{aligned}(\mathrm{g}) + (\mathrm{h}) &= -\frac{6\alpha^2}{32f^2L^3}\sum_{\vec{p}}\frac{1}{E_{\pi,\vec{p}}} \to -\frac{6\alpha^2}{32f^2}\mathcal{I}(0,1) \\ &= -\frac{3\alpha^2 m_\pi^2}{128\pi^2 f^2}\left(-\frac{1}{\varepsilon} - 1 + \gamma_{\mathrm{E}} - \log(4\pi) + \log\left(\frac{m_\pi^2}{\mu^2}\right)\right) + \mathcal{O}(\varepsilon)\,.\end{aligned} \tag{B.17}$$

Combining this with the result of diagram (e), and also including the LO result from diagram (a), $\alpha^2/2$, one finds for the B meson decay constant in the static limit

$$\hat{f}^{\,2} = \alpha^2\left(1 - \frac{3+9g^2}{64f^2\pi^2}m_\pi^2\log\left(\frac{m_\pi^2}{\mu^2}\right) + 2A(\mu)m_\pi^2\right)\,. \tag{B.18}$$

The logarithmic corrections agree with the results found in [29, 171, 180] after squaring them and taking different normalisations for f into account. $A(\mu)$ is a linear combination of the renormalised LECs $\delta_i^{\mathrm{R}}(\mu)$ and the finite parts of the loop integrals which are not proportional to logarithms. The exact form of $A(\mu)$ depends on the renormalisation scheme.

Another diagram which can in principle lead to higher order corrections of the two-point function is diagram (i). For now, only the interaction vertices at LO are considered, which are given in Eq. (A.9). Considering the form of the diagram, it is easy to see that it can only contribute to the self-energy of the B meson: the propagator of the pion starts and ends at the same point in spacetime and is therefore independent of the insertion time, see Eq. (A.4). On the other hand, the propagator of the heavy mesons are proportional to Heaviside functions, which means that the integral over the insertion time of the interaction vertex is given by

$$\int_{-\infty}^{\infty} \mathrm{d}t'\,\theta(t-t')\theta(t') = t\,\theta(t)\,. \tag{B.19}$$

The result for the diagram is therefore proportional to t and can thus only contribute to the self-energy of the B meson. It turns out that for the LO interaction vertices, this diagram vanishes. This can be easily seen from the fact that the pion propagator is proportional to $1/E_\pi$, whereas the derivative w.r.t. time brings down a factor of the pion energy. The sum over the pion momentum is therefore given by

$$\frac{1}{L^3}\sum_{\vec{p}} 1 \to \mathcal{I}(0,0) = 0\,, \tag{B.20}$$

where it was used that scaleless integrals vanish in dimensional regularisation.

For the sake of completeness, the corrections to $\hat{f}$ stemming from diagrams (c) and (d) are also presented. Adding the relevant pieces from the two diagrams, one has

$$-2\frac{3g\alpha^2\beta_1}{16f^2L^3}\sum_{\vec{p}}\frac{\vec{p}^{\,2}}{E^2_{\pi,\vec{p}}} \to -\frac{3g\alpha^2\beta_1}{8f^2}\mathcal{I}(1,2) = -\frac{3g\alpha^2\beta_1 m_\pi^3}{32\pi f^2} + \mathcal{O}(\varepsilon)\,, \tag{B.21}$$

and it follows that

$$\hat{f}^{\,2} = \alpha^2\left(1 - \frac{3+9g^2}{64f^2\pi^2}m_\pi^2\log\left(\frac{m_\pi^2}{\mu^2}\right) + 2A(\mu)m_\pi^2 - \frac{3g\beta_1}{16f^2\pi}m_\pi^3\right)\,. \tag{B.22}$$

Before arguing that there are no further $\mathcal{O}(p^3)$ pieces, one should remember that the chiral dimension of the diagrams is given by i) the chiral dimension of the LECs of the interpolating fields and the Lagrangian, and ii) the number of pion propagators of which each increases the chiral dimension by two. From this consideration alone, it is clear that diagrams with two pion lines contribute at order p^4 or higher.

First, consider only diagrams with the LO interpolating fields of the B mesons and insertions of interaction vertices. The NLO interaction vertices given in Eq. (A.11) contain only terms with at least two pions. This means, they can only enter in diagram (i) in Fig. B.1. But it has been argued above, that those terms only contribute to the self-energy of the B meson. A computation shows that these terms lead to logarithmic corrections of the form $d_i m_\pi^4 t/f^2\log(m_\pi^2/\mu^2)$. Moving to the NNLO Lagrangian, one can use simple power counting to show that it also only contributes terms of chiral dimension 4 or higher. First, one should notice that the NNLO Lagrangian is of chiral order 3, an odd number. This means that the Lagrangian contains at least one derivative since the quark mass matrix is of order 2. Derivatives of the heavy mesons are forbidden by LFN symmetry or can be eliminated using a field redefinition by making use of the LO equations of motion. The derivative therefore has to act on a pion which implies that the diagrams have to contain at least on pion line, this is already an order p^2 contribution. The LECs of the Lagrangian on the other hand are of order p^2 and all diagrams will therefore be at least of order p^4. The terms of the NNLO Lagrangian can be found in [163].

Another set of diagrams has to be considered when one inspects the contributions of the higher order terms in the B meson interpolating fields. Throughout the following discussion, it is assumed that one of the interpolating fields is still the LO piece, only the second is of higher order. This means only contributions of the form

$$\left\langle P^{\mathrm{LO}}(x)P^{\mathrm{N^nLO}\dagger}(0)\right\rangle\,, \qquad \left\langle P^{\mathrm{N^nLO}}(x)P^{\mathrm{LO}\dagger}(0)\right\rangle\,, \tag{B.23}$$

with $n \geq 1$ are considered. Here, P is the heavy-light pseudoscalar density and not the field destroying a heavy meson. First, consider the term proportional to β_2 in the NLO part of the interpolating field. It couples two pions to the heavy meson and therefore only diagrams (g) and (h) of Fig. B.1 are of interest. But the form of the interpolating field given in Eq. (A.20) (the local version only differs in the LECs) shows that it contains a single time derivative acting on a pion. It has already been discussed above that this leads to a result which is proportional to $\mathcal{I}(0,0) = 0$ when diagram (i) with the LO interaction vertex was considered. Turning to the $\mathcal{O}(p^2)$ terms of the B meson interpolating fields, only diagram (a) in Fig. B.1 is of interest. All other diagrams contain an additional pion line which increases the chiral dimension by two, leading to chiral dimension four. But the contributions of diagram (a) with one p^2 and one LO piece of the interpolating field were already used to renormalise the logarithms in Eq. (B.18), they enter in the function $A(\mu)$. Finally, the order p^3 piece of

the interpolating field has to contain a derivative acting on a pion field. As a consequence, the diagrams must contain a pion line and all contributions from this term to the two-point function are at least of chiral dimension five. For the same reason, the β_1 piece in the NLO interpolating field contributes an order p^3 term to the decay constant.

The last terms to consider are of the form

$$\left\langle P^{\mathrm{N^nLO}}(x) P^{\mathrm{N^mLO}\dagger}(0) \right\rangle , \tag{B.24}$$

with $n, m \geq 1$. But the three relevant cases $m = n = 1$, $m = 2$ and $n = 1$, and $m = 1$ and $n = 2$ do not lead to Feynman diagrams without a pion line, they therefore contribute at order p^4 at best.

This concludes the discussion of the order p^3 corrections of the heavy-light decay constant. The result for $\hat{f}$ (and not its square) in the static limit and including corrections up to $\mathcal{O}(p^3)$ is

$$\hat{f} = \alpha \left(1 - \frac{3 + 9g^2}{128\pi^2} m_\pi^2 \log\left(\frac{m_\pi^2}{\mu^2}\right) + A(\mu) m_\pi^2 - \frac{3g\beta_1}{32\pi f^2} m_\pi^3 \right) . \tag{B.25}$$

C. Higher Order Corrections of $\delta h_\perp$

In this appendix, the higher order corrections of $\delta C_{3,k}$ are discussed. These can be obtained in parts by computing diagrams (d)-(o) of Fig. C.1 (these are the same diagrams which can be found in Fig. 5.6). These terms are of the same order in the chiral expansion as δC_2^B and $\Delta m_{B,\text{eff}}$. As before, only contributions which contain at most one factor of β_i, $\tilde{\beta}_i$, or d_i are kept in the results. The latter are the LECs of the NLO HM ChPT Lagrangian, see Eq. (3.36). An explicit computation shows that diagrams (g), (h), and (m) do not satisfy this requirement and are thus neglected. When computing the diagrams, one encounters results of the form

$$\sum_{\vec{p}} f(\vec{p}^{\,2}) p_k \tag{C.1}$$

with some function $f(\vec{p}^{\,2})$. This sum vanishes since the sum runs over a symmetric domain while the summand is an odd function of $\vec{p}$. For this reason, diagrams (d), (e), and also some contributions from other diagrams vanish. Another useful identity is given by

$$\sum_{\vec{p}} f'(\vec{p}^{\,2}) \vec{p}\cdot\vec{q}\, p_k = \frac{1}{3} \sum_{\vec{p}} f'(\vec{p}^{\,2}) \vec{p}^{\,2} q_k \,. \tag{C.2}$$

Evaluating the diagrams and taking the ratio (5.30), one again finds terms which do not fall off in time. These are higher order corrections to the form factors and are therefore neglected. For the $B\pi$ excited states, the result splits into

$$\delta C_{3,k}^{\text{SL}}(\vec{q}, t, t_\text{v}) = \sum_{\vec{p}} \left[A(\vec{p}, \vec{q}) e^{-E_{\pi,\vec{p}}\, t_\text{v}} + B(\vec{p}, \vec{q}) e^{-E_{\pi,\vec{q}}\, t_\text{v}} \right] . \tag{C.3}$$

The interpretation of the two terms is the following: the first term is a tower of $B\pi$ states as can be inferred from the exponential. It falls off with the energy $E_{\pi,\vec{p}}$ which is a function of the momentum which is summed over. The term proportional to the coefficient B on the other hand describes a single pion with fixed momentum $\vec{q}$, the momentum of the final state pion. This contribution can be thought of as a higher order correction of $\delta h_\perp^{\text{dom}}$ defined in Eq. (5.36), since it is proportional to the same exponential.

There are some complications which arise when computing the diagrams. These are due to integrals over the interaction vertices which lead to terms of the form

$$e^{-E_{\pi,\vec{q}}\, t} \sum_{\vec{p}} c(\vec{p}^{\,2}) \int_0^{t_\text{v}} \mathrm{d}t_\text{I}\, e^{-(E_{\pi,\vec{p}} - E_{\pi,\vec{q}}) t_\text{I}} = \sum_{\vec{p}} c(\vec{p}^{\,2}) \begin{cases} \frac{e^{-E_{\pi,\vec{p}}\, t_\text{v} - E_{\pi,\vec{q}}(t - t_\text{v})} - e^{-E_{\pi,\vec{q}}\, t}}{E_{\pi,\vec{q}} - E_{\pi,\vec{p}}} \,, & |\vec{p}| \neq |\vec{q}| \\ t_\text{v}\, e^{-E_{\pi,\vec{q}}\, t} \,, & |\vec{p}| = |\vec{q}| \end{cases} \tag{C.4}$$

with some function $c(\vec{p}^{\,2})$. The problem here is that one has to split the result into terms for which $|\vec{p}| \neq |\vec{q}|$, and others for which the two momenta are equal. There are more convoluted integrals which yield a slightly different result for the individual terms, but they still have to be handled in the same way due to the denominator $1/(E_{\pi,\vec{q}} - E_{\pi,\vec{p}})$. Whereas the first case in the above equation makes it clear which term contributes to the coefficients A and B in Eq. (C.3), it is not so clear for the second term since it mixes terms from both contributions. Nevertheless, it is clear that the full result is finite for $|\vec{p}| = |\vec{q}|$, even if the individual contributions to A and B are not.

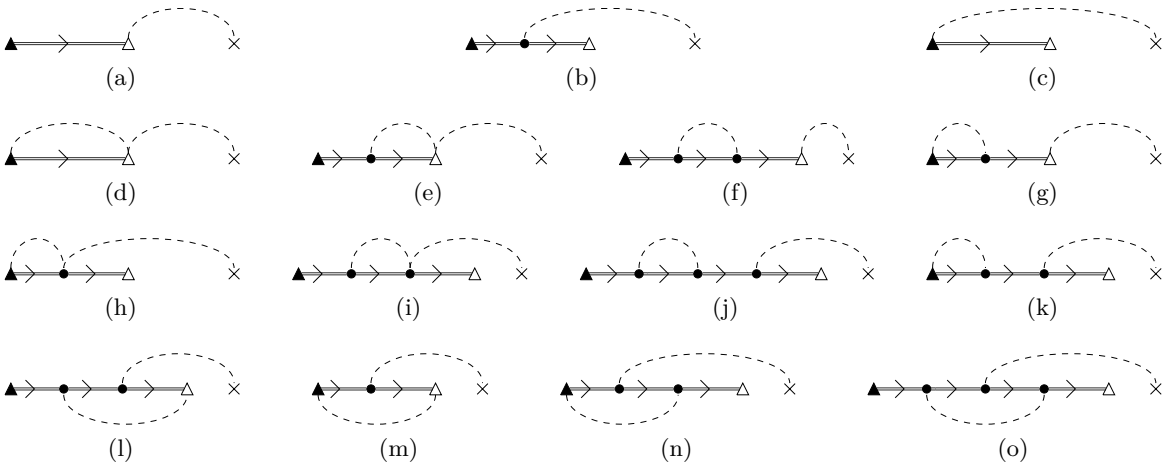

Figure C.1.: A subset of Feynman diagrams contributing to $h_\perp$, $h_\parallel$, and the $B\pi$ excited states contamination of these form factors. See the caption of Fig. 5.1 for an explanation of the symbols.

With these remarks out of the way, one can split the result into several parts. First, the result which falls off in time with the exponential $e^{-E_{\pi,\vec{p}}\,t_\mathrm{v}}$, i.e. those terms which contribute to a tower of $B\pi$ states:

$$\begin{aligned}\delta C_{3,k}^{\mathrm{SL},1}(\vec{q},t,t_\mathrm{v}) = \frac{1}{1-\beta_1 E_{\pi,\vec{q}}/g}\Bigg\{&\sum_{\vec{p}}\frac{\vec{p}^{\,2}q_k}{f^2L^3}\beta_1 g\left(\frac{1}{24E_{\pi,\vec{p}}^2}-\frac{3E_{\pi,\vec{q}}}{8E_{\pi,\vec{p}}^3}\right)e^{-E_{\pi,\vec{p}}\,t_\mathrm{v}}\\ &+\sum_{\vec{p},|\vec{p}|\neq|\vec{q}|}\frac{\vec{p}^{\,2}q_k}{f^2L^3}\Bigg[\frac{\gamma E_{\pi,\vec{q}}}{3E_{\pi,\vec{p}}^2(E_{\pi,\vec{q}}-E_{\pi,\vec{p}})}\\ &+\frac{g^2+g\tilde{\beta}_1 E_{\pi,\vec{p}}}{E_{\pi,\vec{q}}-E_{\pi,\vec{p}}}\left(\frac{3E_{\pi,\vec{q}}}{8E_{\pi,\vec{p}}^3}-\frac{1}{24E_{\pi,\vec{p}}^2}\right)\Bigg]e^{-E_{\pi,\vec{p}}\,t_\mathrm{v}}\Bigg\}\,.\end{aligned} \tag{C.5}$$

The terms proportional to β_1 are finite at $|\vec{p}|=|\vec{q}|$, they stem from diagrams (f) and (l). The reason is that these diagrams simply do not lead to the troublesome integrals which introduce a factor of $1/(E_{\pi,\vec{q}}-E_{\pi,\vec{p}})$. Another interesting thing to note here is that the LECs of the NLO Lagrangian (3.36) again combine to $\gamma = d_3 - d_1/4$, the same combination already found in the excited states contamination of $g_{B^*B\pi}$. The above sum has no UV divergence since the exponential suppresses the large-$|\vec{p}|$ terms.

The second contribution combines all terms which fall off with $e^{-E_{\pi,\vec{q}}\,t_\mathrm{v}}$ and for which $|\vec{p}|\neq|\vec{q}|$:

$$\begin{aligned}\delta C_{3,k}^{\mathrm{SL},2}(\vec{q},t,t_\mathrm{v}) = \frac{1}{1-\beta_1 E_{\pi,\vec{q}}/g}\Bigg\{&\sum_{\vec{p},|\vec{p}|\neq|\vec{q}|}\frac{\vec{p}^{\,2}q_k}{f^2L^3}\Bigg[\frac{\gamma}{3E_{\pi,\vec{p}}(E_{\pi,\vec{p}}-E_{\pi,\vec{q}})}\left(\frac{E_{\pi,\vec{q}}}{E_{\pi,\vec{p}}}-2\right)\\ &+\frac{g^2+g\tilde{\beta}_1 E_{\pi,\vec{q}}}{E_{\pi,\vec{q}}-E_{\pi,\vec{p}}}\left(\frac{1}{24E_{\pi,\vec{p}}^2}-\frac{3}{8E_{\pi,\vec{p}}E_{\pi,\vec{q}}}\right)\Bigg]\Bigg\}e^{-E_{\pi,\vec{q}}\,t_\mathrm{v}}\,.\end{aligned} \tag{C.6}$$

It is clear that this sum is UV divergent since the exponential does not depend on $\vec{p}$ and thus does not render the sum finite. On the other hand, it shows the same exponential decay as $\delta h_\perp^{\mathrm{dom}}$. This is in some sense reminiscent of the discussion of logarithmic corrections of the two-point function in App. B: a finite leading order result is modified by diagrams with additional

pion lines. These additional diagrams have to be regularised and, after renormalisation, lead to a finite correction. For this reason, it can be expected that $\delta C_{3,k}^{\mathrm{SL},2}$ leads to higher order, maybe even logarithmic, corrections to the large excited state in $\delta h_\perp^{\mathrm{dom}}$. But in order to renormalise these contributions, one also needs the interpolating fields at order p^2 and higher. The LECs of these terms would also yield finite corrections to $\delta h_\perp$, but the values of these LECs are not known at present. It is therefore currently not possible to investigate the size of the excited states at orders p^2 and p^3.

The last pieces which are now missing are the terms of the sums for which $|\vec{p}| = |\vec{q}|$. As exemplified in Eq. (C.4), the integrals are still finite at this point. Indeed, if one adds the summands from Eq. (C.5) which diverge at $|\vec{p}| = |\vec{q}|$ and Eq. (C.6), one sees that the pole at $1/(E_{\pi,\vec{q}} - E_{\pi,\vec{p}})$ is a removable singularity, and one arrives at the finite result

$$\delta C_{3,k}^{\mathrm{SL},3}(\vec{q},t,t_{\mathrm{v}}) = \frac{1}{1-\beta_1 E_{\pi,\vec{q}}/g}\left\{\sum_{\vec{p},|\vec{p}|=|\vec{q}|}\frac{\vec{p}^{\,2}q_k}{f^2L^3E_{\pi,\vec{q}}^2}\left[\frac{\gamma}{3}(2+t_{\mathrm{v}}E_{\pi,\vec{q}})+\frac{g^2}{E_{\pi,\vec{q}}}\left(\frac{3}{4}+\frac{t_{\mathrm{v}}E_{\pi,\vec{q}}}{3}\right)\right.\right.$$
$$\left.\left.+\tilde{\beta}_1 g\left(\frac{5}{12}+\frac{t_{\mathrm{v}}E_{\pi,\vec{q}}}{3}\right)\right]\right\}e^{-E_{\pi,\vec{q}}\,t_{\mathrm{v}}}\,. \tag{C.7}$$

The result shows in parts a linear dependence on t_{v}, the insertion time of the vector current. For the excited states contamination of the two-point function and $g_{B^*B\pi}$, these terms were identified with corrections to the heavy meson mass since the diagrams which lead to these terms had the typical form of self-energy diagrams. This is not so clear here, because these terms arise only for one special momentum configuration, and furthermore there are also diagrams in Fig. C.1 which do not look like a diagram with a self-energy insertion. As discussed in App. B, it is also necessary that these terms form the leading order of a series expansion, with the higher orders provided by Feynman diagrams with additional interaction vertices. At the moment, this seems unlikely and one therefore should consider the result in Eq. (C.7) as a contribution to the excited states contamination.

Finally, it should be mentioned that the diagrams in Fig. C.1 constitute only a subset of all diagrams which can contribute at order p^2 and p^3 to the excited states contamination of $\delta h_\perp$. Fig. C.2 shows the remaining ones. Comparing with the diagrams encountered in App. B, it is clear that some of the diagrams are UV divergent and need to be renormalised. As discussed above, a numerical evaluation of the renormalised result is not possible as long as the numerical values of the finite parts of the counterterms is not known. For this reason, the computation of the additional diagrams is omitted for now.

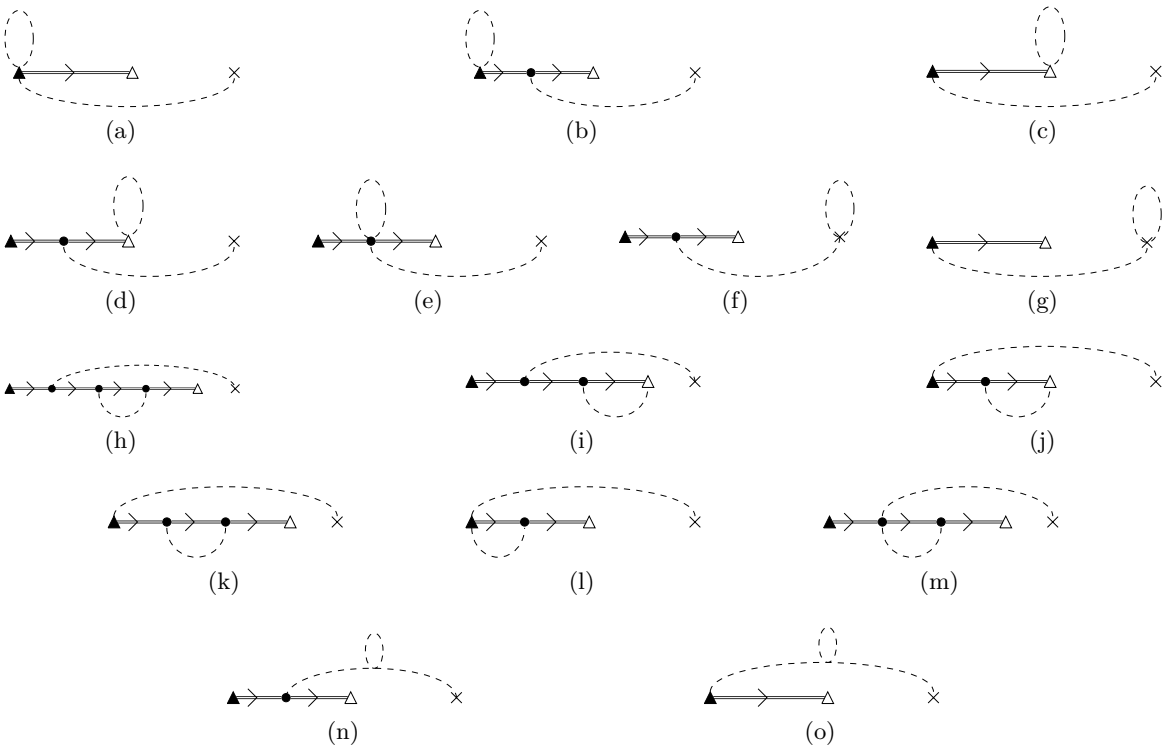

Figure C.2.: More diagrams which contribute to the $B\pi$ excited states contamination of the form factors. The relevant pieces fall off with $\exp(-E_{\pi,\vec{q}}\, t_{\mathrm{v}})$, the same exponential which shows up in $\delta h_\perp^{\mathrm{dom}}$.

Bibliography

[1] G. Aad et al. (ATLAS), 'Observation of a New Particle in the Search for the Standard Model Higgs Boson with the ATLAS Detector at the LHC', Phys. Lett. B **716**, 1–29 (2012).

[2] S. Chatrchyan et al. (CMS), 'Observation of a New Boson at a Mass of 125 GeV with the CMS Experiment at the LHC', Phys. Lett. B **716**, 30–61 (2012).

[3] F. Englert and R. Brout, 'Broken Symmetry and the Mass of Gauge Vector Mesons', Phys. Rev. Lett. **13**, 321–323 (1964).

[4] P. W. Higgs, 'Broken Symmetries and the Masses of Gauge Bosons', Phys. Rev. Lett. **13**, 508–509 (1964).

[5] G. S. Guralnik, C. R. Hagen and T. W. B. Kibble, 'Global Conservation Laws and Massless Particles', Phys. Rev. Lett. **13**, 585–587 (1964).

[6] R. L. Workman et al. (Particle Data Group), 'Review of Particle Physics', PTEP **2022**, 083C01 (2022).

[7] N. Cabibbo, 'Unitary Symmetry and Leptonic Decays', Phys. Rev. Lett. **10**, 531–533 (1963).

[8] M. Kobayashi and T. Maskawa, 'CP Violation in the Renormalizable Theory of Weak Interaction', Prog. Theor. Phys. **49**, 652–657 (1973).

[9] D. J. Gross and F. Wilczek, 'Ultraviolet Behavior of Non-Abelian Gauge Theories', Phys. Rev. Lett. **30**, 1343–1346 (1973).

[10] H. D. Politzer, 'Reliable Perturbative Results for Strong Interactions?', Phys. Rev. Lett. **30**, 1346–1349 (1973).

[11] K. G. Wilson, 'Confinement of Quarks', Phys. Rev. D **10**, 2445–2459 (1974).

[12] M. Lüscher and U. Wolff, 'How to Calculate the Elastic Scattering Matrix in Two-Dimensional Quantum Field Theories by Numerical Simulation', Nucl. Phys. B **339**, 222–252 (1990).

[13] B. Blossier, M. Della Morte, G. von Hippel, T. Mendes and R. Sommer, 'On the Generalized Eigenvalue Method for Energies and Matrix Elements in Lattice Field Theory', JHEP **04**, 094 (2009).

[14] S. Weinberg, 'Nonlinear Realizations of Chiral Symmetry', Phys. Rev. **166**, 1568–1577 (1968).

[15] J. Gasser and H. Leutwyler, 'Chiral Perturbation Theory to One Loop', Annals Phys. **158**, 142–210 (1984).

[16] J. Gasser and H. Leutwyler, 'Chiral Perturbation Theory: Expansions in the Mass of the Strange Quark', Nucl. Phys. B **250**, 465–516 (1985).

[17] J. Gasser, M. E. Sainio and A. Švarc, 'Nucleons with Chiral Loops', Nucl. Phys. B **307**, 779–853 (1988).

[18] T. Becher and H. Leutwyler, 'Baryon Chiral Perturbation Theory in Manifestly Lorentz Invariant Form', Eur. Phys. J. C **9**, 643–671 (1999).

[19] O. Bär, 'Nucleon-Pion-State Contribution to Nucleon Two-Point Correlation Functions', Phys. Rev. D **92**, 074504 (2015).

[20] O. Bär, 'Nucleon-Pion-State Contribution in Lattice Calculations of the Nucleon Charges g_A, g_T and g_S', Phys. Rev. D **94**, 054505 (2016).

[21] O. Bär, 'Nucleon-Pion-State Contribution in Lattice Calculations of Moments of Parton Distribution Functions', Phys. Rev. D **95**, 034506 (2017).

[22] O. Bär, 'Three-Particle $N\pi\pi$ State Contribution to the Nucleon Two-Point Function in Lattice QCD', Phys. Rev. D **97**, 094507 (2018).

[23] O. Bär, '$N\pi$-State Contamination in Lattice Calculations of the Nucleon Axial Form Factors', Phys. Rev. D **99**, 054506 (2019).

[24] O. Bär, '$N\pi$-State Contamination in Lattice Calculations of the Nucleon Pseudoscalar Form Factor', Phys. Rev. D **100**, 054507 (2019).

[25] O. Bär, '$N\pi$ States and the Projection Method for the Nucleon Axial and Pseudoscalar Form Factors', Phys. Rev. D **101**, 034515 (2020).

[26] O. Bär and H. Colic, '$N\pi$-State Contamination in Lattice Calculations of the Nucleon Electromagnetic Form Factors', Phys. Rev. D **103**, 114514 (2021).

[27] M. B. Wise, 'Chiral Perturbation Theory for Hadrons Containing a Heavy Quark', Phys. Rev. D **45**, 2188–2191 (1992).

[28] G. Burdman and J. F. Donoghue, 'Union of Chiral and Heavy Quark Symmetries', Phys. Lett. B **280**, 287–291 (1992).

[29] J. Goity, 'Chiral Perturbation Theory for SU(3) Breaking in Heavy Meson Systems', Phys. Rev. D **46**, 3929–3936 (1992).

[30] P. L. Cho, 'Heavy Hadron Chiral Perturbation Theory', Nucl. Phys. B **396**, [Erratum: Nucl. Phys. B **421**, 683–686 (1994)], 183–204 (1993).

[31] E. Eichten, 'Heavy Quarks on the Lattice', Nucl. Phys. B Proc. Suppl. **4**, 170–177 (1988).

[32] H. D. Politzer and M. B. Wise, 'Effective Field Theory Approach to Processes Involving Both Light and Heavy Fields', Phys. Lett. B **208**, 504–507 (1988).

[33] N. Isgur and M. B. Wise, 'Weak Decays of Heavy Mesons in the Static Quark Approximation', Phys. Lett. B **232**, 113–117 (1989).

[34] E. Eichten and B. R. Hill, 'An Effective Field Theory for the Calculation of Matrix Elements Involving Heavy Quarks', Phys. Lett. B **234**, 511–516 (1990).

[35] E. Eichten and B. R. Hill, 'Renormalization of Heavy-Light Bilinears and f_B for Wilson Fermions', Phys. Lett. B **240**, 193–199 (1990).

[36] E. Eichten, G. Hockney and H. B. Thacker, 'Application of Heavy-Light Methods to B Meson Physics', Nucl. Phys. B Proc. Suppl. **17**, 529–532 (1990).

[37] H. Georgi, 'An Effective Field Theory for Heavy Quarks at Low Energies', Phys. Lett. B **240**, 447–450 (1990).

[38] E. Eichten and B. R. Hill, 'Static Effective Field Theory: 1/m Corrections', Phys. Lett. B **243**, 427–431 (1990).

[39] B. Grinstein, 'The Static Quark Effective Theory', Nucl. Phys. B **339**, 253–268 (1990).

[40] C.-N. Yang and R. L. Mills, 'Conservation of Isotopic Spin and Isotopic Gauge Invariance', Phys. Rev. **96**, 191–195 (1954).

[41] C. A. Baker et al., 'Improved Experimental Limit on the Electric Dipole Moment of the Neutron', Phys. Rev. Lett. **97**, 131801 (2006).

[42] C. Abel et al., 'Measurement of the Permanent Electric Dipole Moment of the Neutron', Phys. Rev. Lett. **124**, 081803 (2020).

[43] G. 't Hooft and M. J. G. Veltman, 'Regularization and Renormalization of Gauge Fields', Nucl. Phys. B **44**, 189–213 (1972).

[44] G. 't Hooft and M. J. G. Veltman, 'Scalar One-Loop Integrals', Nucl. Phys. B **153**, 365–401 (1979).

[45] J. C. Collins, *Renormalization: An Introduction to Renormalization, the Renormalization Group, and the Operator Product Expansion*, Vol. 26, Cambridge Monographs on Mathematical Physics (Cambridge University Press, Cambridge, 1986).

[46] W. Pauli and F. Villars, 'On the Invariant Regularization in Relativistic Quantum Theory', Rev. Mod. Phys. **21**, 434–444 (1949).

[47] C. G. Callan Jr., 'Broken Scale Invariance in Scalar Field Theory', Phys. Rev. D **2**, 1541–1547 (1970).

[48] K. Symanzik, 'Small Distance Behaviour in Field Theory and Power Counting', Commun. Math. Phys. **18**, 227–246 (1970).

[49] S. Scherer and M. R. Schindler, *A Primer for Chiral Perturbation Theory*, Lecture Notes in Physics 830 (Springer Berlin, Heidelberg, 2012).

[50] S. L. Adler, 'Axial Vector Vertex in Spinor Electrodynamics', Phys. Rev. **177**, 2426–2438 (1969).

[51] S. L. Adler and W. A. Bardeen, 'Absence of Higher Order Corrections in the Anomalous Axial Vector Divergence Equation', Phys. Rev. **182**, 1517–1536 (1969).

[52] J. S. Bell and R. Jackiw, 'A PCAC Puzzle: $\pi^0 \to \gamma\gamma$ in the σ Model', Nuovo Cim. A **60**, 47–61 (1969).

[53] Y. Nambu, 'Axial Vector Current Conservation in Weak Interactions', Phys. Rev. Lett. **4**, 380–382 (1960).

[54] J. Goldstone, 'Field Theories with Superconductor Solutions', Nuovo Cim. **19**, 154–164 (1961).

[55] J. Goldstone, A. Salam and S. Weinberg, 'Broken Symmetries', Phys. Rev. **127**, 965–970 (1962).

[56] C. Vafa and E. Witten, 'Restrictions on Symmetry Breaking in Vector-Like Gauge Theories', Nucl. Phys. B **234**, 173–188 (1984).

[57] I. M. Barbour, P. Gibbs, J. P. Gilchrist, H. Schneider, G. Schierholz and M. Teper, 'Strong Evidence for Spontaneous Chiral Symmetry Breaking in (Quenched) QCD', Phys. Lett. B **136**, 80–86 (1984).

[58] M. Gell-Mann, 'Symmetries of Baryons and Mesons', Phys. Rev. **125**, 1067–1084 (1962).

[59] M. Gell-Mann, 'The Symmetry Group of Vector and Axial Vector Currents', Physics Physique Fizika **1**, 63–75 (1964).

[60] J. C. Ward, 'An Identity in Quantum Electrodynamics', Phys. Rev. **78**, 182 (1950).

[61] Y. Takahashi, 'On the Generalized Ward Identity', Nuovo Cim. **6**, 371–375 (1957).

[62] G. 't Hooft, 'Renormalization of Massless Yang-Mills Fields', Nucl. Phys. B **33**, 173–199 (1971).

[63] J. C. Taylor, 'Ward Identities and Charge Renormalization of the Yang-Mills Field', Nucl. Phys. B **33**, 436–444 (1971).

[64] A. A. Slavnov, 'Ward Identities in Gauge Theories', Theor. Math. Phys. **10**, 99–107 (1972).

[65] M. Lüscher, S. Sint, R. Sommer and P. Weisz, 'Chiral Symmetry and O(a) Improvement in Lattice QCD', Nucl. Phys. B **478**, 365–400 (1996).

[66] M. Lüscher, S. Sint, R. Sommer and H. Wittig, 'Nonperturbative Determination of the Axial Current Normalization Constant in O(a) Improved Lattice QCD', Nucl. Phys. B **491**, 344–364 (1997).

[67] J. S. Bell, 'Current Algebra and Gauge Variance', Nuovo Cim. C **50**, 129–134 (1967).

[68] M. Creutz, *Quarks, Gluons and Lattices*, Cambridge Monographs on Mathematical Physics (Cambridge University Press, Cambridge, 1983).

[69] J. Smit, *Introduction to Quantum Fields on a Lattice: A Robust Mate*, Cambridge Lecture Notes in Physics 15 (Cambridge University Press, Cambridge, 2002).

[70] C. Gattringer and C. B. Lang, *Quantum Chromodynamics on the Lattice*, Lecture Notes in Physics 788 (Springer, Berlin, 2010).

[71] P. F. Bedaque, 'Aharonov-Bohm Effect and Nucleon-Nucleon Phase Shifts on the Lattice', Phys. Lett. B **593**, 82–88 (2004).

[72] M. Lüscher and S. Schaefer, 'Lattice QCD Without Topology Barriers', JHEP **07**, 036 (2011).

[73] M. Lüscher and S. Schaefer, 'Lattice QCD with Open Boundary Conditions and Twisted-Mass Reweighting', Comput. Phys. Commun. **184**, 519–528 (2013).

[74] K. Symanzik, 'Schrödinger Representation and Casimir Effect in Renormalizable Quantum Field Theory', Nucl. Phys. B **190**, 1–44 (1981).

[75] M. Lüscher, R. Narayanan, P. Weisz and U. Wolff, 'The Schrödinger Functional – A Renormalizable Probe for Non-Abelian Gauge Theories', Nucl. Phys. B **384**, 168–228 (1992).

[76] K. G. Wilson, 'Quarks and Strings on a Lattice', in 13th International School of Subnuclear Physics: New Phenomena in Subnuclear Physics (Nov. 1975), pp. 69–142.

[77] C. Sturm, Y. Aoki, N. H. Christ, T. Izubuchi, C. T. C. Sachrajda and A. Soni, 'Renormalization of Quark Bilinear Operators in a Momentum-Subtraction Scheme with a nonexceptional Subtraction Point', Phys. Rev. D **80**, 014501 (2009).

[78] K. Jansen, C. Liu, M. Lüscher, H. Simma, S. Sint, R. Sommer, P. Weisz and U. Wolff, 'Nonperturbative Renormalization of Lattice QCD at all Scales', Phys. Lett. B **372**, 275–282 (1996).

[79] H. B. Nielsen and M. Ninomiya, 'Absence of Neutrinos on a Lattice. I. Proof by Homotopy Theory', Nucl. Phys. B **185**, [Erratum: Nucl. Phys. B **195**, 541 (1982)], 20–40 (1981).

[80] H. B. Nielsen and M. Ninomiya, 'Absence of Neutrinos on a Lattice. II. Intuitive Topological Proof', Nucl. Phys. B **193**, 173–194 (1981).

[81] H. B. Nielsen and M. Ninomiya, 'No Go Theorem for Regularizing Chiral Fermions', Phys. Lett. B **105**, 219–223 (1981).

[82] D. Friedan, 'A Proof of the Nielsen-Ninomiya Theorem', Commun. Math. Phys. **85**, 481–490 (1982).

[83] M. Lüscher, 'Exact Chiral Symmetry on the Lattice and the Ginsparg-Wilson Relation', Phys. Lett. B **428**, 342–345 (1998).

[84] P. H. Ginsparg and K. G. Wilson, 'A Remnant of Chiral Symmetry on the Lattice', Phys. Rev. D **25**, 2649–2657 (1982).

[85] G. Colangelo, S. Dürr and C. Haefeli, 'Finite Volume Effects for Meson Masses and Decay Constants', Nucl. Phys. B **721**, 136–174 (2005).

[86] M. Kurth and R. Sommer (ALPHA), 'Heavy Quark Effective Theory at One-Loop Order: An Explicit Example', Nucl. Phys. B **623**, 271–286 (2002).

[87] U. Wolff (ALPHA), 'Monte Carlo Errors with Less Errors', Comput. Phys. Commun. **156**, [Erratum: Comput. Phys. Commun. **176**, 383 (2007)], 143–153 (2004).

[88] S. Schaefer, R. Sommer and F. Virotta (ALPHA), 'Critical Slowing Down and Error Analysis in Lattice QCD Simulations', Nucl. Phys. B **845**, 93–119 (2011).

[89] M. Lüscher, 'Volume Dependence of the Energy Spectrum in Massive Quantum Field Theories. I. Stable Particle States', Commun. Math. Phys. **104**, 177–206 (1986).

[90] K. Symanzik, 'Continuum Limit and Improved Action in Lattice Theories. (I). Principles and ϕ^4 Theory', Nucl. Phys. B **226**, 187–204 (1983).

[91] K. Symanzik, 'Continuum Limit and Improved Action in Lattice Theories. (II). O(N) Nonlinear Sigma Model in Perturbation Theory', Nucl. Phys. B **226**, 205–227 (1983).

[92] N. Husung, P. Marquard and R. Sommer, 'Asymptotic Behavior of Cutoff Effects in Yang–Mills Theory and in Wilson's Lattice QCD', Eur. Phys. J. C **80**, 200 (2020).

[93] N. Husung, P. Marquard and R. Sommer, 'The Asymptotic Approach to the Continuum of Lattice QCD Spectral Observables', Phys. Lett. B **829**, 137069 (2022).

[94] B. Sheikholeslami and R. Wohlert, 'Improved Continuum Limit Lattice Action for QCD with Wilson Fermions', Nucl. Phys. B **259**, 572–596 (1985).

[95] R. Sommer, 'A New Way to Set the Energy Scale in Lattice Gauge Theories and its Applications to the Static Force and α_s in SU(2) Yang-Mills Theory', Nucl. Phys. B **411**, 839–854 (1994).

[96] M. Lüscher, 'Properties and Uses of the Wilson Flow in Lattice QCD', JHEP **08**, [Erratum: JHEP **03**, 092 (2014)], 071 (2010).

[97] M. Lüscher, 'Construction of a Selfadjoint, Strictly Positive Transfer Matrix for Euclidean Lattice Gauge Theories', Commun. Math. Phys. **54**, 283–292 (1977).

[98] G. Parisi, 'The Strategy for Computing the Hadronic Mass Spectrum', Phys. Rept. **103**, 203–211 (1984).

[99] G. P. Lepage, 'The Analysis of Algorithms for Lattice Field Theory', in Theoretical Advanced Study Institute in Elementary Particle Physics (June 1989), pp. 97–120.

[100] J. Bulava, M. Donnellan and R. Sommer, 'On the Computation of Hadron-to-Hadron Transition Matrix Elements in Lattice QCD', JHEP **01**, 140 (2012).

[101] S. Güsken, 'A Study of Smearing Techniques for Hadron Correlation Functions', Nucl. Phys. B Proc. Suppl. **17**, 361–364 (1990).

[102] C. R. Allton et al. (UKQCD), 'Gauge-Invariant Smearing and Matrix Correlators Using Wilson Fermions at $\beta = 6.2$', Phys. Rev. D **47**, 5128–5137 (1993).

[103] M. Papinutto, F. Scardino and S. Schaefer, 'New Extended Interpolating Fields Built from Three-Dimensional Fermions', Phys. Rev. D **98**, 094506 (2018).

[104] M. Lüscher, 'Chiral Symmetry and the Yang-Mills Gradient Flow', JHEP **04**, 123 (2013).

[105] L. Maiani, G. Martinelli, M. L. Paciello and B. Taglienti, 'Scalar Densities and Baryon Mass Differences in Lattice QCD with Wilson Fermions', Nucl. Phys. B **293**, 420–444 (1987).

[106] S. J. Dong, K. F. Liu and A. G. Williams, 'Lattice Calculation of the Strangeness Magnetic Moment of the Nucleon', Phys. Rev. D **58**, 074504 (1998).

[107] S. Capitani, B. Knippschild, M. Della Morte and H. Wittig, 'Systematic Errors in Extracting Nucleon Properties from Lattice QCD', PoS **LATTICE2010**, 147 (2010).

[108] T. Mannel, W. Roberts and Z. Ryzak, 'A Derivation of the Heavy Quark Effective Lagrangian from QCD', Nucl. Phys. B **368**, 204–217 (1992).

[109] U. Aglietti and S. Capitani, 'A New formulation of the Effective Theory for Heavy Particles', Nucl. Phys. B **432**, 315–336 (1994).

[110] J. G. Körner and G. Thompson, 'The Heavy Mass Limit in Field Theory and the Heavy Quark Effective Theory', Phys. Lett. B **264**, 185–192 (1991).

[111] L. L. Foldy and S. A. Wouthuysen, 'On the Dirac Theory of Spin 1/2 Particles and its Non-Relativistic Limit', Phys. Rev. **78**, 29–36 (1950).

[112] R. Sommer, 'Introduction to Non-Perturbative Heavy Quark Effective Theory', in Les Houches Summer School: Session 93: Modern Perspectives in Lattice QCD: Quantum Field Theory and High Performance Computing (Aug. 2010), pp. 516–590.

[113] R. Sommer, 'Heavy Quark Effective Theory: A Predictive EFT on the Lattice', in Effective Field Theory in Particle Physics and Cosmology: Lecture Notes of the Les Houches Summer School: Volume 108 (July 2020), pp. 616–649.

[114] U. Aglietti, M. Crisafulli and M. Masetti, 'Problems with the Euclidean Formulation of Heavy Quark Effective Theories', Phys. Lett. B **294**, 281–285 (1992).

[115] U. Aglietti, 'Consistency and Lattice Renormalization of the Effective Theory for Heavy Quarks', Nucl. Phys. B **421**, 191–216 (1994).

[116] O. Bär, A. Broll and R. Sommer, '$B\pi$ Excited-State Contamination in Lattice Calculations of B-Meson Correlation Functions', Eur. Phys. J. C **83**, 757 (2023).

[117] S. Hashimoto, T. Ishikawa and T. Onogi, 'Nonperturbative Calculation of Z_A/Z_V for Heavy-Light Currents Using Ward-Takahashi identity', Nucl. Phys. B Proc. Suppl. **106**, 352–354 (2002).

[118] F. Palombi (ALPHA), 'Non-Perturbative Renormalization of the Static Vector Current and its O(a)-Improvement in Quenched QCD', JHEP **01**, 021 (2008).

[119] A. V. Manohar and M. B. Wise, *Heavy Quark Physics*, Cambridge Monographs on Particle Physics, Nuclear Physics and Cosmology 10 (Cambridge University Press, 2000).

[120] M. B. Voloshin and M. A. Shifman, 'On the Annihilation Constants of Mesons Consisting of a Heavy and a Light Quark, and $B^0 \leftrightarrow \bar{B}^0$ Oscillations', Sov. J. Nucl. Phys. **45**, 292–294 (1987).

[121] H. D. Politzer and M. B. Wise, 'Leading Logarithms of Heavy Quark Masses in Processes with Light and Heavy Quarks', Phys. Lett. B **206**, 681–684 (1988).

[122] M. Kurth and R. Sommer (ALPHA), 'Renormalization and O(a) Improvement of the Static Axial Current', Nucl. Phys. B **597**, 488–518 (2001).

[123] J. Heitger, M. Kurth and R. Sommer (ALPHA), 'Non-Perturbative Renormalization of the Static Axial Current in Quenched QCD', Nucl. Phys. B **669**, 173–206 (2003).

[124] M. Della Morte, P. Fritzsch and J. Heitger, 'Non-Perturbative Renormalization of the Static Axial Current in Two-Flavour QCD', JHEP **02**, 079 (2007).

[125] B. Blossier, M. della Morte, N. Garron and R. Sommer, 'HQET at Order $1/m$: I. Non-Perturbative Parameters in the Quenched Approximation', JHEP **06**, 002 (2010).

[126] M. E. Peskin and D. V. Schroeder, *An Introduction to Quantum Field Theory* (Addison-Wesley, Reading, USA, 1995).

[127] Y. Aoki et al. (Flavour Lattice Averaging Group (FLAG)), 'FLAG Review 2021', Eur. Phys. J. C **82**, 869 (2022).

[128] I. Adachi et al. (Belle), 'Evidence for $B^- \to \tau^- \bar{\nu}_\tau$ with a Hadronic Tagging Method Using the Full Data Sample of Belle', Phys. Rev. Lett. **110**, 131801 (2013).

[129] B. Kronenbitter et al. (Belle), 'Measurement of the Branching Fraction of $B^+ \to \tau^+ \nu_\tau$ Decays with the Semileptonic Tagging Method', Phys. Rev. D **92**, 051102 (2015).

[130] B. Aubert et al. (BaBar), 'Search for $B^+ \to \ell^+ \nu_\ell$ Recoiling Against $B^- \to D^0 \ell^- \bar{\nu} X$', Phys. Rev. D **81**, 051101 (2010).

[131] J. P. Lees et al. (BaBar), 'Evidence of $B^+ \to \tau^+ \nu$ Decays with Hadronic B Tags', Phys. Rev. D **88**, 031102 (2013).

[132] D. Bećirević, S. Prelovšek and J. Zupan, '$B \to \pi$ and $B \to K$ Transitions in Standard and Quenched Chiral Perturbation Theory', Phys. Rev. D **67**, 054010 (2003).

[133] E. Dalgic, A. Gray, M. Wingate, C. T. H. Davies, G. P. Lepage and J. Shigemitsu, 'B Meson Semileptonic Form Factors from Unquenched Lattice QCD', Phys. Rev. D **73**, [Erratum: Phys. Rev. D **75**, 119906 (2007)], 074502 (2006).

[134] J. A. Bailey et al. (Fermilab Lattice, MILC), '$|V_{ub}|$ from $B \to \pi \ell \nu$ Decays and (2+1)-Flavor Lattice QCD', Phys. Rev. D **92**, 014024 (2015).

[135] J. M. Flynn, T. Izubuchi, T. Kawanai, C. Lehner, A. Soni, R. S. Van de Water and O. Witzel, '$B \to \pi \ell \nu$ and $B_s \to K \ell \nu$ Form Factors and $|V_{ub}|$ from 2+1-Flavor Lattice QCD with Domain-Wall Light Quarks and Relativistic Heavy Quarks', Phys. Rev. D **91**, 074510 (2015).

[136] P. del Amo Sanchez et al. (BaBar), 'Study of $B \to \pi \ell \nu$ and $B \to \rho \ell \nu$ Decays and Determination of $|V_{ub}|$', Phys. Rev. D **83**, 032007 (2011).

[137] J. P. Lees et al. (BaBar), 'Branching Fraction and Form-Factor Shape Measurements of Exclusive Charmless Semileptonic B Decays, and Determination of $|V_{ub}|$', Phys. Rev. D **86**, 092004 (2012).

[138] H. Ha et al. (Belle), 'Measurement of the Decay $B^0 \to \pi^- \ell^+ \nu$ and Determination of $|V_{ub}|$', Phys. Rev. D **83**, 071101 (2011).

[139] A. Sibidanov et al. (Belle), 'Study of Exclusive $B \to X_u \ell \nu$ Decays and Extraction of $\|V_{ub}\|$ Using Full Reconstruction Tagging at the Belle Experiment', Phys. Rev. D **88**, 032005 (2013).

[140] B. Colquhoun, S. Hashimoto, T. Kaneko and J. Koponen (JLQCD), 'Form factors of $B \to \pi \ell \nu$ and a Determination of $|V_{ub}|$ with Möbius Domain-Wall Fermions', Phys. Rev. D **106**, 054502 (2022).

[141] A. J. Buras, W. Slominski and H. Steger, '$B^0 - \bar{B}^0$ Mixing, CP Violation and the B-Meson Decay', Nucl. Phys. B **245**, 369–398 (1984).

[142] A. J. Buras, M. Jamin and P. H. Weisz, 'Leading and Next-to-Leading QCD Corrections to ϵ-Parameter and $B^0 - \bar{B}^0$ Mixing in the Presence of a Heavy Top Quark', Nucl. Phys. B **347**, 491–536 (1990).

[143] G. Buchalla, 'Renormalization of $\Delta B = 2$ Transitions in the Static Limit Beyond Leading Logarithms', Phys. Lett. B **395**, 364–368 (1997).

[144] T. Inami and C. S. Lim, 'Effects of Superheavy Quarks and Leptons in Low-Energy Weak Processes $K_L \to mu\bar{\mu}$, $K^+ \to \pi^+\nu\bar{\nu}$ and $K^0 \to \bar{K}^0$', Prog. Theor. Phys. **65**, [Erratum: Prog. Theor. Phys. **65**, 1772 (1981)], 297–314 (1981).

[145] A. J. Buras, W. Slominski and H. Steger, 'B-Meson Decay, CP Violation, Mixing Angles and the Top Quark Mass', Nucl. Phys. B **238**, 529–560 (1984).

[146] R. J. Dowdall, C. T. H. Davies, R. R. Horgan, G. P. Lepage, C. J. Monahan, J. Shigemitsu and M. Wingate, 'Neutral B-Meson Mixing from Full Lattice QCD at the Physical Point', Phys. Rev. D **100**, 094508 (2019).

[147] A. G. Grozin, T. Mannel and A. A. Pivovarov, 'Towards a Next-to-Next-to-Leading Order Analysis of Matching in B^0-$\bar{B}^0$ Mixing', Phys. Rev. D **96**, 074032 (2017).

[148] A. G. Grozin, T. Mannel and A. A. Pivovarov, 'B^0-$\bar{B}^0$ Mixing: Matching to HQET at NNLO', Phys. Rev. D **98**, 054020 (2018).

[149] F. Palombi, M. Papinutto, C. Pena and H. Wittig (ALPHA), 'A Strategy for Implementing Non-Perturbative Renormalisation of Heavy-Light Four-Quark Operators in the Static Approximation', JHEP **08**, 017 (2006).

[150] J. M. Flynn, O. F. Hernandez and B. R. Hill, 'Renormalization of Four-Fermion Operators Determining B-$\bar{B}$ Mixing on the Lattice', Phys. Rev. D **43**, 3709–3714 (1991).

[151] V. Gimenez and J. Reyes, 'Calculation of the Continuum Lattice HQET Matching for the Complete Basis of Four Fermion Operators: Reanalysis of the B^0-$\bar{B}^0$ Mixing', Nucl. Phys. B **545**, 576–606 (1999).

[152] H. Leutwyler, 'On the Foundations of Chiral Perturbation Theory', Annals Phys. **235**, 165–203 (1994).

[153] S. R. Coleman, J. Wess and B. Zumino, 'Structure of Phenomenological Lagrangians. I', Phys. Rev. **177**, 2239–2247 (1969).

[154] C. G. Callan Jr., S. R. Coleman, J. Wess and B. Zumino, 'Structure of Phenomenological Lagrangians. II', Phys. Rev. **177**, 2247–2250 (1969).

[155] S. Weinberg, 'Phenomenological Lagrangians', Physica A **96**, 327–340 (1979).

[156] S. R. Sharpe and R. L. Singleton Jr, 'Spontaneous Flavor and Parity Breaking with Wilson Fermions', Phys. Rev. D **58**, 074501 (1998).

[157] W.-J. Lee and S. R. Sharpe, 'Partial Flavor Symmetry Restoration for Chiral Staggered Fermions', Phys. Rev. D **60**, 114503 (1999).

[158] O. Bär, 'Chiral Perturbation Theory at Non-Zero Lattice Spacing', Nucl. Phys. B Proc. Suppl. **140**, 106–119 (2005).

[159] F. Bernardoni, P. Hernandez and S. Necco, 'Heavy-Light Mesons in the ϵ-Regime', JHEP **01**, 070 (2010).

[160] C. D. Carone, 'Superflavor Symmetry for Heavy Vector Mesons and Heavy Quarks', Phys. Lett. B **253**, 408–410 (1991).

[161] M. Heiles, M. König and M. Neubert, 'Effective Field Theory for Heavy Vector Resonances Coupled to the Standard Model', JHEP **02**, 204 (2021).

[162] A. Gérardin, J. Heitger, S. Kuberski, H. Simma and R. Sommer (ALPHA), 'Precision $B^*B\pi$ Coupling from Three-Flavor Lattice QCD', PoS **LATTICE2021**, 540 (2022).

[163] S.-Z. Jiang, Y.-R. Liu and Q.-H. Yang, 'Chiral Lagrangians for Mesons with a Single Heavy Quark', Phys. Rev. D **99**, 074018 (2019).

[164] B. Grinstein, E. E. Jenkins, A. V. Manohar, M. J. Savage and M. B. Wise, 'Chiral Perturbation Theory for f_{D_s}/f_D and B_{B_s}/B_B', Nucl. Phys. B **380**, 369–376 (1992).

[165] O. Bär, A. Broll and R. Sommer, '$B\pi$-State Contamination in B-Meson Observables', PoS **LATTICE2022**, 402 (2023).

[166] C. Aubin and C. Bernard, 'Staggered Chiral Perturbation Theory for Heavy-Light Mesons', Phys. Rev. D **73**, 014515 (2006).

[167] O. Bär and M. Golterman, 'Chiral Perturbation Theory for Gradient Flow Observables', Phys. Rev. D **89**, [Erratum: Phys. Rev. D **89**, 099905 (2014)], 034505 (2014).

[168] B. C. Tiburzi, 'Chiral Corrections to Nucleon Two- and Three-Point Correlation Functions', Phys. Rev. D **91**, 094510 (2015).

[169] O. Bär and M. Golterman, 'Excited-State Contribution to the Axial-Vector and Pseudoscalar Correlators with two Extra Pions', Phys. Rev. D **87**, 014505 (2013).

[170] O. Bär, A. Broll and R. Sommer, 'Estimating Excited States Contamination of $B \to \pi$ Form Factors Using Heavy Meson Chiral Perturbation Theory', PoS **LATTICE2022**, 406 (2023).

[171] A. F. Falk and B. Grinstein, '$\bar{B} \to \bar{K}e^+e^-$ in Chiral Perturbation Theory', Nucl. Phys. B **416**, 771–785 (1994).

[172] C. Aubin and C. Bernard, 'Heavy-Light Semileptonic Decays in Staggered Chiral Perturbation Theory', Phys. Rev. D **76**, 014002 (2007).

[173] F. Bahr, D. Banerjee, F. Bernardoni, M. Koren, H. Simma and R. Sommer, 'Extraction of Bare Form Factors for $\mathrm{B_s} \to \mathrm{K}\ell\nu$ Decays in Nonperturbative HQET', Int. J. Mod. Phys. A **34**, 1950166 (2019).

[174] W. Detmold and C. J. D. Lin, 'Matrix Elements of the Complete Set of $\Delta B = 2$ and $\Delta C = 2$ Operators in Heavy Meson Chiral Perturbation Theory', Phys. Rev. D **76**, 014501 (2007).

[175] J.-W. Lee, 'Matrix Elements of $\Delta B = 0$ Operators in Heavy Hadron Chiral Perturbation Theory', Phys. Rev. D **91**, 094511 (2015).

[176] N. Isgur and M. B. Wise, 'Weak Transition Form Factors Between Heavy Mesons', Phys. Lett. B **237**, 527–530 (1990).

[177] L. Randall and M. B. Wise, 'Chiral Perturbation Theory for $B \to D^*$ and $B \to D$ Semileptonic Transition Matrix Elements at Zero Recoil', Phys. Lett. B **303**, 135–139 (1993).

[178] M. Böhm, A. Denner and H. Joos, *Gauge Theories of the Strong and Electroweak Interaction* (B. G. Teubner, Stuttgart/Leipzig/Wiesbaden, 2001).

[179] I. S. Gradshteyn and I. M. Ryzhik, *Table of Integrals, Series, and Products*, edited by V. Moll and D. Zwillinger, Eighth Edition (Academic Press, Boston, 2014).

[180] A. F. Falk, 'Excited Heavy Mesons and Kaon Loops in Chiral Perturbation Theory', Phys. Lett. B **305**, 268–274 (1993).

Selbständigkeitserklärung

Ich erkläre, dass ich die Dissertation selbständig und nur unter Verwendung der von mir gemäß § 7 Abs. 3 der Promotionsordnung der Mathematisch-Naturwissenschaftlichen Fakultät, veröffentlicht im Amtlichen Mitteilungsblatt der Humboldt-Universität zu Berlin Nr. 42/2018 am 11.07.2018 angegebenen Hilfsmittel angefertigt habe.

Ort, Datum

Unterschrift